Development of a robust myoelectric control architecture for lower limb robotic prosthetic applications

by

Talon Garikayi

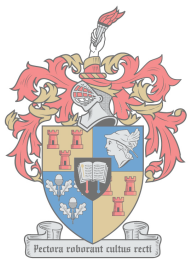

UNIVERSITEIT
iYUNIVESITHI
STELLENBOSCH
UNIVERSITY

Dissertation presented for the degree of Doctor of Philosophy in the Faculty of Engineering at Stellenbosch University

100
1918·2018

Supervisor: Dr. Dawie van den Heever
Co-supervisor: Dr. Stephen Matope

December 2018

Declaration

By submitting this dissertation electronically, I declare that the entirety of the work contained therein is my own, original work, that I am the sole author thereof (save to the extent explicitly otherwise stated), that reproduction and publication thereof by Stellenbosch University will not infringe any third party rights and that I have not previously in its entirety or in part submitted it for obtaining any qualification.

Date: December 2018

Abstract

Development of a robust myoelectric control architecture for lower limb robotic prosthetic applications

Talon Garikayi

Department of Mechanical and Mechatronic Engineering,
University of Stellenbosch,
Private Bag X1, Matieland 7602, South Africa.

Dissertation: PhD (Mechatronic Engineering)

December 2018

Traumatic events such as accidents or vascular and circulatory disorders often lead to amputation of the lower limb. To increase mobility most amputees are fitted with a passive prosthetics. However, the use of a passive foot with a fixed ankle has short term effects, such as asymmetric gait, increased muscle contraction on the intact side and higher metabolic energy expenditure. The long-term effects are osteoarthritis, osteoporosis, back pain and to a large extent musculoskeletal problems. As a result, artificial prosthetic limbs are regarded by the amputees as exotic lifeless attachments to the body and not as a non-biological extension of the human body. Mechatronic systems coupled with intelligent control architectures provide the platform to restoring an amputee's overall mobility related lifestyle. However, the recovered gait is largely influenced by the extent of amputation and functional level of the prosthesis. The transtibial osteomyoplastic amputation technique offers residual muscles that are active throughout the gait cycle. These muscles offer potential sites for extracting surface electromyography (sEMG) signals.

The study presents a novel methodology which seeks to utilise these residual signals to control an artificial limb by predicting the human movement intentions. A protocol was developed for the acquisition and analysis of electromyography signals from the identified muscles. The available SENIAM and ISEK standards were found to be insufficient during the recording of signals from the residual stump as some of the anatomical landmarks were missing. The Soleus muscle responsible for plantarflexion was not accessible on the residual limb thereby providing challenges on using the SENIAM standards for selecting a muscle for the plantarflexion movement. Tibialis anterior, Medialis Gastrocnemius and Lateralis Gastrocnemius muscles were able to provide sEMG signals with sufficient signal properties for developing a myoelectric pattern recognition architecture. The main goal was to develop a robust intelligent control system architecture for a robotic prosthetic lower limb capable of enhancing human mobility with great stability. The functionality of a robotic limb is highly governed by kinetics, kinematics and the dynamics of the mechanical structure when interfaced with the human body. Therefore, the structure and parameters of the actuation model for complex joint angle prediction and an intuitive neural interface mechanism for intention detection were developed based on experimental results from

biomechanics experiments.

A pattern recognition algorithm was developed based on 23 signal features. Principal component analysis was used for dimensionality reduction on the extracted feature set. A total of 22 classifiers were tested and the Linear Support Vector Machine produced an average of 100% classification accuracy on training data with 20% of the training data being reserved for validation. The intelligent architecture produced an average of 99.25% classification accuracy on new unlabelled test data.

The system was optimised using force sensitive resistors to detect heel strike, toe off and beginning of the swing and stance phases of gait. A dual inertial measurement system was used to predict the position of the limb in space thereby providing feedback on limb performance to the main controller. The use of adaptive filters on signal acquisition improved signal quality and the use of Kalman filters on feedback sensors provided a robust system which was able to achieve the desired control objective even in the event of partial or missing input signal as they predicted the intended signal based on the previously correct signal input. This study revealed that the concept developed has the potential to improve the lives of many amputees as it has the ability to restore normal gait to the satisfactory level of the amputee. The intuitive control of the prosthetic limb provided by the sEMG signals and the inertial sensor feedback system minimises the need for the situational attentiveness of the amputee with regards to the operation of the powered prosthetic.

Uittreksel

Ontwikkeling van 'n robuuste myoelektriese kontrole-argitektuur vir robotiese prostetiese toepassings in die onderste ledemaat

Talon Garikayi

Departement Meganiese en Megatroniese Ingenieurswese,
Universiteit van Stellenbosch,
Privaatsak X1, Matieland 7602, Suid Afrika.

Proefskrif: PhD (Megatroniese Ingenieurswese)

Desember 2018

Traumatiese gebeurtenisse soos ongelukke of vaskulêre en bloedsomloopafwykings lei dikwels tot amputasie van die onderste ledemaat. Om die mobiliteit te verhoog, word die meeste geamputeerde toegerus met 'n passiewe prostese. Die gebruik van 'n passiewe voet met 'n vaste enkel het kort termyn effekte soos asimmetriese gang, verhoogde spierkontraksie op die ongeskonde kant en hoër metaboliese energieverbruik. Die langtermyn-effekte is osteoartritis, osteoporose, rugpyn en tot 'n groot mate muskuloskeletale probleme. Gevolglik word kunsmatige ledemate deur die geamputeerde beskou as eksotiese lewenslose aanhangsels binne die liggaam en nie as 'n nie-biologiese verlenging van die menslike liggaam nie. Megatroniese stelsels, tesame met intelligente beheer-argitekture, bied die platform om 'n geamputeerde se algehele mobiliteitsverwante leefstyl te herstel. Die herstelde gang is egter grootliks beïnvloed deur die mate van amputasie en funksionele vlak van die prostese. Die transtibiale osteomyoplastiese amputasietegniek bied oorblywende spiere wat aktief is in die loopsiklus. Hierdie spiere bied potensiële areas vir die opneem van oppervlak-myo-elektroniese seine.

Die studie bied 'n nuwe metodologie aan wat daarop gemik is om hierdie residuele seine te gebruik om 'n kunsmatige ledemaat te beheer deur die menslike bewegings bedoelings te voorspel. 'n Protokol is ontwikkel vir die verkryging en analise van elektromyografiese seine van die geïdentifiseerde spiere. Die beskikbare SENIAM- en ISEK-standaarde was onvoldoende tydens die opname van seine van die oorblywende stomp, aangesien sommige van die anatomiese landmerke ontbreek. Die Soleus-spier wat verantwoordelik is vir plantarfleksie, was nie toeganklik op die oorblywende ledemaat nie en bied dus uitdagings om die SENIAM-standaarde te gebruik om 'n spier vir die plantarfleksie-beweging te kies. Tibialis anterior, Medialis Gastrocnemius en Lateralis Gastrocnemius spiere was in staat om sEMG seine te voorsien met voldoende sein eienskappe vir die ontwikkeling van 'n myoektriese patroon herkenning argitektuur. Die hoofdoel was om 'n robuuste intelligente beheerstelselargitektuur vir 'n robotprotese-onderste ledemaat te ontwikkel wat die menslike mobiliteit met hoë stabiliteit kan verbeter. Die funksionaliteit van 'n robot-ledemaat word sterk beheer deur kinetika, kinematika en die dinamika van die meganiese struktuur wanneer dit met die menslike liggaam inmeng. Die struktuur en parameters van die

aktuasie model vir komplekse gesamentlike voorspelling en 'n intuïtiewe neurale koppelvlak meganisme vir voornemende opsporing is daarom ontwikkel op grond van eksperimentele resultate uit biomeganiese eksperimente.

'n Patroonherkenningsalgoritme is ontwikkel op grond van 23 seinmerke. Die hoof komponent analise is gebruik vir dimensionaliteitsreduksie op die opgeneemde stel seine. 'n Totaal van 22 klassifikasie algoritmes is getoets en die Lineêre Ondersteuningsvektormasjien het gemiddeld 100% klassifikasie akkuraatheid op opleidingsdata geproduseer met 20% van die data wat vir validering gereserveer is. Die intelligente argitektuur het 'n gemiddeld van 99,25% klassifikasie akkuraatheid op nuwe ongemerkte toetsdata opgelewer.

Die stelsel is geoptimaliseer deur gebruik te maak van kraggevoelige weerstande om hakstaking, tone-af en begin van die swaai- en houdingsfases van die gang te bepaal. 'n Dubbele traagheidsmetingsisteem is gebruik om die posisie van die ledemaat in die ruimte voor te stel en sodoende terugvoer te gee aan ledemate-prestasie aan die hoofbeheerder. Die gebruik van adaptiewe filters op sein verkryging verbeter sein kwaliteit en die gebruik van Kalman-filters op terugvoer-sensors het 'n robuuste stelsel gelewer wat in staat was om die verlangde beheerdoelwit te behaal, selfs in die geval van gedeeltelike of ontbrekende insetsein, aangesien hulle die beoogde sein voorspel het gebaseer op die voorheen korrekte seininvoer. Hierdie studie bewys dat die konsep wat ontwikkel is die potensiaal het om die lewens van baie geamputeerdes te verbeter aangesien dit die vermoë het om normale gang te herstel tot die bevredigende vlak van die geamputeerde. Die intuïtief beheer van die prostetiese ledemaat wat deur die elektromyografiese seine en die traagheidssensor terugvoerstelsel verskaf word, verminder die behoefte aan die situasionele aandag van die geamputeerde ten opsigte van die werking van die aangedrewe prostese.

Acknowledgements

I would like to express my sincere gratitude to my supervisor Dr. Dawie van den Heever and my co-supervisor Dr. Stephen Matope for their continuous support, encouragement, guidance and advice, trust, stimulating discussion, proposed ideas and constructive suggestions during my studies.

Also, I would like to express my deepest appreciation to all Dr. John Cockcroft for his constant support, interest in the topic, immeasurable contributions, kind assistance and wonderful friendship throughout the studies. Thanks are given to all of my colleagues at the Biomedical Engineering Research Group at Stellenbosch University. My work and discussion with them were always a pleasure that created an ideal working environment for my research.

I would also like to thank Theodorus Kriel for the technical advice with regards to working with amputees (Amputee Clinic, South Africa), Madeleine Dreyer and Cara Mills (Human Motion Analysis Unit, Central Facility, South Africa) on assisting with data collection and experimental set-up. Lastly, I would want to thank Ben and Mike who made this study a success through their unwavering support.

Contents

List of Figures

List of Tables

Chapter 1

Introduction

1.1 Background

Lack of a healthy diet and the rising prevalence of health issues such as diabetes, as well as degenerative joint diseases such as arthritis and osteoporosis, are building the demand for prosthetics [1]. In addition, traumatic events such as accidents or vascular and circulatory disorders often lead to amputation of the lower limb below the knee joint [2]. South Africa has the highest number of amputations in the Southern Africa region with an amputee population of approximately 311 139. There were over 2000 new cases of amputations reported in South Africa in 2009, the highest in Southern Africa per year [3]. According to the report released by Stats SA in 2011, out of the population of 51 777 560 in South Africa, 53% of the elderly population was disabled. As a result, this causes a strain on the national economy as the dependency ratio increases annually. According to [4], the production cost of a transtibial mechanical passive limb for daily living activities is approximately $25 196. With basic electronic components, the cost increases to approximately $31 196. Therefore the microprocessor-based limbs will cost close to $45 563. In South Africa, the average purchase price of a passive mechanical limb is approximately R75 000 while the cost of a powered active prosthetic is R1.4 million. As a result, the cost of prosthetic limbs is far beyond the reach of many South Africans. Therefore, most South African amputees have resorted to using unorthodox methods to achieve mobility, ranging from simple walking sticks to home-made crutches.

The need and desire for developing powered prosthetic limbs to improve the lifestyle of amputees has been well researched and justified [5]. However, less progress has been made so far with regard to improving the performance of the devices with the aid of sensory feedback [6]. The use of powered prosthetic limbs with the aid of myoelectric signals began as early as the 1980 [7]. However, the introduction of pattern recognition systems has resulted in the investigation of the clinical applicability of myoelectric control systems for commercial devices [8]. The advantage of a natural lower limb over a prosthetic limb is the variability of ankle stiffness with respect to gait type, walking speed and terrain [9], this pattern could be matched if pattern recognition systems are implemented on the current commercial devices. The ideal myoelectric control system should be able to match the variable ankle stiffness in order to meet the gait demands. However, this presents a design challenge given that the quality of electromyography (EMG) signals at the residual limb are affected by the type of amputation, cause of amputation and extent of amputation [10], [11], [12]. Although pattern recognition algorithms have been extensively used in image processing, it is not yet clinically viable to implement such techniques without comprehensive, computationally intensive and complex signal processing techniques in

prosthetic designs [13].

Depending on the level of amputation, there is a change in the body structure associated with surgery and, as a result, there will be a limited number of active muscles for the intended task [14].The lower limb amputees often exhibit non-symmetric gait pattern [15]. Although the use of passive prosthetic limbs increases mobility, this will, however, cause an increased energy expenditure of approximately 60% as compared to a non-amputee [16]. Regardless of the tremendous efforts made to commercialise powered limbs, there has been a high rejection ratio from the amputees for up to 66% of the population [17], [18]. Although this is an improvement from the 75% rejection reported on the highly mechanical systems there is still a lot to be done with regard to intuitive control for myoelectric prosthetics [19]. Major complaints emanated from high power consumption, extended reaction times and lack of dexterousness of the powered limbs. However, concepts that may have been impractical at the time of their inception have become possible with developments in biomedical engineering technologies, thereby providing high chances of increasing device performance. Advances in signal acquisition and data processing technologies have provided new platforms for physiological signals to be used for control and monitoring purposes in the development of active prosthetic limbs. Therefore, there is hope for increased reliability with regard to functionality on new designs.

A myoelectric control system is one that addresses the fundamentals of controllability, which includes the accuracy of movement control, the intuitiveness of actuating control and the response of the control system [20] with the aid EMG signals. The major attributes of an active prosthesis, such as observability, controllability and stability, are affected by uncertainty in either the model, disturbances at control input signal or noise in the sensor input [21]. According to [10], the ability to decode the EMG signals can prove to be extremely useful in restoring some or all of the lost motor functionality in amputees. Hargrove et al. [22], suggested that the clinical application of robotic technology to active prosthetic knees and ankles is limited by the lack of a robust control strategy. Furthermore, robustness, adaptability, and situational awareness are the three complementary machine intelligence pursuits which can be used to enhance the expected clinical effectiveness of conventional and emerging myoelectric control systems [23].

Robustness and plasticity are essential features of all biological systems [24]. Thus, if the emerging technologies are to imitate biological systems then these features form the basis of the control architectures. According to [25], robustness describes the insensitivity of a system to external perturbations, and plasticity describes the changeability of a system in response to changes in external conditions. Surprisingly, biological systems somehow always manage to find a trade-off between these two properties [25]. Therefore, there is a need to develop a robust myoelectric control system architecture that is capable of overcoming the plasticity-stability dilemma intelligently. This is mainly attributed to the fact that intelligent control architectures enhance development of powerful, flexible and efficient prosthetic designs [26]. If achieved, this will go a long way to improving the functionality of active prosthetics and ultimately the lifestyle of the amputees [27].

1.2 Problem statement

A large population of amputees use passive mechanical limbs for their daily ambulatory activities. However, the use of these passive prosthetics with a fixed ankle has negative short-term effects such as asymmetric gait, increased muscle contraction on the intact side and higher metabolic

energy expenditure. Hence, this can lead to long term-effects such as osteoarthritis, osteoporosis, back-pain and, to a large extent, musculoskeletal problems. As a result, these mechanical limbs are regarded by amputees as exotic lifeless attachments to the body and not as a non-biological extension of the human body. Therefore, the application of intelligent myoelectric control systems will enhance reliability of the powered prosthetics.

1.3 Aim

The aim of this study is to develop an autonomous myoelectric control system architecture for an active powered prosthetic lower limb with the aid of myoelectric and inertial signals.

1.4 Objectives

To achieve this aim, the following objectives were accomplished:

- To analyse the effect of the passive mechanical prosthetic ankle on lower limb amputee gait.
- To characterise electromyography signal properties for ankle movements on transtibial amputees.
- To investigate the use of inertial sensors as feedback signals in-order to improve adaptability, reliability and robustness of the architecture.
- To design and test a multichannel surface electromyography signal acquisition and processing system.
- To develop a robust myoelectric control architecture for a multifunctional artificial ankle.
- To test the functionality of the control system.

1.5 Motivation

The desire to develop technologies that can assist the physically challenged to overcome obstacles related to lifestyle improvement resulted in the pursuit of the development of intelligent myoelectric control architectures. The general norm known to the disabled is that *disability does not mean inability*. However, without technology interventions, this statement is far from being a reality. It leaves the burden of mobility achievement to the amputee leading to a stressful lifestyle. This study seeks to help the lifestyle of the amputees with regard to ambulatory related activities by improving already existing mechanical and powered limbs to become more reliable, dependable and autonomous. Ultimately, this will reduce the burden on using the device as it *intuitively* predicts the intended movement and executes the motion effortlessly.

The *detectability* and *measurability* of muscle signals from the skin surface have motivated the use of surface sEMG signals as input signals to the proposed control architecture. The need to orient the limb in space to achieve recommendable ground clearance and smooth normal gait has resulted in the possible use of inertial measurement unit (IMU) sensors. These sensors have been widely applied in gait analysis, sports science and motion picture development. However, with seamless integration with the sEMG signals, these IMU sensors can be used to develop robust control architectures capable of adapting to dynamic changes in signal quality. As a result

of the multichannel signal based control system (sEMG and IMU sensors), feedback on actuator performance is possible. Dual systems improve reliability and reduce the responsibility of the user on the overall performance of the system.

These IMU sensors could also provide the possibility of controlling the below-the-knee artificial limb based on the thigh orientation. Therefore the possibility of developing a hybrid system of inertial sensors and sEMG signals has resulted in the need to pursue this study as the demand for robust and self-adapting control architectures is increasing. Furthermore, the applicability of learning algorithms was investigated to improve robustness and adaptability as it requires minimum human intervention. The success of a robotic prosthetic limb is determined by its adaptability to changes in torque demands, skeletal structure, growth in human tissue, body weight and changes in terrain while still achieving the intended goal of improving human mobility. Fekri et al. [28] suggested that if one explicitly state the specifications for the required stability and performance robustness for the adaptive closed-loop system, then one can evolve the present control system architectures so that they can be confidently used in real applications.

The proposed control architecture will be able to achieve the desired control objectives in the situations of both known and unknown uncertainties. Englehart and Hudgins [20] outlined that by exploiting the processing power inherent in current computing systems, substantial gains in classifier accuracy and response times are possible as main characteristics of a high-level control system. The function of the IMU sensors was to achieve acceptable tracking characteristics of the robotic prosthetic limb under variable gait speeds and ambulatory activities. According to [29], information extracted from multiple channels of sEMG recording sites can be used as inputs to control systems for active limb prostheses. Therefore, implementing such a technique along with other signals (i.e. using inertial sensors to detect movement) can increase functionality and reduce the load from the user as the intentions can be detected intuitively in real-time.

The current powered limbs lack adequate control interfaces which could allow amputees to operate them in an intuitive and close-to-natural way, such as the user's movement prediction methods. Therefore, the goal of this project is the development of a myoelectric control system architecture which can predict the user's movement intention with the aid of learning algorithms, search algorithms, cognitive reasoning and adaptation laws to correctly position the limb.

Thus, this study presents the development of a myoelectric control system that will enable improved mobility, thereby improving the lifestyle of the amputee.

1.6 Unique contribution

This study contributes to the field of biomedical engineering through:

- The development of an intuitive neural interface from which the user's intent can be determined in real-time.
- The development of a model for utilising both muscle and inertial sensor signals to accurately control desired lower limb motions.
- The development of a learning algorithm for control system architecture to improve the adaptability of an active prosthetic limb in a dynamic environment.

- Extending the literature on how biomechatronic systems can be utilised for the development of powered prosthetic limbs.

1.7 Research scope

The research seeks to address the applicability of EMG signals and inertial signals as dual input control signals for a control architecture in a systematic manner in order to improve robustness and adaptability of active prosthetic lower limbs. The research is organised as follows:

- Experiments for gait analysis were designed to study the gait of unilateral transtibial osteomyoplastic amputees in real time during ambulatory-related activities. Experimental protocols were then developed taking into consideration all regulations governing the use of human beings in research. The research protocols were approved by the Ethics Committee. The data collected was then used to understand the effects of passive limbs on amputee gait. The data was analysed and gait parameters such as gait speed, step length and step frequency were determined. Further analysis was done on anatomic angles and orientation angles for the hip, knee and ankle in an effort to understand how the passive prosthetic limb supports the body weight.

- The feasibility of attaining sEMG signals from the residual limb was investigated. Therefore, experiments were developed to determine which residual muscles could be used to achieve a multifunctional prosthetic limb and also the quality parameters of the available signals were investigated. Experimental protocols aligned to SENIAM and ISEK standards were designed to collect and analyse the data. Algorithms for signal analysis were developed to analyse the signal quality and feasibility of using the EMG signal as a control signal.

- From the determined EMG signal parameters, such as time domain, frequency domain and time-frequency domain in the initial experiments, a multichannel data acquisition system was developed to acquire the signals in real-time for a multifunctional lower limb. Experimental protocols were developed aligned to International Electrotechnical Commission, IEC 60601-1 standards for the design and development of electronic medical equipment. The protocol took into cognisance the Application of Risk Management to Medical Devices (ISO 14971) standard. The main goal was to develop a miniaturised front end device that can accommodate a multi-nodal system and investigate signal processing techniques for real-time control. Techniques such as Common Mode Rejection (CMRR), amplification, anti-aliasing, notch filtering, low pass and high pass filtering were investigated. The developed data acquisition unit formulated the initial module for the control system architecture.

- The applicability of inertial sensors so as to determine limb orientation and methods for attaining a synergistic integration with the EMG signal were developed. Experimental protocols developed were governed by the approved Research Protocol by the Ethics Committee. The objective was to study the anatomical angles related to the knee and ankle to determine the feasibility and effectiveness of such signals for active limbs. The main goal was to develop a single nodal sensor integrated into the developed EMG data acquisition module. The IMU signals were used to determine the position of the limb according to the gait of the participant and controlling the ankle actuator. Algorithms for signal analysis and conversion were developed so as to achieve a feedback and prediction mode for

the control architecture. It was highly anticipated that algorithms such as Kalman and Complimentary filtering will improve the robustness and adaptability of the architecture to external perturbations.

- The applicability of machine learning was investigated with a bias towards pattern recognition systems. Experimental protocols were developed with an emphasis on improving system performance. Learning based control and other modern control systems such as the MIT Rule and Lyapunov Principle were analysed with the aim of increasing stability and improving plasticity of the control architecture. Algorithms were developed so as to achieve a more reliable and dependable control system architecture capable of improving the performance of an active prosthetic lower limb.

- Finally, the functionality of the developed control architecture was tested on the amputee. The experimental protocol initially used to determine the effects of passive limbs was then used to test the functionality of the developed powered limb. The main major concern was to evaluate the extent to which the powered limb had restored the normal gait. The amputee was equipped with the newly developed powered limb and tasked to walk on a treadmill. The special treadmill had force plates embedded in it. Noraxon IMU sensors were used to determine the orientation and anatomical angles of the participant. The results were compared to the normative data.

1.8 Conclusion

The aim of the study and the scope of the work was determined. The elimination of the development of the mechanical structure provided enough time to focus on the development of the control architecture. The objectives developed addressed how the aim was achieved in a more systematic way. The developed research scope was well aligned to the methodology used in the study as each step involved experimental design approach on realising every objective. The justification of the developed control architecture was presented and the major contributions in the field of biomedical engineering were identified as providing intuitive control of the powered prosthetic limbs and improvement of ambulatory-related activities of the amputee.

Chapter 2

Literature review

2.1 Introduction

This section evaluates the concepts of using sEMG signals as control input and other feedback mechanisms for controlling robotic prosthetic limbs. The capabilities and limitations of the use of EMG signals for prosthetic control are well understood in research settings and are now under scrutiny in the context of clinical application [30]. Therefore emphasis is on the theories, principles and philosophies governing the development, modelling, parameter estimation and control of a robotic prosthetic lower limb for clinical applicability. The main thrust of the literature survey is on the applicability of the extracted signal from the muscles using sEMG signal extraction technique and inertial signals on embedded control systems architecture to achieve the intended objective intelligently. Other concepts which will be reviewed include:

- State of the art lower limb prosthetics;
- Recent trends in myoelectric control;
- Electromyography signal acquisition, processing and classification;
- Inertial measurement sensors;
- Control systems architecture design techniques; and
- Pattern recognition and intelligent algorithm techniques.

Often, the study of bionics emphasises implementing a function found in nature, such as detecting human intentions rather than just imitating biological structures; this will formulate the basis for this study. Such technologies are being applied in the field of rehabilitation device manufacturing with an emphasis on achieving a seamless integration with the attached assistive device to the amputee. However, the prevailing challenge is on developing control architectures that can predict human intentions in a dynamic environment and correctly position the prosthetic limb. This has resulted in the need for more robust and intelligent active powered prosthetic limbs.

sEMG interface provides an alternative way of communication that will open up possibilities for comprehensive human and device interaction. The advantages that it offers to the user over existing control methods include subtle and intimate communication, independence of portable control devices, and avoidance of direct eye contact or deep attention by the user. These features

are, however, not yet in existence on any of the commercially available devices [7], [31]. The anticipated challenge in developing sEMG-based prosthetics in the future is to achieve robust classification in long-term use without making the classifier training procedure too cumbersome. While relatively simple classifiers and feature vectors have been sufficient to provide high classification accuracy using simulated signals, the future trend in sEMG studies seems to be towards more complicated control systems as well as utilisation of online training and sensor fusion techniques (i.e. using sEMG with other sensor modalities) that are likely to allow development of more robust and versatile user interfaces [32].

2.2 Commercially available powered prosthetic limbs

The use of pwered prosthetic limbs is relatively new and commercial microprocessor based prosthetic products are still in their infancy. The field of prosthetic control is slowly evolving due to the need to improve the adaptability and robustness of the devices. Much effort is currently being channelled towards reducing power consumption, improving usability, reducing dependence on the user and improving neural interface [33]. Established manufacturers in the field of prosthetic limbs include Otto Bock, Ossur, Touch Bionics, Endolite and Bedford [34].

Otto Bock manufactures microprocessor prosthetic products based on the hydraulic fluid control technology [35]. However, these microprocessor-based power limbs do not use sEMG signals but utilises only the inertial sensors are implemented. The system lacks the achievement of other independent motions that an amputee may be require to do during ambulatory activities. Notable innovations in the field of stuble recovery are inherent in Genium and C-Leg prostheses. Such a technique provide high resistance on the ankle to achieve *stumble recovery* [36]. This technique does not make use of the intuitive control of the limb but is based on prediction control of the preprogrammed individual gait. The Triton Smart Ankle, which utilises the Europa^{TM} technology for the moment and force determination to provide data for ankle adaptation. This improved amputee balance on slopes but had no significant improvements on gait [37].

The LiNX prosthesis was developed by Endolite and utilises an integrated system of microprocessors, sensors and actuators for simultaneous control of the foot and the knee [38]. Other products include the Orion-2 and the Smart-IP [39], these products make use of the microprocessor as a means of improving the system performance. However, they utilise gait estimations to improve stability. Such devices still requires the involvement of the amputee in terms of providing feedback to the system performance [40]. There is a lack of intuitive control from the user when using these microprocessor-based limbs.

As a benchmark to lower limbs, Touch Bionics developed the *i*-limb prosthesis. However, the technology is only applied to upper limbs but can be benchmarked for lower limbs [41]. The *i*-limb utilises surface myoelectric signals to mimic the human hand. It has the capability of achieving most basic motions expected on the hand such as opening, closing and griping [42]. The functionality of the device is based on a feed forward control system, whereby there is no feedback on whether the desired activity has been achieved or not [43]. Rather, the performance of the *i*-limb is highly governed by the triggering technique [44]. The technique monitors the number of impulses required to achieve a certain motion. Every individual is therefore trained on his specific triggering capabilities. Recently, Touch Bionics has improved the accuracy of the *i* -limb by introducing the grip Chips^{TM} technology, which involves placing the Bluetooth based

grip chips onto the object to be gripped or close to it to achieve lateral grip [45]. The technology is based on the need to improve proximity control of the device. Currently, the technology is implemented in the *i*-limb quantum and the *i*-limb revolution.

Bedford developed the BiOM powered anklewhich utilises the V-shaped carbon spring for propulsion, thereby improving propulsion by 50% as compared to standard springs [46]. The device is too expensive and the minimum cost is $ 50 000. Hence, by November 2013, healthcare insurers were not prepared to cover it and considered it to be cosmetic [47]. Yet, the major benefits anticipated from the use of the BiOM include reduced back pain, hip pain and knee pain [48]. In the long term the device has the capability of improving cardiovascular health and those cost associated with such comorbidities.

The aforementioned technologies from the LiNX, *i*-limb, BiOM, C-Leg and Triton Smart Ankle and other technologies all utilised position measurement and force sensors so as to improve the user's gait [44], [33]. The technologies require the amputee to begin the gait and the sensors will monitor the gait and then improve the actuation system as the amputee continuously moves. The greatest set-back of these technologies is that the user has to move for some specified distance [7]. As a result, the technologies are more dependable on long walks and the user has no intuitive control of the device [33].

2.3 The electromyography signal

When a group of specialized cells are capable of performing contraction and relaxation collectively, resulting in motion or providing stabilization and generating heat in the body, they are termed muscles [49]. The depolarisation and repolarisation of the muscle fibre during contraction due to ionic transmission from the axons generates measurable action potentials [50]. Muscle contraction can easily be regarded as the intention of a user to carry out a specific limb movement; however, reflexes do occur and these cause unnecessary control challenges for powered prosthetic limbs. These muscles can be classified as skeletal, smooth and cardiac muscles. It is the skeletal muscles which are attached to the skeleton and facilitate movement and position of the body through the EMG signals [51].

2.4 The deep muscle electromyography signal

The posterior compartment of the leg contains two classes of muscles, namely the superficial and the deep muscles [52]. The superficial muscles are mainly used for the analysis of surface EMG signals and the deep muscles had been analysed for deep muscle EMG and mostly achieved using fine-wire or needles. However, a patented technology developed by Dr. Lester John and colleagues at University of Cape Town allows the non-invassive measurement of deep muscles [53]. A good correlation was found on sEMG for superficial and deep mucles, thus creating avenues for using additional muscles for prosthetic control. However, the technology is yet to be tested on residual stump muscles. The results could be different since the amputation procedure does affect muscle and anatomical orientation during bone bridging. The separation of the deep muscles and the superficial muscles is achieved through the band of fascia. Appropriate placement of surface EMG electrodes could allow the analysis of deep muscles [54]. However, in the case of amputees, the use of deep muscles could present challenges as the amputation technique has

effect on residual muscle orientation. The residual muscles are terminated as flaps and attached to existing tibial bone. Therefore, the use of the deep muscles will not give a true representation of the muscle activity. Furthermore, the level of muscle crosstalk in amputees is very high. The soleus is one of the deep muscles which is difficult to access on amputees [55] while the plantaris a small muscle which is even absent in almost 10% of the people [56]. According to Koshio et al,[57], there is notable interference between deep muscles and superficial muscle EMG signals. It is therefore difficult to use these deep muscle EMG for prosthetic control given that the muscle crosstalk on amputees is further increased [50].

2.5 The fine-wire (needle) electromyography signal acquisition technique

The acquisition of EMG signals could further be achieved using fine-wire EMG (fEMG) techniques. The technique could be implemented for both deep muscles and superficial muscles [58]. Fine-wire EMG technique has the capability of minimising muscle crosstalk and eliminates the movement artefacts. In addition, fEMG allows the analysis of targeted muscle activation performance [59]. However, the technique requires great skill and involves insertion of needles on amputees [60]. Even though the skin impedance challenges could be eliminated, the technique brings about discomfort among the amputees and increases the shunning of powered prosthetic limbs [50]. It should however be noted that the interpretation of sEMG is more difficult than fEMG signals due to the previously mentioned changes in skin impedance, movement artefacts and muscle cross talk when comparing non-amputees [61].

2.6 The surface electromyography signal acquisition technique

The sEMG signal is, however, a superposition of individual motor unit action potentials (MUAPs) within the pick-up range of the surface electrodes [62]. The MUAPs are generated by nerve cells and muscle cells. Their basic source is the cell membrane potential which, under certain conditions, may be excited to generate an action potential. According to [63] and [64], as amplitude and frequency content changes with the contraction-force level, it is possible to associate the muscle contractions of the user to the control of the device concerned. The muscular contraction can be detected and, using surface electrodes, the signal can be acquired and processed for further use with the aid of an embedded electronic circuit [8]. These detectable signal patterns can be used in a myoelectric control system to aid the control of prosthetic devices.

Every signal has its distinct properties; hence these properties are used for pattern recognition and signal detection. The EMG is no exception; with important stochastic data both in the time and frequency domain, these signals present a basis for intelligent control.The electric field generated by the action of many cells constitutes the bio-electric signal [65], as illustrated on Figure 2.1. The MUAP is the generalised muscle action potential which can be detected either by invasive or non-invasive methods. Therefore, the generalised model representation of the EMG signal is represented as:

$$x(n) = \sum_{r=0}^{N-1} h(r)e(n-r) + w(n) \tag{2.1}$$

where $x(n)$ is the modelled EMG signal, $e(n)$ is the point processed which represents the firing impulse, $h(r)$ is the MUAP, $w(n)$ is the zero mean addictive white Gaussian noise and N, is the number of motor unit firings [65].

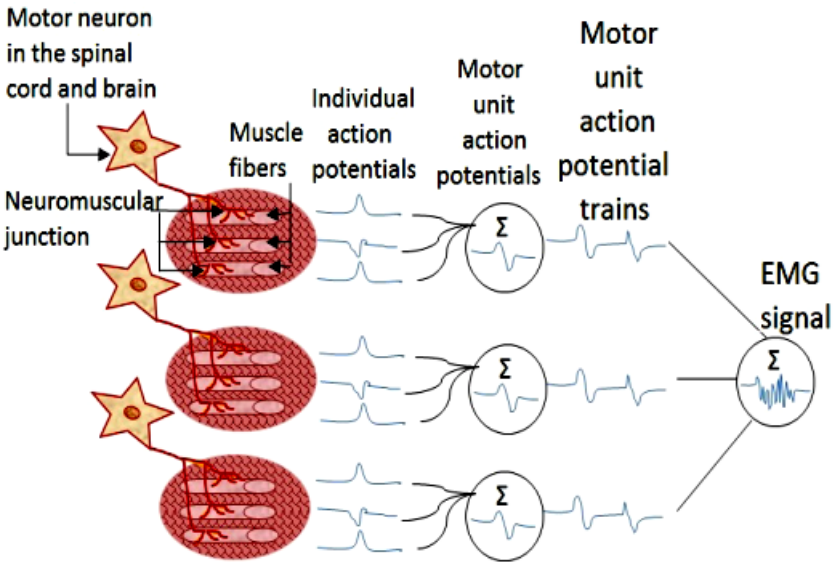

Figure 2.1: Illustration of EMG signal generation

The strength of every biomechatronic design is the synergistic integration of the mechanical, electronic and control systems with the aid of data acquisition and signal processing. However, myoelectric signals are very low amplitude and low frequency electrical signals [66]. The different physiological electrical signals can be classified according to the function of its source, frequency and amplitude range.

The gurus in designing control architectures for powered prosthetic limbs such as [30], [50] and [67] concluded that various approaches have attempted to decompose the multi-muscle synergies into the activity of constituent muscles, but the models are very sensitive to anatomical and electrophysiological factors that may change during use. Achieving simultaneous, independent control using intramuscular EMG is still a challenging task because a stable muscle synergy map must be developed for each user [30]. Quantitative clinical analysis of EMG signals involves the measurement of either the individual MUAPs, which are extracted from an EMG signal recorded during a weak voluntary contraction, or the interference pattern, obtained during a strong voluntary contraction where individual MUAPs become superimposed in the recorded signal and cannot be identified individually [68]. It has been reported that sEMG signals recorded from the amputee muscles after amputation are similar to the sEMG of healthy participants [69]. Therefore, there is still muscle firing when the amputee intends to perform a movement.

The movement and positioning of limbs is controlled by electrical signals travelling back and forth between the muscles and the peripheral and central nervous systems. Until recently, sEMG signals were recorded primarily for exploratory or diagnostic purposes; however, with the advancement of bioelectric technology, sEMG signals have also become a fundamental tool in achieving artificial control of limb movement, for instance, functional electrical stimulation (FES) and rehabilitation. If properly detected, processed and transmitted, the signals in the muscles can

be used to determine the principal movements of the limb. According to [49], there is a need to consider the key problems and corresponding solutions of sEMG signal clarification which consists of recognition rate, algorithm complexity, robustness and real-time characteristics. However, there is no significant difference in classification accuracy as a result of using the intramuscular EMG measurement technique when compared to the sEMG measurement technique [50]. This suggestion increases the relevance of sEMG in clinical application. Furthermore, impressive classification accuracy (97%) of human intended movements could be achieved by optimally selecting only a few channels of sEMG [50]. This provides a potential implementation of sEMG in designing robust control architectures thus promoting wearable rehabilitation designs.

2.7 Factors affecting sEMG signal acquisition

The low amplitude and stochastic nature of sEMG signals brings about complexity in myoelectric based control systems. Transient changes are basic factors that confound the use of sEMG and are a result of short- and long-term variations in the recording environment during use. The inherent noise within the electrical circuits and the general power line frequency (50 Hz in South Africa) result in the need for a more robust signal processing technique [70]. Due to the external interference, electrode impedance changes, electrode shift and lift, and muscle fatigue there is an alteration on the sEMG signal quality and present challenges to clinical robustness [30]. These factors can emanate from physiological and non-physiological factors from during signal acquisition. Therefore, it is recommended that it is important to perform source separation before data recording, processing and analysis with regard to sensor readings [71].

According to Scheme and Englehart [30], the main clinical advantage of sEMG is that it is non-invasive, but its robustness is limited by inherent problems of electrode movement and lift, skin impedance changes over time and motion artefact. An EMG signal may be affected by various factors such as muscle anatomy, muscle physiology, contraction, crosstalk and recording instruments such as electrode types and sites [72]. Physical artefacts had been of great concern in some studies showed promising results after using recessed electrodes [73]. Tam and Webster [74], proposed the more economical way of scratching the skin to minimise skin impedance effect. In general, all the proposed methods were not feasible for wearable devices. The electrode placement procedure has to be simple and user-friendly. As a result, intelligent filtering techniques are relevant for both for firmware and hardware. Encouraging results were obtained by Podrug and Subasi [75] using the wavelet technique as it maintains all the signal features after filtering, although the skin preparation was also intensive. Selecting proper electrode size and achieving proper electrode placement can minimise muscle crosstalk [76].

Unfortunately, due to a number of these factors, sEMG signal is currently of limited use in clinical testing [7]. Although it is challenging and nearly impossible to eliminate the presence of artefacts, there is a need to develop mitigation methods to minimise the effect of these factors that affect the acquisition of the sEMG signal. The use of high pass and low pass filters within the signal acquisition system improves the signal quality, hence the use of a high precision instrument amplifier before band pass filtering guarantees the improvement of the signal-to-noise ratio (SNR). However, the filtering processes also cause an attenuation of the signal properties, such as the amplitude of the MUAPs in time.

The signal measured by surface electrodes is mainly influenced by muscles close to the skin. However, due to electrode placement, there is a high possibility of *crosstalk* between muscles

[19]. Internal measurement techniques allow for a high-quality EMG measurement which is relatively free from crosstalk. Currently, there is no reported clinical use of invasive electrodes for the purpose of prosthetic control. Weir et al. [77] proposed a new implantable myoelectric sensor (IMES) which transmits data through the skin using a wireless link. These IMESs were housed in BION II packaging capsules with a sample rate of 1.2 kHz. It is neither convenient nor practical, though, to use percutaneous wires during chronic use due to the risk of breakage and infection [30]. Generally, the use of invasive electrodes is not recommended due to the discomfort it causes to the user. Podrug and Subasi [75], recommended the use of extensive signal processing techniques both in hardware and software platforms. However, the system proved to be computationally tedious, and the removal of artefacts is only dealt with during final signal processing, thereby presenting opportunities for losing valuable information. In such a system, errors are amplified during the initial signal filtering and amplification stage.

2.8 sEMG signal acquisition technique

Limited information content in the available control signals and a large amount of data required to choose the desired function are the current limitations for accelerated implementation of multi-function myoelectric control systems [78]. Therefore, there is a need to develop a data acquisition system which can preserve the information from the raw signal. This can be achieved by minimising and carefully selecting positions for signal conditioning in the system. Unnecessary filtering, poor selection of cut-off frequencies and poor amplification gains can easily distort the signal quality. Thus the data acquisition module consists of signal detection, filtering, amplification and sampling as sub modules as shown in Figure 2.2. These sub-modules are all integrated in most designs [79]. In some applications, the amplification is applied after filtering while in other designs the filtering is applied after amplification. The argument is that if amplification is applied before filtering then there are higher chances that the noise artefacts will be amplified. Hence, filtering before amplification reduces the presence of noise signal [80].

Figure 2.2: Signal acquisition sub-modules

2.8.1 Surface electrodes

Electrodes form an integral part of the data acquisition module as they are the initial signal detection system. These sensors can be bipolar, monopolar or an array of electrodes. Although the electrode construction is beyond the scope of this study, the literature on its design considerations and interface methods were both evaluated with regard to the signal acquisition circuit requirements. The sEMG electrodes provide a non-invasive technique for measurement and detection of the signal. They form a chemical equilibrium between the detecting surface and the skin of the body through electrolytic conduction so that current can flow into the electrodes

[81]. According to [82] and [81], there are two types of surface electrodes, namely gelled and dry electrodes. For gelled electrodes, a silver-silver chloride ($Ag/AgCl$) layer is the main metallic composite electrolytic while the dry electrodes are simply metallic plates of given diameter.

The $Ag/AgCl$ electrode is very stable electrically; as a result, it makes a small noise [83] which reduces the need for high level filtering techniques. Gelled electrodes are mainly used for clinical application as they require extensive skin preparation and proper gel concentration. Therefore, these electrodes are not suitable for rehabilitation devices, especially wearable devices. For rehabilitation and wearable devices, dry electrodes are used either as bar electrodes or array electrodes. However, these electrodes have decreased efficiency as compared to gelled electrodes and sometimes require a built-in pre-amplifier which in turn increase electrode weight and reduce stability [84]. According to Luca [85], electrodes can further be categorised into passive and active electrodes. Passive electrodes require an external amplification while active electrodes contain a pre-amplification attachment.

2.8.2 Signal detection and amplification

Differential mode and the monopolar mode are the most common detection methods used. However, the differential mode is most popular due to the prevailing use of the bipolar electrodes. The peak-to-peak amplitude voltage has been reported differently, ranging from 0 mV to 10 mV before amplification [49]. The recommended differential amplifier gain used in most lower limb studies was 1000 [31]. However, the amplifier gain used in upper limb studies ranged from 1000-5000 [86], [87]. A general recommendation is that the amplifier gain has to be 60 dB on the logarithmic scale. Although the input impedance and common mode rejection ratio (CMRR) depends highly on the overall instruments used within the system, the amplifier must have a high input impedance and high CMRR so as to maximise its performance. Wojtczak et al. [88] suggested the use high-resolution data on analogue-to-digital systems as a mitigation measure to the use of high gain amplifier and the results were satisfactory although other authors argued that there will be a loss of relevant information due to the early conversion.

2.8.3 Signal sampling

According to the recommended SENIAM standards [72], [84], [89], [90] sEMG signal is usually recorded within the frequency range of 0 Hz to 500 Hz as compared to fine wire EMG with a frequency range of 0 Hz to 1000 Hz. Therefore, there are higher chances of having noise interference for sEMG signals due to its low frequency range. As a result, the recommendable sample rate is between 1000 Hz to 1200 Hz as compared to the 2000 Hz for the fine wire insertion electrodes. Luca [85] also supported the adherence to the Nyquist Theorem as a way of improving signal quality.

Luca [85] suggested that the usable energy of sEMG signals should be limited to a frequency range of 0 Hz to 500 Hz, as a result, the minimum sampling frequency should be set to 1000 Hz. However, a higher sampling rate is preferred to improve both data resolution and accuracy [91]. Contrarily, [92] and [93] reportedly used lower frequencies, resulting in the use of lower sampling rates in an effort to improve the robustness of the systems and the results were not as impressive as those achieved when one adheres to the Nyquist Theorem of doubling the sampling frequency. This is because the power density function of the sEMG signals have negligible contributions outside the high pass filter range of 5 Hz to 10 Hz to low pass filter range of 400 Hz to 450 Hz [89], [94]. Therefore, a 1000 Hz sampling frequency is sufficient to provide a quality signal [95].

2.8.4 Filtering

Filtering is the basis of signal processing, especially for bioelectric signals such as sEMG which has noise inherent in them. According to Li et al. [96], appropriate adjustment of analysis window length, sampling rate, and cut-off frequency in sEMG conditioning and processing would be potentially useful in reducing computational cost and ensuring classification performance. Noise is always part of the detected signal and its continuous presence can result in malfunctioning of the system due to the poorly presented control input signal characteristics [97].

The sources of noise prevailing in sEMG signal are arguably unavoidable, but the noise due to electrode performance can easily be minimised through the use of proper electrodes. As for other types of noise, the use of filers is the only notable option. In fact, the high pass filter usually is within 10 Hz to 15 Hz with a low pass filter of 500 Hz to 600 Hz [89], [94]. Therefore, the pass band of 15 Hz to 500 Hz is mostly used. Considering that artefacts can produce frequencies as high as 30 Hz , it is challenging to work with sEMG due to the high pick up area which presents high potential of crosstalk from adjacent muscles. The high pass filter with a cut-off frequency of less than 15 Hz is used to remove motion artefacts and the inherent instability of the sEMG signals [98]. The presence of spikes in the detected signal results in unwanted frequencies above 500 Hz and they can be removed with the use of a low pass filter with a cut-off frequency of 500 Hz [99].

The presence of noise signal from power line interference, which arises at 50 Hz to 60 Hz [100], requires the use of a notch filter to remove the ambient noise. However, some authors argued that this is not a recommended method as it distorts the signal quality [101] as it is reported that the 50 Hz to 60 Hz frequency range contains valuable information [102]. There are several types of filters that can be implemented in sEMG circuits and these include Butterworth, Chebyshev, Elliptic and Bessel filter [98]. Unfortunately, there is no readily available filter which can approach all the attributes of the ideal filter.

2.9 The state of the art myoelectric control systems

Myoelectric control systems are control systems that utilise the sEMG as the main input signal. This control signal is regarded as the intent signal that emanates from actuation of muscles in human beings. Human locomotion, for instance, requires multi-dimensional coordinated rhythmic patterns that need to be correctly tuned so as to satisfy multiple constraints. This includes the capacity to generate forward motion, with low energy, without falling over, while adapting to possibly complex terrain and while allowing the modulation of speed and direction [103]. This relevance of locomotion both for biology and for robotics has led to multiple interesting interactions between the two fields. These interactions have mainly been in one direction, with robotics taking inspiration from biology in terms of morphologies, modes of locomotion, and control mechanisms [104]. However, for lower limb control, the proximity of the amputation to the knee increases the complexity of the artificial limb systems required to replicate or mimic ankle movement in the sagittal plane.

During the last three decades, researchers have been working effortlessly to optimise myoelectric control systems [105], [106] and successes and failures have been equally reported as early as 1993 [107]. After the discovery of the reliability of myoelectric signal for prosthetic control, efforts shifted to developing a control system architecture that can achieve multiple functions

from a single channel. There have been tremendous efforts by researchers [105], [106], [108], [109], [14] and [29] on the development of control system architectures for artificial limb movements. However, none of them has fully integrated electronics, signal processing and mechanics for clinical applicability of the architectures. Each proposed system had its own challenges,ranging from complex computation, poor reliability, lack of intuitive control and lack of hardware support, resulting in the slow adoption of the technologies for clinical applications.

According to Hudgins et al. [107] many commercially available systems in the 1990s were based on EMG amplitude estimates or rate of change of the EMG. Such systems had a limited number of functions for the intended use. Simultaneous control of different devices using the same EMG signal apparently became difficult. Since these systems are amplitude dependent, they were not recommended for high level amputees with weak EMG signal amplitude. State control has been deemed a failure for multifunction prostheses [110]. As a result, [107] proposed an artificial neural network pattern recognition system. This was necessitated by the fact that an EMG is one-dimensional and methods for pattern recognition may be applicable. Hudgins' suggested system was based on the fact that [107] given an electrode site the signal features are reproducible for a given movement. The proposed system was successful on classifying four classes of contraction types of the upper arm at an accuracy of 91.2% for non-amputees and 85.5% for amputees. The results were convincing but not clinically viable, however this formed the basis of most 20^{th} Century control architectures. A follow up to this suggestion was attempted a decade later in the 21^{st} Century and the results remain not clinically viable [20]. The shortcomings of the proposed system was s lack of an integrated electromechanical system. As a result, the proposed decision system was not coupled to any electromechanical system and controllability was not evaluated through functionality.

Nishikawa et al. [108] proposed a controller that utilises a real time learning algorithm. The controller learns an operator's characteristics and generates control signals from the EMG signals simultaneously. The controller consists of the analysis unit, the adaptation unit and the trainer unit so as to achieve real time learning. The strength of the design was on the analysis unit which was able to produce invariability of feature vectors in the same motions, thus shortening the learning steps, which is an important characteristic in real-time learning. However, level of performance of the device differed from one participant to another. The performance of the device was also related to the quality of the training data as other units of the architecture highly depended on the first unit. The group further proposed the need for better learning algorithms and interface technologies as this contributed to the short fall on the device's overall performance. The major short comings of this research were the limited number of motions for the limb and poor learning rate of 507.1 to 1294 Hz , the experiment produced 91.5% accuracy. Such extended processing times caused the system to be deemed as undesirable for prosthetic control since the recommendable time is should be below 300 ms. With regard to classification, the device performed well but was based on a virtual system. Therefore the functionality of the proposed system could not be validated for robustness and adaptability which are relevant for clinical applicability.

Ajiboye and Weir [109] proposed a heuristic fuzzy logic approach to multiple EMG pattern recognition for multifunctional prosthetic control. The developed system was transparent to, and easily âĂIJtweakedâĂİ by, the amputee. The main goal was to improve the update rate for real-time control. The most notable weakness of the proposed design was on its inability to adjust control parameters with relation to changes in participant's condition, such as increase in

weight, which will in turn affect changes in torque demands within the joints. The investigation was based on the classification of signals as it ignored the interface with the mechanical structure; hence a good synergy is required between the control algorithm and the mechanical actuation system which will be responsible for joint configuration. The most notable achievement was the ability of the system to allow for seamless control of multiple degrees-of-freedom in a multifunctional prosthesis; however the system did not address issues regarding robustness or adaptive control resulting in poor reliability. The fact that this design was based on trial-and-error learning made it undependable as the fuzzy rules are based on probability rules and not well known distinct parameter functions. The rules of combining membership functions used were known as the minmax rule for conjunctive (AND) and disjunctive (OR) reasoning. These rules are not robust as they are based only on predictions and not trained data [111].

Li [112] suggested an electromyography pattern recognition based control of powered multifunctional upper limb prostheses. The results obtained revealed that once a pattern has been classified, a command is sent to a prosthesis controller to implement the movement. With this new control method, the user elicits the contraction corresponding to the degrees of freedom (DOF) that they want to control, and the classifier chooses the appropriate class of motion. The system was based on an offline parameter estimation and a general switching based adaptive control system. As a result, the user has intuitive control of each function, as the intended movement matches the prosthesis function. However, the switching system generates bad transients with adverse effects on system performance. These bad transients ultimately increase controller bandwidth and lead to system instability in the presence of high frequency unmodeled dynamics. Although the system was able to use pattern recognition as a tool for determining the partcicipant's intended action, it lacks the ability to predict the movements in case where the pattern is not clear due to poor signal acquisition and processing. Again there is an issue of conflicting rules during classification of patterns resulting in poor response of the control architecture [113]. Hence for the lower limb, EMG signals are stochastic and the presence of load increases torque demands on the ankle actuator resulting in increased complexity.

Hargrove et al. [29] proposed a noble system that was based on the use of electromyography (EMG) signals from natively innervated and surgically re-innervated residual thigh muscles in a patient who had undergone knee amputation. The system was based on offline training data for specific human tasks such as sitting, standing and walking on stairs. The greatest set-back of the proposed system was on the process of redirecting the nerves to a certain area [114]. This surgical procedure requires great skill; it is tedious and not clinically viable for an off-the-shelf product. The system was based on targeted muscle reinnervation (TMR) surgery, making the design expensive, and reliability of the control signal largely depends on the success of the surgical procedure. Such a control system would take time to implement and if the TMR is not performed during amputation then the patient has to undergo two successive amputation procedures [115]

To a greater extent, the aforementioned technologies [29], [108], [109], [112],[114] and [115] all exhibit the technology readiness levels from conceptual design and mathematical models to demonstrated prototypes in active robotics. However, functionality is still a cause for concern as all of the suggested control architectures were either based on virtual systems or offline data and were simply too complex for the available hardware. Although there is evidence of incremental innovation among all the designs mentioned above, they were not clinically viable as some require surgical procedures for implementation. In robotic prosthesis, the major difference is on actuation. With active prosthetic joints the prosthesis is considered as an independent machine

designed to fulfil an objective related to position [116]. The sugestions considered by [116] and [117] were arguably incorrect as this will cause the amputee to consider the active limb as a lifeless mechanical structure attached to the human body. Furthermore, such suggestions will result in the development of prosthetic limbs that do not address the need for intuitive neural interface with the amputee. Designs based on such notions increase the physical role of the amputee on the functioning of the limb, resulting in increased energy expenditure and ultimate rejection by the participant. It can be concluded that for the system to correctly detect amputee's intended movement it has to utilise pattern recognition based control systems, learning algorithms and adaptive control strategies.

2.10 Machine learning

Nowadays, the term *machine learning* gathers together a set of methods that can automatically detect patterns in data, and then use the uncovered patterns to predict future data, or to perform other kinds of decision making under uncertainty [118]. Controlling the mobility of the human body with the aid of artificial limbs is a complex goal as the parameters to be controlled changes very often. These parameters include variable body weight, unpredictable height gain, change in body structure and reflex action based movements. Determination of Cartesian space and joint space in powered prosthetic limbs is of great importance and there is a need to improve the stability of the mechanism. Non-intuitive control is one of the few reasons amputees have lost intrest on the use of their prostheses [30]. Switched or gated control is considered to be slow and non-intuitive, requiring both time and sustained cognitive effort on the part of the user [119]. Challenges and limitations of conventional or traditional control methods have motivated researchers to think in other terms, including the implementation of intelligent systems.

Extensive work done so far demonstrated that an adaptive neural control scheme is particularly suitable for controlling highly uncertain, nonlinear, and complex systems [120]. The control scheme can learn the full dynamics of a non-holonic system on-line, and can deal with parametric as well as non-parametric uncertainties, yet guarantees tracking errors asymptotically converge to zero [121]. Miao et al. [122] developed a recurrent neural network control system without requiring explicit knowledge of the system dynamics and the results were convincing for adaptive control for lower limb control.

Furthermore, [123] suggested that predictions are a key component of intelligence and necessary for accurate motor control. In reinforcement learning, such predictions can be made through general value functions (GVFs). These are temporally extended predictions about a signal of interest that have been applied to building up real-time anticipatory knowledge in relation to human-machine interactions. Their main contribution was on improving robotic artificial limb performance through real-time learning and utilisation of temporally extended predictions. This was achieved through the use of multilayer predictions, that is, predictions based on predictions using simulations.

According to Degris et al. [124] reinforcement learning methods are often considered as a potential solution to enable a machine to adapt to changes in real time to an unpredictable environment. When developing a control architecture, one can choose to have hierarchies based on tasks, for example sitting, standing and walking. If well-structured, an off-line learning algorithm can be developed so as to switch between a specific set of decisions depending on the hierarchy being executed. A novel idea was proposed by [125] regarding 3D model retrieval and

classification by semi-supervised learning with content-based similarity. Using this technique, status of terrains can be identified and classified and a set of decisions can easily be activated. However, such a system has limitations when applied to sEMG signals.

The most common machine intelligence feature used in active limbs is Artificial Neural Networks (ANN). According to Elsafi [126] ANN retains two characteristics of the brain as primary features: the ability to *learn* and to *generalize* from limited information. The approximation between the field of ANNs and probability theory has led to a new domain called Statistical Machine Learning (SML) [127]. It is clear from these previous applications of Feed Forward Artificial Neural Networks (FFANN) that once the network is trained using input−output examples, it learns and generalises the input−output relation. As a result, it serves as a surrogate model to prevent repetition of time-consuming calculations. A trained neural network can make a real-time prediction of output for a new set of inputs or a real-time classification of a new input pattern [128].

Learning is undoubtedly one of the most relevant contributions of ANNs to the sphere of information processing systems. Three basic classes of learning can be considered as supervised, unsupervised and reinforcement and they allow for [129]:

- Implementing a process with no need to know the mechanism model that lies beneath.
- Using the same model to deal with different tasks.
- Adapting the system to changes in the surrounding environment.

The basic tasks that can be performed through a learning process are [130]:

- Pattern association.
- Pattern recognition.
- Function approximation, including system identification, parameter estimation and inverse modelling.
- Computation of the suitable parameters of a control system.

Morita et al. [131] managed to achieve torque control of each joint in the upper limb. The joint torque was estimated from many EMG signals using an artificial neural network, hence the learning system was based on the feedback error schema. Apart from being off-line learning, all these systems learn from a policy already well known to the problem using pattern generator type policies. However, there is a need to develop a new prediction method to overcome the problems of the training process in artificial neural networks. Therefore, the requirements to develop models customised for several applications still exist regardless of the fact that the architecture of the ANN is universal.

The applicability of machine learning in rehabilitation systems is highly limited by hardware availability and the need for miniaturisation of the available technology [7]. Most of the aforementioned techniques were applied on offline systems using the Matlab software platform and large working stations. However, for clinical viability and wearable device technology size, power consumption and weight of hardware do matter most. In this study, machine learning will be used for pattern recognition in EMG signal classification. Signal classification, if well utilised, will assist in correctly predicting the partcipant's intentions in real-time, thereby improving active limb's adaptability and robustness [132].

2.11 Inertial measurement system

According to [133], physical activity is any bodily movement. As a result, these activities can easily be detected and quantified to determine the rate of locomotion or the extend of movement of the user. Accelerometers and gyroscopes have been widely used as inertial measurement units during gait analysis [134]. In some cases, these sensors are used to determine both anatomical and orientation angles of the participant during gait analysis [135]. The sensor placement procedure and the calibration of these sensors have been regarded as complex and tedious. This is mainly because the human body is not flat, neither is it uniform nor similar from one individual to another. Therefore, results can either be reported for static or dynamic experiments. When these sensors are used for clinical diagnosis, it is advisable to report the timing accuracy of the classifications instead of the accuracy on event counts [136]. Although these sensors had been used within a system, it is possible to measure the behavior or the orientation of a single limb in space [137] using the individual sensor technique.

The introduction of an orientation measurement system in myoelectric control systems enables the use of control interlocks within the control architecture. The position of the thigh and the shank is known to vary with the stage within the gait cycle [138]. Therefore, individual sections of the limb could be monitored independently. It is then prudent to use the individual sensor outputs to determine the position of the limb. The output from such sensors could also be used as feedback systems to provide a complete closed loop control system. This will, in turn, allow for adaptive control resulting in a more robust control architecture.

The main characteristic of a control system designed for prosthetic applications is to achieve the desired trajectory with minimum to no errors. As a result, the determination of kinematic models of the lower limb is a prerequisite for proper motion planning. Computations of the position and orientation are based on the joint position and kinematics of the limb, hence these transformations require actuator space, joint space and Cartesian space [139]. The success of lower limb rehabilitation designs are constrained by foot-ankle motion, degrees of freedom and forces determined by computational models. However, a combination of reliable measurements and mathematical modelling techniques has proved to be a powerful tool for investigating the complicated behaviour of human joints for the past three decades [139], [140], [141] Any model of a joint, often inspired by engineering, is related to an idea of a mechanical analogy (hinge joint, ball-and-socket joint, universal joint) that behaves in a similar manner as a biological joint [142]. The kinematics model represents the motion of the prosthetic limb without considering the forces that cause the motion. The dynamic model establishes the relationships between the motion and the forces involved, taking into account the masses and moments of inertia, for instance, the dynamic model considers the masses and inertias involved and relates the forces with the observed motion, or instead calculates the forces necessary to produce the required motion [139].

Su et al. [143], clearly outlined that the validation of the two or four segment models proposed by [144], [145] and [146] have not yet been done regarding repeatability and reliability. Therefore, the applicability of such models is still questionable during the design of rehabilitation devices of the lower limb. According to [143], a three-dimensional motion analysis of the foot and ankle is more relevant.

A prosthetic foot is a key element of the lower limb prosthetic leg, literally forming the basis

for a stable and efficient amputee gait [147]. Motion at the ankle joint is usually divided into that at the ankle and at the subtalar joints [148]. Tulchin et al. [149] argued that the previous work done by [150] and [151] of modelling a foot as a single rigid body was not adequate since the detailed motion between individual joints within the foot cannot be appreciated. The group went on to propose a multi-segmented foot model which comprises of a two joint model of hind-foot and fore-foot motion. This model was successful in determining the foot kinematics during high speeds. However, these early foot and ankle models all lacked the consideration of the internal foot movements [148].

According to [152], the mean overall rotation is much higher at the ankle 63^0 than at subtalar joint (4^0) regarding the flexion on maximal dorsi- to maximal plantar-flexion. Lundgren et al. [153] also reported that during the stance phase of walking, the joint rotations in the three anatomical planes were found to be on a range of about 8^0 to 15^0 at the ankle joint, and about 7^0 to 10^0 at the subtalar joint. Thus, human motor control has always acted as an inspiration in both robotic manipulator design and control. The development of a human lower limb robotic prosthesis is highly motivated by the human foot ankle mechanics, its dexterity, and its vast repertoire of motion. Figure 2.3 shows the terminology for indicating the spatial location, relative position and motion of bones and tissues in the foot, illustrated for a right foot, displayed from the front. The the planes are indicated with bold font, axes names are underlined, directions are indicated with italic font and motions are in capital font [154].

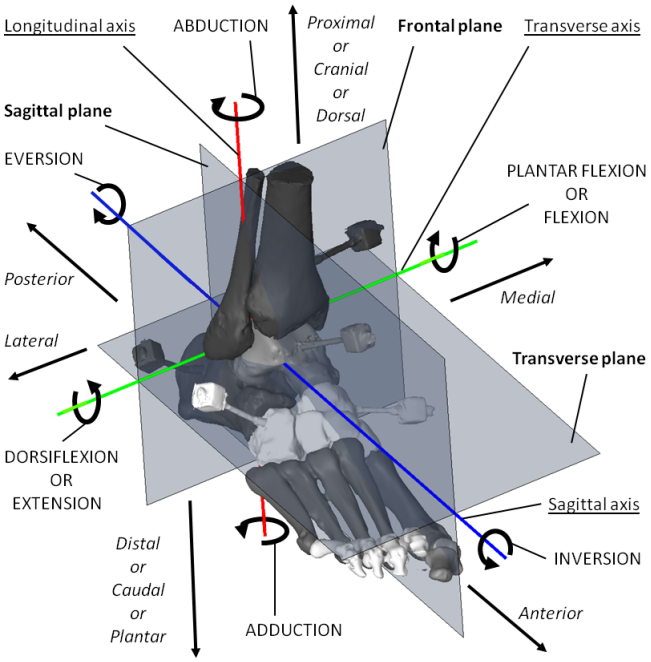

Figure 2.3: The human foot and ankle

An understanding of the mathematical model of the human ankle is of paramount importance in developing a control and electro-mechanical system of the robotic prosthesis. The human shank and foot complex is an intricate, multi-joint mechanism, which is fundamental for the interaction between the lower limb and ground during locomotion [149]. At the same time, the ankle has a very complicated anatomical system. As a result, the large amount of literature on

experimental and modelling studies has not fully described the coupled joint motion, position and orientation of the joint axis of rotation, stress and strain in the ligaments. Even the ankle's role on guiding and stabilising joint motion, conformity and congruency of the articular surfaces, patterns of contact at the articular surfaces, patterns of rolling and sliding at the joint surfaces, and muscle lever arm lengths are yet to be fully exploited [147].

Moreover, most models [155], [156], [157] considered for computational model analysis were based on the hinge joint. The suitability of the hinge joint assumption is supported by early studies [158], [159], [160] which show only one or two rotation axes, but other studies have shown that this may not be true [161], [162], [163]. The much appreciated kinetic profiles in use were achieved by [157] considering the talocrural and talocalcaneal joint rotations as hinge joints acting as a single monocentric one degree of freedom joint [164].

2.12 Robust and adaptive control in assistive devices

The need for intuitive control has necessitated the development of robust control architectures with embedded adaptive capabilities. The majority of commercial prosthetic designs available still require the user to contribute immensely to the device functionality [7]. According to Weir [165] there exists a technological gap with regard to robust simultaneous control schemes between research and commercial applications. This may be in the form of the user initially being required to perform or mimic normal gait for a few strides before the control system detects the intended movements. Thus, robust control refers to the control of unknown systems with unknown dynamics subject to unknown disturbances [166]. Taking into consideration the unpredictable changes in human skeletal structure and body weight, there is a need for robust prosthetic limbs.

The human body is a nonlinear system with unpredictable dynamics. Most electromechanical systems which are interfaced with the human body for rehabilitation purposes require adaptability characteristics so as to achieve optimum performance. If an assistive device is to fail, then it has to fail gracefully. This implies that the control system should not exhibit complete failure in the presence of a fault [167]. Changes in body weight, swelling of the amputated site, noise in the myoelectric signal and changes in body height may cause unexpected failures within the control system. Body weight dynamics affect limb kinematics and torque demands. According to [168], reliability of a system is a measure of the success with which it conforms to some authoritative specification of its behavior. Hence, swelling of the amputated site reduces the amplitude and frequency of the control signal, as a result, this affects the device's reliability. Chandrasekharan [166] argued that the techniques for robust control have been criticised for their accessibility to the practising engineer, the tediousness of the methods, the general application to normal systems and the conservatism that they often present. The achievement of a robust control system largely depends on how the robust performance requirements were defined [28]. Therefore, there is a need to determine the relevant adaptive law for the proposed system.

There have been tremendous efforts on the implementation of robust control in myoelectric based prosthetic limbs [107], [169], [170], [171], [172], [173], [174], [175], [176]. Adaptation and robustness have been introduced at different levels of control. Hudgins et al. [107] improved the feature extraction technique within a pattern recognition system so as to improve classification accuracy. This resulted in improved robustness of the design. However, the system was not able to adapt to sudden changes in signal parameters, such variable frequency and amplitude. Rifay

et al. [175] suggested the use of augment-1 adaptive control. However, even when this was augmented by a non-linear proportional control algorithm the system did not achieve clinically viable results on tracking the trajectory even in the presence of a filter in the design. Furthermore, [165], proposed the improvement of the classifier to reduce the decision making time. In this regard, the proposed system was able to achieve reduction in processing time. However, the issues concerning adaptation were not clearly highlighted as only the improvement of the classifier was suggested as the improvement of system adaptability. Proportional gain control has been utilised mostly for actuator control. Therefore, the implementation of adaptive gain for the control of myoelectric exoskeletons aims to reduce metabolic energy expenditure [177] as some sections of the body will stop compensating by having excessive anatomical angles during gait. However, the proposed system could not take into consideration variations in the control signal parameters.

The previously mentioned designs and suggestions in the field of robust and adaptation control of powered limbs did not address the problem of intuitive control holistically. Some studies focused only on the classifier accuracy, others on the feature extractor optimisation and the bulk of the studies focused on improving control signal quality. The suggestions lacked hardware support and also focused on advanced control theory with no practical backing. Therefore, Weir's [165] suggestions concerning the need to design with the intention to bridge the gap between research and commercial products remains justified. These suggestions included the implimentation of systems such as Model Predictive Control (MPC), Stochastic Control (CS), Model Reference Adaptive Control (MRAC), Polynomial Control Systems (PCS) and Adaptive lambda-tracking as a way of improving performance of the control architecture. According to Sanz et al. [178] adaptive control is different from robust control in that it does not need a priori information about the bounds on these uncertain or time-varying parameters; robust control guarantees that if the changes are within given bounds the control law need not be changed, while adaptive control is concerned with control law changing themselves during execution of the control objective. As a result, there is a need to develop a control system architecture with both adaptability and robustness so as to achieve the desired objective of intelligent active prosthetic limbs.

2.13 Conclusion

There is an overwhelming amount of literature regarding the development of myoelectric control architectures. However, most studies focused on evaluating the classification accuracy rather than the ultimate functionality of the architecture, thereby creating the gap between technology relevance and clinical applicability of the proposed designs. Some of the previously mentioned studies focused on extracting the signal for analysis, resulting in the development of several analogue front-ends. Hence the conditioning of the signal for control systems was overlooked. Suggested myoelectric control systems developed were validated based on their classification capabilities with limited literature and results presented on their functionality on actual powered prosthetic limbs. However, these results provided an insight into which techniques could easily be optimised for better control system performance.

In some instances, success was based on simulated signals in platforms such as Matlab and Labview. As a result, the proposed classifiers could not perform as expected when tested on raw EMG signals due to the noise inherent in the signal which was overlooked during simulations. During simulations, noise was modelled as simple white Gausian noise but in reality the noise inherent in the signal varies with the type of source. There seems to be a lack of commendable

resolutions with regard to the filtering techniques and cut-off frequencies. Most studies developed their protocols based on the SENIAM and ISEK standards. Therefore, high pass filtering and low pass filtering were dominant in most of the aforementioned studies. Hence, notch filtering as a way of removing the 50 Hz power line interference was strongly discouraged in all studies. However, the justification was based on the use of the signal for diagnostic purposes. As a result, there is need to evaluate the significance of such a recommendation when using the signal for control purposes.

There is less literature reported regarding the evaluation of powered commercial prosthetic limbs. Therefore, the derivation of design parameters from the literature was difficult. In most studies the information regarding the applicability of myoelectric control systems on amputees was rather hypothesised based on signals form non-amputees. This led to growing concerns with regard to validity of the signal parameters presented in the literature concerning frequency bandwidth, amplitude and power. Therefore, there is a need to determine the signal parameters on the residual limb of the amputee so as to check for the feasibility of the proposed design. There seems to be consensus on types of signal features used to develop a feature set. However, the recommended feature set size is unknown. As a result, the general rule of thumb used on these studies was such that the feature set should be large enough to provide good classification accuracy without increasing computational complexity of the system. The 350 ms processing time was reported on several studies within the literature, hence the time was only determined during classification and overlooked the controller and actuator time delays.

The technological gaps that existed in the previous studies could only be eliminated if the relevance of the proposed technologies is validated based on the functionality of the powered ankles and not on the performance of the classifiers only. Recommendations concerning the signal processing for control purposes should be clearly stated and differentiated from recommendations for diagnosis. Therefore, there is a need to develop a control system architecture that could provide the platform for the applicability of machine learning in a real time environment.

The systematic review of all elements that are applicable for the construction of an intelligent and robust myoelectric architecture revealed that there is still a technological gap between scientific findings and clinical relevance. The majority of the technology frontiers aforementioned lacked hardware support for implementation within wearable devices. The success rate of most of the suggested pattern recognition systems was highly influenced by pre-processing techniques used and noise reduction techniques used for the control signal. The majority of the studies were based on offline data as real-time online algorithms presented challenges with respect to the unpredictability of incoming data quality.

Chapter 3

Research methodology

3.1 Introduction

A pragmatic methodology was employed in this study to determine the design parameters and the realisation of the development of an intelligent and robust myoelectric control architecture. This approach was chosen based on the literature survey which indicated conflicting paradigms on how the development of prosthetic devices should be carried out [179]. Even though the SENIAM and ISEK standards [180] are regarded as standards for recording and reporting EMG based studies, they were found to be insufficient when applied to amputees [132]. As a result, the majority of data presented in this study was based on experiments carried out using modified standards to achieve the required design parameters.

3.2 Research design

The engineering design method implemented in this study was based on the *VDI 2221: Systematic approach to the design of technical systems*, a method developed by the German Association of Engineers [181]. This method enabled the evaluation of results at each stage and presented the opportunity to work iteratively on all stages of the design process [182], [183]. The main reason for implementing the VDI 2221 approach was to develop the control architecture, not as a theoretical framework but as a consideration of the issues regarding clinical applicability. The complimentary phase model methodology that was also used and that works well with the VDI 2221 was the Parl and Beitz model [184].

Section 1.7 explained the standards which were adhered to during product design whereas this section is highlighting the standards which were adhered to during clinical experiments, type of experiments, experimental set-ups and the signal processing employed. The study was highly diversified covering the fields of biomechanics, mechanics, artificial intelligence, control theory and electronics. As a result, the methodology was presented such that the technique and methods used per each engineering field was clearly indicated. This section is an expansion to the research scope presented earlier in section 1.7 concerning an overview on how the study was carried out.

The main thrust of the study was to initially qualitatively determine the actual challenges being experienced by the amputees. Then, a quantitative analysis was carried out on the effects of the current non-powered lower limb prosthetics being used with the aid commercial testing

equipment. The results recorded enabled the justification of the need of the powered lower limbs. An experimental analysis was then carried out on the feasibility of the amputated residual limb to check if it can provide EMG signals through surface electrodes, sufficient enough to control a powered limb. The results were then used as design specifications for the control architecture as they highlighted the signal features and quality. A control architecture was then developed along with the relevant sensor fusion and actuator interface technologies. The developed control architecture was coupled to a mechanical limb to come up with a biomechatronic powered ankle. The performance of the new design was evaluated based on the normative data within the commercial gait $MR3$ system. Optimisation algorithms were then developed and implemented to improve adaptability, robustness and intelligence of the biomechatronic powered ankle.

The experimental design approach used in this study enabled comparison of alternatives, identification of significant inputs that is separating the vital few from the trivial many, facilitated variability reduction, robustness design and also balancing trade-offs. As a result, the methodology enabled collection of information effectively and in a reproducible manner.

3.3 Standards

The research involved experimenting with human beings and as a result, an Ethical Clearance (S16/05/093) for human testing was approved by the Health Research Ethics Committee, Stellenbosch University (see Appendix A). Recording and reporting of the EMG data was based on the SENIAM and ISEK standards [180], [185] and there was strict adherence to the ISEK and SENIAM standards during recording and post-processing of the signals extracted from the non-amputated leg. However, amendments were made to the SENIAM standards during the recording of the signals from an amputated leg since some of the anatomical landmarks mentioned in the standards were now missing on the residual stump. Furthermore, other standards adhered to during the study were:

- National Core Standards for Health Establishments in South Africa.
- National rehabilitation policy, rehabilitation for all of 2000.
- The Occupational Health and Safety Act 85 of 1993.
- The Health Professions Act 56 of 1974.
- WMA Declaration of Helsinki - Ethical Principles for Medical Research Involving Human Subjects.
- National Health Act. No. 61.2003 (NHA) and regulations relating to research involving human participants.
- National Health Research Ethics Council (NHREC).
- Promotion of Access to Information Act 2 of 2000 (PAIA).
- Protection of Personal Information Act (POPI).
- Health Research Ethics (HREC) Standard Operating Procedures (SOP), 2^{nd} Edition, Stellenbosch University.

3.4 Recruitment of participants

The amputees were recruited as recommended by the Amputee Clinic under the guidance of Jayson Chin and Associates, Cape Town, South Africa. The study was conducted under the approved research protocol (S16/05/093). The experimental protocol was explained both orally and in writing to all participants before written consent was obtained. The study consisted of two, unilaterall mal amputees (left leg amputated), with participant 1 weighing 81 Kg, with a height of 1.75 m and aged 43. The second participant weighed 79 Kg with a height of 1.73 m and aged 46. Both participants had received osteomyoplastic transtibial amputation surgery. The stump length for participant 1 was 15 cm and that of participant 2 was 17 cm and the residual stumps were 33.7% and 36% of the length of sound limb respectively when measured from the knee towards the ankle. According to Isakov et al. [186] there is no significant difference between signal parameters among amputees who have received similar amputation. The initial test results (pilot test) also reported similar findings [132]. The main reason for having a small sample size was that it has been justified that the nature of sEMG signals in healthy participants are similar concerning signal features such as amplitude and frequency. Also, the availability of amputees who had received similar amputation on the same leg, within same year and being of closely similar weight contributed to the reduced sample size. As a result, our sample size was reduced to two amputees. Such small sample sizes are common in EMG based studies [187].

To work only with amputees with sEMG signals that are recommendable for myoelectric control systems, the exclusion criteria included myopathy patients, in other words participants with low sEMG signal amplitude. The myopathies are neuromuscular disorders in which the primary symptom is muscle weakness due to dysfunction of muscle fibre [188]. Other symptoms of myopathy can include muscle cramps, stiffness, and spasm [189]. Also to be excluded were the neuropathy patients. Neuropathy refers to the conditions that result when nerves that carry messages to and from the brain are damaged or diseased. This exercise was carried out at Jayson Chin and Associates Amputee Clinic in Cape Town. Only the individuals who passed the inclusion criteria were presented for further trials. Both the amputees signed the consent form in order to be included in the study. This was followed by a safety induction with regard to the nature of activities to be carried out.

The participants had reported no history of diagnosed musculoskeletal and neurological pathology. They had also reported independent ambulatory with medium to high daily activities. The participants have been using a passive limb for the past two years. The criteria for inclusion was based on the independence of community ambulatory living with an assistive device. This eliminated the need to train the participants on how to use the limb before the experiments. Also considered was the need for participants with a comfortable surface bearing socket and no medical history related to limb injuries or comorbidities that could affect gait, joint angles or sEMG signals.

3.4.1 Population size

The sample size was limited to two subjects mainly because the initial pilot experiments evaluation showed no significance difference between subjects with respect to distance variables. These experiments were carried out with our own non-commercial equipment. The commercial laboratories (Human Motion Analysis Unit, Central Facility, South Africa) we were using were charging an hourly rate. As a result, the decision was made to use two subjects as a cost effective measure. Furthermore, several experiments were then carried out on the two amputees in order

to provide reliable information and large data sets to work on. The use commercial laboratory was to improve on quality of results in order to meet international standards with regards to equipment and quality of work. This in turn assisted on providing validated data. The use of equipment designed at the University will limit the authenticity of the data as they were not commercially approved instruments and equipment. Another driving factor for using a small sample that the large sample initially assembled were amputees of different age groups with different amputee types and different level of amputation. However, we chose these two subjects because they received the same amputation surgery and the level of amputation was almost the same and they are of the same age group (Middle aged men). They were also amputated on the left leg during the same year and the amputation surgeries were simply 21 days apart. Therefore, this was a good sample to use.

3.5 Procedure

Although the SENIAM and ISEK standards were very detailed and helpful, they lacked proper guidance for the users as they failed to provide choices one could use when working with EMG signals. Therefore the procedure used in this study was highly motivated by the guide provided by [190] with regard to using and interpreting of kinesiologic electromyographic data. Their suggestions and the proposed guide were useful from planning experiments to methods and techniques for reporting the data. The procedure involved in the study included:

- Developing of research protocol S16/05/093.
- Submitting and amending the research protocol S16/05/093 for approval by the Ethical Committee.
- Recruiting of participants with similar amputation and on the same side of the leg.
- Attaining the written and oral consent from the participants.
- Screening the participants by eliminating myopathy and neuropathy participants at the Amputee Clinic in Cape Town.
- Carrying out a short training course on using the equipment and apparatus at the laboratory.
- Carrying out a small pilot study to validate the developed protocol and type of activities.
- Developing a multi-channel hybrid data acquisition.
- *Experiment 1*: Investigating the nature of available sEMG signals on the residual amputated limb.
- *Experiment 2*: Analysing amputee normal gait cycle.
- *Experiment 3*: Determining of anatomical and orientation angles of the participants.
- *Experiment 4*: Determining the applicability of inertial sensors for myoelectric control architectures.
- Designing pattern recognition system for robust myoelectric control.

- *Experiment 5*: Testing an integrated sensor system which included the inertial measurement units (IMU), EMG sensors and force resistive sensors on a pattern recognition control architecture.
- Validating of the developed pattern recognition control system architecture based on classification accuracy on test data.
- Validating of the developed concept using gait analysis at the Neuromechanics Unit.

All of the above steps addressed the goal of developing a robust autonomous myoelectric control architecture.

3.6 Data acquisition and experimental set-up

The apparatus and data acquisition tools used in this study differed concerning the objective being carried out. The main experiments included EMG acquisition using surface electrodes, normal gait analysis using cameras and reflective markers, orientation and anatomical angles analysis using IMU sensors and signal analysis. However, a generalised description of the equipment is presented in this section. Detailed descriptions are given in the next sections. The experiments were carried out at the Human Motion Analysis Unit, Central Analytical Facilities, Stellenbosch University, South Africa. Validation tests were carried out at Neuromechanics Unit, Stellenbosch.

The raw signals sEMG were acquired using the Noraxon active electrode system, which has an onsite amplifier. The system has a 10 GΩ impedance with a common mode rejection ratio of 115 dB at 50 Hz. The signals were sampled at 1500 Hz as required by the SENIAM and ISEK standards. The measurement function accuracy (MFA) of the sensors was $\pm 2\,\mu V_{RMS}$. The baseline noise was less than $1\,\mu V_{RMS}$. The electronic gain was set at 200 with an overall gain of 500. The 50 Hz notch filter was not applied during data acquisition. Wireless communication was used between the electrodes and the data acquisition unit to minimise cable movement artefact.

The experimental protocol involved the acquisition of maximum voluntary contraction (MVC) level from the participants by holding a movement contraction for at least 5 s, since the recommended processing time for the targeted processor is 300 ms. As a result, the 5 s duration provided enough data without the participants experiencing fatigue. The participants were tasked to perform five motions of dorsiflexion and plantarflexion movements with a resting pause in-between (dorsiflexion-rest-plantarflexion). The second set of five motions included performing dorsiflexion and plantarflexion continuously without a resting pause (dorsiflexion-plantarflexion). All these initial experiments were conducted while the participants were seated. Another set of data was carried out when the participants were walking along a 10 m walking envelope. The reason for removing the resting pause in the second set of data was to facilitate an evaluation to determine whether there is muscle crosstalk and also testing the ability of the developed system to classify the movements in the event of fast reactions. The signals were recorded using the Noraxon MyoMotion System, also known as MyoResearch3 (MR3), USA. Ten data sets were collected for each motion on normal gait activity. The activities were carried out during design parameter considerations and in evaluating the performance of the developed design. The raw data sets were stored for further processing. The post-processing of the signals was done using MR3 Noraxon MyoMotion System. In the MR3 platform, filtering using digital filters was implemented. The results were exported to Matlab 2017a for further analysis.

The signal analysis was carried out based on the method proposed by [72] and [180] and supported by [98]. However, much guidance for signal processing was based on ISEK standards since it is more focused on sEMG signals. The raw signal was filtered using a finite impulse response band pass Butterworth filter between 15 to 50 Hz with the aid of a Hamming window which allows for 50% overlap. A 60 db/oct was utilised as a method of minimising overshoot reduction of settling time. Further amplification was achieved with a 60 dB gain. The removal of the 50 Hz interference from the power line was achieved using a bidirectional infinite impulse response filter during post-processing in MR3 software. Rectification was then applied to allow calculations related to time domain, frequency domain and time-frequency domain features of the signals. Smoothing of the signal was done using a three-stage algorithm which involves the mean (moving average), mean absolute (the mean average with combined rectification) and root mean square techniques.

The processed results from the MR3 Noraxon Software were then exported to Matlab for further analysis. The power spectral density analysis was based on the Welch method, hence Fast Fourier Transform was applied for the power spectral analysis. The recording of the positional data enabled the labelling of the events during post-processing of the data for analysis. Furthermore, individual modules could easily be integrated with the whole system or work freely.

The Noraxon IMU MyoMotion system consists of 16 individual wireless sensors. The system was able to acquire orientation and anatomical data in real-time. During post-processing, the user can export data as quaternions or even raw accelerometer, gyroscope and magnetometer values. In dynamic mode, the system has an accuracy of $\pm 1.2^0$. The IMU sensors had an internal sampling frequency of 400 Hz for both gyroscopes and accelerometers. However, when integrated to the data logger, the data sampling frequency is reduced to 200 Hz. The gyroscopes had a full scale of ± 2000 deg/s and the accelerometers had a full scale of ± 1.7 g. The Nexus Motion System from Vicon, USA was used for the anatomical and orientation angle analysis. The system consists of motion tracking cameras and an algorithm used to develop a 3D skeletal model of the participant. Reflective markers were installed on selected anatomical landmarks such as the foot, tibia, thigh and pelvis of the participants. These reflective markers were then detected by the high-resolution cameras during gait analysis, provided that the participant was within the calibrated working envelop. In this study, the working envelop was a 10 m by 15 m platform with force plates at the centre. It was a complimentary technique for gait analysis. The modules within the MR3 software system include motion, EMG, force and video [191], as illustrated in Figure 3.1.

Working in Nexus platform was made easy due to the availability of the *Biomechanics Workflow* feature, which enabled the development of a custom-made data collection protocol that was developed to best suit the study of amputees. This feature has been used successfully in other previous studies [192]. Other features which were explored were Optimum Common Shape Technique (OCST), Symmetrical Center of Rotation Estimation (SCoRE) and Symmetrical Axis of Rotation Analysis (SARA), as they enabled easy data acquisition and analysis within Nexus Software.

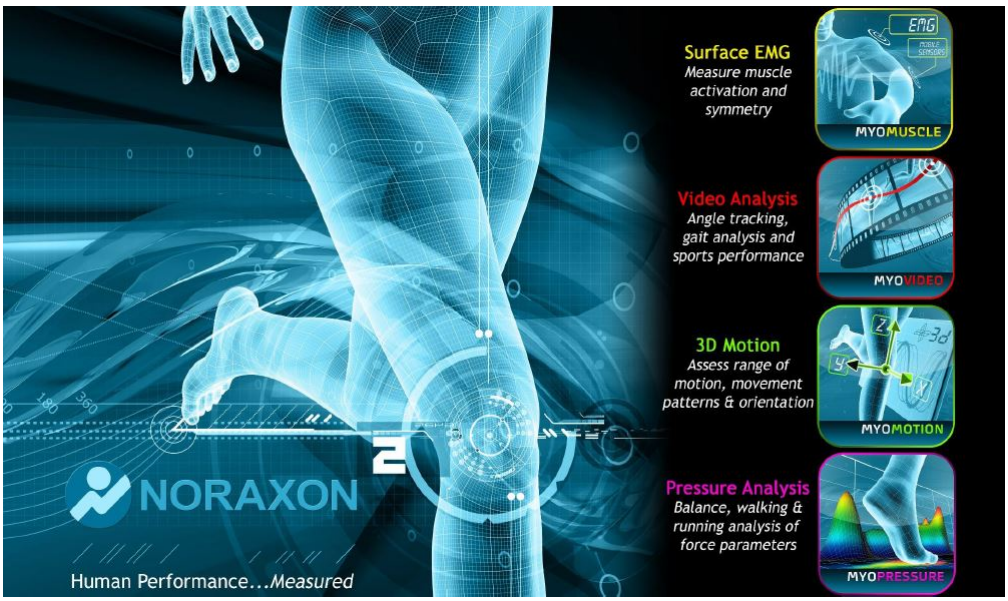

Figure 3.1: MyoResearch3 recording Noraxon System modules

The Noraxon MyoMotion System and the Vicon Nexus Motion System were both calibrated before the recordings. This enabled the validation of the recorded results using normative data already pre-loaded within the system. The name and activity number (Label, e.g. Participant1.Activity1.) was used for every recording. The participants were instructed to stand straight, with arms flexed along the hips. In the software, the chosen body segments were compared to the known starting position of all body joints on the skeletal avatar hence compared to the known starting position of all body joint. The calibration position was maintained for a period of 1 s or more after triggering the calibration module within the software. After initial calibration, recalibration was carried out after every five sets of activities. That was done to continuously develop a reliable measuring system. An audible sound was heard, notifying the user of the beginning of the calibration process and another sound was heard during the end of the calibration process.

3.7 Activities

The proposed system was expected to be able to predict the intended limb movement. Hence every limb movement was systematically associated with an expected activity to be performed. To develop a data set for the design parameters, the participants performed the following mobility related activities in the laboratory:

- Walking with sEMG sensors, IMU sensors and reflective markers (Gait analysis and EMG Analysis were carried out simultaneously). The Vicon Nexus system and the Noraxon Motion system were used at once to validate data.
- Sitting with sEMG sensors and performing dorsiflexion and plantarflexion movements using amputated leg.
- Standing with both legs spread and feet pointing forward during calibration procedure.

A pilot study was carried out to determine the best possible duration of each activity. The findings were similar to [193] where the average stride duration was 5.6 s and each step duration was 1.2 s, hence the average velocity was 1.5 ms . The recording equipment was sampling at 1500 Hz . Therefore, to achieve sufficient data sets, a minimum of 196 s per activity was sufficient. This was an average of four minutes of walking and provided an average of 653 windows. Each window length was 350 ms. Therefore, each activity lasted about five minutes and every activity was repeated ten times. That is an average of twenty minutes of participation.

The participants were expected to wear the sensors for at most an hour. This included set-up and calibration time. However, participant 1 visited the laboratory three times; the initial visit was for the pilot study and training of both the participants and the researchers on the use of the equipment and familiarisation with the activities. The second visit was for the data collection intended for determining the design parameters. The third visit was for testing and validating the developed control architecture. The second participant did not participate on validation of the design, therefore, he only visited the laboratory twice.

The gait analysis and the recording of sEMG data was carried out at the same time when the participant was walking. Initially, the participants were made to sit down, and data was recorded as they moved their limbs to determine active muscles on the residual limb. The participants were tasked to perform both movements at the same time with both legs. As a result, data was recorded on the residual limb and the sound leg. This was done to analyse the extent to which the sEMG was active and on which muscles:

- Dorsiflexion/ plantarflexion
- Inversion/ eversion
- Abduction/ adduction

After completion of these activities performed when seated, the participants were tasked to walk using a normal gait. The EMG signals were then extracted on the identified muscle sites when the participants were walking on a 10 m wooden platform with embedded force plates. It was during this walking activity that the Vicon Nexus Motion system, Noraxon IMU system and Noraxon EMG system were synchronised to monitor participant's gait and sEMG performance.

3.8 EMG data acquisition using Noraxon MyoResearch-3 (MR3) system

The sEMG data were recorded from the identified lower limb muscles. The SENIAM standards were used mainly to select the muscles which were responsible for lower limb motion. Issues with regard to electrode placement are discussed in the following section. The raw signals were acquired using the Noraxon active electrode system which has an on-site amplifier. The system has a 10 GΩ impedance with a common mode rejection ratio of 115 dB at 50 Hz . The signal was sampled at 1500 Hz. The measurement function accuracy (MFA) of the sensors was $\pm 2\,\mu V_{RMS}$. The baseline noise was less than $\pm 1\,\mu V_{RMS}$. The electronic gain was set at 200 with an overall gain of 500. The 50 Hz notch filter was not applied during data acquisition. Wireless communication was used between the electrodes and the data acquisition unit to minimise movement artefacts. The signals were recorded using the Noraxon Myomotion System, USA. The number of data sets collected for each motion was as explained in section 3.7 and the raw data sets were

stored for further processing.

The post-processing of the signals was done using MR3 and Matlab R2017a. The three dimension positional data was also simultaneously recorded at 200 Hz using the Noraxon's MyoResearch3 (MR3) System's IMU module, which can measure anatomical and orientation angles, along with the Vicon's Nexus Motion system. The modules were synchronised and this enabled real-time data recording. To acquire reliable data, signals were recorded from both legs simultaneously for every participant. This enabled the consideration of the data from the normal leg as control data for the study. Furthermore, a comparison to normative data within the Noraxon MR3 system was carried out.

3.9 Selection of muscles and sensor placement

The selection of muscles to use for the study was based mainly on SENIAM and ISEK standards. However, other methodologies [194] which closely adhere to the recommended standards were used. Although all the agreed standards for recording were followed, difficulties emanated when working on the residual limb. As a result, some amendments were made which included a vigorous trial and test in real-time of EMG amplitude at targeted sites [132], as illustrated in Figure 3.2. The main reason for using these standards for selecting muscle sites was to avoid muscle redundancy [195], which may have a negative impact on the control architecture performance. The goal was to achieve the control objective with lowest number of signal channels.

Figure 3.2: EMG recording using the MR3 System, Noraxon

The selection of muscle sites was, however, governed by the probability calculation suggested by [196] such that the behaviour of the signal is regarded as zero-mean Gaussian process $s(t)vN(0, s_s)$ corrupted by a zero-mean Gaussian additive noise $n(t)vN(0, s_n)$. Assuming that

P_d is the probability of detection, then the double threshold is given by:

$$P_d = \sum_{k=r_0}^{m} (mk) P_d^k (1 - P_d)^{(m-k)} \tag{3.1}$$

where r_0 is the threshold and m is the length of the window. The methodology suggested by [197] was also considered as it takes into consideration innervation zone activity of lower limb muscles. Their study presented an overview of which muscles will ultimately be active on the surface given their innervation behaviour [198]. However, their suggested method was only applicable to the sound leg, hence the missing anatomical landmarks on the residual limb resulted in the use of MR3 software in real-time, as illustrated in Figure 3.3, on searching for active muscle sites. The MyoMotion module within the MR3 system had a pre-designed protocol on sensor placement and was also used to aid in the placement of the EMG sensors on the participants as illustrated in Figure 3.3.

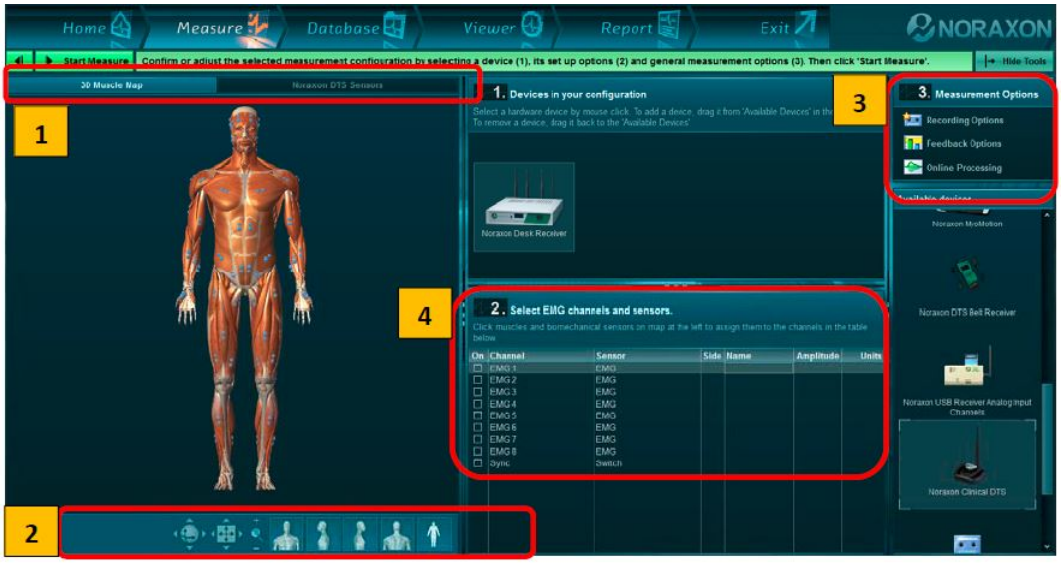

Figure 3.3: EMG sensor placement illustration within the MyoMotion module

The 3D muscle map is illustrated in window (1) while the rotation tools are shown in window (2). These rotation tools were used to visualise Gastrocnemius muscles at the back. Window (4) indicates the channels that were ready for use while window (3) was used to select the measurement and recording options. A detailed evaluation of the system indicated that the system is well aligned to the SENIAM and ISEK standards for recording the signals. The pre-configured signal recording enabled the use of external triggering systems, thereby giving the participant enough time to get familiar with the environment before recordings began. This also enabled correct recording of start/stop scenarios. The threshold was set as the minimum duration the signal must stay above to activate the trigger. Such a technique enabled the validation of the recorded results as well as visual playback. The comprehensive measurement system enabled reduction in experimental time and easy analysis of the results in real-time. The sEMG signals were recorded from the Soleus, Tibialis Anterior, Gastrocnemius Lateralis and the Gastrocnemius Medialis muscles of the sound leg, as illustrated in Figure 3.4.

Proper skin preparation procedures were performed, which included shaving the limb and cleaning with alcohol. The use of alcohol was to reduce signal distortion due to increased skin impedance. The electrodes were then placed on the Tibialis Anterior, Gastrocnemius Lateralis and Gastrocnemius Medialis of the amputated leg, as illustrated in Figure 3.4. After amputation the Soleus could not be accessed and, as a result, it was not considered on the amputated left leg. The Soleus muscle was only considered for the normal leg. Challenges were experienced during the sensor placement for the recording of EMG signal due to the absence of foot anatomical landmarks. The position of the EMG sensors is shown in Figure 3.4 for both the amputated and the non-amputated leg.

Figure 3.4: Illustration of (a) SENIAM electrode position on a normal leg, (b) the residual limb and (c) the electrode positioning on the functional leg.

Pre-gelled, bipolar $Ag/AgCl$ surface EMG electrodes of 10 mm diameter were used. The electrodes were placed 20 mm apart, longitudinally concerning the muscle fibre to be measured, as recommended by the SENIAM and ISEK standards [89]. The SENIAM and ISEK standards were difficult to apply on the amputated leg since some of the anatomical landmarks from the ankle were missing. This presented challenges on determining proper electrode placement. As a result, the procedure for placing electrodes on the amputated leg included having the MR3 MyoMotion on-line and selecting locations that exhibited high amplitudes during dorsiflexion and plantarflexion movements concerning the Tibialis Anterior, Gastrocnemius Lateralis and the Gastrocnemius Medialis muscles.

3.10 Gait analysis using the Vicon Nexus II motion system

The quantitative gait analysis has been recognised as a useful tool for extracting dynamic and kinematic data [199]. The gait protocol adopted for the study was derived from reviews, comparisons and studies carried out by [150] and [200]. The all-inclusive modelling and processing tool for movement analysis, Vicon Nexus Motion Systems, was used to capture the three-dimensional data. Three force plates were correctly positioned in the middle of the walkway. The behaviour of the myoelectric signals was evaluated based on the normal gait of the amputees. The objective was to analyse the signal profile of the identified muscles during normal gait. Anatomical angles were only calculated provided that there were at least two sensors located around the joint. As a result, the experimental set-up included the placement of two reflective markers around a joint on the participant, as illustrated in Figure 3.5.

The three force plate orientation system on the wooden floor was used for force measurements, as illustrated in Figure 3.5. The wooden floor was used because it reduces the risk of bruises in the unfortunate event of a fall by the participant. Although any sensor configuration was acceptable by the system, caution was taken by beginning with the pelvis or upper thoracic sensor and then creating an uninterrupted sensor chain to distal segments. The Nexus system has the capability of intelligently label the data in real-time. This also enabled real-time participant calibration to be carried out automatically. The native integration with Matlab allowed the generation of scripts for further signal processing. The Vicon cameras were set as illustrated in Figure 3.5 to capture sufficient data within the working envelope. The Automatic Quality Assessment Tool within Nexus enabled the automatic detection of gaps, thereby improving the reliability of the readings.

The Vue Video system within Nexus enabled full frame synchronisation up to $120Hz$ or $1920 * 1080$ HD from a single point connection for both power and data. This was made possible by the embedded dynamic video and optical calibration. The SCoRE and SARA Functional Calibration enabled quick set-up and provided real-time visual feedback in the workspace to assist with participant calibration. Data management was achieved via the use of ProEclipse, which is embedded within Nexus. The working envelope and the *c3d* lower limb model generated for the right leg is shown in Figure 3.5. The recorded data was then further exported as *c3d* files to Matlab R2017a for post-processing. The processed results revealed the anatomical and orientation angles of the participant.

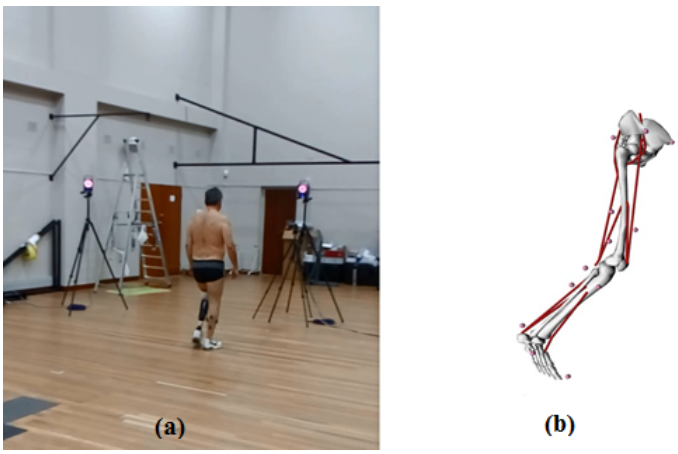

Figure 3.5: Gait analysis using (a) Vicon Motion System and (b) the output *c3d* file of the lower limb

3.11 Determination of anatomical and orientation angles using Noraxon Sensor system

The EMG signal was used as a control signal, in other words it was modelled as the user's intent to carry out a movement using the limb under investigation. However, initial experiments carried out as discussed in section 3.7.3 reavealed that there is a need for a feedback mechanism within the control architecture. Although forward dynamics could be used to generate a feedback estimate this has not been a recommendable technique for physiological motor control based systems [201]. As a result, the position and orientation of the limb in space were determined

using inertial measurement sensors from Noraxon, USA. The expected draw-backs of the system included positional data reliability, drift, inhibited movement and global positioning. However, the benefits of direct measurement and real-time data acquisition outweighs the draw-backs as a result of using the sensors.

There is a known standard on IMU sensor placement [202]. Hence, the Noraxon IMU system has a validated model embedded in its MR3 software that was used to record the signals. The participants were tasked to perform the activities as discussed earlier in section 3.7. The recorded data was synchronised with the visual system to enable data labelling. The sensor placement was based on the objective of obtaining anatomical and orientation angles. The set-up worked well during initial experiments for determining design specifications through determination of anatomical and orientation system while the participant was wearing the passive limb. However, challenges with regard to calibration emerged when the Noraxon IMU system was used in the presence of the powered prosthetic limb. Each time the DC motor was activated it established a magnetic field which affected the performance of the Noraxon IMU measuring sensors. The two MPU6050 IMU sensors dedicated for control architecture were not affected since the magnetometer values within the algorithm were used for real-time calibration and each time a double support was registered the IMU sensor carried out a self-calibration procedure. Magnetic interference, which is one of the expected challenges, was not present during the testing of the powered ankle on the developed control system. The wireless connection between the sensors and the main terminal computer was preferred to reduce other effects such as voltage drops.To minimise the effects of magnetic interference, the Vicon Nexus motion system and the Noraxon IMU system were synchronised. Hence, the experimental set-up was as illustrated in Figure 3.6.

Figure 3.6: Illustration of all IMU sensor and reflective marker positions

3.12 Prototype testing and design validation

A prototype powered ankle was developed to test the functionality of the developed hardware and control algorithms. The developed mechanical foot could fit the structure of only one of the participants (participant number 1) as, due to the high cost involved in developing the prosthetic powered limb only one participant was tested. The previously reported results showed that there is no significant difference between amputees who had a similar amputation. Therefore, one participant was used for testing the functionality of the powered ankle.

The designed mechanical powered ankle was fitted onto the participant's left amputated leg. Necessary adjustments were made concerning height and alignment of the device. The control box was attached to the thigh of the same leg. Two IMU sensors were mounted, one on the thigh and the other on the shank (metallic part of the prosthetic leg). The sEMG sensors were placed inside the socket, and the cable leads were connected to the main data acquisition unit which had an SD Card for data recording. The performance of the sEMG sensors was initially visualised using Labview as a way of confirming the level of noise interference before recording.

The system was calibrated and the participant was instructed to walk on a flat surface until he was comfortable walking with variable gait speeds. The Noraxon IMU sensors were then placed on the foot, shank, thigh and pelvis of the participant for both legs. These Noraxon IMU sensors were used to monitor the gait of the participant. Furthermore, Noraxon EMG sensors were placed on the sound leg of the participant. After final calibration (when the participant had all sensors mounted on him), the participant was instructed to walk on the treadmill. The treadmill speed was selected as 0.5 ms^{-1} and 0.8 ms^{-1}. The results were recorded using Noraxon MR3 software. The recorded results were then preprocessed to determine classification accuracy and device gait performance by analysing the anatomical and orientation angles.

3.13 Risk and side effects involved in the study

The study was confined only to the design of the control system architecture, which included the signal acquisition and control systems. It does not include the design of the limb's mechanical structure. The equipment used for this study was certified to be used on humans. The risk and side effects discussed in this section cover the following experiments:

- Analysis of sEMG signals from the residual stump and the sound leg using gelled and dry electrodes.
- Determination of anatomical and orientation angles of the lower limb using Noraxon IMU sensors.
- Gait study of osteomyoplastic transtibial amputees.
- Testing of an sEMG multichannel signal acquisition electronic device.
- Validation of a functional powered ankle prosthetic limb.

The risk and side effects associated with each experiment and the study as a whole are discussed in the following sections.

3.13.1 Potential risks associated with analysis of sEMG signals from the residual stump and the sound leg using gelled and dry electrodes

This experiment was carried out in two phases. The initial test used gelled electrodes, and the aim was to determine the sEMG signal quality on the residual limb and the sound leg. The second phase involved testing the feasibility of using dry electrodes and evaluating whether there is significant difference between the electrode types. Both electrode types were linked to an active amplifier with an operating voltage of 3.3 V at 0.1 mA, which was too low to cause fibrillation of the heart. The sensors had an embedded protection circuit. Each electrode weighed 0.6 g; therefore, the additional load to the human body was almost negligible. The possible risks associated with the research were:

- *Skin irritation* - The surface electrodes are mainly found in two types, that is the gel and the dry electrode type. For gelled electrodes, a silver-silver chloride ($Ag/AgCl$) layer is the main metallic composite electrolytic substance. All types required the cleaning of the skin surface using methylated spirits. This may cause skin irritation. Since the future endeavours in myoelectric control systems include using sEMG signals recorded using dry electrodes on the non-shaved skin, in experiments there was a need to acquire data from surfaces cleaned using alcohol and those from alcohol-free cleaned surfaces. Shaving of the

skin was considered during experiments. The H124SG Covidien electrode type was used, it has a pre-gelled adhesive side with non-irritating gel, specifically developed to prevent allergic reactions. The foam electrode was latex free and therefore suitable for every skin type. The dry electrodes had no skin irritation risks as they were stainless steel electrode bars with smooth surfaces.

- *Voltage surges* - The electronic circuits use low voltage and low current components, hence the result is a high impedance circuit. The section for the surface electrodes contains a Darlington Pair configuration for protection circuit and high-value resistors in the kilo-Ohm ($k\Omega$) range to increase the circuit impedance. The high input impedance amplifiers also enable secure protection against unwanted voltage surges.

3.13.2 Potential risks associated with determination of anatomical and orientation angles of the lower limb using Noraxon IMU system

The determination of anatomical angles was carried out using Noraxon IMU sensors. These commercially available sensors were deemed safe to be used on humans. The only possible risk expected was electronic surges which were very unlikely to occur due to the electronic protection circuit and effective grounding techniques used in the system. There was no direct physical link between the participant and the main data logger, which was powered from the 230 V/13 A supply due to the wireless communication between the sensors and the main system. Since the participants were expected to walk several times on a 10 m walking platform, this may result in unexpected falls. However, measures such as clearing obstacles and having the participants familiarise themselves with the platform were taken to avoid such events.

3.13.3 Potential risks associated with gait study of osteomyoplastic transtibial amputees using Vicon Nexus System

This experiment was carried out to determine the distance variables of a normal gait of the participants. The results were used to determine the effects of using passive prosthetic limbs. The risks associated with this experiment were similar to those discussed earlier on using the IMU systems. Furthermore, the skin irritation was regarded as one of the major irritations since the reflective markers were mounted using double sided tape on the participant's anatomical landmarks such as the high, thorax and pelvis. The removal of the reflective makers may cause skin discomfort as tape will be in contact with any hair follicles on the skin surface. The discomfort is mainly caused by the speed and angle of removal of the gelled electrodes from the skin surface.

3.13.4 Potential risks associated with testing of an sEMG multichannel signal acquisition electronic device

The developed multichannel electronic signal acquisition module was tested using surface gelled electrodes and dry electrodes. An additional risks associated with this experiment was mainly fibrillation of the heart since the new circuit made use of the zenner diode barrier system. The system allowed voltage to flow only from the participant to the electronic circuit, thereby suppressing the reverse voltage flow. The participant was tasked to perform activities only associated with normal gait therefore, the risks discussed in section 3.9.1 were all taken into consideration.

3.13.5 Potential risks associated with testing the developed prototype

Although the study was confined to the development of a control architecture, the validation of the concept involved testing the control architecture using a powered ankle prototype. The developed electronic signal acquisition module and the main control card were linked to a DC powered motorised actuator. The actuator used a lead-screw technique to provide displacement. The risks associated with this experiment included all the risks listed in section 3.9.1 and those of section 3.9.4. The validation was carried out on a treadmill, and this presented high risks associated with falling. To avoid the risks, the participant was carefully instructed on the use and operation of the treadmill before testing. Also, rails were mounted on the treadmill so that in the unfortunate event of a fall, the participant could use the rails to regain balance. Additional to the Noraxon IMU sensors, two custom made MPU6050 IMU sensors were included that were installed on the shank and thigh of the amputated leg, thereby increasing the risk of electric shock. However, the 5 V operating voltage reduced the risk of electronic shock. Since the IMU sensors were not measuring anything directly on the skin, they were isolated using a plastic box. A safety switch accessible to the participant was also used on the control box.

3.14 Statistical analysis and data processing

The analysis of signals was carried out in Matlab R2017a, R-Studio, SPSS and MR3 to achieve perfect presentation and analysis. MR3 was mainly used for real-time analysis of the signals, as previously discussed in Figure 5. The initial analysis carried out on the data investigated the relationship between data acquired from the muscles on the sound leg against data acquired on the amputated leg. To achieve this, the Pearson Product Moment Correlation (PPMC) coefficient was determined. The greater the positive value of the coefficient, r, the greater the variation between the data sets. Therefore, when $r = 0$, there was no variation in the two samples. If x (amputated limb) and y (sound leg) are variables representing two data sets, then the PPMC is determined as:

$$r = \frac{n(\sum_{n=1}^{N} xy) - \sum_{n=1}^{N} x \sum_{n=1}^{N} y}{\sqrt{(n(\sum_{n=1}^{N} x^2) - (\sum_{n=1}^{N} x)^2)(n(\sum_{n=1}^{N} y^2) - (\sum_{n=1}^{N} y)^2))}} \tag{3.2}$$

where N is the total number of samples in a data set.

Although this technique was able to show that there was a relationship between the data sets, it was not able to show the difference between the dependent and independent variables. As a result, the strength of the relationship was measured using the coefficient of determination, r^2, with the significance expressed as probability level, p. Therefore, the larger the correlation, the stronger the relationship. The sample size was selected such that the difference between what we observed and what was expected was large enough to be significant. The $t - test$ ($p < 0.05$) was carried out on all feature sets produced during different movements to determine if there was any significant difference. The relationship could be strong and yet not significant and in some instances the relationship could be weak but yet significant, and as a result, the key factor was the sample size. Where small data samples were used, much attention was given to the significance and where large samples were used, much attention was given to the strength of the correlation.

The signal bar graphs, shrinking circles and sinusoidal wave forms were all used as signal representation and analysis tools in MR3 in real-time. These features were responding directly to the performance of muscle behaviour in real-time. The easy-to-visualise system also enabled

trigger settings. The recordings were either exported as *csv* files or *mat* files for post-processing. The mean, mean absolute and the root-mean-square smoothing techniques were all tested with a 350 ms smoothing window. According to [49], the nature of the EMG signal is such that it is stochastic and its model, $x(n)$, comprises of additive white Gaussian noise, w_n:

$$x(n) = \sum_{r=0}^{N-1} h(r)e(n-1) + w(n) \tag{3.3}$$

where $e(n)$ is the point processed, $h(r)$ represents the motor action unit potential and N is the number of motor units firing. The nature of the signal allows the determination of time and frequency domain features using statistical methods. To achieve a comparison between participants, the methodology suggested by [198] was considered such that if y is the current reading, y_{norm} is its normalised value as y_m and y_M are the lower and upper threshold values such that:

$$y_{norm} = \frac{y - y_m}{y_M - y_m} \tag{3.4}$$

The quantitative analysis of the EMG signals included the determination of mean frequency, median frequency, total power and mean power of the signal. Furthermore, a quantitative analysis of the gait including mean, peak and minimum values was also conducted. Kinetic data, such as vertical ground reaction force and ankle, knee, and hip powers, were compared with normative data. Anatomical and orientation angles were also determined. These included hip, knee and ankle rotation and ankle dorsiflexion and plantarflexion. To a greater extent, the distance variables such as the cadence, velocity, stride duration, stride length, step and stance phase were recorded and analysed. Linear discriminant analysis (LDA) was applied to all the signals from the targeted muscles to analyse signal classification based on the acquired features. According to [203] and [204], the Lilliefors test is a requirement when working with data on unknown behaviour such as EMG. The initial test carried out on each data set was the Lilliefors test, to determine whether there was a normal distribution on the data. This was carried out in Matlab R2016a, MathWorks Inc. Whenever the static variable k, was greater than the critical value c, the result was $h = 1$ indicating a rejection of the null hypothesis at the proposed 0.05 significance test level [205]. In situations where the actual value of p was required, the Monte Carlo approximation was carried out such that the standard error, SE was determined as:

$$SE = \sqrt{\frac{\widehat{p}(1-\widehat{p})}{n_{rep}}} \tag{3.5}$$

Where $\widehat{p}$ is the estimated p-value of the hypothesis test and n_{rep} was the number of Monte Carlo replications performed. Furthermore, the assessment for the quantitative data was mainly based on the one way non-parametric Friedman ANOVA, a pair-wise comparison was further carried out using Dunn's posthoc test [198],[206] as a method for testing for statistically significant differences among the variables was carried out in R Studio [207], [208]. The data was then evaluated to provide normative information for the amputee population when performing ambulatory related activities.

3.15 Conclusion

The protocol used to achieve the set objectives was too broad and ever-changing as the conditions of testing continuously changed. The standards associated with the test carried out were

all taken into consideration. The experiments were carried out indoors at the Human Motion laboratory, Stellenbosch Biomedical Engineering Research Group laboratory, Stellenbosch Neuromechanics Unit and also at the home of the first participant (participant 1). The results for the environments were compared. Since there was no significant difference ($p = 0.8$), the validation of the device was carried out at the Neuromechanics Unit. The initial training and pilot test carried out before the main test and validation test were very helpful as they provided an in-depth understanding of biomechanics measuring equipment and calibration procedures.

The validation of the developed control architecture was carried out in two phases. The initial phase involved the determination of the classification accuracy of the control architecture. During this phase parameters such as repeatability, processing time and percentage classification accuracy were determined. The results were compared to the standard values determined from the literature. The acceptable classification accuracy was any value greater than 90% and the processing time should be less than or equal to 350 ms. The second validation involved carrying out normal gait analysis of the participant using the developed crude prototype powered limb. The distance and anatomical spatial variables were then compared to those of the non-amputees provided as normative data. In addition, the results were also compared to those acquired using the passive mechanical prosthetic limb. Recommendations, conclusions and limitations of the study were made with regard to the developed architecture performance.

Chapter 4

Analysis of sEMG signal features

Published Journal article [1]

4.1 Introduction

Electromyography (EMG) is a process which involves detection, analysis and use of signals extracted from muscle sites emanating from muscle activation [49]. The signals have been used in clinical diagnosis, assistive technology and engineering [209]. In this study, the focus is on assistive technology for rehabilitation of lower limb amputees. Lower limb amputees have struggled for a long time to acquire neural intuitive powered ankle devices to aid mobility [1]. As a result, this has reduced the confidence the amputees have in the reliability of the prosthetic limbs.

The ankle dorsiflexion and plantarflexion movements are responsible for the proper toe-off and heel-strike during normal gait. The propulsive force generated by the ankle enables smooth forward body projection and minimises hip rotation. The natural ankle intuitively adapts to the desired gait, thereby assisting the body to achieve a full range of motion for all anatomical angles, such as the hip and the knee. However, the use of stiff mechanical prosthetic ankles results in some difficulties related to ambulatory activities for amputees, which may lead to abnormalities within the gait [210]. The poor range of motion and lack of intuitive control of the ankle may result in short-term effects such as bruises and long-term effects such as lower back-pain. Therefore, there is a need for naturally controlled ankle prosthesis, and this can be achieved with the use of sEMG signals. Such a technique will present the amputees with intuitive control of the ankle, thereby achieving close to natural gait [8]. However, challenges exist in selecting the proper muscles to use and also in the poor signal quality of the sEMG signal available at the amputated residual limb.

The *Standards for reporting EMG Data*, popularly known as the ISEK-EMG standards, were developed by Dr Roberto Merlitti [72] and endorsed by the International Society of Electrophysiology and Kinesiology (ISEK). They describe how EMG data is recorded, processed, analysed and reported. The standards sufficiently explain the nature of the recording sensors and signal processing. In 1996, the Biomed-2 program by the European Community resulted in the formulation of the *surface EMG for non-invasive assessment of muscles* (SENIAM) standard

[1] Garikayi, T., Van den Heever, D. and Matope, S., 2018. Analysis of surface electromyography signal features on osteomyoplastic transtibial amputees for pattern recognition control architectures. *Biomedical Signal Processing and Control*, 40, pp.10-22.

to integrate basic and applied research on surface EMG and to solve key issues with regard to clinical application [83],[180]. The SENIAM standards highlighted the locations of electrode placements for sEMG recording while the ISEK standards are more aligned to signal processing. Furthermore, the SENIAM standards only focus on surface EMG while ISEK takes note of both surface and invasive EMG signals. However, the standards complement each other very well. Key issues for both standards are sEMG sensor types and sensor placement procedures, sEMG signal processing and surface EMG modelling. Other methods and guides proposed later were merely an extract of the ISEK and SENIAM standards [190].

According to [211], there is notable variation with regard to electrode placement, inter-electrode distance and determination of landmark morphology during EMG measurement. As a result, there is a need to carefully implement SENIAM and ISEK standards when working with amputees as the missing part of the leg provides difficulties in the use of the standard operation procedures. During the recording of EMG signals, there are several factors that may lead to the distortion of the signals and these include muscle crosstalk, skin impedance and power line interference [212].

As an amputee sustains a contraction, the amplitude of the surface EMG signal increases as a result of the synchronisation of the activated and newly recruited motor units [213]. However, in some cases, this is regarded as symptoms of fatigue [214]. Although the sEMG signal is affected by muscle crosstalk, it can easily be described in terms of amplitude, frequency and phase [49]. Therefore, the goal is to determine safe operating amplitude levels and at the same time achieve optimum control of the prosthetic ankle. According to [215], the analysis of EMG signals is mainly for muscle fatigue, muscle geometry and muscle force. However, it is muscle force that mainly affects the performance of myoelectric control systems since the EMG signal amplitude is proportional to the muscle force [190]. Contrary to that, for amputees, the extent of amputation has an adverse effect on muscle behaviour. The median frequency and the mean power frequency are the most common and reliable indicators of muscle performance [216].

Myoelectric control systems for lower limb prosthetics are often regarded as complex systems due to the nature of the available signals at the residual limb. The implementation of pattern recognition based systems for myoelectric control has been extensively investigated, and recommendations for non-amputees were made [109],[217]. However, challenges still exist for implementation of such robust techniques on amputee related designs [7]. The pattern recognition system's accuracy and reliability are highly influenced by the classification accuracy which is affected by the quality and nature of signal features. Pattern recognition based systems are complex but are a reliable control architecture since they use the signal features instead of signal threshold values. In the time domain these features include zero-crossing per second, integrated EMG, mean absolute value and root mean square value [209]. The performance of pattern recognition systems is highly affected by White Gaussian Noise (WGN) inherent in the dominant frequency bandwidth [218],[209]. The WGN is difficult to eliminate using bandpass filtering. Therefore, there is a need to develop a robust feature set that can guarantee optimal classifier performance in the presence of WGN. Since the establishment of the Hudgins features in 1993 [107], efforts had been made to improve the feature sets and evaluations were done to develop a grading system for the EMG features. Boostani et al. [219] and [209] evaluated the features based on sensitivity to noise, hence the Willison amplitude feature was superior to all the features. However, the analysis was based on simulated noise, hence the results differ from real-time EMG noise interference.

In this study, it was hypothesised that the residual limb muscles still contain active myoelectric signals. However, the signal characteristics are affected by the type of amputation. As a result, this affects the extent of the functionality of the active powered ankle. The objective was to determine the strength of the available myoelectric signals for sagittal plane ankle movements. The results of these statistical analysis techniques are presented in the following sections.

4.2 Methods and materials

The participants, activities, experimental set-up, data acquisition and statistical analysis used for the study is detailed in section 3 of the report. However, in this section, the actual signal acquisition procedure was presented. The methods used for electrode placement, signal acquisition, processing and reporting were strictly based on the SENIAM and ISEK standards. The approved research protocol was an extract from the SENIAM standards with slight modifications to suit amputees. The SENIAM standards were mainly utilised for electrode selection, selection of muscles and also electrode placement. However, they were not clear on data acquisition and reporting for data acquired from amputee participants. Therefore, ISEK standards were used for sampling, filtering and processing of the signals.

4.2.1 Participants

The study consisted of two male amputees. The selected sample of amputees were unilateral amputees (left leg amputated) with first participant weighing 81 Kg with a height of 1.75 m and aged 43. The second participant weighed 79 Kg with a height of 1.73 Kg and was aged 46. Both participants have received osteomyoplastic transtibial amputation surgery. The stump length for participant 1 was 15 cm and that of participant 2 was 17 cm and the residual stumps were 33.7% and 36% of the length of the sound limb respectively when measured from the knee to the ankle. The participants reported independent ambulatory related activities with medium to high daily activities. The participants have been using the passive limb for the past two years. The criteria for inclusion was based on the ability of the participant to effectively use the prosthetic limb inside the laboratory testing environment without the need for assistance. This eliminated the need to train the participants on the use of the limb before the experiments. Another consideration was for the participants to have a comfortable surface bearing socket which utilises the vacuum system and have to had no medical history related to limb injuries or comorbidities that could affect gait, joint angles or electromyography signals. None of the participants had a history of neuromuscular disorders.

4.2.2 Skin preparation and electrode placement

The sEMG signals were recorded from the Soleus, Tibialis Anterior, Gastrocnemius Lateralis and Gastrocnemius Medialis. Proper skin preparation procedures were performed, which included shaving the limb and cleaning with alcohol. The use of alcohol was to reduce signal distortion due to increased skin impedance. The electrodes were then placed on Tibialis Anterior, Gastrocnemius Lateralis and Gastrocnemius Medialis of the amputated leg. After amputation, the Soleus could not be accessed and,as a result, the Soleus was not considered on the amputated left leg. However, the Soleus muscle was considered for the sound leg. Pre-gelled, bipolar Ag/AgCl surface EMG electrodes of 10 mm diameter were used. The electrodes were placed 20 mm apart, longitudinally, with respect to the muscle fibre to be measured, as recommended by the SENIAM and ISEK standards [72].

4.2.3 Data acquisition and signal processing

The raw sEMG signals were acquired using the Noraxon active electrode system. The system has a 10 GΩ impedance with a common mode rejection ratio of 115 dB at 50 Hz. The signals were sampled at 1500 Hz, as required by the SENIAM and ISEK standards. The measurement function accuracy (MFA) of the sensors was $\pm 2\,\mu V_{RMS}$. The baseline noise was less than $\pm 1\,\mu V_{RMS}$. The electronic gain was set at 200 with an overall gain of 500. The 50 Hz notch filter was not applied during data acquisition as suggested in the literature [8]. Wireless communication was used between the electrodes and the data acquisition unit to minimise cable movement artefact.

The experimental protocol involved the acquisition of maximum voluntary contraction (MVC) level from the subjects by holding a movement contraction for at least 5 s since the recommended processing time for the targeted processor is 300 ms. As a result, the 5 s duration provided enough data without the subjects experiencing fatigue. The subjects were tasked to perform five motions of dorsiflexion and plantarflexion movements with a resting pause in-between (dorsiflexion-rest-plantarflexion). The second set of five motions included performing dorsiflexion and plantarflexion continuously without a resting pause (dorsiflexion-plantarflexion). All these initial experiments were conducted while the subject was seated. Another set of data was acquired when the participant was walking along a 10 m walking envelope. The reason for removing the resting pause in the second set of data was to facilitate an evaluation to determine whether there is muscle crosstalk and also to test the ability of the developed system to classify the movements in the event of fast reactions. The signals were recorded using the Noraxon MyoMotion System, also known as MyoResearch3 (MR3), USA. Five data sets were collected for each motion during normal gait activity. The activities were carried out during design parameter considerations and were used to evaluate the performance of the developed design. The raw data sets were stored for further processing. The post-processing of the signals was done using the MR3 Noraxon MyoMotion System. When using the MR3 platform, the filtering using digital filters was implemented. The results were exported to Matlab 2017a for further analysis.

4.3 Statistical analysis

The Pearson's correlation coefficient was used to determine the relationship between data from different muscle sites on the sound and the amputated leg on the same participant and across participants with respect to time domain and frequency domain features. The t-test ($p < 0.05$) was carried out on all feature sets produced during different movements to determine if there is any significant difference. All statistical analyses was carried out using Excel, Matlab and MR3 software. The spectral frequency analysis and spectral density frequency analysis were used mainly to select which muscles are still active and to determine the level of firing. The targeted control architecture was based on pattern recognition, and as a result the ability to distinguish signals from different muscles based on feature sets was mandatory. Signal power or signal strength per muscle site concerning dorsiflexion and plantarflexion movements of the ankle was determined. The evaluation of EMG signals was carried out in frequency and time domain. The quantitative analysis included the determination of mean frequency, median frequency, total power and mean power of the signal. Linear discriminant analysis (LDA) was applied to all the signals from the targeted muscles in order to analyse signal classification based on the acquired features

4.4 Results

It has been extensively reported as to which muscles are responsible for lower limb movements through the application of ISEK and SENIAM standards. However, the challenge was whether the muscles would still be available after amputation and, if so, to what extent their features could be utilised for pattern recognition algorithms. The results presented in this section highlighted the determination of active muscles during plantarflexion and dorsiflexion movements of the ankle, signal classification feasibility and the behaviour of the EMG signals during normal gait.

4.4.1 Determination of active muscles on the residual amputated limb

The osteomyoplastic amputation procedure performed on the participant preserved the activeness of the muscles at the residual limb even though the mean amplitudes of the signals differed from the sound leg, as shown in Figure 4.1. The study protocol revealed the gait events that can be monitored using the same muscles responsible for the ankle movement. The Tibialis Anterior, Medialis and Lateralis Gastrocnemius muscles were all monitored during both the stance and swing phase and the sEMG signals emanating from those muscles are as illustrated in Figure 4.1.

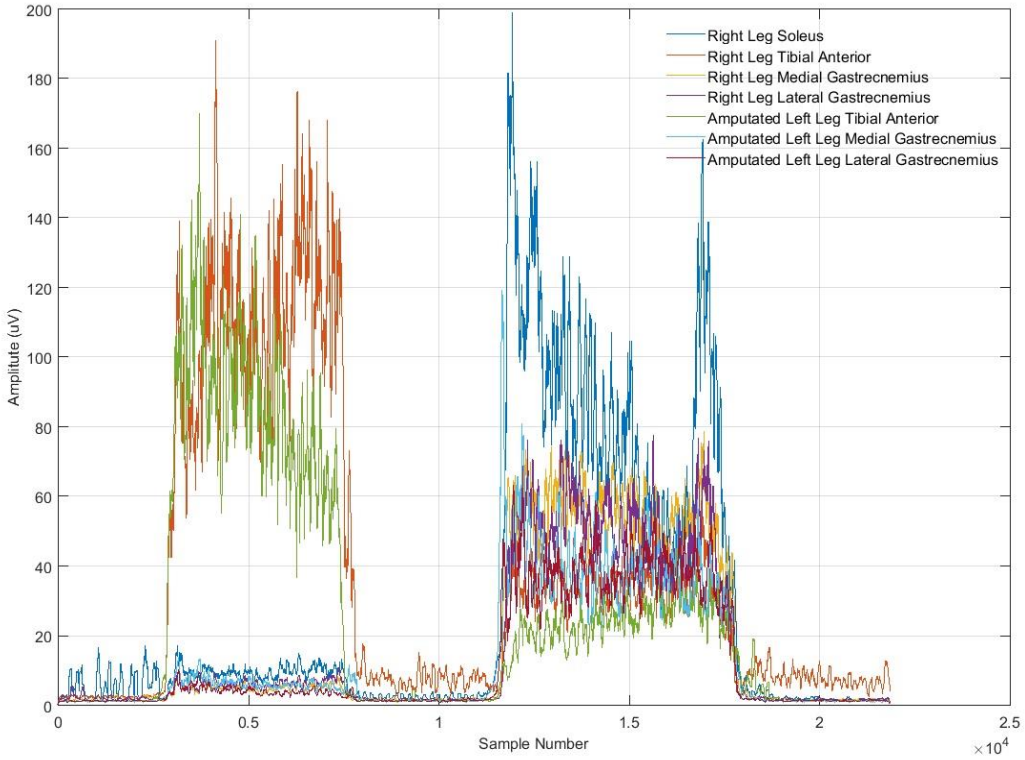

Figure 4.1: Comparison of mean amplitudes of right sound leg and left amputated leg

The Tibialis Anterior, Medial Gastrocnemius and Lateral Gastrocnemius were all active at the residual limb with variable amplitudes. The Soleus muscle on the residual stump was inaccessible. However, when tested on the sound leg, the Soleus muscle was dominant during plantarflexion with a mean amplitude of $82.53 \pm 7\mu$V as compared to the Gastrocnemius sEMG

signals, as shown in Figure 4.2. There was a significant difference ($p = 0.03$) between the signal power of the Soleus muscle and the Gastrocnemius medial and lateral EMG signals. The variation in signal power as shown in Figure 4.2 was a cause of concern for developing myoelectric control architectures since the Soleus muscle was inaccessible to provide a plantarflexion sEMG signal. The significant test performed illustrated that there is significant difference ($p = 0.001$) between the signals acquired at the amputated stump and the sound leg. Although there are several signal features that can be used by signal classifiers [209], the most dominant ones are integrated EMG (IEMG), mean absolute value (MAV), modified mean average value (MMAV), variance of EMG (VAR), waveform length (WL) and Wilson amplitude (WAMP). These are the main features which formulated the basis of the 12 time domain features. Some of the features included among these features were merely a derivative of the main features. The comparison of the signal characteristics from the amputated leg and the intact leg was based on the evaluation of time domain based features. The results are illustrated in Figure 4.3.

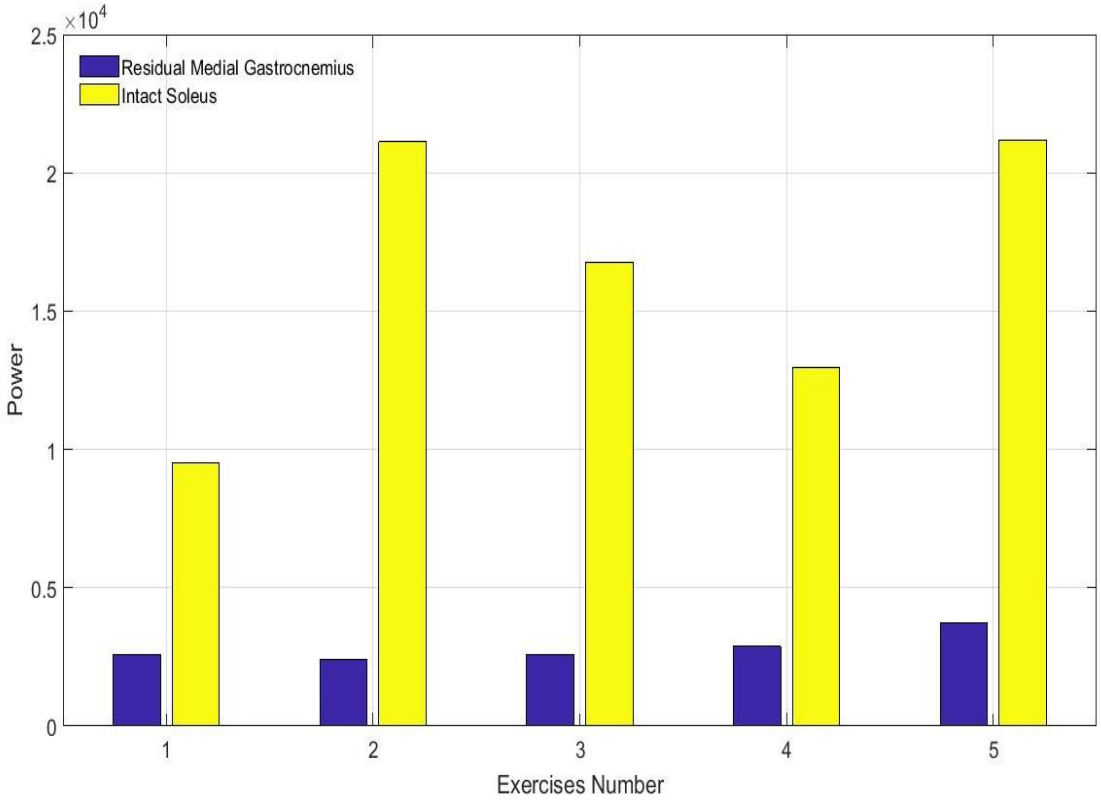

Figure 4.2: Comparison of signal power of Soleus and Medial Gastrocnemius muscle EMG signals

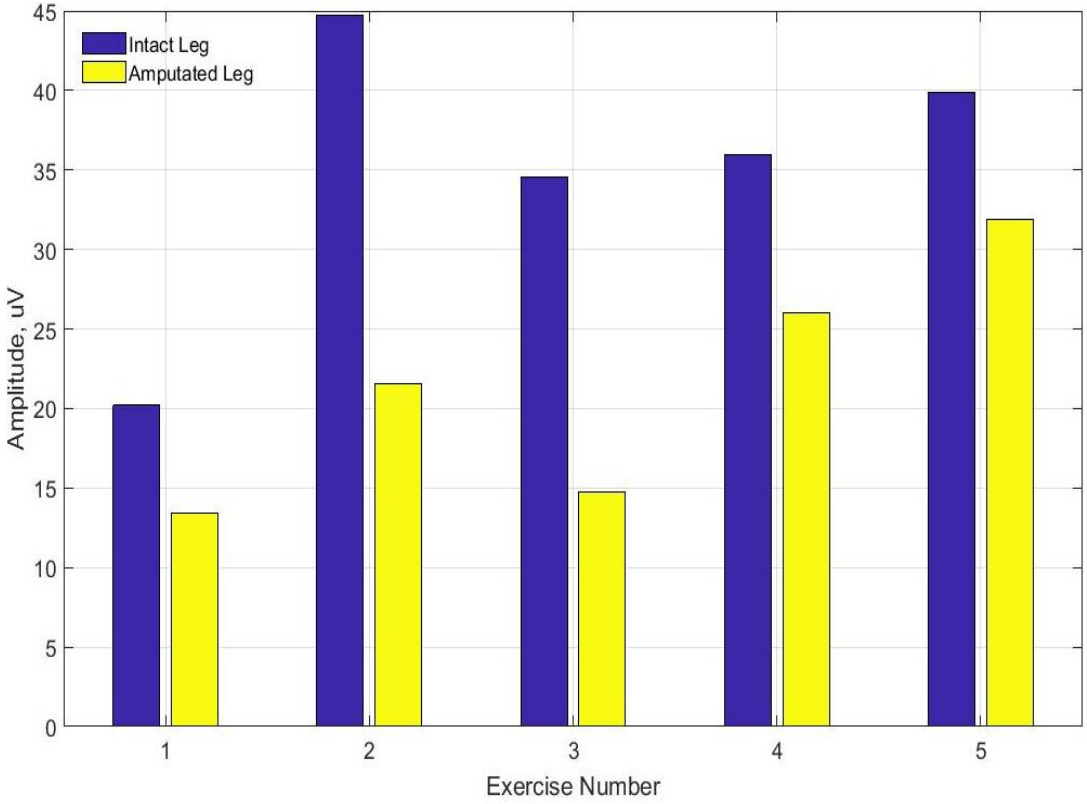

Figure 4.3: Comparison of mean amplitudes of intact leg and amputated leg

4.4.2 Analysis of the plantarflexion movement of the ankle

The EMG signal profile illustrated in Figure 4.1 shows how the plantarflexion movement highly depends on the performance of the Soleus muscle EMG signal. However, in the absence of the Soleus muscle, the Gastrocnemius (Lateralis and Medialis) muscles and the Tibialis anterior muscle were evaluated for their ability to provide meaningful signal features during plantarflexion. Figure 4.4 illustrates the nature of the rectified signals of the available sEMG signals on the amputated leg. There was significant difference ($p = 0.01$) between the features of the Tibialis Anterior and the Gastrocnemius sEMG signal. Figure 4.5 shows the mean amplitudes for the three signals. The mean amplitudes were $27.50\,\mu$V, $26.20\,\mu$V and $16.83\,\mu$V for Gastrocnemius Lateralis, Medialis and Tibialis Anterior respectively. The mean values were for five repeated exercises per participant, and during plantarflexion, the Tibialis Anterior muscle on the amputated leg had a mean value of $31.86\,\mu$V as compared to$50.75\,\mu$V on the intact leg. The amputated leg had a minimum amplitude of $11.93\,\mu$V and a maximum amplitude of $21.14\,\mu$V with a mean value of $16.83\,\mu$V.

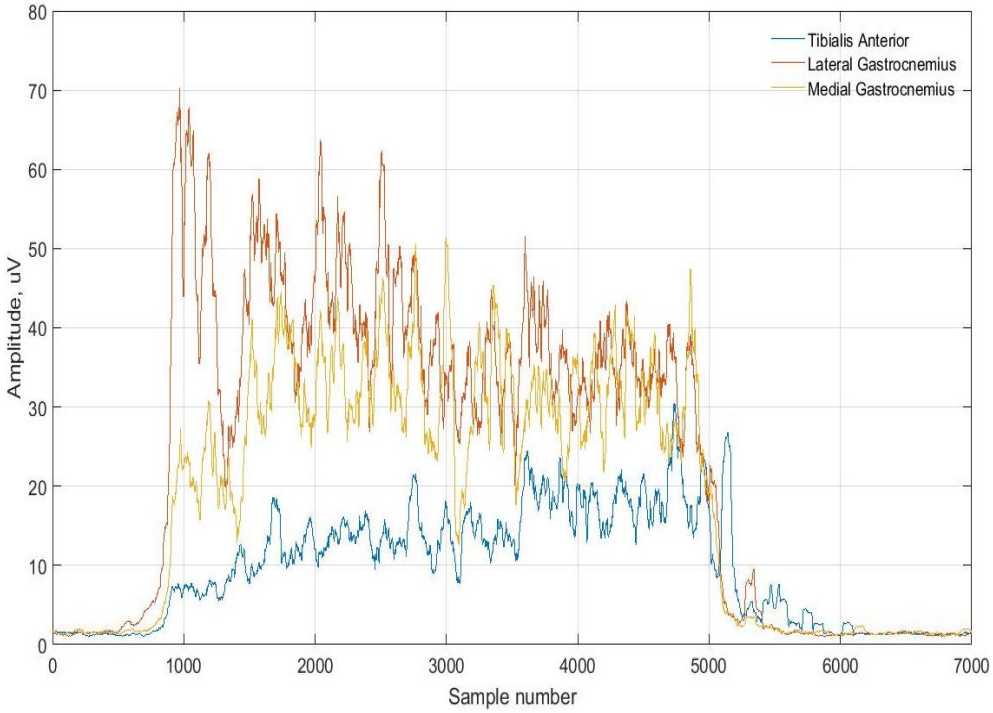

Figure 4.4: Tibialis Anterior, Medial and Lateral Gastrocnemius EMG signals during plantarflexion

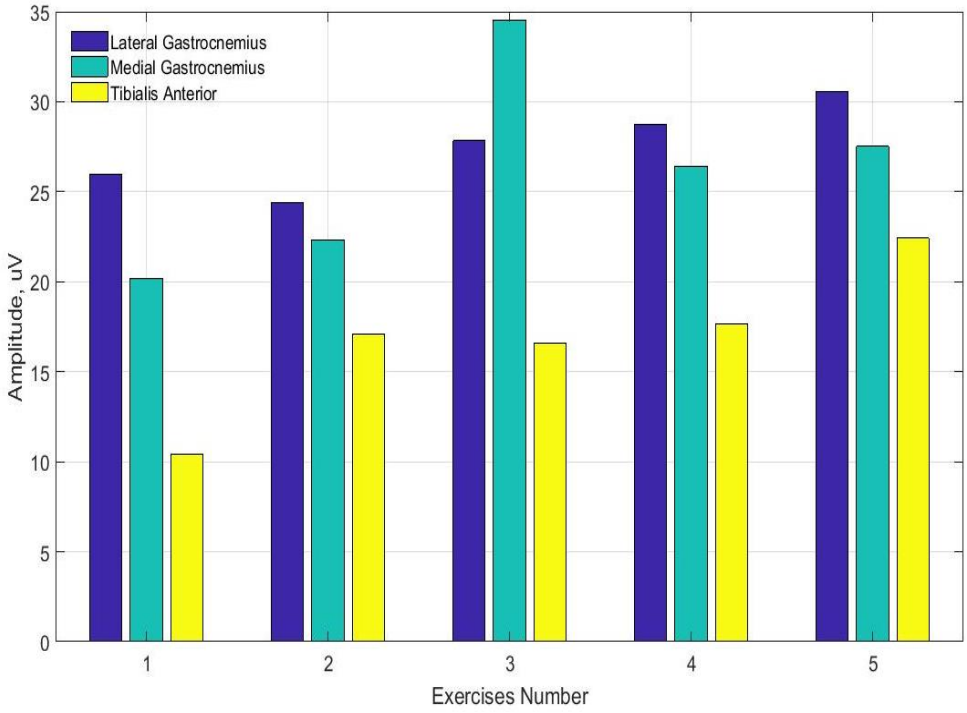

Figure 4.5: Amplitude comparison of Tibialis Anterior, Medialis and Lateralis Gastrocnemius sEMG signals during plantarflexion

4.4.3 Analysis of dorsiflexion movement of the ankle

The myoelectric prosthetic ankle is expected to perform dorsiflexion movement, which is one of the principal movements of the ankle within the sagittal plane. According to the standards for recording surface EMG signals [72], the Tibialis Anterior muscle is responsible for dorsiflexion movement. The frequency features of the Tibialis Anterior is shown in Table 4.1, for both the amputated and the normal leg. The features included the total power bandwidth and mean and median frequency of the signal.

Table 4.1: Tibialis Anterior signal frequency features

Features	Normal Leg	Amputated Leg
Mean frequency	103.9968	70.09102
Median frequency	86.8540	58.8219
99 % occupied bandwidth	372.5115	330.95016
Power bandwidth	1.4599	1.5307

The signal profile of Tibialis Anterior is shown in Figure 4.6. There was no significant difference ($p = 0.12$) between the intact and the amputated leg mean amplitudes of Tibialis Anterior during dorsiflexion. The mean amplitude is $89.38 \pm 11.45\,\mu$V on the normal leg as compared to $73.35 \pm 4.98\,\mu$V on the amputated leg.

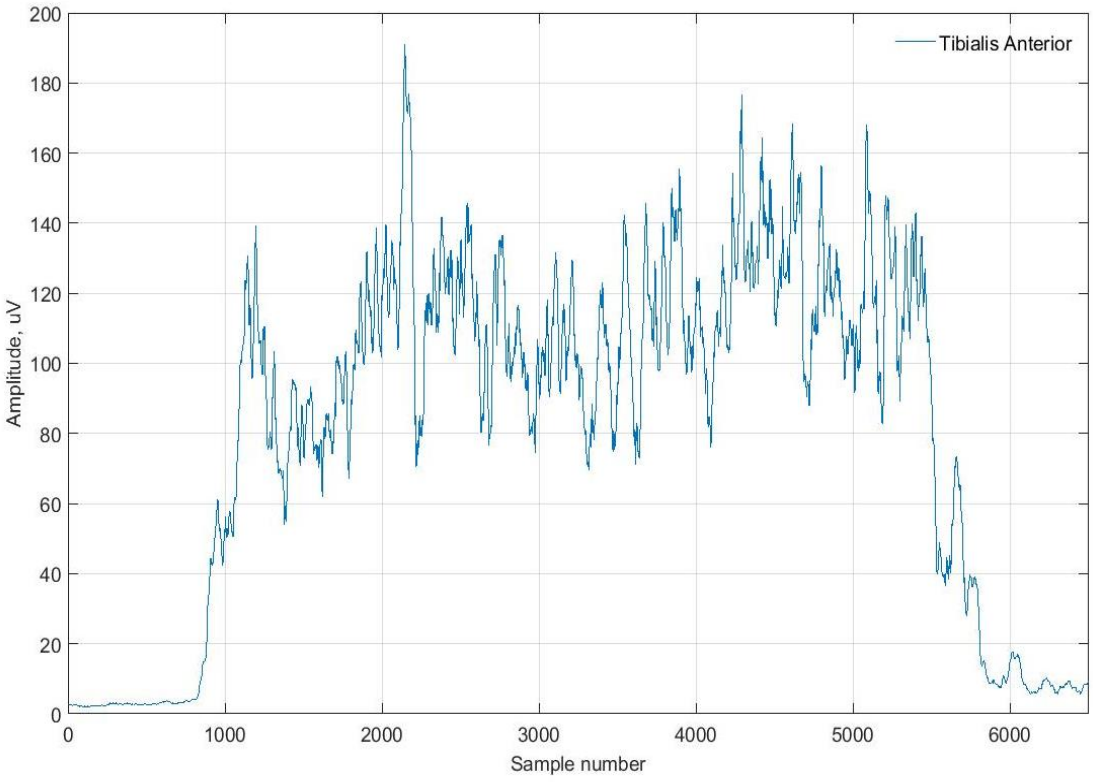

Figure 4.6: Rectified Tibialis Anterior signal profile during dorsiflexion

The signal mean frequency of the amputated leg was 67% of the normal leg. However, there was no significant difference between the 99% occupied bandwidth between the signals. When an overlapping hamming window was considered, the signal strength was distinct as shown in Figure 4.7. The sEMG signal amplitude of the amputated leg is approximately 50% less than that of a intact leg. This would in-turn cause a high demand for amplification and filtering techniques which may cause distortion of the signal.

The results presented in Figure 4.7 and 4.8 indicate that the lower frequencies are dominant in both the Tibialis Anterior muscle and the Medialis Gastrocnemius muscle. The signal power of the Gastrocnemius muscles is nearly half that of Tibialis Anterior during dorsiflexion. However, the results in Figure 4.7 and 4.8 indicate the presence of muscle crosstalk. This may result in challenges during feature extraction, contributing to notable classification errors during pattern recognition.

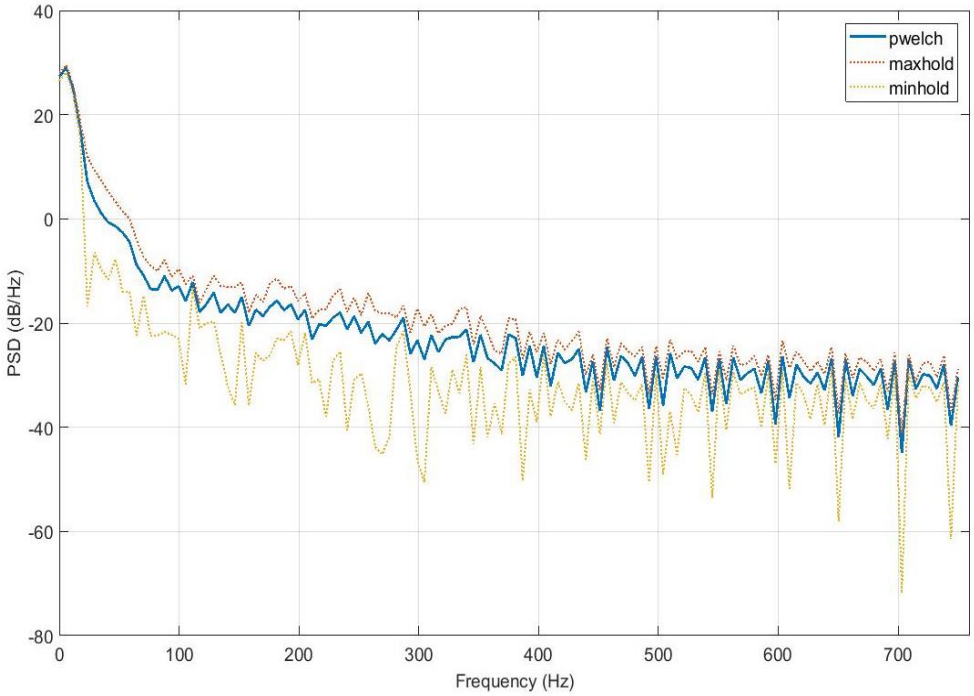

Figure 4.7: Tibialis Anterior power spectrum for dorsiflexion movement on the amputated leg

The peak power of approximately 30 dB/Hz was recorded for the Tibialis Anterior muscle in Figure 4.8, while a peak power of approximately 15 dB/Hz is recorded for the Medialis Gastrocnemius muscle. In Figure 4.8, the peak power of the Gastrocnemius muscles was half the expected power, this indicated the presence of muscle crosstalk emanating from the residual stump's load bearing point where the muscles are attached to the same bone.

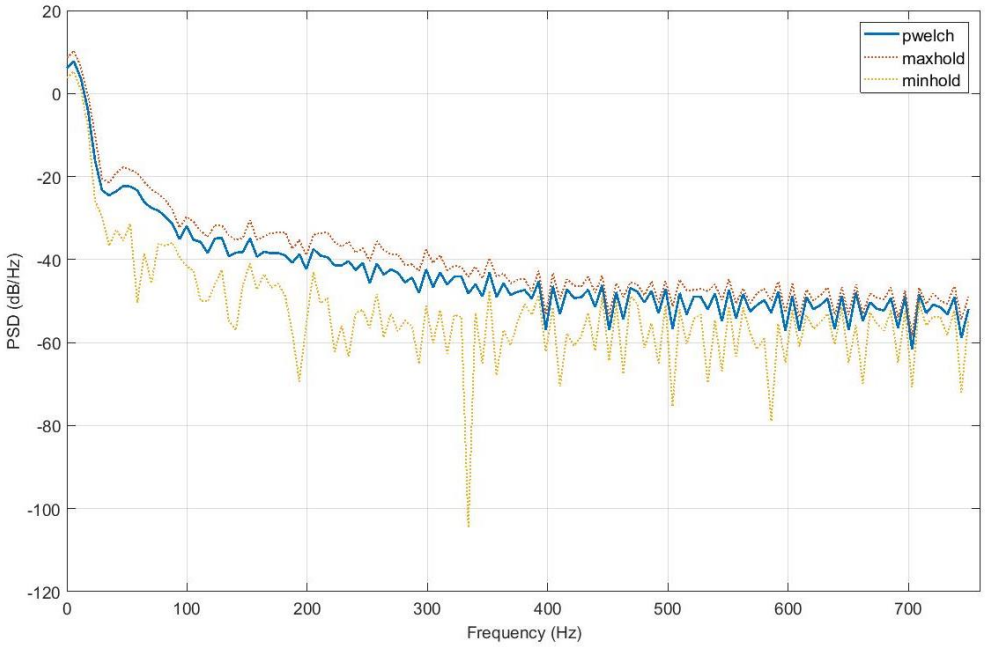

Figure 4.8: Medial Gastrocnemius power spectrum for dorsiflexion movement on the amputated leg

4.4.4 Signal classification feasibility analysis

The signals were tested for their classification feasibility with respect to the extracted features. The Tibialis Anterior muscle was analysed with regard to the generated EMG signals classification capabilities using linear discriminant analysis (LDA). The classification was based on the main time domain features, which were the mean and standard deviation values, and the results are shown in Figures 4.9, 4.10 and 4.11. The Tibialis Anterior and Medialis Gastrocnemius muscles recorded 100% classification accuracy as, shown in Figure 4.12. However, there were challenges in classifying signals from the Lateral Gastrocnemius muscle which recorded a classification error of 0.0769% as shown in Figure 4.11. The error was, however, negligible as the classification accuracy was approximately 99.92%.

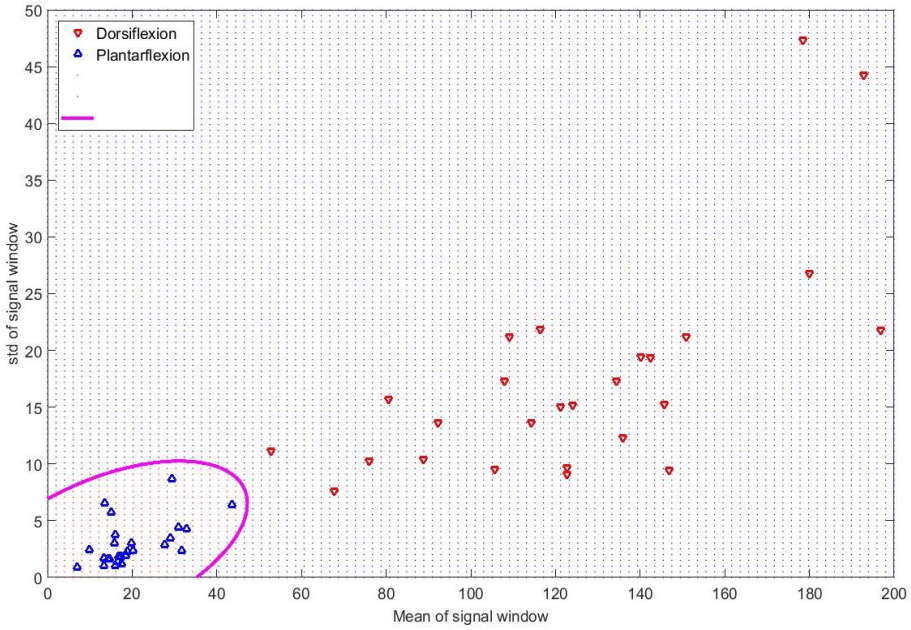

Figure 4.9: Tibialis Anterior EMG signal classification for dorsiflexion and plantarflexion movement

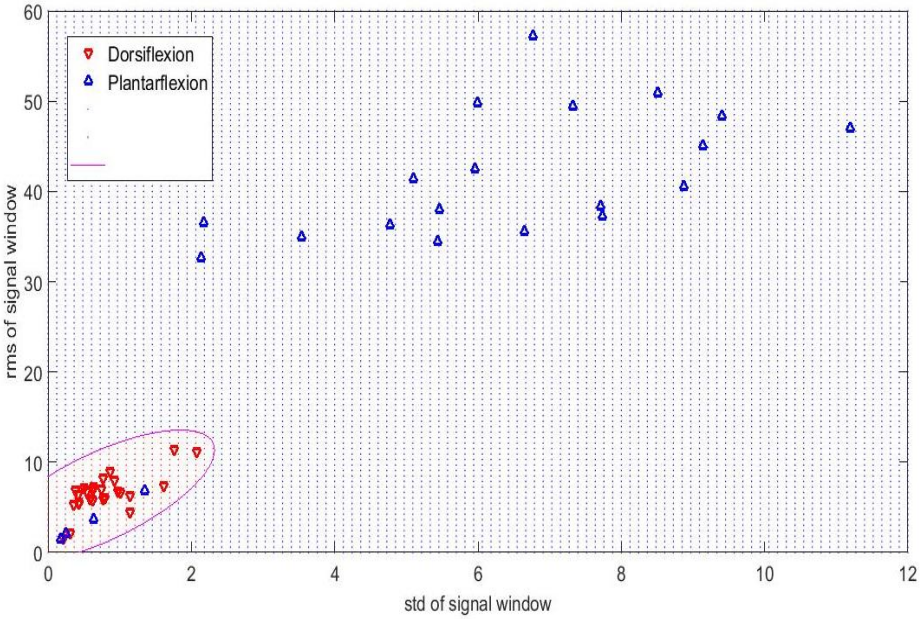

Figure 4.10: Lateralis Gastrocnemius EMG signal classification for dorsiflexion and plantarflexion movement

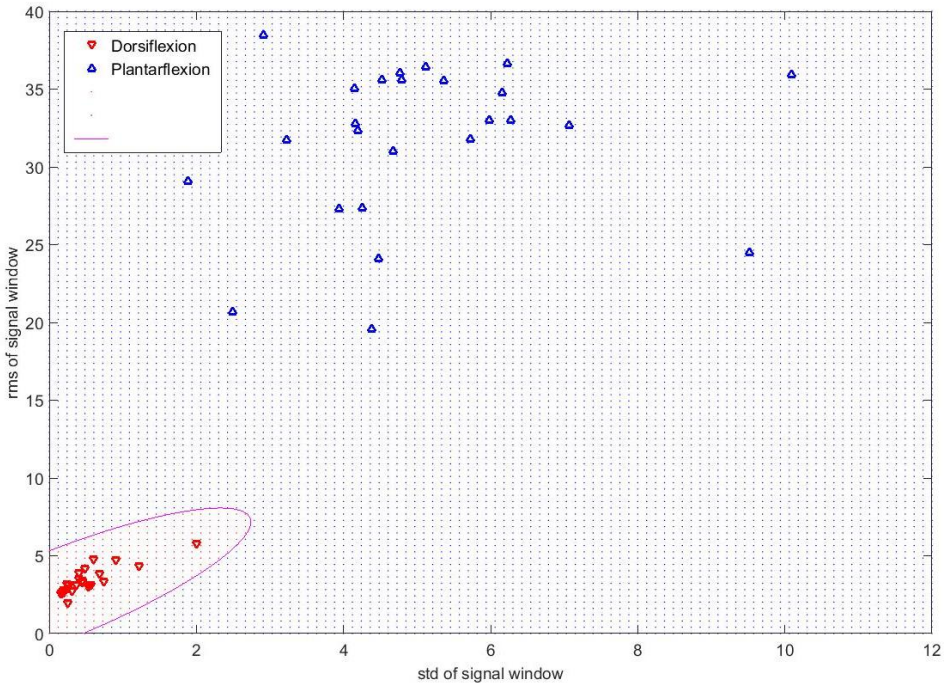

Figure 4.11: Medial Gastrocnemius EMG signal classification for dorsiflexion/plantarflexion movement

4.4.5 Analysis of myoelectric signal behavior during normal gait

The behaviour of the myoelectric signals was evaluated based on the normal gait of the amputee. The objective was to analyse the signal profile of the identified muscles during normal gait. After rectification, bandpass filtering and signal smoothing, the sEMG signal from the Tibialis Anterior, the sEMG was modelled as a rectified sinusoidal signal, as shown in Figure 4.12. The resultant model approximately follows the normal distribution curve characteristics. Although the sEMG signal for a complete stride does not follow perfectly a normal distribution curve as illustrated in Figures 4.12, 4.13 and 4.14, the complete removal of muscle crosstalk and other noise artefacts could result in a good approximation of a bell curve. However, expectations of a normal distribution are such that the mean, mode and median are equal with the curve being symmetrical at the centre. This was, however, a challenge as the swing phase was at approximately 60% of the gait cycle. Therefore, the approximate properties facilitate the use of pattern recognition algorithms as feature extraction becomes easy.

The Tibialis Anterior muscle was activated during the terminal stance, hence the peak value was during the pre-swing phase and a second peak was evident during the toe-off phase. The muscle was deactivated during the mid-swing phase. The mid-swing and the terminal swing events occurred at the lower mean amplitude of $5.72\,\mu$V. The Lateralis Gastrocnemius sEMG signal was initially fired during the mid-swing. However, the peak amplitude was evident during the terminal swing phase, as shown in Figure 4.14. As a result, the muscle firing strength was decreased during the heel strike (initial contact) phase and an average amplitude of $5.03\,\mu$V was maintained during the single support phase. There was no marginal difference with regard to peak amplitudes of the Medialis and Lateralis Gastrocnemius sEMG signal during heel strike, as illustrated in Figures 4.13 and 4.14 respectively. However, the amplitude of the Medialis

Gastrocnemius sEMG signal was notably twice that of Lateralis Gastrocnemius sEMG signal during terminal swing.

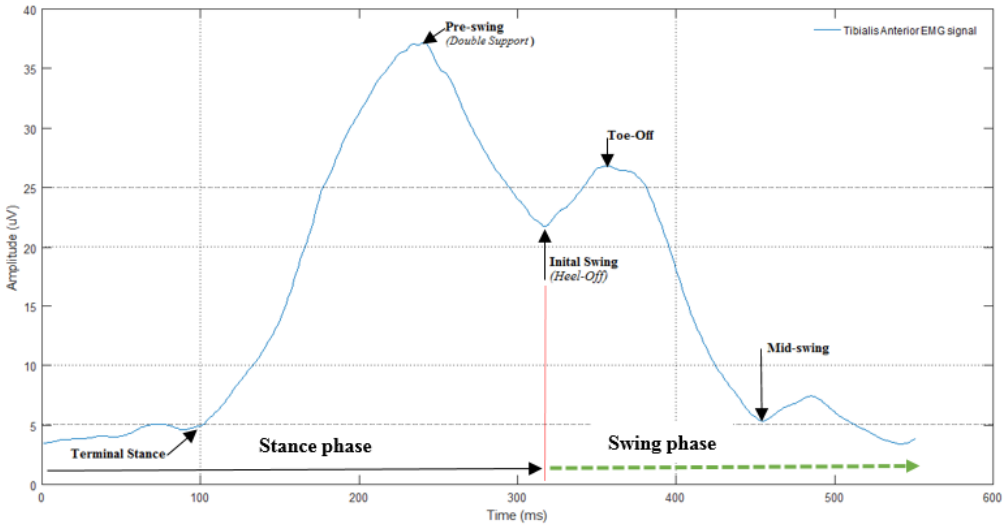

Figure 4.12: The illustration of the Tibialis Anterior muscle EMG signal during normal gait

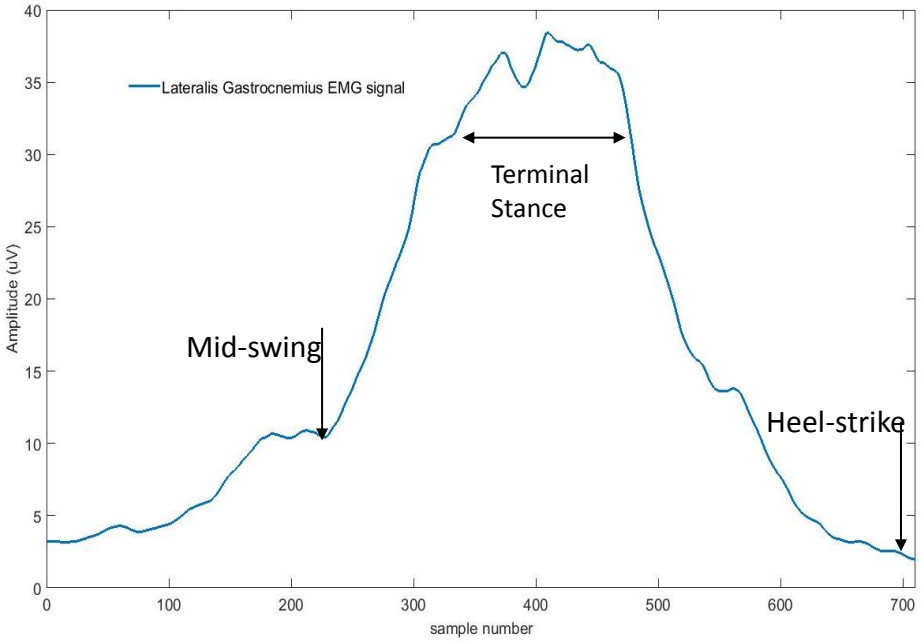

Figure 4.13: The illustration of the Lateralis Gastrocnemius muscle EMG signal during normal gait.

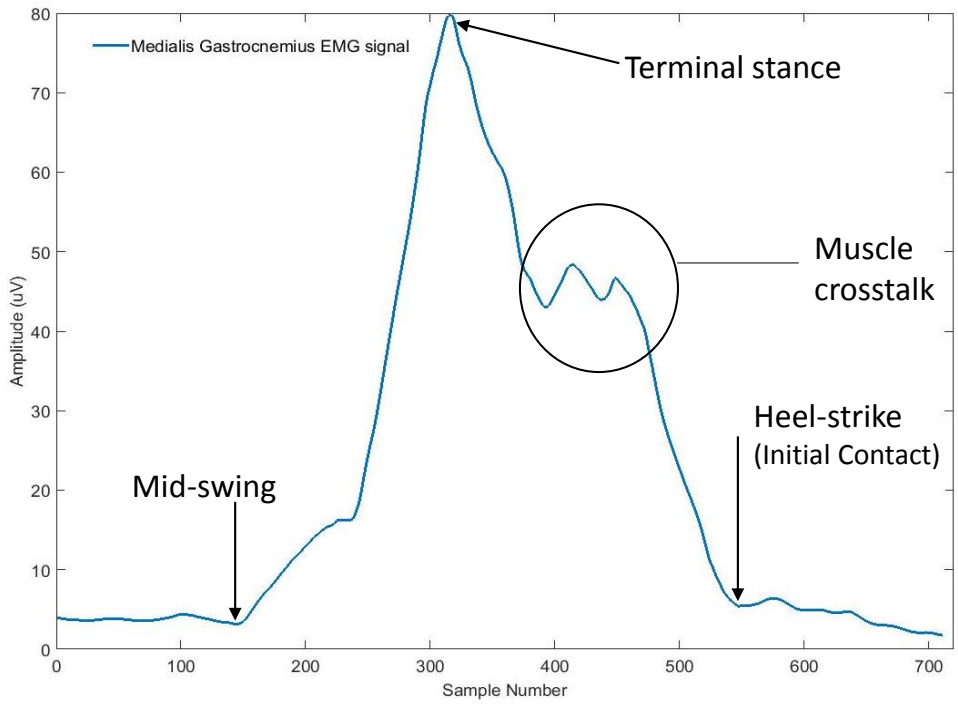

Figure 4.14: The illustration of the Medialis Gastrocnemius muscle EMG signal during normal gait

The analysis of the Tibialis Anterior, Medialis Gastrocnemius and the Lateralis Gastrocnemius revealed that all the muscles were fired during the swing phase. The Tibialis Anterior had its mean peak amplitude at 38.09 μV during the pre-swing phase. The Medialis Gastrocnemius and the Lateralis Gastrocnemius muscles registered mean peak amplitudes of 43.64 μV and 26.56 μV respectively during the terminal phase, as shown in Figure 4.13 and 4.14 respectively.

4.5 Discussion

The current SENIAM and ISEK standards are specifically meant for determination of signal sites and signal characteristics of a sound full-length leg. The majority of the related studies on the characterisation of sEMG signals for myoelectric control were based on normal full length limbs [32],[220]. This has been attributed mainly to challenges that arise when determining the signal characteristics from a residual stump where some of the anatomical landmarks are missing. As a result, this has a negative impact on the commercialisation of myoelectric control architectures since the proposed methods and techniques were not clinically viable.

The results from the study protocol revealed that there is a significant difference ($p = 0.001$) between the signal features from sound legs and amputated legs, indicating the need for the establishment of standards for reporting sEMG signals from amputees. This was mainly because the quality of the signal features was highly influenced by the level of amputation and amputation technique implemented. Pure biological signals are rare, if ever obtained, and methods for noise detection, filtering and signal analysis in both time and frequency domains were evaluated. According to SENIAM standards, the Soleus muscle is responsible for plantarflexion of the ankle [83]. The recommended electrode placement for Soleus [180], [221] is well detailed in the SENIAM standards, however, the recommended electrode location was below the amputation line

and, therefore, this muscle was inaccessible after amputation. As a result, only the Gastrocnemius muscles were available as a source of sEMG signals for plantarflexion.

During the plantarflexion movement, the Medial and Lateral Gastrocnemius muscles were very active with mean amplitudes above 25 μV. A comparison of signal strength between the Soleus from a sound right leg and the available Gastrocnemius muscles from the amputated leg (Figure 4.2) revealed that the available Gastrocnemius muscles only pose an average of 17.04% signal power as compared to the desired value and mean amplitude of 43.73%. This is because the Soleus muscle is not accessible on the amputated leg. Furthermore, there was evidence of muscle crosstalk, as shown in Figure 4.4, between the Medialis and Lateralis Gastrocnemius sEMG signals.

During the swing phase, the Medialis Gastrocnemius muscle fires first, as shown in Figure 4.14. When the Lateralis Gastrocnemius muscle is activated in the later stage of the terminal swing, it causes a signal distortion of the Medialis Gastrocnemius muscle. The Tibialis Anterior and the Gastrocnemius muscles vary in sEMG signal features both during static and dynamic conditions. The signal amplitude for Tibialis Anterior during dorsiflexion on the amputated leg is approximately 50% less than that from the normal leg during the same exercise. The frequency domain features, illustrated in Table 1, also revealed that the mean frequency for the Tibialis Anterior from the amputated leg (70.09 Hz) is approximately 32% less than the sound leg (104.00 Hz).

The 100% classification accuracy achieved on Tibialis Anterior EMG signals was an indication of the capability of the low amplitude signals to be utilised for pattern recognition. The 0.0769% classification error on the Lateralis Gastrocnemius muscle was due to muscle crosstalk with Tibialis Anterior, which occurred during the dorsiflexion movement. The muscle crosstalk may have been inherited from the osteomyoplastic amputation procedure. All the signals are of lower signal strength and amplitude during the swing phase. All three available muscles were not activated during the stance phase. As a result, it would be difficult to predict the stance phase for myoelectric control architectures using the available signal channels. Comparison for the significant difference was done on feature sets and not among individual features, and also between amputees, and there was no significant difference between the signal features from one amputee to the other. Even though variations could be detected among some features, to a greater extent a universal pattern recognition control architecture can be developed for amputees who have undergone the same procedure of osteomyoplastic amputation.

The low mean amplitudes from the amputated leg revealed evidence of low force being produced by Lateralis and Medialis Gastrocnemius muscles during plantarflexion movement. If the implementation of myoelectric control architecture in powered prosthetic lower limbs is to be pursued then efforts have to be made for it to function with the available low amplitude, low energy and low power sEMG signals from the Medialis and Lateralis Gastrocnemius muscles. However, under such conditions, they would be high signal infidelity. The low amplitudes would demand the use of high gain amplifiers to optimise the resolution. Therefore, the low signal power and low signal amplitude would result in the need for a high input impedance system. The DC signal suppression in low amplitudes would thus remain a challenge. The DC component of the signal was caused by skin impedance and chemical reactions between the skin and the measurement electrodes. This resulted in common mode disturbances. However, such signal processing techniques result, in noise being inherent in the control signal, regardless of the implementation

of filters. Therefore, the strength of the signal to be used for the myoelectric control was weak, resulting in the need for more robust pattern recognition algorithms.

4.6 Limitations of the study

The study used a small sample of two amputees mainly due to the lack of availability of amputees who have received similar type of amputation and are living an active life style. However, the number of activities were increased and the length of each activity was also increased in an effort to increase the number of data samples. Instead of using EMG signals from non-amputees, the signals from the sound leg were compared to those of the amputated leg of the same subject. The main reason being that the skin impedance of amputees is significantly different from that of non-amputees. In order to increase the efficacy of the study and to provide more generalised recommendations, there is a need to increase the number of amputees of same age group with similar amputations. However, the findings were conclusive in the determination of signal qualities on amputated legs. The effect of residual muscle activation performance on signal amplitude and frequency both in the time and frequency domain were also determined.

4.7 Conclusion

The study revealed that there are sEMG signals present on the residual limb after amputation. However, there were significant differences in signal features. As a result, their signal strength was much lower than that of non-amputees. Tibialis Anterior, Medialis and Lateralis Gastrocnemius sEMG were still active on the residual limb. However, the Soleus muscle was not accessible as a source of the myoelectric signal. Furthermore, myoelectric signals were classified during dorsiflexion and plantarflexion movements.

When the amputation surgery is carried out as a rehabilitation procedure, it usually takes into consideration the ability of the residual stump to heal fast and also to be able to be interfaced with the socket of the prosthetic limb. Emphasis is also mainly on the load-bearing points of the stump. However, less attention is given to the need to harvest sEMG signals from the amputated leg. As a result, it was a challenge to achieve reasonable signal features from the residual muscles. When the muscles are cut and shortened during the amputation procedure, the resulting contraction strength of the muscles is also reduced, resulting in reduction of the usable signal features. During osteomyoplastic amputation, some muscles are joined together resulting in muscle crosstalk during the acquisition of myoelectric signals. Furthermore, there were active myoelectric signals at the residual stump which are characterised by high level of noise due to muscle crosstalk and the skin at the stump was too loose, thereby resulting in electrode movement. The success of myoelectric control systems for lower limb rehabilitation is highly affected by poor signal features. Leading to the growing demand of robust and adaptive pattern recognition systems as compared to simple logic threshold systems. These new generation pattern recognition systems would be capable of dealing with imprecise and partial features.

Chapter 5

Investigating the effects of a passive mechanical ankle

Published Journal article [1]

5.1 Introduction

There are basically four standard requirements for gait, which are equilibrium, locomotion, musculoskeletal integrity and neurological control [222]. However, as a result of amputation, amputees often struggle to achieve all these basic requirements leading to limited ambulatory-related activities. According to [223], transtibial osteomyoplastic amputees, often recover their mobility capabilities earlier than transfemoral amputees mainly due to the presence of the knee. During rehabilitation, different surgical procedures are usually applied depending on the cause leading to the amputation [224]. These methods include long posterior flap (Burgess and Brackner technique), anterior/posterior fish mouth flap, sagittal flap, skewed flap and Ertl procedure [224], [225]. In general the technical aspects which are highly regarded during the aforementioned surgical procedures include nerves, bone, haemostasis, skin and muscle flaps [226].

Each technique has its own advantage, hence none of the proposed procedures was regarded as more superior or more highly recommended than the other. An amputee can receive a short, average (medium) or long amputation with respect to the position of amputation along the lower limb. When selecting the level of amputation there is a trade-off between increased function of the more distal level versus decreased complication rate with more proximal level [227]. As a result, as the level of amputation moves proximally, the walking speed of the individual decreases and ultimately the oxygen consumption increases. Therefore, the level of amputation has a direct impact on the recovered gait for lower limb amputees.

The motivation for osteomyoplastic amputation is the need to develop a residual limb for an amputee who is highly involved in ambulatory related activities. Therefore, there is bone bridging between the tibia and the fibula resulting in a more stable end bearing limb [225]. The loss of ankle mortise causes fibular instability. However, the myoplasty technique brings about stability of the residual limb [228]. Furthermore, the blood flow and recovery of normal length-tension of

[1] Garikayi, T., Van den Heever, D. and Matope, S., 2017. Investigating the effects of passive mechanical ankle on unilateral osteomyoplastic transtibial amputees. *Journal of Musculoskeletal Research.* Vol. 20, No. 3 (2017) 1750015 (13 pages)

the muscles is also improved [225].

This study investigated the temporal variables, anatomical and orientation angles during normal gait for lower limb amputees. Quantitative gait analysis was used to determine possibilities of long and short term health effects.

5.2 Methods and materials

The subjects, experimental set-up, data acquisition and statistical analysis used for the design under study in this section was outlined in section 3 and the detailed procedure is on sections 3.7.3 and 3.7.4. The Noraxon MR3 normative data with regard to gait analysis was also used in this study. The MR3 database at the Human Motion Analysis Unit was a compilation of able bodied subjects performing normal gait within the same laboratory and having the same ranges of age, height and weight ranges with the amputee participants. The design specifications were based on the results extracted from the experiments carried out using Vicon Nexus II Motion System, as explained in section 3.7.3.

5.3 Results and discussion

The spatial-temporal and kinematic measurements have been useful in the analysis of gait parameters [229]. The objective was to determine if there are any gait anomalies on unilateral amputees as a result of using passive mechanical prosthetic ankles. Therefore, the distance variables and anatomical angles were evaluated. The use of state of the art recording equipment, such as the Noraxon MyoMotion System and processing the data in MR3, minimised the need for excessive filtering. The results presented in this section are categorised as distance variables, orientation and anatomical angles. A t-test was performed on all the distance variables, anatomical and orientation angles so as to determine the significance of the study and the significant difference between the amputees and the normal subjects.

5.3.1 Analysis of distance variables

The results presented in this section include cadence, velocity, stride time, stride length, step time and stance, as illustrated in Table 5.1. These parameters were evaluated so as to determine anomalies using a benchmark of normal ambulators and knowledge of gait. The results of the t-test are presented in Table 5.1.

Table 5.1: Average and standard deviations of temporal distance factors

Item	Parameter	Unit	Normal Value	Average Amputee Value	p-value
1	Cadence	$steps/min$	110	107.23 ± 3.50	0.211
2	Velocity	m^{-s}	1.5	1.41 ± 0.07	0.088
3	Stride time	s	5.6	5.60 ± 0.18	1.00
4	Stride length	m	0.8	0.79 ±0.03	0.878
5	Step time	s	1.12	1.13 ± 0.05	1.876
6	Stance phase	gait % cycle	60	59.00 ±2.58	0.562

The results presented in Table 2 revealed that there is no significant difference ($p > 0.05$) with respect to distance variables for normal subjects and amputees. Such results were also reported in previous studies [193]. However, there was evidence of unequal step length with respect to the amputees, resulting in an asymmetrical gait. The amputees were able to perform all ambulatory activities and hence achieve the same results as the normative data from the MR3 system, despite minimum variations. The step size was reduced each time the amputated leg with the prosthetic attachment was used as the leading leg. The difference was approximately 0.15 m, therefore it was too small to be significant ($p = 0.878$). Furthermore, the stance time on the amputated limb was slightly lower than on the normal side, resulting in limited stance time and early swing. The amputees exhibited decreased cadence as compared to normal subjects as a result of the reduction in self-selected walking velocity. However, the 2.8% decrease in cadence caused no significant difference in the walking velocity ($p = 0.211$) of the amputees.

In previous studies, it was shown that healthy subjects have the unique capability of utilising the dorsiflexors and plantarflexors to reduce the dorsiflexor moment at heel strike so as to rapidly reach foot-flat, resulting in an early stance. However, the stiff ankle on mechanical prosthetic limbs used by amputees generated an extended moment which affects the transition from stance to early swing gait phase.

The reduction in stance time was as a result of reduction in the time taken during mid stance (single support) as the amputee avoids loading the amputated leg for a long period of time. The load bearing positions of the residual limb were sensitive to increased load, hence the stance phase occurs at 58% during the gait cycle.

5.3.2 Analysis of anatomical angle parameters

The anatomical angles investigated include the hip, knee and ankle for the unilateral amputees. The two-sample t-test was performed assuming unequal variances. The results prompted further investigations into the gait cycle of the amputee as there existed a significant difference (since $p < 0.05$) between the gait of a normal subject and that of an amputee. The results presented in Table 5.2 indicated that there is significant difference between the amputee and the non-amputee normative data with respect to hip flexion-extension, knee flexion-extension and the ankle dorsiflexion-plantarflexion movements. The significant difference ($p = 0.0060$) recorded on the ankle inversion is as a result of a lack of an intuitive control of the prosthetic limb by the user. The prosthetic limb orientation was being governed by the stiff ankle mechanism, hence the only possible motions were along the sagittal plane.

Table 5.2: t-test: analysis of anatomical angles

Item	Movement	p - value
1	Hip flexion	0.0290
2	Hip abduction	0.0001
3	Hip rotation	0.0010
4	Knee flexion	0.0020
5	Ankle dorsiflexion	0.0300
6	Ankle inversion	0.0060
7	Ankle abduction	0.0400

The analysis involved evaluation of the hip flexion-extension, pelvis tilt and dorsiflexion-plantarflexion movement of both the amputated and the sound leg as follows:

- *Hip flexion-extension and the pelvis tilt*

The hip flexion recorded a mean peak of 36^0 on the amputated left leg as compared to the mean peak of 25^0 on the amputee's intact right leg, as shown in Figure 5.1. The 44% additional flexion was as a result of the amputee's effort of trying to compensate for the lack of propulsion force on the passive ankle during toe-off. The plantar flexors were absent on the amputated leg, hence the quadriceps assisted in achieving the toe-off position. The hip forms the basis for human gait as it generates the power for all the movements. Previous findings also suggested that the excess hip abduction and flexion will result in unstable lumbar movements leading to a decrease in gluteus medius and internal oblique activity [230].

The changes in hip flexion-extension angle as the gait cycle progresses is illustrated in Figure 5.2. There was an early swing phase due to limited stance phase with regard to the amputated leg, this is illustrated in Figure 5.2 and also compliments the values of the stance phase in Table 3, although this was insignificant ($p = 0.562$). The basic function of the lateral pelvic tilt (pelvic obliquity) is to control the vertical excursion of the centre of mass. The lateral pelvic tilt is important as it lowers the centre-of-mass, hence causing a decrease in energy expenditure [231]. Similar effects of pelvic tilt on acetabular retroversion were also reported in literature [232]. The poor range of motion of the hip during flexion and extension as illustrated, in Figure 5.2, is as a result of poor propelling force during heel-off and toe-off events. The mechanical ankle is stiff and provides limited propulsive force during these events. Therefore, the excessive hip tilt has adverse short and long term effects to the amputee's health and well-being.

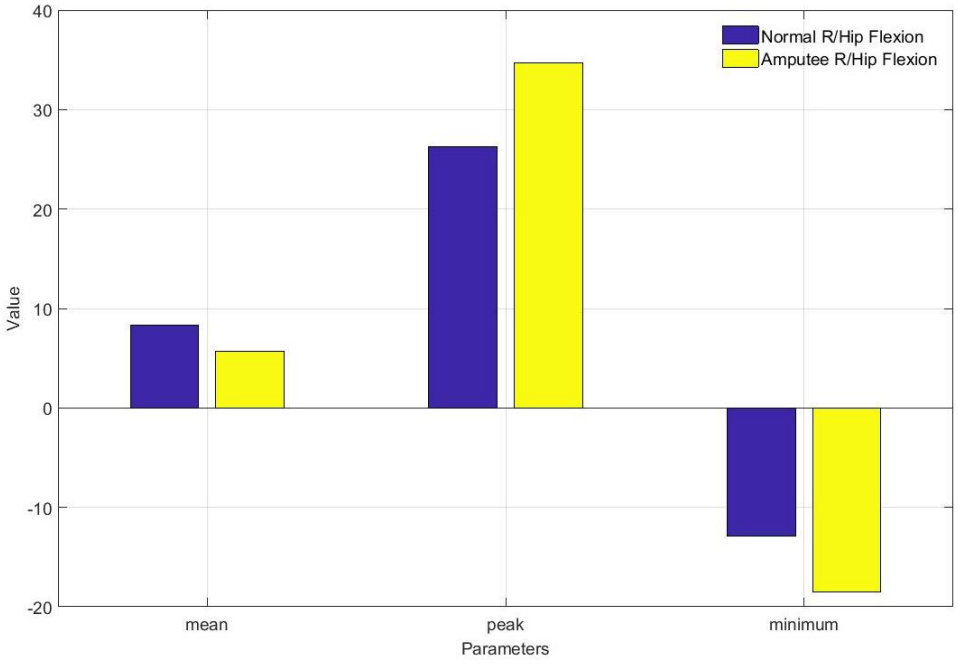

Figure 5.1: Illustration of the hip flexion-extension mean, peak and minimum values

The lack of hip extension during the terminal stance, as illustrated in Figure 5.2 was mainly attributed to lack of balance which is usually provided by the dorsiflexors and plantarflexors: these were absent on the amputated limb. The hip rotation in Figure 5.2 exhibited poor range of motion during the stance phase with a 60% deviation from the mean of the normal subjects. The poor hip rotation was due to the dragging of the affected limb resulting in the circumduction of the hip.

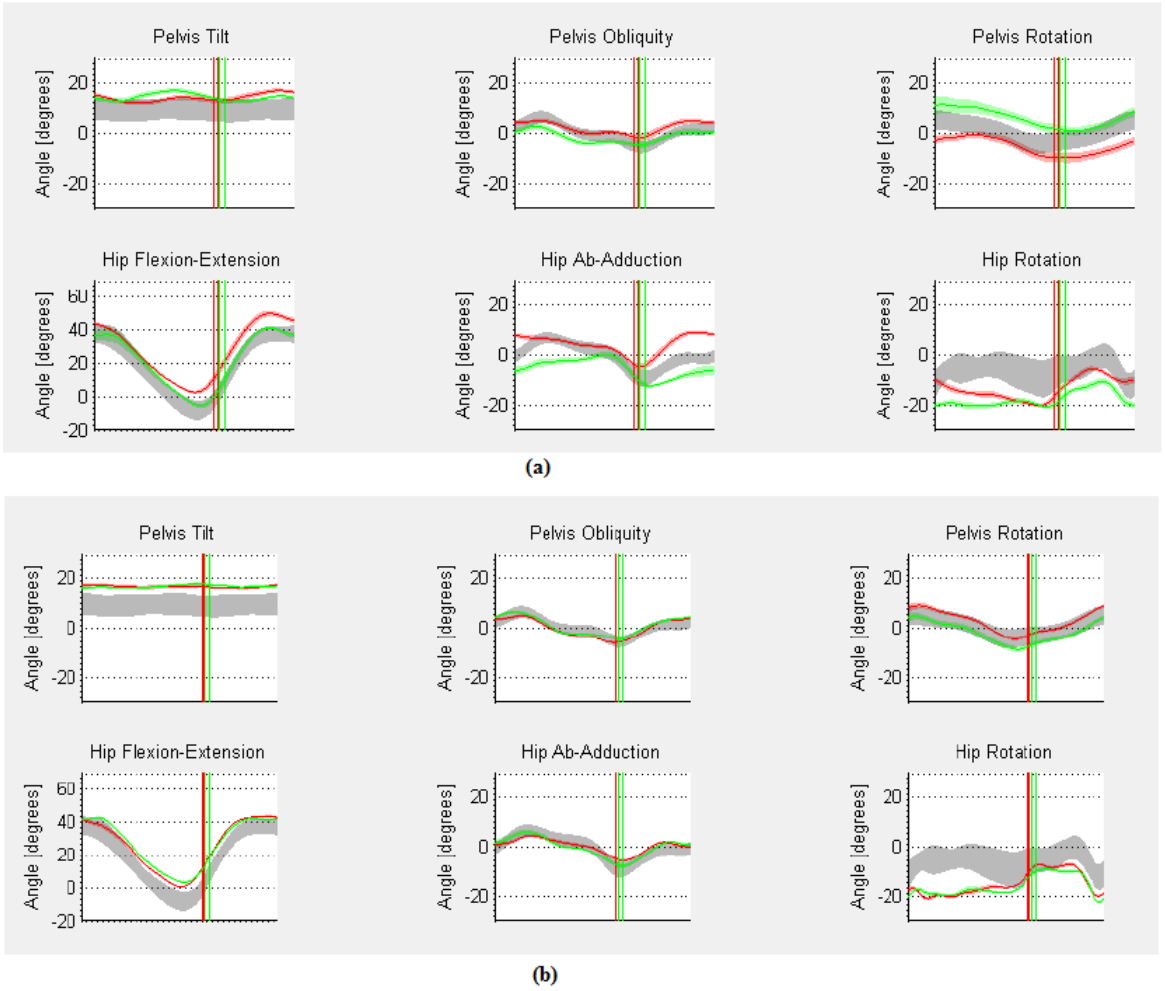

Figure 5.2: Hip flexion-extension and pelvis during normal sagittal gait for amputee participant 1 (a) and Amputee participant 2 (b). The grey band is the normative data: mean $\pm$ 1 SD, the red line is the amputated leg and green line is the intact leg

The mean hip flexions during the terminal stance for both subjects were well above 42^0. This was as a result of the amputee leaning on the unaffected leg so as to create sufficient heel clearance. This may result in posture challenges since posture is adapted from the hip. Taking into consideration that the hip flexors connect the femur to the lower back, the excessive use of the flexors may result in lower back pain [231]. The limited range of motion in hip extension contributes much to the long term development of anterior pelvic tilt [233]. Thus, there is a need to have a complete range of motion for the hip flexion and extension as a way of postural

correction and of limiting the causes of lower back pain [234].

The mean pelvis tilt for the amputees was 18^0, that is a 50% deviation from the expected mean of 12^0. The expected pelvic tilt is 5^0 to 18^0 with 12^0 being the average and 18^0 being the worst case scenario in most cases. During normal gait, the pelvis was expected to oscillate along the z-axis between -2^0 and 6^0. However, due to the compensation within the hip flexion, the oscillation shifted gradually towards the 2^0. The pelvis tilt is mostly used to identify the possibility of gait anomalies and their relationship to short and long term effects on the spinal cord [235]. The lateral pelvis tilt is controlled by the hip abductors of the stance leg. As a result, there is notable change in lateral tilt, as shown in Figure 28 when the amputated leg is within the stance phase.

Pelvis tilt is an important parameter to determine the possibility of lower back pain in the future for most amputees. The most important parameter is the pelvic anterior tilt; however, during the gait, only the pelvis pitch, roll and yaw were monitored as orientation parameters. Therefore, the tilt was derived from these three parameters. The status of the hip flexors and the hamstrings determine the level and type of tilt which may result. The hip flexors were affected by the excessive hip flexion and hip extension, the hamstrings were affected mostly by the excessive knee extension and flexion. However, the extreme changes in the pelvis affect the degree of lumbar lordosis [236]. This may result in lower back pain. Similar results were recorded on trunk kinematics analysis revealing an asymmetrical gait due to compensatory mechanisms based on 54 subjects [237]. These compensatory mechanisms put the lumbar spine under immense stress [232].

- *The knee flexion-extension analysis*

The knee angle has a direct effect on velocity and other distance variables. The status of the knee angle is illustrated in Figure 5.3 during the normal gait. The knee angle achieved the expected range of motion for the amputees. However, these achievements were as a result of excessive knee flexion rotation. The results presented in Figure 5.3 show that there is neither excessive extension nor excessive flexion of the knee. However, during the early stance there is evidence of extension when flexion is expected and also a poor range of motion with respect to knee rotation.The poor range of motion and excessive rotation has an adverse effect on the patellofemoral joint [238]. The principle role of the knee is to allow movement and stability by absorbing, transmitting and redistributing forces. However, such excessive rotations will affect the performance of the knee resulting in long term health effects related to joints.

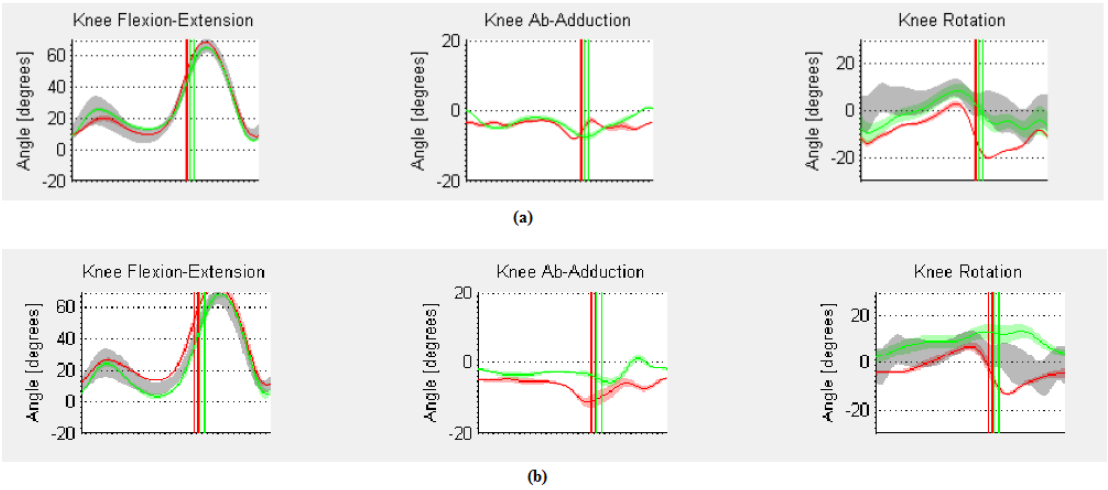

Figure 5.3: (a) Knee extension-flexion during normal gait for amputee participant 1 and (b) amputee participant 2. The grey band is the normative data: mean $\pm 1SD$, the red line is the amputated leg and green line is the normal leg

- *The ankle dorsiflexion and plantarflexion analysis*

The ankle dorsiflexion and plantarflexion plays an important role during the toe-off period and assisted in moving the body mass forward, as shown in Figure 5.4.

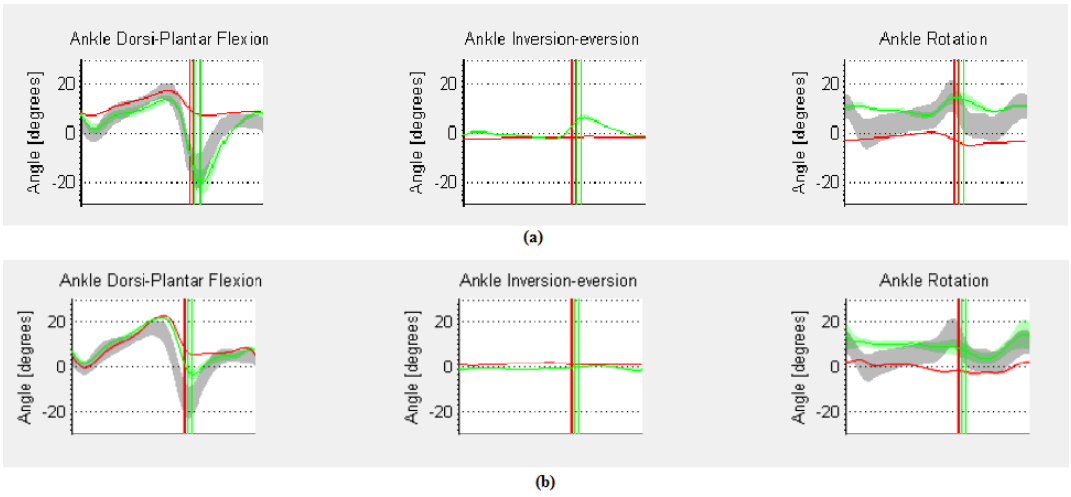

Figure 5.4: (a) Ankle movements for amputee participant 1 and (b) Amputee participant 2. The grey band is the normative data: mean ± 1 SD, the red line is the amputated leg and the green line is the normal leg

However, in amputees the passive ankle does not achieve much. The amputated leg does not even achieve 25% of the expected range of motion during both the dorsiflexion and the plantarflexion for both amputees, as shown in Figure 5.4. As a result, the intact limb of the subject will be used to develop compensation for moving the mass of the body forward. The plantarflexion movement experienced during heel-strike provides balance and smooth tibia projection. Using

the phases suggested by [229], the lack of power absorption between 5% - 40% of the stride at the ankle on the amputated leg results in the excessive hip flexion on the normal leg due to contraction of the plantarflexors. The absence of the flexible and adaptive ankle results in the lack of power generation by the ankle during the 40% - 60% stride cycle. When addressing long term effects associated with asymmetrical gait, foot alignment is a major contribution, hence the ankle dorsiflexion and plantarflexion angles should be monitored [239]. The lack of power absorption from initial contact to approximately 15% of the stride on the amputated leg results in the absorption of power within the socket, thereby increasing the risk of bruises on the contact surfaces.

The minimum, maximum and mean angles of the amputee have exceeded those of the non-amputated leg in all respects, as shown in Figures 5.5. The results revealed that the mechanical prosthetic ankle was exceeding expected angles as a way of compensating for poor hip flexion and extension as the lack of intuitive control of the device leaves the user with no control over range of motion. The four-bar ankle linkage model suggested by, [240], shows that the calcaneofibular ligament and the tibiocalcaneal ligament provides stable and controlled dorsiflexion for the proper positioning of the ankle as a result of the Tibialis Anterior muscle activation.

The subtalar movement permits the foot to change from being flexible to a rigid structure during normal gait, thereby assisting as a rigid force lever for force transition. However, the passive ankle could not achieve such transformation, as illustrated in Figure 5.5, during the early swing phase at 58% gait. The double support occurred late in the gait cycle, as illustrated in Figure 5.4. The decrease in the double support time shows evidence of notable balance disorder. The step duration varied depending on the side being measured; however, comparing the amputated leg and the intact leg, the duration decreased with respect to the amputated leg.

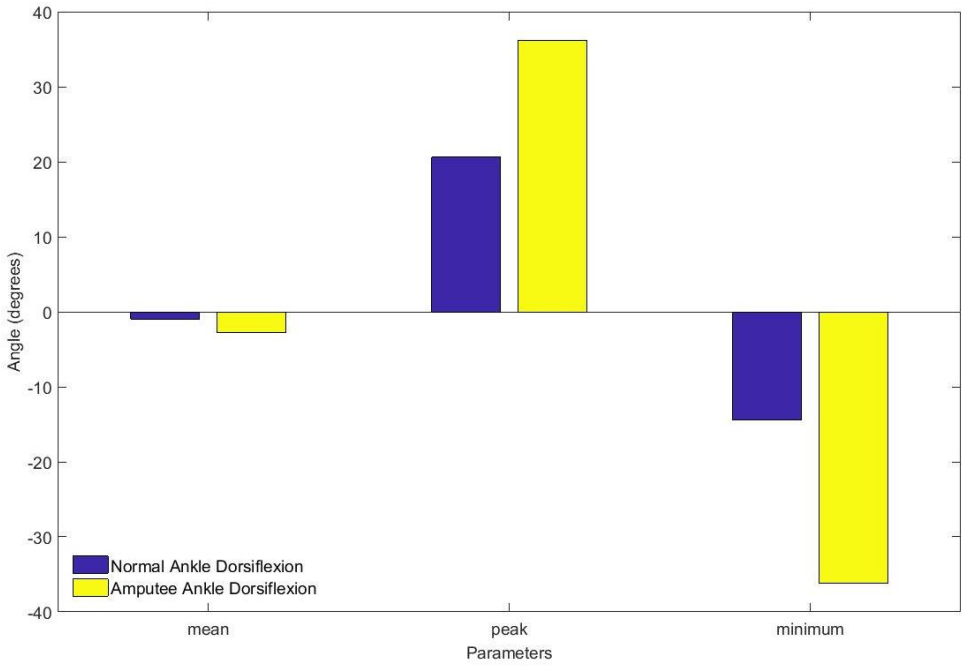

Figure 5.5: Dorsiflexion-plantartflexion Amputee minimum, maximum and peak angles

5.4 Limitations of the study

The amputees were using prosthetic limbs manufactured from two different suppliers. The extent to which this has impact on the amputee's gait was not evaluated as the devices could not be interchanged between the amputees as they were custom made. However, same Prosthetist was used to fit the passive prosthetic limbs and his recommendation was that they were fit for purpose. Even though the amputees did not report any difficulties on using the prosthetic limbs, the swelling of the stump was noted at the end of every two hour walking session. The sample of participants was small (two amputees), however, the number of gait activities was increased per amputee and the number of days were increased in an effort to increase the number of data sets for statistical analysis. A comparison was made to previously completed studies [241], [242], [243]. The small sample has an effect on diagnosis studies, but has less significance when a patient specific device is being designed. In this study, the analysis of the signals were only meant for determination of signal quality in order to develop design specifications.

5.5 Conclusion

The experimental study revealed that the use of stiff mechanical prosthetic ankles causes asymmetries in the gait cycle leading to possible lower back pain injuries and bruises on the load bearing points of the socket. There is no significant variation in stride duration, cadence and step size between the amputee data and the normative results. This may have been attributed on the fact that the amputees were well aware that they were under investigation, resulting in proper movement within the laboratory. The amputees had a great desire to achieve walking capabilities, hence they usually achieved these distance variables regardless of the type of artificial limb being used. However, the short term effects of such efforts are bruises at the load bearing surfaces of the residual stump.

There is poor range of motion (ROM) management on the knee flexion/extension and also on the hip extension. This can affect the psoas muscles which are directly connected to the five lumbar vertebrae. Therefore, this may also result in anterior pelvic tilt. The long term effects of anterior pelvic tilt includes hip pain, lower back pain and flat foot on the non-amputated leg. The fundamental principle is that the lumbar is affected by the action of the hip flexors which are monitored by means of the hip flexion angle. This could have an adverse effect on the anterior pelvic tilt which may lead to long term effects of lower back pain. Furthermore, the continual gait asymmetries may lead to difficulties in walking, thereby causing significant health problems. The asymmetries in gait may be due to injury, pain or tissue damage that may result in musculoskeletal, cardiovascular, pulmonary and physiological problems for the amputees.

Therefore, there is a need to develop an active prosthetic limb which is capable of achieving the desired dorsiflexion and plantarflexion movements intuitively. The active ankle should have a control architecture that is capable of predicting the position of the limb in space during the gait cycle and ultimately minimising anomalies in the gait cycle. Robustness and adaptability should be the key characteristics of the control system of the active prosthetic ankle so as to adapt to changes in body weight, height and posture of the amputee, thereby minimising deviations from normal gait.

Chapter 6

Development of an activity prediction system

Published as conference proceedings.[1]

6.1 Introduction

The functionality of a device is regarded as its suitability for a specific task [244]. However, the means of determining the suitability of prosthetic limbs in developing nations has currently been a challenge. Most prosthetic lower limbs in developing countries are not tested using proper gait analysis equipment once fitted. This is due to the cost associated with the analysis and the limited availability of the resources in some of the remote areas [7]. As a result, it is assumed that once the prosthetic limb fits well on the amputee, then it will perform as expected.

The leg is regarded as the lower limb of the human being [245] and by monitoring the segments of the leg, one can monitor the activity of the human being. It has long been reported that active powered prosthetic limbs use sEMG signals and orientation sensors to predict the human intention [246]. However, the clinical applicability of this technology is limited due to lack of sensor fusion techniques and proper supporting hardware. At times the reported results were based on the experiments carried out using smart-phone data recorded on able-bodied participants and, in some cases, the feasibility was simply based on classification accuracy of the data recorded. The challenges concerning the hardware development and real-time data acquisition are yet to be fully reported. Issues of sensor calibration, mounting and reliability are not present in most reported results.

Electromyography signals have been successfully analysed for clinical diagnosis, however, their applicability in the control architectures is still a cause for concern [31], [30]. The previous study reported in section 4.3.1 revealed that after amputation not all muscles are available for myoelectric control [132]. The EMG signals are either too weak to overcome noise interference, or they are simply a result of muscle crosstalk, leading to certain stages of gait being difficult to predict using the available muscle signals. The Soleus, Tibialis Anterior, Medialis Gastrocnemius and Lateralis Gastrocnemius are responsible for the ankle movements concerning dorsiflexion and

[1] Garikayi, T., Van den Heever, D. and Matope, S., 2016. *Development of a rehabilitation activity monitoring system for transtibial amputees.* Proceedings of the South Africa Institute for Industrial Engineering Conference, 27-28 October, Stonehenge, Parys, South Africa, (p.177-190).

plantarflexion. As reported earlier, during toe-off or pre-swing only the Soleus sEMG signal was active, but this muscle was not accessible on the residual stump. Another stage of concern is the initial swing whereby only the tibia is activated with approximately 30% strength signal as compared to the non-amputated leg, leading to possible classification errors during actuation of the powered ankle.

According to [247], the major drawback that existed in the 1990s' designs was the need for visual attention by the amputees when using powered limbs. There was less use of feedback systems and, as a result, this increased the involvement of the amputee with the functionality of the device. The same sentiments were echoed by [30] for the current designs with regard to lack of acceptable functionality. Therefore, challenges there still exist on achieving a total intuitively controlled prosthetic limb. These challenges result in limited dexterity of most available powered limbs, resulting in low acceptance level by the amputee community [247], [30]. Therefore, there is a need to develop a more reliable intent recognition system which will make use of both surface EMG signals and other additional sensors, such as the inertial measurement unit (IMU) sensors and force sensitive resistors or mechanical sensors [246]. The IMU sensors will have the capability of determining the position of the limb in space with respect to ground and subsequently deduce the anatomical angles. Therefore, the use of inertial sensors will assist in the determination of the thigh and shank orientation with respect to the gravity [248], resulting in a robust control architecture.

Anatomical and orientation angles had reportedly been measured using inertial sensors [249]. The use of body-mounted sensors has been extensively established and the results obtained were satisfactory [250]. However, this has been mainly for clinical use only during gait analysis. Challenges still exist concerning the application of such technology on integrating them for prosthetic control systems. The three fundamentals regarding the applicability of wearable technology are *acceptability*, *applicability* and *adaptability* [251]. Therefore, the technology is mainly evaluated on its appropriateness for the task at hand and for the user rather than by its modernity or ease-in-use for developers. The benefits of wearable technology for amputee rehabilitation include, among other things, to promote healthy lifestyles, aid in clinical decision making by health professionals as well as patients, and enhance healthcare quality by improving access to medical and health information and facilitating instantaneous communication in places where this was not previously possible [252].

Inertia sensors can easily be classified into two distinct groups, accelerometers which measure the linear change in inertia and gyroscopes which measure radial changes in inertia [248]. Also, magnetometers are included in some IMU packages. Orientation measurement is an important fundamental principle in human movement. Although there are several gyroscope sensors, vibrating mass gyroscopes are considered suitable for determining limb orientation [253].

The use of accelerometers for gait analysis as a biomechanical quantification method is becoming popular as the demand for outdoor experiments increases [254]. An accelerometer consists of a proof mass suspended by compliant beams anchored to a fixed frame [255]. According to [253], there are several types of accelerometers, but most human movement applications use piezo-resistive accelerometers or variable capacitance accelerometers, both of which respond to gravitational acceleration as well as to acceleration due to movement. The most common types are piezo-resistive devices, which consist of silicon piezo-resistors in their suspension beam and capacitive devices, which have the changing capacitance between the proof mass and a fixed

conductive electrode separated from it with a narrow gap [253]. The capacitive devices have a good DC response, low drift, high sensitivity and low power dissipation. However, they are susceptible to electromagnetic interference [256]. Other less common devices are tunnelling, resonant, thermal and optical.

With the rapid development in microelectronics, it is now possible to build miniaturised instrumentation [257]. The advantage of using IMU sensors is that the devices are small in size, have low power consumption, high accuracy and repeatability, high shock tolerance, and application-specific performance programmability [252]. The MP6050 IMU miniaturised device from Inverse Technology, shown in Figure 6.1, was used to determine the orientation of the limb [258]. The sensor is equipped with an internal Digital Motion Processor (DMP) which allows 3D motion processing algorithms to be implemented [258].

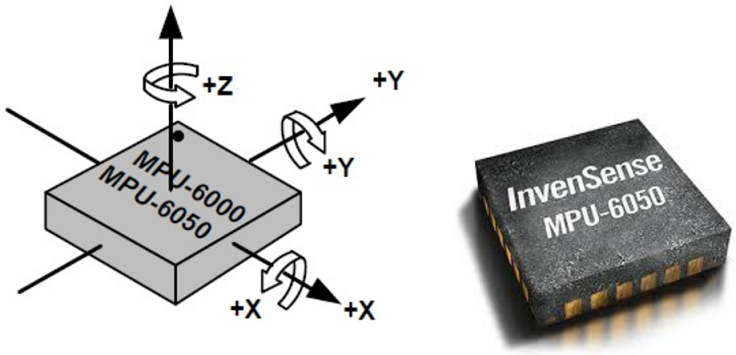

Figure 6.1: Orientation of axes of sensitivity and polarity of rotation

According to [248],[252],[253] and [259], parameters for motion analysis in humans can be measured in relation to stride and running characteristics. Therefore, the use of accelerometers can be extended to detect movement signatures and features in limbs. Myagoitia et al. [250] suggested that the method for finding kinematics by using body mounted accelerometers and rate gyroscopes is as accurate as a camera motion capturing systems. This justifies the use of IMU based technologies so as to minimise experimental cost as the optical systems are too expensive and are restricted to indoor measurements for accurate results. The greatest niche of accelerometer sensors is that they can be used to determine orientation of the limb with respect to earth's gravity, as components of gravity are aligned orthogonal to the accelerometer axis [260]. The possibility of using the inertial sensors is based on the reliability of the position algorithm to calculate the linear acceleration of the knee from accelerometer data and it depends on the distance between the proximal tangential accelerometers on thigh and shank at the knee joint [250].

IMU sensors provide higher integration, greater functionality, lower cost and higher performance on control systems [261]. The application of IMU sensors is abundant in the field of tracking and navigation. Foxlin [262], developed a tracking shoe based on IMU. In his justification was that the only practical solution would be to compensate for drift in gyroscopes to determine roll and pitch. Although these sensors are susceptible to errors, there are several methods which are used to improve their accuracy [263]. A generalised methodological layout of

inertial sensor application and the technology of inertial sensors was well explained by Sprager and Juric [249].

6.2 Methods and materials

The methodology for the development of the limb orientation system was developed based on methodologies proposed for activity monitoring system by [264] and [265] using smart-phone data. The study involved the use of five non-amputated participants. The participants were aged between 32 and 36 years. The mean height of the participants was 1.6 m and the mean weight was 78 Kg. Since there was no significant difference in distance variables between non-amputees and amputees from results reported in section 5.3.1 of the study. It was hypothesised that, even if the system is developed and tested on non-amputees it will work well on amputees when integrated with the targeted control architecture. However, the design parameters used in the study were extracted from the results reported in section 5.3.2 for orientation angles of lower limb on osteomyoplastic transtibial amputees. The systematic procedure used to achieve the objective of activity monitoring of the limb orientation was as follows:

- The IMU data acquisition circuitry was developed based on MPU6050.
- On-board filtering was implemented as firmware for embedded sensors.
- Sensor fusion technique was implemented for integrating two IMU sensors.
- An inertial measurement unit was mounted on the legs along with the two sensors.
- A data acquisition algorithm was developed and deployed and participants were task with carrying out the activities.
- The acquired data was imported into Matlab R2017a and post-processed using bandpass filters was implemented.
- Data was segmented between training data (with activity labels) and test data.
- Feature extraction and classification of the activities.

The activities considered for classification were walking, walking upstairs, walking downstairs, sitting, standing and laying. The experiments were carried out at the Biomedical Engineering Research Laboratory, Stellenbosch University. The results generated were used during the development and testing of the final powered limb prototype when the IMU sensors were integrated with other sEMG sensors and force sensitive resistors. However, in this section emphasis was on hardware design and testing concerning the IMU sensors independent of the other sensors.

6.3 Design of the limb orientation measuring system

There were two possible methods of determining the position of the shank; the first method was to place a sensor on the thigh and another one on the shank and then determine the angle between the two sensors. The angle will then be modelled to determine the position of the shank during gait. The second method was to use one sensor placed at the shank and then determine the tilt angle.

The objective was to acquire the accelerometer, gyroscope and magnetometer values to formulate a data set which can easily be used for tracking the position and orientation of the shank. To achieve such a data set, there was a requirement for proper filtering and sensor fusion techniques. The design made use of arbitrarily defined zero-identity orientations, which makes perfect physical alignment unnecessary and reduces the difficulties associated with extracting desired outputs. The sensors were embedded with an internal Digital Motion Processor^{TM} (DMP) which allows 3D motion processing algorithms to be implemented in real-time, thereby reducing the processing load on the main signal processor within the system. The human body was not uniform, leading to the possibility of imperfect sensor placement. Therefore, the quaternion orientation output and the quaternion operations were developed and deployed to account for the body's irregularities, thereby achieving accurate forward and downward vectors. The algorithm used for detection of angles also incorporated a Kalman filtering technique. IMU sensors have been used for recording gait in many previous studies and the methodology for signal acquisition and data processing is well documented in past studies [266]. However, the use of IMU sensors for controlling actuators in the field of Body-Sensor Network (BSN) is highly limited. As a result, this presents challenges with regard to data segmentation and filtering which is easy for offline systems but somehow complex for real-time control systems [267].

6.3.1 Orientation estimation for activity monitoring purposes

The use of IMU sensors for activity monitoring is well researched and documented, however, the application for control systems is rather limited. The available literature on orientation estimation mainly utilised smart-phone data in real-time, or made use of pre-recorded data for offline analysis. As a result, issues with regards to orientation errors, misalignment and noise interference are not well dealt with. The major challenge of implementing inertial sensors is that they can directly measure physical quantities that are related to the motion of the amputatee and not necessarily the position and orientation of the amputated limb [268]. As a result, there are several mathematical modelling techniques which are implemented to extract relevant information that could be used to determine orientation of the limb with respect to gravity vector [269]. These include sensor fusion algorithms (accelerometers, gyroscopes and magnetometers), filtering algorithms, zero-velocity update algorithms, orientation algorithms and heading algorithms.

The sensor orientation errors can introduce system errors, hence major challenges arise in sensor misalignment considerations. This is mainly defined as the angular difference between the sensor's axis of rotation and the system defined inertial reference frame (global frame). Although [266] suggested the elimination of magnetometers and foregoing the sensor-to-segment mounting assumptions, this study considered these eliminations as bottlenecks for proper angle estimation. The results presented by [266] did not justify the significance of the elimination of magnetometers. The resultant matrices (R_x, R_y and R_z) are a result of the roll, pitch and yaw rotational matrices operating on the gravitational vector ($\mathbf{g}$) about x, y and z coordinate system. The basic coordinate systems are based on the sensor coordinate system describing its movement, F_m and the global reference frame, F_R, independently of the sensor movements. The F_m, is therefore regarded as the frame attached to the limb (thigh and shank). The IMU is positioned so that the orientation is measured in the earth's gravitational field such that the acceleration output is $\pm g$ for earth's downward gravitational field alignment. As a result, the IMU sensor undergoes linear acceleration, a_r when oriented in the earth's gravitational field g, given that G_p, is the representation of the three-axis accelerometer IMU orientation in native

units, then:

$$G_p = \begin{bmatrix} G_{px} \\ G_{py} \\ G_{pz} \end{bmatrix} \tag{6.1}$$

$$G_p = R(g - a_r) \tag{6.2}$$

The initial positioning of the sensor is illustrated in Figure 33 such that the earth's gravitational field, g, is aligned to the z-axis of the sensor and there is no linear acceleration, such that $a_r \approx 0$. With such assumptions:

$$G_p = \begin{bmatrix} G_{px} \\ G_{py} \\ G_{pz} \end{bmatrix} = Rg = R \begin{bmatrix} 0 \\ 1 \\ 1 \end{bmatrix} \tag{6.3}$$

The description of rotation of a body in 2D space is explained using the use of complex numbers such that operations with $\mathbf{i}$ in a 2D plane result in several rotations. The complex numbers are on the y-axis with the real numbers on the x-axis such that:

$$i = 90^0 \tag{6.4}$$

$$i^2 = 180^0 \tag{6.5}$$

$$i^4 = 360^0 \tag{6.6}$$

In 3D space, the rotation introduces the three planes as $\mathbf{i}$, $\mathbf{j}$ and $\mathbf{k}$. The quaternion, Q_t, is used to estimate the frames as they rotate independently from each other. A quaternion, Q_t, is a fourth-dimensional vector that can be interpreted as a third-dimensional rotation vector. It is mainly conformed by a scalar constant, ω, and a 3D vector, $\mathbf{q}$, such that:

$$\boldsymbol{q} = a + b\boldsymbol{i} + c\boldsymbol{j} + d\boldsymbol{k} \tag{6.7}$$

where$a$, b, c and d are real numbers. Hence:

$$i^2 = j^2 = k^2 = 1 \tag{6.8}$$

and this can further be translated as:

$$ij = k, \quad ji = 1, \quad jk = 1, \quad ji = -1, \quad ki = k \quad and \quad ik = -j \tag{6.9}$$

In the end $\mathbf{i}$, $\mathbf{j}$ and $\mathbf{k}$ form a Euclidean frame. The quaternion, q, will however, return the form $q = (t, \mathbf{v})$ where t is a scalar part and $\mathbf{v}$ is the vector part. Therefore for any quaternion, the map,

$$\varphi_q(\omega) = \frac{q\omega\widehat{q}}{Q_{(q)}} \tag{6.10}$$

is a rotation about the vector, $\mathbf{v}$, with half turn:

$$h = \frac{|v|}{t} \tag{6.11}$$

where Q is the quadrance. However, when one has a point in space the quaternion, ω, is a pure imaginary quaternion therefore, $t = 0$. Therefore for the projection of the sensor in 3D space:

$$\boldsymbol{q} = \begin{bmatrix} q_1 \\ q_2 \\ q_3 \end{bmatrix} \tag{6.12}$$

$$Q_t = \boldsymbol{q}, \omega \tag{6.13}$$

The rotational vector, Q_t, is associated with sine and cosine of the rotational angle, γ, with respect to each axis (x,y,z). As a result, γ is a combination of the roll (ϕ), pitch (θ) and yaw (φ) such that:

$$\gamma = [\phi, \theta, \varphi] \tag{6.14}$$

This rotation about the main axis results in the rotational vector representation in time as:

$$Q_t = \frac{1}{2}[cos\gamma, \boldsymbol{q} sin\gamma] \tag{6.15}$$

The quaternions can easily be composed so as to represent several rotations through a quaternion product, Q_c, considering a three dimensional space:

$$Q_c = Q_a \otimes Q_b \tag{6.16}$$

$$Q_c = Q_z(\varphi) \otimes Q_y(\theta) \otimes Q_x(\phi) \tag{6.17}$$

$$G_p = \begin{bmatrix} cos\varphi cos\theta cos\phi + sin\varphi sin\theta sin\phi \\ cos\varphi cos\theta sin\phi - sin\varphi sin\theta cos\phi \\ cos\varphi sin\theta cos\phi + sin\varphi cos\theta sin\phi \\ sin\varphi cos\theta cos\phi - cos\varphi sin\theta sin\phi \end{bmatrix} \tag{6.18}$$

However, the composed quaternion can be represented by individual rotational matrices along individual axis as R_x, R_y and R_z. These matrices are regarded as roll, pitch and yaw respectively:

$$R_x(\phi) = \begin{bmatrix} 1 & 0 & 0 \\ 0 & cos\phi & sin\phi \\ 0 & -sin\phi & cos\phi \end{bmatrix} \tag{6.19}$$

$$R_y(\theta) = \begin{bmatrix} cos\theta & 0 & -sin\theta \\ 0 & 1 & 0 \\ sin\theta & 0 & cos\theta \end{bmatrix} \tag{6.20}$$

$$R_z(\varphi) = \begin{bmatrix} cos\varphi & sin\varphi & 0 \\ -sin\varphi & cos\varphi & 0 \\ 0 & 0 & 1 \end{bmatrix} \tag{6.21}$$

The yaw, $R_z(\varphi)$, is aligned to the earth's gravitational field, as a result only the roll, $R_x(\phi)$ and the pitch, $R_y(\theta)$, are considered. Since the z-axis is aligned to the gravitational field, the normalised sensor output will be in terms of roll and pitch angles:

$$\frac{G_p}{\|G_p\|} = \begin{bmatrix} -sin\theta \\ cos\theta sin\phi \\ cos\theta cos\phi \end{bmatrix} \tag{6.22}$$

$$\Rightarrow \frac{1}{\sqrt{G_{px}^2 + G_{py}^2 + G_{pz}^2}} \begin{bmatrix} -sin\theta \\ cos\theta sin\phi \\ cos\theta cos\phi \end{bmatrix} = \begin{bmatrix} -sin\theta \\ cos\theta sin\phi \\ cos\theta cos\phi \end{bmatrix} \tag{6.23}$$

Solving for the roll and pitch angle according to the rotation sequence $\boldsymbol{R}_{xyz}$:

$$R_{xyz} \begin{bmatrix} 0 \\ 0 \\ 1 \end{bmatrix} = R_x(\phi)R_y(\theta)R_z(\varphi) \begin{bmatrix} 0 \\ 0 \\ 1 \end{bmatrix} \tag{6.24}$$

$$roll, \phi = actan(\frac{G_{py}}{G_{pz}}) \tag{6.25}$$

$$pitch, \theta = \frac{-G_{px}}{G_{py}sin\phi + G_{pz}cos\phi} = \frac{-G_{px}}{\sqrt{G_{py}^2 + G_{pz}}} \tag{6.26}$$

The design was such that the pitch was being tracked as the elevation of the limb within the sagittal plane.

6.3.2 Single sensor placement

The use of a single node sensor system would reduce the weight of the system on the user. Therefore, measuring the tilt of the limb relative to the ground was explored. The tilt angle (β) of the lower limb from the original position when the subject is seated or standing in the absence of linear acceleration can be determined. The angle is between the gravitational vector and the initial orientation with the gravitational field pointing downwards along the z-axis, as shown in Figure 6.2. The initial test, however, revealed that if the sensor is placed on the shank alone, the orientation of the shank when seated and when standing is the same. However, the orientation for walking was different from that of standing.

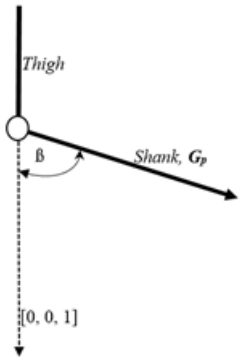

Figure 6.2: Tilt measurement

Taking into consideration the accelerometer reading, $G_p(x, y, z)$ in the absence of linear acceleration, the tilt angle is determined. If a_z is the acceleration along the z-axis then:

$$R_p \begin{bmatrix} 0 \\ 0 \\ 1 \end{bmatrix} = a_z \tag{6.27}$$

$$G_z = |G_p| cos\beta \tag{6.28}$$

$$cos\beta = \frac{a_z}{\sqrt{a_x^2 + a_y^2 + a_z^2}} \tag{6.29}$$

$$\beta = arcos \frac{a_z}{\sqrt{a_x^2 + a_y^2 + a_z^2}} \tag{6.30}$$

6.3.3 Dual inertial sensor system

In the targeted control system, the objective was to manipulate the ankle angle (α) with respect to the outputs (τ and ψ) from the inertial sensors. However, since the outputs are used for generating a control signal, it is the orientation of the inertial sensors with respect to the gravity vector that was considered. Figure 6.3 illustrates the mounting of the sensors on the participants. The proposed system of avoiding calculation of anatomical angles but rather calculating the orientation of the individual limbs (shank and thigh) enabled the development of a more robust algorithm. Such a system enabled the implementation of the base coordinate system (roll, pitch and yaw) with the aid of the normalised readings of G_p as additional control conditional statements within the algorithm.

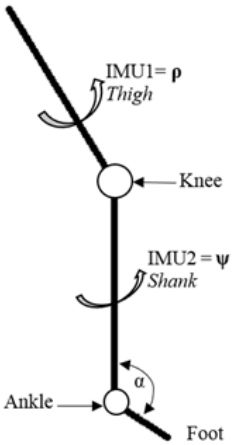

Figure 6.3: Dual IMU measurement system

It should be noted that the acquired inertial sensor outputs were not a derivation from the anatomical angles of the subjects but the orientation of the inertial sensor. The availability of the dual inertial system resulted in increased system accuracy with regard to different gait stages. The definition of the available measurement signal was based on [266] derivation. Considering the dual sensor system, the accelerations, a_1(t),a_2(t) ε R^3 and angular rates, g_1(t), g_2(t) ε R^3, are determined at some sample period, $\triangle t$. Determining the derivatives of the angular rates, (a_{g1}) ÌĞ(t),(a_{g2})(t) ε R^3, using the third order approximation:

$$a_{g1/g2}(t) \approx \frac{g_{1/2}(t - 2 \triangle t) - 8g_{1/2}(t + \triangle t) - g_{1/2}(t + 2 \triangle t)}{12 \triangle t} \tag{6.31}$$

However, during data collection, the expected accelerometer data set, D_i was recorded as a text file and exported and as a *csv* file to Matlab R2017a as:

$$D_i = (a_x, a_y, a_z, g_x, g_y, g_z) \tag{6.32}$$

Magnetometer values (m_x, m_y, m_z) were not recorded as outputs but they were used within the embedded algorithm during calibration within the DMP and also as inputs to a Kalman and as complimentary filters. Furthermore, the combination of accelerometer, gyroscope and magnetometer values assisted in the determination of the correct angle relative to the ground.

6.4 Results and discussion

This section presents the results on the signal acquisition, filter performance and classification feasibility of the acquired signals. The signal acquisition units were based on the MPU6050 architecture developed to output values to a microprocessor. The Kalman filter and the complimentary filter were compared so as to determine the best optimum filter for the design. In literature the Kalman filter is reported to be superior of the complimentary filter in terms of signal output quality but has a complex computational method that could increase processing time. The signals from the IMU sensor systems could be used as inputs to the pattern recognition systems. Therefore, classification feasibility was evaluated based on the recorded data set in an off-line set-up.

6.4.1 Evaluating accelerometer performance

The results presented in this section were recorded after calibration of the sensors to reduce the errors from offset and sensitivity mismatch. Tilt can easily be determined by direct integration of the output of the gyroscope. However, the error associated with the null bias stability affected the results as the signal period increased. This caused an apparent rotation even when the observed subject was stationary. Therefore, this is not a recommendable method for a signal to be recorded over a period of hours or days. As a result, the inclination angle was determined using accelerometer values under static conditions. The results were to be used to determine the movement of the lower limb when the amputee is performing normal gait. In this regard, the participants (non-amputees) were tasked to walk and stand with the aim of initially determining the four states (walking, standing and walking up and down stairs). Even though the targeted control architecture was limited to the normal gait of amputees walking on flat surfaces, walking on stairs was included during this test. The algorithm was developed such that during standing, the accelerometer values normal to the z-axis will produce acceleration oscillating around 10 /ms while other axes will produce values close to zero. Figure 6.4 illustrates the results generated during standing and walking on a flat platform.

The results presented in Figure 6.4 illustrate that the use of accelerometer values alone will not be able to provide the actual limb orientation. Therefore, recommendations were that the monitoring of the individual limbs concerning gait events would provide rather convincing results. Determination of either walking or standing was not sufficient to provide a reliable control signal since single and double support events both produced the same results as standing. Furthermore, the whole swing phase could be categorised as walking. As a result, there was a need to optimise the generation of a reliable feedback system to optimise the targeted control architecture if IMU sensors are to be incorporated in the targeted design.

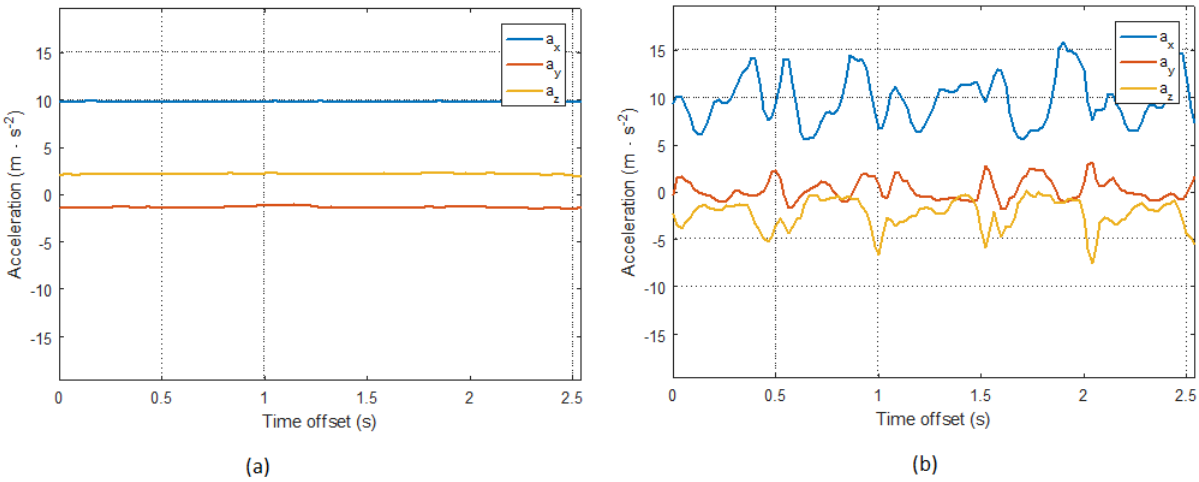

Figure 6.4: Illustrating the stability of accelerometer values during walking and standing

The frequencies generated by the signals during walking upstairs and walking on a flat platform are shown in Figure 6.5 and Figure 6.6. The spectral density comparison revealed a close correlation of the signals within the frequency domain. The autocorrelation was useful for frequency estimation, especially for the low-pitch frequencies such as accelerometer values. The magnetometer signal was very difficult to utilise for activity recognition as it was affected largely by the presence of metallic objects. Even after the use of a plastic casing, the readings were still affected. As a result, direct activity monitoring will not be suitable for providing a feedback signal to the targeted control architecture.

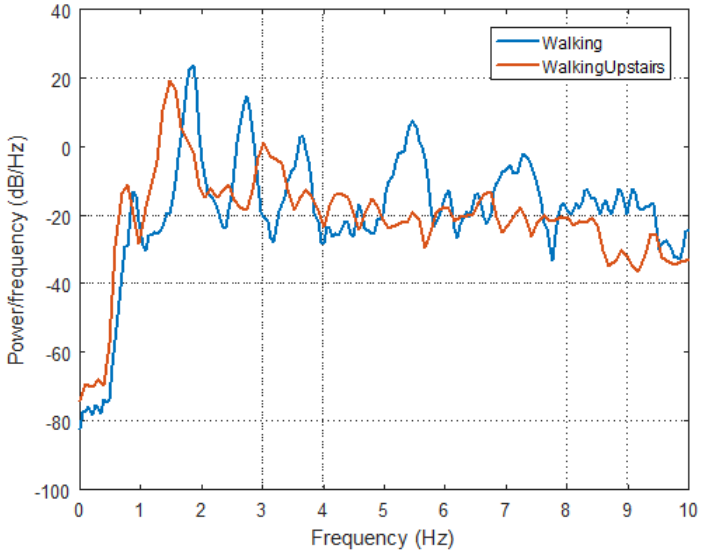

Figure 6.5: Comparison between walking on a flat platform and walking upstairs using signal frequency

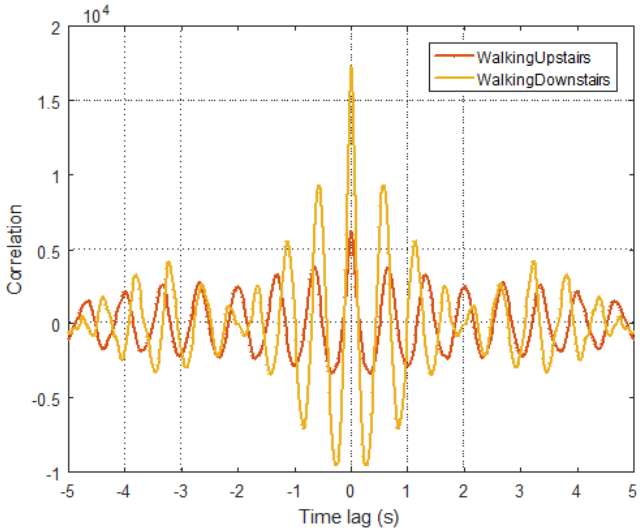

Figure 6.6: Correlation comparison between walking on a flat platform and walking upstairs using signal frequency

6.4.2 Kalman filtering and signal processing

The gyroscope had notable drift under small periods, and its raw values could not be used for activity detection. The movement of the legs during walking could not provide convincing information for the adoption of raw gyroscope readings. The accelerometer returned true values when the acceleration was progressive but suffered greatly from vibrations. As a result, there was a need for the implementation of a Kalman filter and complimentary filter as methods to extract useful signal features. The two filters were both tested under the same conditions and the results are presented in Figure 6.8. The results showed that the Kalman filter provides a smooth useful signal with a steady state error of zero. The Kalman filter is an optimal estimator [270], it infers parameters of interest from indirect, inaccurate and uncertain observations. The underlying principle is that if all noise is Gaussian, the Kalman filter minimises the mean square error of the estimated parameters [271]. It is thus regarded as the best tool to achieve optimal estimatation for linear systems through online real-time processing [272]. The implementation of the Kalman filter was based on the fact that prior knowledge was not necessary as the filter relies on the last state and covariance matrix that defines the probability of the sate being correct. The strength of a Kalman filter is on adaptation and robust sensor fusion through the use of the prediction and the update equations [273]. The prediction equations predict the current position of the artificial limb based on the previous position (state). The update equations check for IMU output reliability as well as the reliability of the predicted state. The input data sets to the Kalman filter were arranged as:

$$accelerometer \quad values, \quad A_{acc} = [a_x, a_y, a_z] \tag{6.33}$$

$$gyroscope \quad values, \quad G_{gyr} = [g_x, g_y, g_z] \tag{6.34}$$

$$magnetometer \quad values, \quad M_{mag} = [m_x, m_y, m_z] \tag{6.35}$$

Therefore, if X represents the state (x, y, z) of the limb with the signals to be filtered while U is the action or filtered signal (roll (ϕ), pitch (θ) and yaw (φ), then the A_{acc}, G_{gyr} and M_{mag} value were then inputs to the following *updating* equations. The sensor model (H) was initialised

as a diagonal identity matrix and then frequently adjusted during design. The IMU signals had noise inherent in the signal which was represented as a covariance, Q. The IMUs (thigh and shank) were integrated together so that the readings from both IMU sensors were accurate and the confidence of the sensors (R) was optimised so that P is improved since it was the confidence coefficients of the filter responsible for exhibiting the reliability of the filter:

$$K = pH^T(HpH^T + R)^{-1} \tag{6.36}$$

$$x_k = X + K(z - HX) \tag{6.37}$$

$$P_{x_k} = (I - KH)p \tag{6.38}$$

The *update equations* above will be performing an iterative process with the *prediction equations* bellow to determine the state estimates as:

$$X = A_{x_{k-1}} + Bu_{k-1} \tag{6.39}$$

$$P = APA^T + Q \tag{6.40}$$

The outputs from the algorithm were Kalman filtered acceleration (kal_x, kal_y, kal_z), the gyroscope values (g_x, g_y, g_z), roll (ϕ), pitch (θ) and yaw (φ). It is, however, the pitch that was utilised for limb orientation prediction. The prediction equations have the capability of generating outputs (z) returned from each sensor position and in the unfortunate event of a missing input data (X), the Kalman filter uses z to estimate the missing position. Given I is a diagonal identity matrix, the Kalman filter is able to determine the reliability (P) of the filter outputs and constantly adjusts it using model matrices **A** and **B** which represents how the system changes from one state to the next in real-time.

After initial calibration, the algorithm begins with the current state, $x_{(k-1)}$, the initial covariance matrix $P_{(k-1)}$ and the current input $u_{(k-1)}$ to get the predicted state **X** and predicted covariance matrix **p**. This results in the achieved measurement y_k. The update equations are then used to correct the initial predictions in order to get the new state matrix x_k and new covariance P_k. The process was then iterated in the algorithm. All this was performed in the microprocessor as the real-time acquisition of the signals occur. The available Digital Motion Processor within the MPU6050 sensor allows the implementation of magnetometer readings (m_x, m_y, m_z) for calibration of the sensors in real-time. The resultant output after the implementation of the Kalman Filter is illustrated in Figure 6.7.

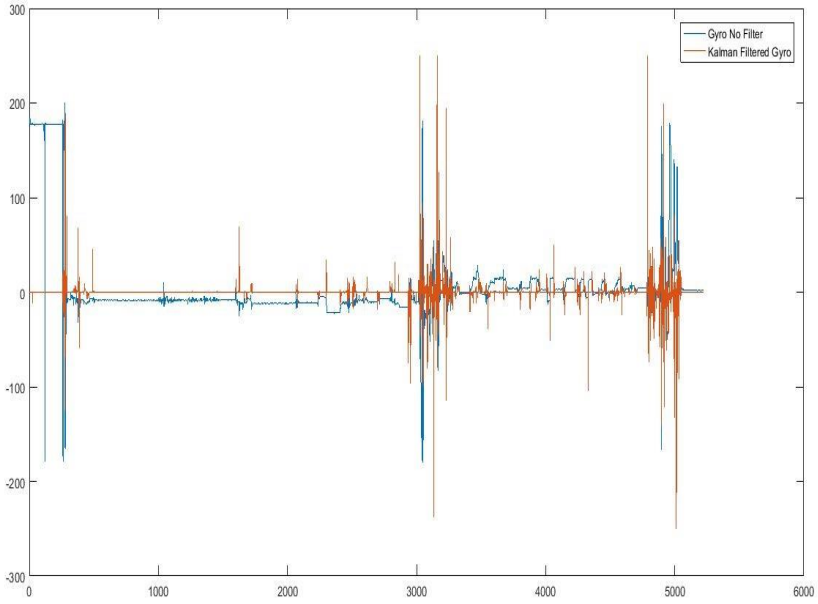

Figure 6.7: Illustrating the effects of Kalman filtering

6.4.3 Evaluating feasibility of activity classification

The activities (walking, walking upstairs, walking downstairs, sitting, standing and laying) were identified using both threshold technique and pattern recognition system. According to [70], the clinical viability of the proposed system is largely dependent on the underlying recognition module ability to detect a variety of activities that are performed routinely in many different manners by different individuals under different environmental conditions. However, this presents a bottleneck as the real world data is noisy and complex. The data set comprising of the accelerometer values was used as an input to a feature extractor. There were only six features used to develop the feature vector which was then used as an input to an artificial neural network classifier. There was clear distinction between walking on flat surface and walking upstairs, as illustrated in Figure 6.8. The contribution of low frequencies on walking upstairs as compared to walking on a flat surface was then detectable during feature extraction and used as a distinct feature. The results in Figure 6.8 were a representation of classes related to walking only.

Two additional activities (sitting and laying) were then added, and the classification learner in Matlab R2017a was used to determine the classification accuracy. The confusion matrix shown in Figure 6.9 illustrates how the system was able to classify the activities (1. walking, 2. walking upstairs, 3. walking downstairs, 4. sitting, 5. standing, 6. laying). The system achieved 93.3% classification accuracy. The main contribution to the 6.7% error was largely on classifying between sitting, standing and laying. There were also notable errors in the system on classifying between walking upstairs and walking downstairs. However, to a greater extent, the system was able to classify all mobility activities.

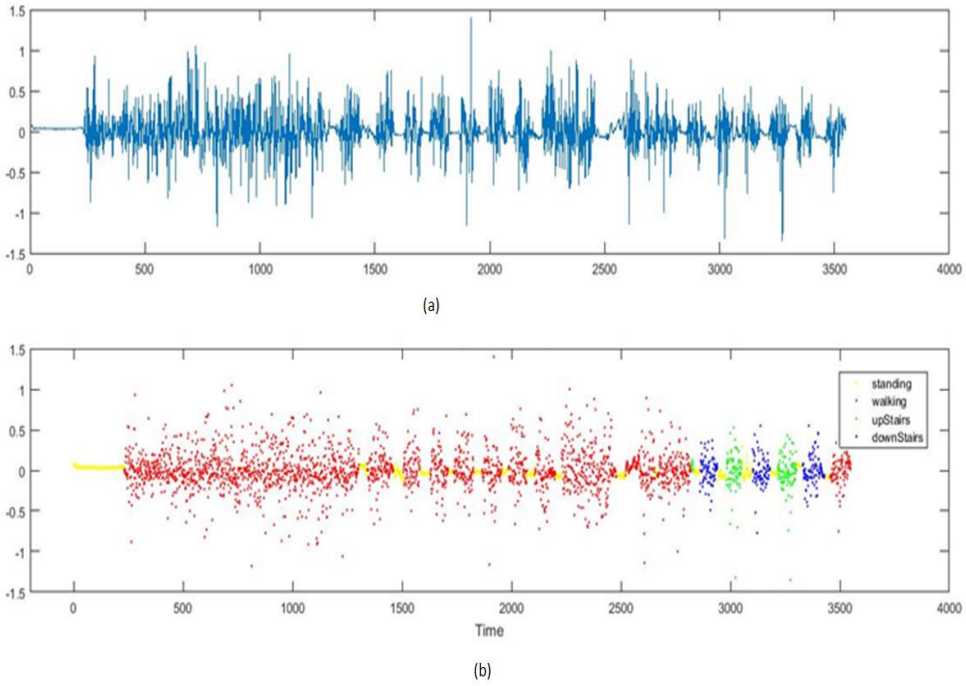

Figure 6.8: Scatter plot for (a) raw signal and (b) classified activities

The designed electronic circuit and the proposed system architecture provided reliable information for the development of a Rehabilitation Monitoring System (RMS) for transtibial amputees who have received prosthetic limbs. The system is capable of recording daily activities responsible for mobility. The results can easily be used by clinicians to make informed decisions regarding the usage of the artificial limb. However, the developed system does not show the gait cycle parameters as it is only limited to activity recognition, length of activity and period of when the activity was performed.

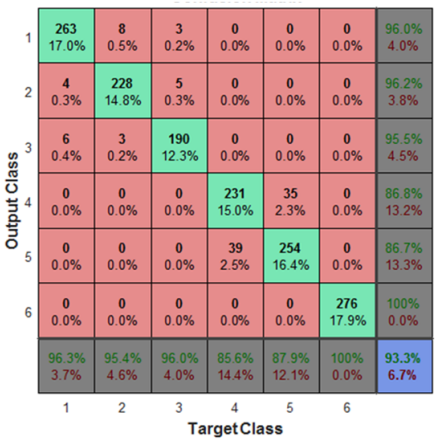

Figure 6.9: Confusion matrix for classified activities

6.5 Limitations of the study

The initial design specifications for the IMU circuitry was derived from anatomical and orienation angles of non-amputees. This procedure was done in-order to avoid taking device specifications from amputees who had already developed skeletal disorders as deduced in Section 5 discussions. The sample of participants was five which was small with regards to biomechanics experiments. However, the objective was to determine angles and not for diagnosis of any skeletal or muscular disorders. Therefore, the sample size presented sufficient data to derive the design specifications. It is also necessary to note that by implementing inertial sensors one can only directly measure physical quantities that are related to the motion of the amputee and not necessarily the position and orientation of the amputated limb. Algorithms were further developed to determine position and orientation parameters. Furthermore, the circuitry was affected by presence of a magnetic field and ferromagnetic materials. Additional magnetic shielding was highly recommended.

6.6 Conclusion

The results presented in this section were based on activity monitoring and it was well related to the limb orientation monitoring. The study revealed that it is very much possible to include IMU sensors as orientation estimation sensors in a control architecture. The electronic hardware circuitry developed enabled the extraction of individual sensor values such as gyroscope, accelerometer and magnetometer values independently. However, there were limitations on using raw gyroscope values, as the test carried out revealed that the presence of ferromagnetic materials cause sudden spikes on raw gyroscope signals. The use of a high pass filter to remove low frequencies caused by sudden drift of gyroscope signals improved classification accuracy and signal presentation.

The results in this section revealed that activity monitoring would not be a suitable method of creating a feedback signal for a pattern recognition system. Although the pattern recognition algorithm worked well for classification of activities it will be challenging to classify gait events based on accelerometer values. This is due to the small signal detection windows between gait events. Previously mentioned results in section 5.3.1 revealed that the stride duration is approximately 1.2 s and that there are eight distinct events in a gait cycle (one stride). Such sudden changes in activity will be difficult to classify.

Recommendations were that, on integrating within the targeted pattern recognition system, IMU sensors will be used to detect orientation. As a result, the pitch would be recorded and classified as compared to the individual accelerometer or gyroscope values. In addition, the two IMU outputs will be used individually as two pitch values. The suggested set-up will enable the detection of the two sections (thigh and shank) individually and the outputs will be used as feedback to the control architecture. Activities, such as sitting and laying, were also deemed unnecessary to monitor or detect since they are not core events of the normal gait.

Chapter 7

Development of a robust myoelectric pattern recognition and IMU based control system architecture

Published as conference proceedings.[1]

7.1 Introduction

Proportional and direct control strategies based on threshold systems are currently regarded as the best solutions to control powered prosthetic limbs [274]. However, the number of degrees of freedom or movements expected surpasses the available signal channels. As a result, the clinical viability of powered limbs is still regarded as a challenge for assistive technologies. The goal of pursuing a pattern recognition based control system is to improve multifunctional capabilities of the powered limb [275]. The objective is to improve the applicability of intuitive control of the powered limbs. The use of sEMG signals is well researched and documented, however, the clinical applicability of the technology has been a subject of concern [106], [107], [276], [277].

The failure of sEMG signal based control architectures has been attributed to noise interference inherent in the signals and lack of supporting hardware [274], [7]. Novel ideas had been proposed for both upper and lower limb control [8], [112]. However, the use of simulated data, non-amputee data [278] and virtual systems have led to a decline in reliability of the suggested system on real-world application [274]. Under these simulated environments, noise interferences have been overlooked, hence the success of these systems has been overrated. In real-time applications, the noise inherent in the stochastic myoelectric signal and lack of adequate feedback systems affect the reliability of the powered prosthetic limbs.

According to [8], most myoelectric control systems developed so far are mainly focused on feedforward control. As a result, they add extra load on the user as he will be responsible for completing the feedback loop using visual inspections [278]. In such a context, the reliability of the actuation system becomes questionable [31]. The lack of automated intuitive feedback loop and limited dexterity of the available prosthetic limbs reduces the acceptability of the devices

[1]Garikayi, T., Van den Heever, D. and Matope, S., 2016. *Development of a rehabilitation activity monitoring system for transtibial amputees.* Proceedings of the South Africa Institute for Industrial Engineering Conference, 27-28 October, Stonehenge, Parys, South Africa, (p.177-190).

within the amputee community. Harnessing control signals from EMG signals, researchers have developed crisp control, finite state machine control or on-set analysis as a means of increasing the reliability of the control system [274]. The goal of pattern recognition systems is to increase device reliability by intuitively controlling the device. Extended benefits include a reduction in energy consumption, as amputees currently use 60% more energy [16] as compared to non-amputees performing the same task.

The pattern recognition algorithm is the basis for the machine intelligence of the device. It defines the level of robustness and adaptability of the control architecture. Ever since the *Hudgins features* were reported in 1993 there has been tremendous efforts to develop clinically viable pattern recognition systems [20], [30],[70], [144], [209],[279], [280], [281], [282] and [283]. Although several techniques have been implemented on the development of this pattern recognition system, the methodology and functional blocks of the architecture remains the same. Most 19^{th} Century studies were centralised around work done by [107], while most of the 21^{st} Century studies are centralised around work done by [209]. The major difference is that work carried out by [209] emphasised mainly the applicability of hybrid systems for enhancing classifier performance. The only difference among the findings has been on classification accuracy, and not functionality of the system, as the results are mainly focused on virtual, off-line or simulated data sets.

The goal of the study was to develop a robust control architecture that has the capability of determining the user intent in real-time, actuate the powered ankle and provide feedback on the system performance. This will result in increased dexterity of the powered ankle, thereby improving normal gait for lower limb amputees.

7.2 Method and materials

The subjects, experimental set-up, data acquisition and statistical analysis used for the study in this section was outlined in section 3, and the detailed procedure is in section 3.7.2. The design specifications were based on the results extracted from the experiments carried out using Noraxon MyoMotion inertial sensors as explained in section 3.7.4. The methodology was optimised to overcome the challenges highlighted by [284] concerning the use of sEMG signals for prosthetic control. As a result, further steps were carried out to achieve the desired design and these include the use of additional sensor technologies such as force sensitive resistors, encoders and inertial sensors. The inertial sensors were used as designed in section 6.3.3, which utilised a dual sensors node system. The results from the previous section concerning the applicability of the IMU sensors were considered during the development of the control architecture.

7.2.1 Determination of muscles sites

The location of muscles responsible for the dorsiflexion and plantarflexion, and the abduction and adduction movements of the ankle are well defined within the SENIAM standards [72]. However, these locations were based on non-amputees, hence there was a need to determine these locations on the residual limb. A modified-SENIAM standard was then used to select muscle sites which exhibited optimum signal quality. The Tibialis Anterior, Medialis Gastrocnemius and the Lateralis Gastrocnemius muscles were identified as the only muscles which could be used to achieve the sagittal plane movements. The Soleus muscle was not accessible on the amputated leg. The signal quality deteriorated as the proximity of the amputation to the knee

increase. As a result, only three signal channels were selected, hence this was used as a design parameter. Therefore, a three-channel myoelectric system was proposed. Detailed methodology is well explained in section 3.6.2 of the report.

7.2.1.1 Determination of force measurement points

The results presented previously in section 4 of the report revealed that it is difficult to determine heel-strike and toe-off on the amputated leg due to inaccessibility of the Soleus muscle. As a result, there was a need to devise a way of detecting these gait events and complimenting the sEMG signal. The force plates used during experimentation indicated that a notable reaction force is present on the hind-foot (talus and calcaneus bones) and the fore-foot (metatarsals and phalanges bones) during heel-strike and toe-off respectively. These locations were then mapped to the amputated leg, and the prosthetic foot was fitted with force sensitive resistors at the hind-foot and fore-foot.

7.2.2 Determination of the positions of inertial measurement sensors

The Noraxon sensor system was used to determine correct positioning of the IMU sensors. These positions were optimised to minimise magnetic interference and power line (50 Hz) noise on the output signal. Two sensor modules were developed based on the MPU6050 IMU sensor architecture. The developed sensors were then tested using a mechanical rig which represents the femur and the shank. Also, signal filtering and calibration techniques were then optimised using the mechanical rig. Once the results showed a convincing ($\pm 1\%$) variation from commercial Noraxon sensors, the IMU sensors were placed on the shank and the thigh of the amputee. The amputee was tasked to perform normal gait on a treadmill. The treadmill speeds were then adjusted from 0.5 m/s to 0.8 m/s.

7.2.3 Signal acquisition and processing

The signals from the two IMU sensors and two encoder channels were synchronised and linked up using the I2C communication protocol to the main microprocessor. The force sensitive resistors were hard-wired as analogue inputs to the microprocessor. Wireless technology was used to send the acquired data to a personal computer. The acquired data set consisted of three channels of sEMG signals, two channels of IMU signals, two channels of force sensing resistors (FSRs) and two channels of encoder signal. These signals were represented as columns. The labels were recorded as representatives of the gait phases in real-time and the data set was used for training and validation purposes of the control architecture. Matlab R2016a, SPSS and R Studio were used as signal analysis platforms. The statistical analysis carried out on the data is outlined in 3.6.2 of the study.

7.3 Design considerations

Design considerations for pattern recognition systems were signal quality, data segmentation, number of features, processing time and classification accuracy. The proposed control architecture utilised four different input control signals and each signal had a predefined number of channels. Although the proposed control architecture utilised four different types of signals namely, sEMG, inertial, positional (encoder) and force signals, it was the sEMG signal that was utilised for pattern recognition. This was mainly because the sEMG signals are directly linked to the detection of the user's intent and their impact on the control system determines the success

of the design. The other three signals were used to aid reliability of the control architecture through the establishment of feedback signals and control interlocks in the knowledge base.

During experiments carried out using the protocol explained in section 3, the study revealed that there are three active sEMG channels namely the Tibialis Anterior, Medialis Gastrocnemius and Lateralis Gastrocnemius muscles. The experiments for gait analysis also revealed that the position of the limb could be determined in space. Also, the protocol revealed that the gait can easily be monitored by identifying core events of the gait such as the heel-strike, toe-off and the foot flat. The goal of the study is to develop an optimised system which utilises sEMG sensors, FSRs, encoders and IMU sensors integrated together to reliably control a prosthetic ankle. The integration of sEMG signals, IMU sensors and force sensors will improve the reliability of the proposed system. The toe-off, double support, single support and heel-strike events could be monitored using force sensitive resistors placed within the prosthetic leg. For a detailed block diagram of the proposed architecture refer to Appendix C and Appendix D.

Design factors and considerations were first highlighted in this section followed by the development of analog front ends for the inertial measurement sensor, the myoelectric sensor and the force sensitive resistors. Lastly, a comprehensive presentation of the architecture was carried out. In some cases, the method used to achieve the design is explained with reference to section 3 and supported by findings in sections 4, 5 and 6.

The design and manufacture of medical devices are governed by several standards. The International Electrotechnical Commission (IEC 60601-1) standards for the design and development of electronic medical equipment and the Application of Risk Management to Medical Devices (ISO 14971) were considered. All safety features and assumptions included in the design were based on IEC60601-1 and ISO 14971. The major consideration was such that the device could conform to ISO 13485 Quality Management System for managing medical devices and equipment. Furthermore, the other design considerations were signal input range, bandwidth, noise interference, sampling rate, communication protocols, power consumption robustness and adaptability. According to [98], the notable requirements for the sEMG signal acquisition circuitry are isolation, high gain, high input impedance, low input bias current, wide input common mode range, low noise, low input offset voltage and good common mode rejection ratio (CMRR). Some of the design requirements are:

- *Isolation*: The characteristics of the circuit to provide reliable isolation in the unfortunate event of the amplifiers sending a current to the human body within the electrodes should be clear and well-defined [80]. The isolation should be able to cater for analog power supply, digital power supply and digital data bit stream [285].
- *Data processing*: The reliability of an electronic device is mainly affected by the processing capability of the main processor [286]. Even after sucessfully establishing the feature extraction mechanism and classifiers [107], the need to develop compatible data processors was emphasised. The possible processors include digital signal processors, field programmable gate arrays, microprocessors and microcontrollers. Furthermore, there is the need for on-board processing capability to reduce post-processing requirements. This includes the use of adaptive filters which could adaptively adjust the filter constants in real time.
- *Analog-to-digital converters*: The digital bit-stream conversion from an analog signal is mainly dependent on the sampling rate. For the conversion to occur in real-time, anti-aliasing filters are required and as such there is a need to select analog front-ends that

have such an in-built capability [96]. This is mainly because aliasing is a result of a signal whose highest frequency component is greater than one half of the sampling frequency and this higher frequency component is not distinguishable from lower frequencies. The sEMG signals have a useful frequency range of 15 Hz-500 Hz and the recommended sampling frequency is 1000 Hz or greater.

- *High gain*: The demand for high gain is necessitated by the low amplitude signals available at the amputated limb. The gain will enable the suppression of internal noise of the amplifiers since high gain amplifiers are sensitive to small changes in input signal [287].
- *Low and stable offset voltage*: An unstable and unreasonably high offset voltage can lead to input signal saturation, thereby reducing the reliability of the circuit. There is a need to employ an external nulling potentiometer to adjust the offset voltage to zero [288], [289].
- *High input impedance*: Most signal distortions are as a result of low input impedance, hence the need for high input impedance on the amplifiers to minimise noise due to electrical loading [288].
- *Low input bias current*: The differential input values are very low and as such a low input bias current is a requirement and should usually be less than 10 pA [290]. This is also necessary for human safety and as a junction current for the transistors [285]
- *Wide input common-mode range*: The input common mode must be large enough to avoid distorting the input signal. The rail-to-rail voltage is the expected range for common mode range [291].
- *Common Mode Rejection Ration (CMRR)*: The advantage of using instrumentation amplifiers is that they have a high CMRR, that is they have a high capability of rejecting common signals that appear in phase and at both inputs, thereby increasing the differential signal [289].
- *Low internal noise*: The presence of thermal and flicker noise within amplifiers usually results in the generation of internal noise [292].

7.4 Development of a multichannel EMG signal acquisition module with adaptive filters

The EMG signal was the main control signal for the proposed myoelectric control architecture. The initial experiments carried out [132] indicated that the sEMG signal was available on the residual stump. However, the signal power and amplitude were very low as compared to the signal strength on the non-amputated leg [132]. As a result, the signal acquisition module characteristics for the sEMG signals required additional filtering and amplification.

There have been great efforts on developing EMG front ends and pre-amplifiers [293], [294], [79], [295]. The Liberty Mutual MYO-III is a high input impedance amplifier, developed by Liberty Mutual, that has a fixed bandpass response of 150 Hz, which is simply a third of the expected bandpass [296] for sEMG signals. The Utah EMG preamplifier developed by Motion Control has a high pass filter of 10 Hz and a low pass of 30 Hz [297]. However, the high band pass filtering was unreliable because of the absence of usable high frequency of data. McGill University developed the BMED1 and the BMED2 amplifiers with the latter having adjustable

gain [293]. To reduce noise interference, [297] introduced the AC coupled instrument amplifier configuration on a 60 μA analog front end for biosignals measurements. However, the greatest setback of the aforementioned amplifiers is their inability to provide a reliable signal under uncertain conditions, such as changes in skin impedance and movement artefact.

The EMG quantitative analysis [132] carried out on the amputees revealed that there are three active muscle sites which can be utilised for ankle control and these are the Tibialis Anterior, Medialis Gastrocnemius and the Lateralis Gastrocnemius. The mean amplitudes for Tibialis Anterior, Medialis Gastrocnemius and the Lateralis Gastrocnemius muscles varied with respect to the type of movement being carried out. These values, recorded using the Noraxon Myomotion system provided the necessary signal amplitude ranges that can be achieved from the available muscles on the residual limb. Figure 7.1 illustrates the nature of the available signals and their respective amplitudes [132].

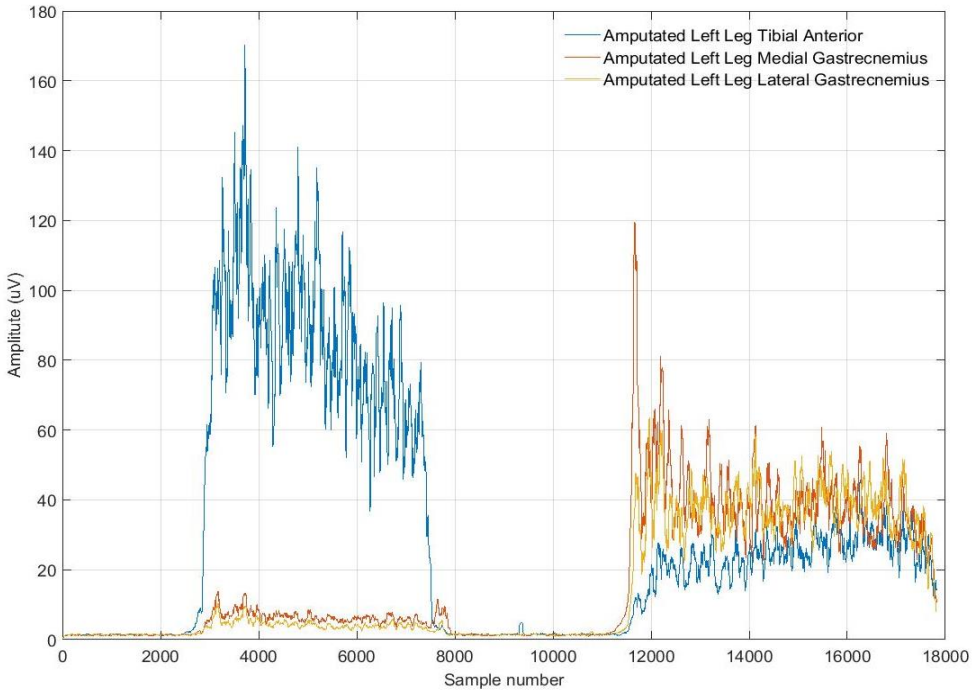

Figure 7.1: Rectified sEMG signals recorded from 3-channels

The signal frequency characteristics were determined from the bandpass filtered signals. Figure 7.2 shows the range of useful frequencies. The frequency spectrum illustrated in Figure 7.2 provided necessary information regarding the useful frequency ranges for the signal acquisition module. The 15 Hz to 500 Hz bandwidth was the useful frequency range, as suggested by the SENIAM and ISEK standards. However, there was 50 Hz power-line interference noise inherent in the signal.

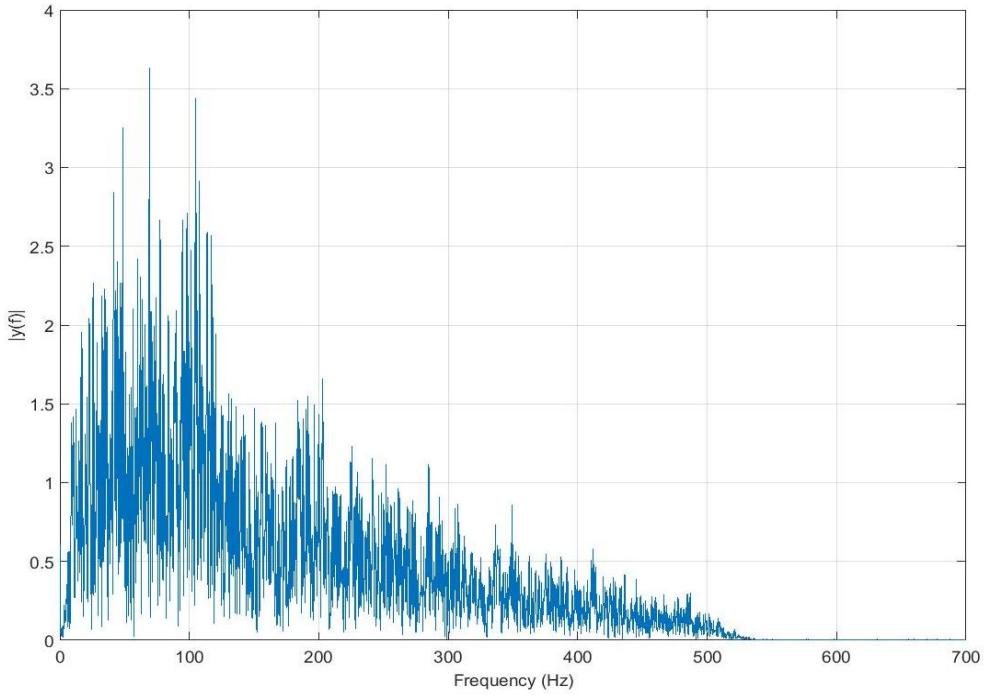

Figure 7.2: Single sided frequency spectrum for a raw EMG signal

7.4.1 Optimising EMG noise reduction system

According to [298], noise is inherent in all bioelectrical signals, hence the need for methods and techniques to reduce the adverse effect of noise on the quality of the EMG control signal. The major sources of common mode interference signals are magnetic induction, cable or electrode movement and displacement currents on the electrodes [99]. Furthermore, other sources of noise that emanated from transduction from ionic to an electron form are DC voltage potential and AC voltage potential. The other form of noise is the power-line interference also known as the AC pickup or hum and this is usually eliminated using a notch filter. However, a notch filter is not recommended for EMG circuits since the signal has valuable information at 50 Hz is regarded to be valuable. In electronic circuits, the best possible method of reducing the effect of noise is to reject common-mode signals [80].

The charge transfer between the electrode and the electrolyte is also an issue of great concern since the level of conduction is highly influenced by the degree of contact between the skin and the electrode via the electrolyte. The electrode-electrolyte interface is usually stabilised by using the $Ag/AgCl$ electrodes [99]. However, for wearable devices, the use of sticky gel is not favourable. Therefore, there is a need to develop a signal acquisition system that could acquire the signal under variable noise levels. The structure of the skin tissue and the related electrical model [299],[300] is shown in Figure 7.3.

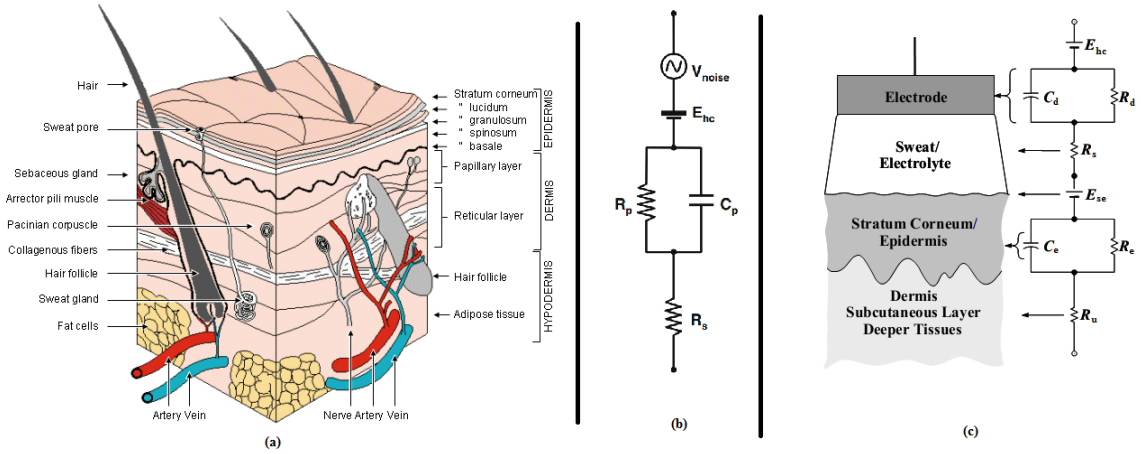

Figure 7.3: (a) Skin anatomy, (b) electrical model of the charge transfer and (c) generalised model of electrode-skin interface

The nature of the skin also influences the quality of the signal, since the skin quality varies from one individual to another. The top layer, the epidermis, has a high impedance due to the presence of dead cells [299]. According to [300], the interface between skin and the electrode can easily be modelled as an RC circuit, as shown in Figure 7.3(b), and also the electrode-skin interface in Figure 7.3(c). E_{hc} is the half-cell potential as a result of the frequency dependent of the circuit, at high frequency the impedance is represented by only R_s and at low frequencies by the sum of skin and electrode impedances $(R_s + R_p)$. The coupling of the electrode to the skin surface results in a semi-permeable membrane resulting in the potential difference, E_{ss}. Thus, the best possible technique to reduce the noise interference within the charge transfer is by using a good electrolyte as in the form of a conducting gel. The use of $(Ag/AgCl)$ electrodes is highly recommended for surface EMG [72],[85],[99].

The metallic-electrolyte interface also generates noise, which is proportional to the increase in thermal noise at frequencies above 100 Hz. However, at higher frequencies, noise generated as a result of the use of amplifiers is more dominant even though operational amplifiers are the building blocks for common-mode rejection circuits [298], [301]. An instrument amplifier will provide the same performance in a more compact way [302], [303]. When selecting the instrument amplifiers, it is also necessary to consider one with high common-mode rejection (CMR). This will suppress the signals common to both inputs before amplification. Thus, the noise reduction system is coupled with pre-amplification circuitry.

Signal loss due to magnetic interference, noise and other environmental effects is a cause of concern in low amplitude biosignals based designs; therefore, measures are always taken to maintain the signal strength and quality. If V_c is the common-mode voltage and i is the electromagnetic filed current generated from the power line and Z_g is the skin-ground impedance (see Appendix B) then:

$$V_c = iZ_q \tag{7.1}$$

Due to the infinite impedance of the amplifiers, Z_i, the common mode voltage, V_c, is greatly affected by the attenuator action of impedance at pick-up points Z_a and Z_b at the skin-electrode interface. Therefore, the gain in the noise level due to these sources is given by:

$$V_1 - V_2 = V_c(\frac{Z_b}{Z_i + Zb} - \frac{Z_a}{Z_i + Z_a}) \tag{7.2}$$

Since Z_i is sufficiently higher than the skin-electrode impedances (Z_a and Z_b) then:

$$V_1 - V_2 = V_c(\frac{Z_b - Z_a}{Z_i}) \tag{7.3}$$

As a result, skin impedance must be minimised and a high input impedance amplifier must be provided. This is the main reason why a pre-amplification circuit is necessary. However, amplifying the raw signal also means amplifying the noise within the signal. This is to avoid the unfortunate event of having an undesirable signal-to-noise ratio in the final amplification circuit.

7.4.2 Development of the active electrode

The low amplitude and weak signals from the amputated residual limb demanded the implementation of active electrode signal pre-amplification and processing. These signals can easily be detected using monopolar or differential configuration mode. However, the differential mode was more preferred as it cancels out common signals. The biopotential amplifier was based on the instrumentation amplifier, and an active high pass filter was also implemented. The advantage of electrode amplification is that it cancels out polarisation of the electrode due to input bias current as a result of poor skin contact.

The choice for instrumentation amplifiers is based on their capability to reject the common signals and only amplify the differential signal. The presence of input buffer amplifiers within the instrumentation amplifier reduces the effect of impedances from input sources, thereby maintaining the desired common-mode rejection. The common mode rejection is effected by the subtractor circuit embedded inside the instrumentation amplifier as the output stage amplifier. The need to regulate the precise DC levels, thus rejecting undesired DC offset voltage and also sudden reset after input levels, is achieved by the additional AC coupling circuit. The output from the electrode circuit was then transmitted to the analogue front end for further filtering. The proposed differential amplifier had a gain of 10 for the whole bandwidth. The expected high pass was 15 Hz as a way of preserving all the signals. This resulted in a bandwidth of 485 Hz since the signal has frequencies as high as 500 Hz. Several instrumentation amplifiers were considered for electrode amplification, and these include AD620, INA333, INA128P and INA141. The INA128P was then selected based on the single supply mode and stability over a wide range of changes in input impedance. The final design was incorporated within the multichannel system (see Appendix C for the detailed circuit).

7.4.3 Myoelectric signal filtering in a multichannel design

Noise in sEMG signals acquisition can result in poor intent classification. Therefore, there is a need to remove the unwanted signal (noise) before classification, and this is achieved by filtering the signal. SENIAM and ISEK recommendations on recording and reporting EMG signals mainly serve as guidance, however, the choice of filtering techniques is governed by the intended application. The filtering techniques used for diagnosis are different to those used for control of powered limbs. Luca et al. [98] used a bandpass filter of 250 Hz to 2 kHz even though the well-known bandpass is 15-500 Hz [49]. Their justification was the need for elimination of the movement artefact. The expected range of frequencies for EMG signals is 10-1500 Hz as determined in experiments carried out in this study [132]. To achieve such desired frequencies,

a high pass filter with a cut-off frequency of 15 Hz and a low pass filter with a cut-off frequency of 500 Hz was designed. An active low pass filter and high pass filter would produce significant results. The filters received a signal from an instrumentation amplifier. The rests of the filtering blocks were as illustrated in Figure 7.4.

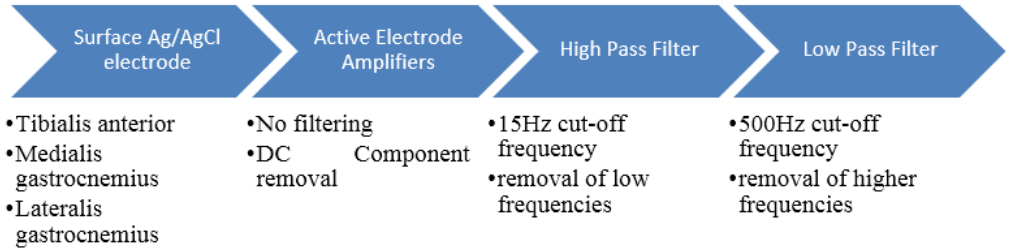

Figure 7.4: The noise filtering block diagram

7.4.4 Modelling the high pass filter

High pass filters remove the artefact noise for low amplitudes which might result from electrode movement or muscle crosstalk. This is also useful for separating signals of different frequencies. If properly designed, the filter will allow the desired signal to pass and attenuate the harmonics. The performance of the designed filter was analysed for its amplitude response. The amplitude response illustrated the ratio of the output amplitude to the input amplitude versus frequency. However, the roll-off increased as the number of poles increased. More poles in the active filter will result in more attenuation at a given frequency in the stop band. The lower cut-off frequency, f_{cH}, is the lower frequency at which the gain is3 dB less than the gain at the centre frequency. Using a second- order filter is recommended as they provide a roll-off of 40 dB/decade as compared to 20 dB/decade provided by first-order filters. After several trials, a second-order high pass filter using the Sallen-Key architecture was designed implemented. The transfer function for the second-order unit gain for a high pass filter is presented as:

$$H_{(s)} = \frac{s^2}{s^2 + \frac{\omega_0 s}{Q} + \omega_0^2} \tag{7.4}$$

where Q is the quality factor which determines the height and width of the peak of the frequency response of the filter and ω_0 is the function of the undamped natural frequency, f_0. One can thus determine $\omega_0 = f_{cH}$ as:

$$f_L = \omega_0 = 2\Pi f_0 = \frac{1}{\sqrt{R_1 R_2 C_1 C_2}} \tag{7.5}$$

$$Q = \frac{1}{2\zeta} = \frac{\omega_0}{2\alpha} = \frac{\sqrt{R_1 R_2 C_1 C_2}}{R_1(C_1 + C_2)} \tag{7.6}$$

where α is the attenuation and ζ is the damping ratio. Hence, the general expression for determining the two unknowns (R_1 and C_1) is:

$$R_1 = mR_2 \tag{7.7}$$

and

$$C_1 = nC_2 \tag{7.8}$$

Therefore, we can deduce that in terms of R_2 and C_2:

$$f_L = \omega_0 = 2\Pi f_0 = \frac{1}{R_2 C_2 \sqrt{mn}} \tag{7.9}$$

And

$$Q = \frac{\sqrt{mn}}{m+1} \tag{7.10}$$

The cut-off frequency, f_c, for a high pass filter is the frequency at which all frequencies below that frequency are eliminated. The value of f_c is actually a pre-set value determined for this design and was 15 Hzas recommended by SEIK and SENIAM standards. However, for Sallen-Key architecture, $R_1 = R_2$ and $C_1 = C_2$. This is because for Sallen-Key architectures $m = n = 1$. Therefore, the quality factor, Q, has a fixed value of 0.5. The use of 15 Hz also addresses the desired characteristics of the control signal for the intended pattern recognition system. As a result, the high pass frequency,f_{cH}, was determined as:

$$f_{cH} = \frac{1}{2\Pi\sqrt{R_1 R_2 C_1 C_2}} \tag{7.11}$$

$$\Rightarrow f_{cH} = \frac{1}{2\Pi\sqrt{(4.7\times10^3)\times(4.7\times10^3)\times(2.2\times10^{-6})\times(2.2\times10^{-6})}} \tag{7.12}$$

Therefore, $R_1 = R_2 = 4.7\,\text{k}\Omega$ and also $C_1 = C_2 = 2.2\,\mu\text{F}$ and ultimately the high pass filter cut-off frequency, $f_{cH} = 1500\,\text{Hz}$. The final circuit schematic developed was part of the broad three channel signal acquisition module, however, these were initial signal conditioning circuits before the multichannel system (see Appendix B).

While the Q factor of an element relates the losses, this also relates directly to the bandwidth of the filter with respect to its centre frequency. Q indicates energy loss relative to the amount of energy stored within the system. Thus, the higher the value of Q, the lower the rate of energy loss and hence oscillations will reduce more slowly, in other words, they will have a low level of damping. With an increasing value of Q or quality factor, the bandwidth of the tuned circuit filter is reduced. As losses decrease, the tuned circuit becomes sharper as energy is stored better in the circuit at the 15 Hz cut-off frequency when the gradient becomes zero. Therefore the Q factor was chosen to be 0.5 as a way of reducing oscillations and bandwidth. As a result, the transfer function representing the high pass filter is:

$$H_{(s)} = \frac{s^2}{s^2 + 193.42s + 9353.17} \tag{7.13}$$

7.4.5 Modelling of the low pass filter design

The low pass filter passes all frequencies from zero up to corner frequency, f_{cL}, and blocks all frequencies above this value. There was a need to implement a second-order filter to achieve the flattest response possible in the passband and most sharply defined stop band. This is achieved by cascading two low pass filters. A low pass filter has a constant gain from zero to a high cut-off frequency. These low pass filters are necessary to avoid aliasing in data acquisition circuits. The cut-off frequency, f_{cL}, is the frequency where the voltage gain is reduced to 0.707; therefore, at f_{cL}, the gain is down by 3 dB and after that, it decreases as frequency increases. The most important aspect when selecting the cut-off frequency for the low pass filter is to take into consideration the sampling frequency for the A/D converter. According to [304], using a high

sampling rate would reduce requirements on an anti-aliasing filter but could increase processing and computational load. The sampling rate should be high enough to attenuate the desired frequency while avoiding increasing the size of the data [305]. Furthermore, higher sampling rates result in hardware constraints. However, [304] suggested that a sampling frequency of less than 2000 Hz is not sufficient to avoid aliasing, hence there is a need to have a trade-off between sampling rate and hardware requirements and data size. The fundamental knowledge governing the sampling frequency is always such that the sampling frequency should be twice the frequency of the sampled raw signal [306]. The initial experiments carried out in the study revealed that a cut-off frequency of 500 Hz will be sufficient, hence the design involved selecting proper filter resistors and capacitors.

Thus, for a signal frequency of 500 Hz, a sampling frequency of 1000 Hz was sufficient. Therefore, the circuit shown in Figure 61 was sufficient to give an output of 500 Hz as the cut-off frequency. The second-order low pass filter was preferred over general RC passive low pass filters as a way of increasing the quality factor above 0.5. The technique is based on the positive feedback technology, localised to the cut-off frequency and as a result any quality factor, Q can be realised. The generalised transfer function for the low pass filter is:

$$H_{LP} = \frac{K}{-(\frac{f}{f_{cL}})^2 + \frac{jf}{Qf_{cL}} + 1} \tag{7.14}$$

where K is the gain constant governed by the feedback resistors R_7 and R_8. The relationship between the frequency, f, and the cut-off frequency, f_{cL}, governs the performance of the filter. When the occurring signal frequency, f, is far less than the cut-off filter frequency, f_{cL}, then the circuit allows all frequencies to pass but multiplies them with the gain, K. However, when the occurring frequency, f, is far greater than the f_{cL}, then all signals are attenuated to the square of the ration of the frequencies. The circuit schematic for the low pass filter is as shown in Appendix B. The second-order filter was based on equal value components such that R_5=R_6=R and C_3=C_4=C. Therefore;

$$Q = \frac{1}{3 - K} \tag{7.15}$$

It is necessary to use the best possible gain, K, during filtering since K affects the performance of the filter and for best operations, it is advisable to select $3 \geq K \geq 2$. However, any K value too close to 3 results in Q being sensitive to variations in the gain resistors. This will result in Q greater than 0.5. Therefore, the low pass cut-off frequency, f_{cL}, is:

$$f_{cL} = \frac{1}{2\Pi\sqrt{R_1 R_2 C_1 C_2}} \tag{7.16}$$

and for equal values components:

$$f_{cL} = \frac{1}{2\Pi RC} \tag{7.17}$$

$$\Rightarrow f_{cL} = \frac{1}{2\Pi\sqrt{(3.9 \times 10^3) \times (3.9 \times 10^3) \times (8.2 \times 10^{-6}) \times (8.2 \times 10^{-6})}} \tag{7.18}$$

Therefore, $f_{cL} = 500$ Hz and $\omega = 3126.95$. As a result, the transfer function, $H_{(s)}$ representing the performance of the filter, is given by:

$$H_{(s)} = \frac{s^2}{s^2 + 6253.90s + 9.78^6} \tag{7.19}$$

Therefore, resulting Sallen-Key filter responsible for both low pass and high pass filtering is illustrated in Figure 7.5.

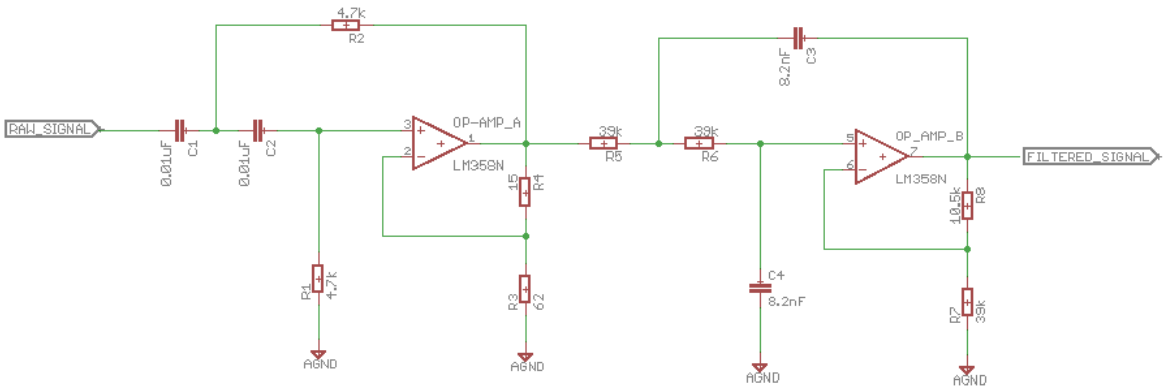

Figure 7.5: The Sallen-Key band pass filter circuit

Thus, the band pass filter has the capability of attenuating all frequencies below15 Hz and those above 500 Hz. This will reduce the computational time during post processing of the signal as low and high frequencies with less information about the signal would have been removed.

7.4.6 The multichannel front-end system

The results presented in section 4.3.1 revealed that there are three active sEMG sites on the residual stump. As a result, multichannel signal processors and conditioning circuits were preferred. The demand for additional muscle sites to provide a much larger set of signal features presented the study with a challenge to develop a system which is compact and still achieves the desired signal acquisition and processing capabilities.

There are several biopotential amplifiers commercially available, and these include the ADS1294, ADS1296 and ADS1298 [307]. These are multichannel, simultaneous sampling, 24-bit, delta-sigma analog-to-digital converters with built-in programmable gain amplifiers (PGAs), internal reference and an on-board oscillator. These features enable the development of compact medical instrumentation systems with low power consumption. The ADS1294 and ADS1296 can both accommodate four channels of signals [308], [309] as per the design specifications and considerations mentioned earlier. However, the ADS1298 was chosen on the basis of having a better sampling capability at low gain. At a gain of 12 and a data output rate of 32 kSPS, the ADS1298 has an input referred noise of 28.6 μV_{RMS}. However, the reduction in output data rate results in a reduction in input-referred noise such that a data output rate of 500 SPS results in 0.5 μV_{RMS} input referred noise. Such characteristics of increased data rate with an increase in input referred noise results in the need to have a trade-off between speed of communication and signal quality.

According to [8], the expected total processing time for a myoelectric control system is 300 ms and any system that achieves a time period less than that is considered clinically viable. One of the advantages of utilising the ADS1298 continuous-time delta-sigma ($CT\triangle\sum$) analog-to-digital converters is the availability of digital communication and extended general inputs-outputs. As a result, the $CT\triangle\sum$ architecture eliminates the need for anti-alias filtering before digitisation.

The full circuit diagram for the multichannel signal acquisition is shown in Appendix D. The following characteristics are considered important for the development and functionality of a biosignal acquisition circuit:

- *Power management*

  The reason for utilising a multichannel ADC is to acquire a large number of signals from different channels simultaneously, using low energy conception. The main considerations during power circuit design was low consumption, low noise generation, compactness and reliability. The analogue supply (AVDD/AVSS) was separated from the digital supply (DVDD). The power management was achieved using low-drop-out (LDO) voltage regulators from Texas Instruments. The TPS73250DBVT was used to achieve the stable +5 V required by the main controller while the TPS73225DBVT was configured so as to achieve +1.8 V digital supply (DVDD), as shown in Figure 7.6.

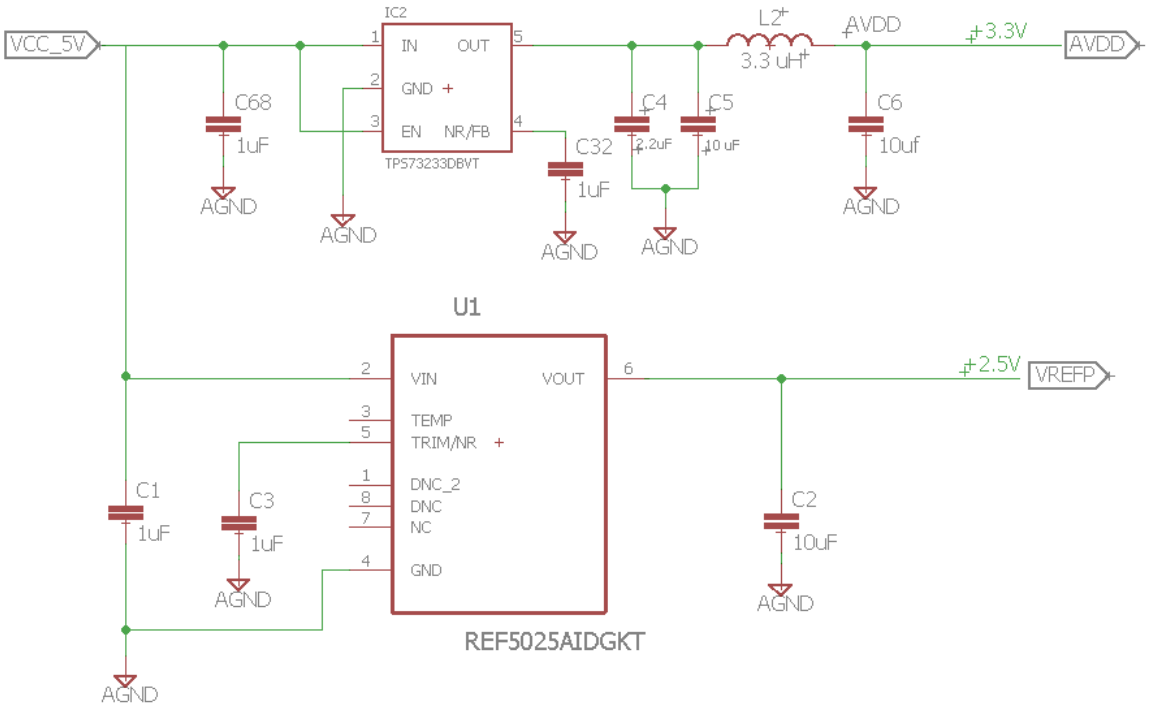

Figure 7.6: The digital supply power management circuit

The use of the voltage divider on the output of the regulator, TPS73225, facilitated the availability of the +1.8 V which is necessary for digital supply. However, the analog supply (AVDD) voltage was set to +3.3 V using the TPS73233 LDO regulator. The external reference was set at +2.5 V using the low-noise, low-drift and high precision voltage reference, REF5025, as illustrated in Figure 7.7.

The power management system is robust with regard to line and load changes. The same reference voltage which was used for the ADC is also utilised for driving the reference electrode with the aid of an amplifier. The power management system employed provides

high reverse blockage and ground pin current that is nearly constant over all values of output current.

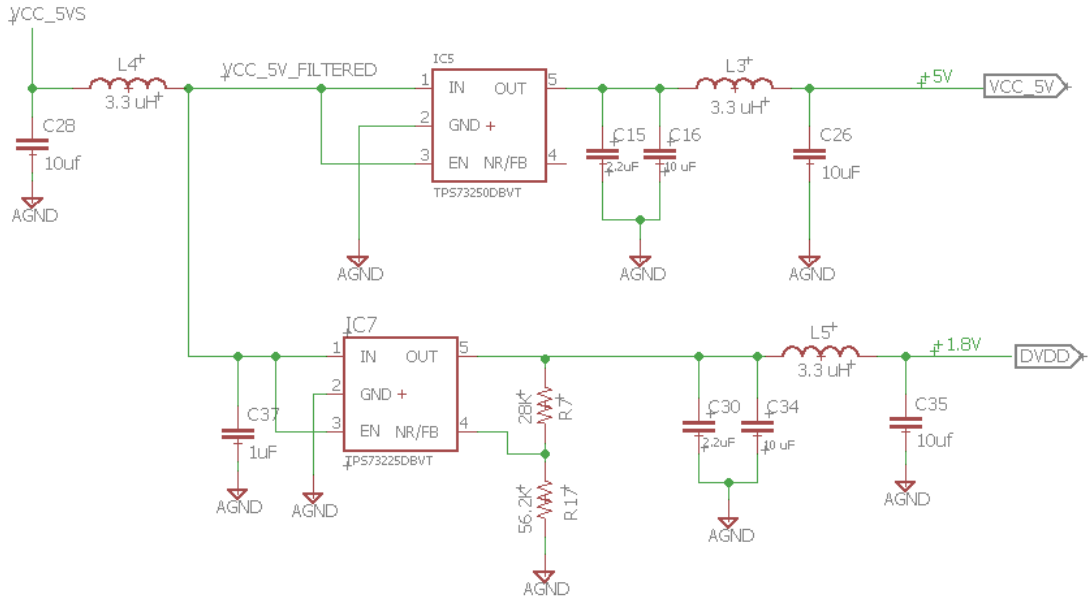

Figure 7.7: The digital supply power management circuit

- *The reference electrode configuration*

  The reference electrode forms the grounding link between the amputee and the electronic device. It is integral in the minimisation and subsequent elimination of noise. Poor reference electrode connection can result in poor signal quality [310]. Previous studies, [311] and [312], suggested that a high input impedance system on the signal detection electrodes circuit may eliminate the need for a reference electrode. However, there is no strong background information to support the suggestions, since these were mere recommendations. Furthermore, the removal of the reference or ground electrode introduced high levels of noise in the signal. The only available anatomical landmark for the reference electrode was the insertion of the Soleus just below the knee, since the soleus was not considered for the circuit as its muscle belly was reportedly inaccessible after amputation [132].

- *Signal sampling*

  The main thrust for sampling is to digitise the signal. Therefore, the parameters used considered the accuracy and reproducibility of the sampled signal. The sampling frequency highly depends on the available bandwidth. The Nyquist Theorem requires that the sampling frequency be at least twice the signal frequency [99], [101]. This was observed so as to avoid aliasing and, as a result, an anti-aliasing filter was not implemented during the post-processing of the signal.

  Higher sampling frequencies improve accuracy and data resolution. Since the system has a low pass filter at 500 Hz, the recommended sampling frequency was 1000 Hz [72]. Low

sampling rates have been reported in some studies [91], [93] and the results presented in the next section indicated acceptable accuracy when applied to classification algorithms.

7.5 Development of the pattern recognition control architecture

The main objective of any myoelectric control system is to assist the mechanical limb to achieve the desired projections during movements by utilising the sEMG as an input signal for the control architecture. However, for lower limb prosthetics, there is the additional desire of supporting the body and providing the required torque during locomotion. The motivation of implementing pattern recognition over other control techniques was to enable the identification of the intended movement with respect to the signal features or structure. Such an application results in a more robust and reliable control architecture.

The development of electromechanical prosthetic devices has outpaced the advancement of techniques to control them. The need for dexterity and high demand for multifunctional artificial limbs has resulted in the development of new modern methods to improve the control architectures. The growing need for achieving multiple movements from limited signal channels have resulted in the establishment of pattern recognition systems. The pattern recognition developed only focused on the dorsiflexion and plantarfleexion movements which are executed within the sagittal plane. This is because, despite the fact that the human ankle has three principle planes which require a minimum of three degrees of freedom to fully execute them, after amputation some movements become irrelevant for normal gait. The gait results presented by [132] indicated that abduction and adduction movements were not relevant during normal gait for amputees. The primary concern was the achievement of dorsiflexion and plantarflexion which are fundamental to locomotion.

The developed architecture considered denoising implementation prior to feature extraction and data windowing (see Appendix C). Furthermore, the system incorporated dimensionality reduction [70], a technique which was intended for the reduction of the size of the feature vector resulting in reduction in computational time and improvement in classification accuracy using principle component analysis (PCA). The stages in pattern recognition highly depended on the quality of the surface myoelectric control signal. However, the low amplitude, low signal strength, domination of low artefact frequencies and small signal bandwidth present in amputee sEMG signals made the use of pattern recognition a challenge [209], [132]. According to [209], the success of the classifier highly depends on the quality of features extracted from the control signal. Hence, the need for a reliable feature set. Therefore, a well distributed input feature-set will improve the classifier performance [281], [282]. The future of robust prosthetic limbs highly revolves around pattern recognition; the following sections describe every step taken to accomplish the proposed control pattern recognition architecture.

7.5.1 Measured input signal

The protocol explained in section 3.6.2 of the study was used to determine the best possible muscle sites with the aid of SENIAM standards as suggested by [213] on detection and conditioning of surface signals. Tibialis Anterior, Lateralis Gastrocnemius and Medial Gastrocnemius were selected as channels to provide control signals from the residual limb [132]. The nature of the detected signals is illustrated in Figure 7.8, recorded during dorsiflexion and plantarflexion respectively. The signals shown in Figure 7.8 were extracted on the amputated limb using the

three channel analog front end based on the ADS1298 presented previously in section 7.4. For a detailed circuit schematic, see Appendix D.

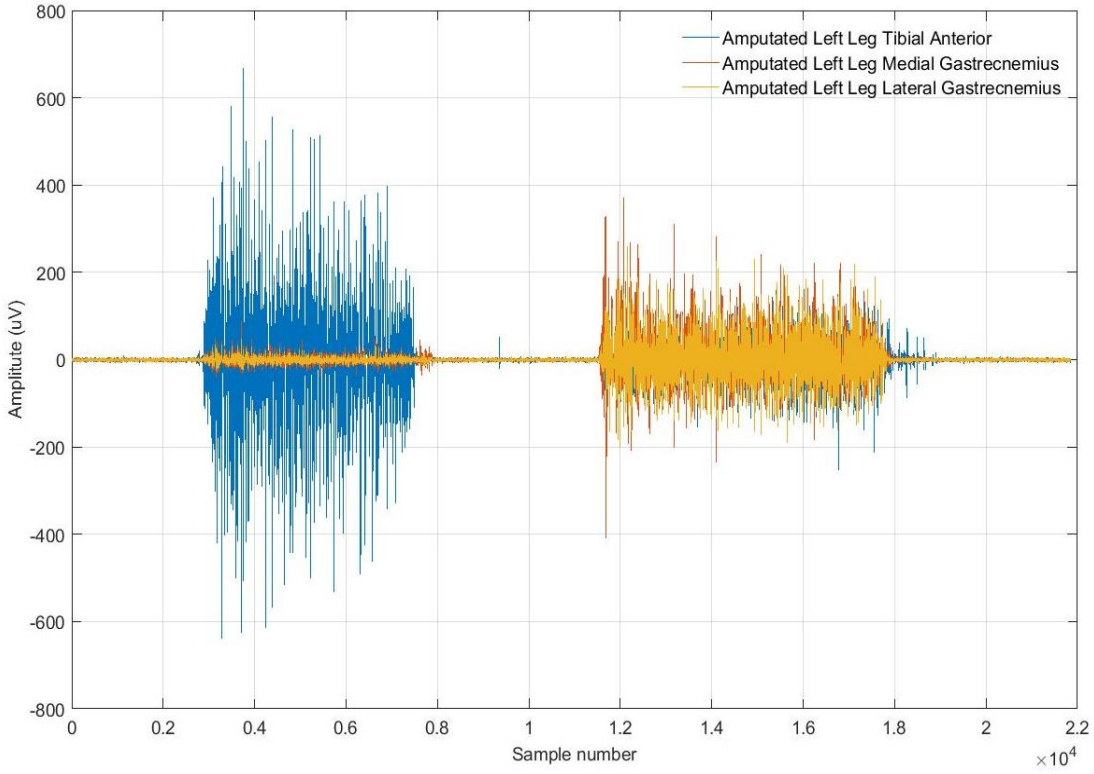

Figure 7.8: Raw sEMG signals recorded from three muscle sites

The measured signal was filtered using the 15 Hz high pass filter and also a 500 Hz low pass filter. A notch filter was not implemented to avoid losing valuable signal information around 50 Hz as this information was affected by the roll-off of the filter. The use of ADS1298 resulted in a more stable and clean signal with regard to minimisation of noise interference because of the adaptive nature of the filters. The gain of 12 used to avoid the amplification of the noise inherent in the signal and also increasing sampling capabilities of the adaptive filter. Furthermore, amplification was then applied after filtering.

7.5.2 Denoising the detected sEMG signal

Noise could not be eliminated, but efforts were made to reduce the effect of the noise both during signal acquisition and post-processing. The ADS1298 has the capability of automatically adjusting the filter constants and further amplify the signal with a gain of 12. The Wavelet denoising technique was implemented during post processing of the signal. Wavelet analysis has been widely applied in the field of image processing, hence the introduction of several techniques within the Discrete Wavelet Transform (DWT) has enabled the analysis of event-related potentials (ERP), such as electromyography signals in biomedical engineering field [313]. The recorded signals were labelled and stored as *mat*-files in Matlab. The sampling frequency and the duration

of each signal were also noted. The following steps were carried out on achieving the suggested denoising technique:

- *Performing a multilevel wavelet decomposition*: This included obtaining the approximations and detail coefficients. The signal was split into low pass sub-bands approximation level, $A1$, and high pass sub-bands, $D1$.
- *Identifying a thresholding technique*: Thresholding of the detail coefficients was then carried out. The available techniques included the universal threshold method, sure-shrink/rigsue method, Heursue method and minmax method. The signal was then analysed, and a suitable threshholding technique was selected between hard and soft thresh holding, where x was the signal and D was the set of first level detail coefficients.
- *Thresholding the detail coefficients and reconstruction of the signal*: This enabled the visualisation of the usable denoised EMG signal. In both techniques, coefficients less than the threshold were reduced to zero. In soft thresholding, the coefficients greater than the threshold were shrunk to zero (x-threshold) while in hard thresholding, the coefficients greater than the threshold were left unchanged.
- *Comparing the results*: The results were then compared with other denoising techniques, such as the Savitzy-Golay technique and the Moving Average technique, using the signal-to-noise ratio (SNR) values.

The choice for Discrete Wavelet Transform (DWT) over the Continuous Wavelet Transform (CWT) was based on the fact that the information CWT displays at closely spaced scales, such as sudden reflexes of the muscles, is highly correlated and therefore unnecessarily redundant for denoising and analytic purposes [314], [315], thus rendering it inefficient. According to [316], DWT utilises a series of half high passband and low passband filters (wavelets) to decompose the input signal into scales (frequency bands), thereby making it possible to analyse nonstationary signals, such as sEMG signals because the surface EMG signals exhibit slowly changing trends punctuated with transients. An effort to use Fourier Transform (FT) was regarded unreliable because the method does not represent abrupt changes efficiently. This is due to the fact that FT represents data as a sum of sine waves which are not localised either in time or frequency domain. The DWT denoising enables the use of the full-scale range of the signal. Although there are several forms of wavelets, such as Morlet, Daubechies, Coiflets, Biorthogonal, Mexican hat and Symlets shown in Figure 7.9, it is the Symlet wavelet which was preferred for this application. These are also known as Daubechies' least asymmetric wavelets. Their symmetric property makes them best suited for sEMG denoising. The properties could be manipulated by varying the number of taps of the filter. The output coefficients of DWT are directly proportional to the number of samples, and, this reduces computational time. The superiority of the Discrete Wavelet Transform (DWT) is that the functions are well localised in time and frequency. The fact that a wavelet is a rapid decaying wave with a zero mean allows for complex EMG signals to be analysed and easily localised. Since the muscle activation can only occur for a short duration, the best technique to use is the wavelet denoising technique. DWT is orthogonal, that is a subset is a selected translation and scaling of the main set and they significantly correlate to each other. The two concepts initially considered when selecting the nature of the Symlet wavelet were scaling and shifting the wavelet. The process of scaling allowed for shrinking the signal in time domain and was achieved as:

$$\varphi(\frac{t}{s}) \qquad for \quad s > 0 \tag{7.20}$$

where s was the scaling factor, a positive constant which corresponds to how much a signal was scaled in time, and was inversely proportional to the frequency such that increasing the scale factor reduced the frequency. The reciprocal relationship between the scale factor and the frequency was the centre frequency, C_f, and it was regarded as the constant of proportionality. This was mainly because the wavelet has a bandpass characteristic in the frequency domain such that the equivalent frequency, F_{eq}, was a relationship between sampling interval, Δt and the centre frequency, C_f:

$$F_{eq} = \frac{C_f}{s\Delta t} \tag{7.21}$$

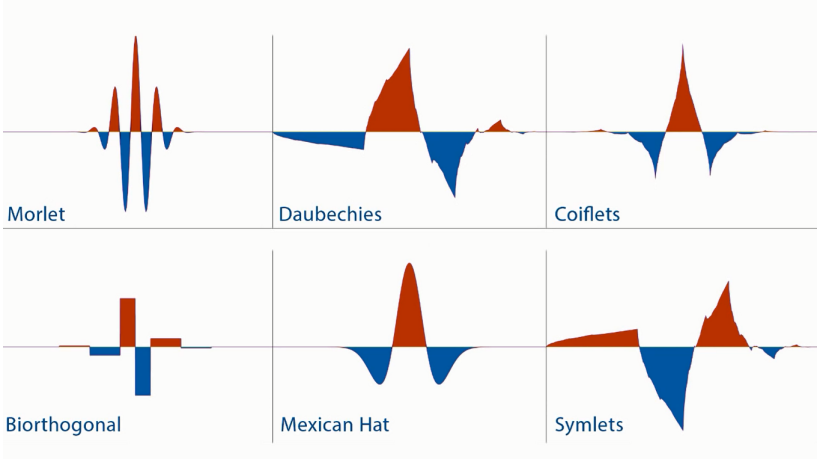

Figure 7.9: Types of wavelets

Stretching the wavelet assisted in capturing slowly varying changes and, in some instances, shrinking ($0 < s < 1$) the wavelet assisted in capturing abrupt changes. Different scales were therefore created from different frequency ranges being analysed. After scaling the wavelet, the resultant wavelet was then applied to selected points along the signal using the process called shifting. The idea was to shift the wavelet and centre it at point k along the signal to denoise the section where a specific feature is being targeted for feature extraction:

$$shifting, \quad \phi(t-k) \tag{7.22}$$

The major advantage of DWT was that one could denoise a signal with few coefficients. It was therefore good for faster processing and presentation of the signal. The scaling and shifting techniques helped in eliminating redundancy in coefficients.

7.5.3 Data segmentation

Data segmentation is one of the important procedures that affect a pattern recognition system. It is fundamental in determining the reliability of a feature extractor with regard to complexity. Ultimately, windowing positively affected the overall complexity and processing time of the architecture. When the data was recorded, it was in the form of a stream of digitalised values in a channel format. However, for analysis to be carried out there was a need to develop a window which focused on the motion of interest. As a result, a segment was regarded as a window where the features were extracted. The summation of all windows resulted in the length

of the original signal. The signal detection and classification was made to occur within 300 Hz to achieve the objective of real-time control [20]. Therefore, a 250 Hz window was selected for this design with an overlap of 32 ms. This was adopted from the protocol implemented by [20] on achieving the proposed robust control architecture. The segment length, state of data and the window technique were the major considerations during the design. These parameters affect the performance of the pattern recognition system [8]. The decisions, D_n, are made at every 250 ms intervals in real-time and, as a result, the processing delay, τ, is a summation of feature extraction and feature discrimination time. Therefore, the total decision time was defined as $(\tau + R_n) < 50$ Hz.

7.5.4 Feature extractor development

Feature extraction was implemented after data segmentation. However, due to signal distortion as a result of noise inherent in the detected signal, it was very difficult to use the raw sEMG signal as an input signal to a myoelectric control system. Therefore, the 15 to 500 Hz band pass filter was implemented during signal detection and transmission. Furthermore, a sixth-order Butterworth filter was implemented during post processing of the signal prior to data segmentation.

Every bioelectric signal has its own distinct features and, due to its stochastic nature, the myoelectric signal is rich in features that can be extracted either in time domain or frequency domain. There are more than ten time domain features and six frequency domain features available for use in myoelectric control systems [317]. Feature extraction techniques employed in any pattern recognition algorithm determines the extent to which the system can give accurate predictions [282], resulting in the need for proper selection of features. Previous studies [107], [318], [70] have proposed several methods of extracting the features of the EMG signal so as to improve its usability. The success of the classifier highly depends on the quality of features extracted from the signal [209]. The features considered in this study were adapted from the features suggested by [70], which were an extension of the features used by [107]. Additionally, the modified Hudgins Features, suggested by [209], namely the Modified Mean Frequency (MMNF) and Modified Median Frequency (MMDF), were also considered so as to increase the feature vector with the aim of improving the classification accuracy. The representation of the features is explained in detail in the following sections. The analysis was applied to every window which was presented as a row within the feature vector and the result was a column of features for every window. The following section discuss some of the features which were used to develop the feature vector.

Mean, μ: The μ analysis was applied on the segmented data, i, of the EMG signal, x, such that each sample value, x_n, is from returned, $\overline{x}_{i(\mu)}$. The length, N_w, of the signal within the window was considered from the total length, N, of the recorded signals. Therefore μ is given by:

$$\overline{x}_{\mu(i)} = \frac{1}{N}\sum_{k=1}^{N_w} x_k \qquad for \quad i = 1, 2, 3, ..., I \tag{7.23}$$

where x_k is the k^{th} sample in a window, i, and I is the total number of windows present in the channel.

Mean Absolute Value, MAV: The MAV analysis was applied on the segmented data, i, of the sEMG signal, x, such that each sample value, x_n, is from returned $\overline{x}_{i(MAV)}$. The length, N_w,

of the signal within the window was considered from the total length, N, of the recorded signals. Therefore, the MAV is given by:

$$\overline{x}_{MAV(i)} = \frac{1}{N}\sum_{k=1}^{N_w}|x_k| \qquad for \quad i = 1, 2, 3, ..., I \tag{7.24}$$

where x_k is the k^{th} sample in a window, i, and I is the total number of windows present in the channel.

Mean Absolute Deviation, MAD: The MAD, analysis was applied on the segmented data, i, of the EMG signal, x, such that the each sample value, x_n, is derived from $\overline{x}_{i(MAD)}$. The length, N_w, of the signal within the window was considered from the total length, N, of the recorded signals. Therefore MAD is given by;

$$\overline{x}_{MAD(i)} = \frac{1}{N}\sum_{k=1}^{N_w}|x_k - \overline{x}_w| \qquad for \quad i = 1, 2, 3, ..., I \tag{7.25}$$

where $\overline{x_w}$ is the mean for the window having N_w samples while x_k is the k^{th} sample in a window, i and I is the total number of windows present in the channel.

Zero crossings, ZC: The ZC analysis was carried out for every window, hence returning a column of values representing the signal, x, per channel. The sEMG signal poses some sine wave characteristics and this included the ability to have a definite number of times it crosses zero. However, due to motion artefact, skin impedance changes and the 50 Hz power line interference, a threshold, ϵ, was set. Such a technique was once applied by [20]. When assuming consecutive samples, x_k and x_{k+1}, the zero crossing counting was only detected when:

$$(x_k > 0 \quad and \quad x_{k+1} < 0) \quad or \quad (x_k < 0 \quad and \quad x_{k+1} > 0) \tag{7.26}$$

and:

$$(|x_k - x_{k-1}| < \epsilon) \tag{7.27}$$

The ZC was treated as a simple frequency measure in a more customised manner.

Slope Sign Change, SSC: This feature is almost similar to the ZC feature, however, instead of determining the behavior of the signal along the datum line, the signal behaviour is monitored based on comparing the current sample value to the previous sample value. Similarly, a threshold, ϕ, was set given three samples, x_{k-1}, x_k and x_{k+1}. The SSC was only incremented when:

$$[x_k > x_{k-1} \quad and \quad x_k < x_{k-1}] \quad or \quad [x_k < x_{k+1} \quad and \quad x_k < x_{k-1}] \tag{7.28}$$

and:

$$(|x_k - x_{k+1}| \geqslant \phi) \quad or \quad (x_k - x_{k-1}) \geqslant \phi \tag{7.29}$$

Waveform Length, WL: The actual length of a waveform within a window length determines the complexity of the cumulative length signal wave form. As such:

$$x_{WL(i)} = \frac{1}{N}\sum_{k=1}^{N_w}|\Delta x_k| \quad where \quad \Delta x_k = x_k - x_{k+1} \tag{7.30}$$

The value, x_{WL}, contains the amplitude, frequency and duration of the waveform. It is a very good indicative measure of the sEMG signal which is stochastic in nature and poses properties of a sine wave.

These signal features were then used to develop a single feature vector of time domain features which was then implemented along with frequency domain features, such as mean frequency, median frequency and signal power, as an input vector to the pattern recognition classifiers. Previous studies indicated that some classifiers use one feature while others utilise two or more features for robustness purposes. The fact that a sEMG signal is stochastic presents a complex task during classification. The strength of the whole active system was determined by the classification accuracy. To develop a less complex system, [319] used the Mean Absolute Value (MAV) as a single signal feature for classifying motions of an upper limb. However, the classification accuracy depended mostly on the activity concerned and, as a result, 55% classification accuracy was recorded. This revealed the need for a large yet manageable feature set, which the author opted to use.

The available literature revealed a lot of conflicting facts with regards to which feature domain to use between time features and frequency domain features. Ever since the 1990s [107] up to the recent studies [320], the size of a feature set has been a subject of debate [318],[20], [220], [70]. However, there is a common trend among all studies that the feature set was large enough to improve classification and small enough to reduce computation complexity. This has resulted in hybrid systems as new and existing techniques were merged together to improve classifier accuracy. It is, however, the use of several signal features in a classifier that usually enables robustness in a system although it increases transient response. The results of the feature vectors are presented in section 8.6.

7.5.5 Dimensionality reduction

The literature survey revealed several types of time and frequency domain features that could be used for the study. In previous studies, the size of the feature set affected the performance of the developed system [220]. As a result, different methods were investigated with regard to feature reduction as a way of system optimisation. Dimensionality reduction is regarded as the removal of redundant features within a feature set to reduce computational complexity and processing time without compromising the classification accuracy [70]. When dimensionality reduction was applied on the initial feature set, the remaining feature set was rich in global information, in other words, a true representation of the actual signal and not just the segment under investigation. The provision of accurate signal representation is fundamental to the reliability of a pattern recognition based control system, and feature sets can be formulated from time domain statistics, autoregressive coefficients and time-frequency information. Such techniques were also applied previously by [71] and [185] as they reported that it was often very difficult to decide the number of features to include in a feature set to optimise classifier performance. As a result, an automated process of identifying relevant features that will optimise classification was developed in the Matlab R2017a environment.

Principal Component Analysis (PCA) and Self Organizing Feature Maps (SOFM) were the most common feature reduction methods in the 1990s [321]. However, [322] argued that the linear supervised feature reduction method, which employs linear discriminant analysis (LDA), was superior to PCA and SOFM. LDA and FisherâĂŹs LDA all strive to find the linear combination

of features. According to [323], LDA performs better on continuous quantities. In an effort to optimise the dimensionality reduction process, some studies reported hybrid systems. Liu [113] and Kushaba et al. [185] developed hybrid systems with the aid of non-linear and fuzzy extension versions of LDA through the incorporation of kernel learning and fuzzy methods, known as generalised discriminant analysis (GDA), and orthogonal fuzzy neighbourhood discriminant analysis (OFNDA), respectively.

From the aforementioned suggestions, there is a relationship between the feature extraction techniques used and also the dimensionality reduction technique implemented. Therefore, some studies avoided the use of dimensionality reduction techniques as they are bound to be limited on feature extraction techniques. The reliability of a classification system is measured by its classification accuracy; however, this property is affected by the complexity of the classification problem and the quality of the signal features. According to [324], the role of dimensionality reduction is to derive a smaller set of features from a multivariate feature set with less redundancy as a clear representation of the original data set. This will result in a classifier with fewer inputs which will have fewer adaptive parameters leading to improved generalisation properties. Ultimately, this will reduce classification complexity and computational time.

Therefore, the study implemented dimensionality reduction using PCA based on the fact that the technique fitted well with the size of the available features within our feature set. Other methods tested included SOFM, but the targeted classifiers such as LDA, Linear Support Vector Machines (LSVM) and Decision Trees did not provide convincing results as they either reduced classification accuracy or increased processing time. However, PCA provided acceptable results when combined with LSVM.

7.5.6 Feature reduction using principal component analysis

A large amount of variables (33) within the feature vector made it impossible to apply basic visualisation and, as a result, PCA dimensionality reduction was applied before classification. The PCA technique has the capability of combining features (variables), F_n, and replacing them with a single principal component, F_{ci}, which is orthogonal, thereby providing a true representation of the original variables. As a result, $F_{ci} < F_n$ indicates a reduction in original feature vector size. Therefore, redundant features are eliminated and, in doing so, the processing time is greatly reduced and classifier performance is optimised. The derived linear orthogonal components represent maximised variance within the original data set [325]. If $\boldsymbol{F_v}$ is the initial feature vector then the population covariance matrix for the time domain and frequency domain features is given by:

$$varF_v = \begin{bmatrix} \sigma_1^2 & \sigma_{12} & . & . & . & \sigma_{1p} \\ \sigma_{12} & \sigma_2^2 & . & . & . & \sigma_{2p} \\ . & . & . & . & . & . \\ . & . & . & . & . & . \\ . & . & . & . & . & . \\ \sigma_{p1} & \sigma_{p2} & . & . & . & \sigma_p^2 \end{bmatrix} \tag{7.31}$$

Then, taking the linear combinations into consideration:

$$Q_1 = r_{11}F_1 + r_{12}F_2 + \cdots + r_{1p}F_p \tag{7.32}$$

and:

$$Q_2 = r_{21}F_1 + r_{22}F_2 + \cdots + r_{2p}F_p \tag{7.33}$$

Therefore:

$$Q_1 = r_{p1}F_1 + r_{p2}F_2 + \cdots + r_{1pp}F_p \tag{7.34}$$

These combinations can be regarded as linear regression, predicting Q_i from the variables $Q_1, Q_2, \cdots, Q_n$. Hence, there is no intercept and, as a result $r_{i1}, r_{i2}, \cdots r_{ip}$ can be regarded as regression coefficients. Therefore the concept is based on selection of $r_{i1}, r_{i2}, \cdots ip$ coefficients that maximises the feature vector,

$$varF_i = \sum_{k=1}^{p}\sum_{l=1}^{p} r_{ik}\sigma_{kl} = r_i^{'}\sum r_i \tag{7.35}$$

However, this is subject to the fact that the sum of squared coefficients adds up to unity [326] and the new derived component will be uncorrelated with all previously defined components. As such:

$$r_i^{'}r_i = \sum_{j=1}^{p} r_{ij}^2 = 1 \tag{7.36}$$

Therefore:

$$cov(Q_{i-1}, Q_i) = \sum_{k=1}^{p}\sum_{l=1}^{p} r_{i-1,k}r_{il}\sigma_{kl} = r_i^{'}\sum r_i = 0 \tag{7.37}$$

Therefore, the technique shows that all the principal components are uncorrelated with one another, resulting in a maximised distinguishing technique for the features under consideration. After the application of the PCA technique on a feature vector with 33 variables, it was reduced to 23 variables resulting in increased classification accuracy and reduction in processing time.

7.5.7 Classifier development using linear support vector machines

There are several motion classes which were evaluated during the determination of design parameters; the results revealed that the sagittal plane motions (dorsiflexion and plantarflexion) at the ankle were the main motions that affect the human gait. Therefore, the two principal motions (dorsiflexion and plantarflexion) within the sagittal plane were used for the development of the classifier. These two motions provided the initial two motion classes (dorsiflexion and plantarflexion) and the *resting* class was included since it was fundamental for gait analysis. Resting was considered to be that moment when none of the muscles was activated, in other words, when no intention was detected. The labelled data was used for training and validation. The motion classes were categorised visually, as illustrated in Figure 7.10.

Visual inspection indicated and increased amplitude of signals from the non-amputated leg as compared to signals from the residual limb. However, the inaccessibility of the Soleus muscle on the amputated leg presents a challenge with regard to detection of plantarflexion motion. As a result, a robust classifier was preferred, taking into consideration repeatability, sensitivity, classification accuracy and processing time of the classifier. The fact that there are mainly two classes which require classification, with the resting class being evaluated as the datum, resulted in the linearity of the data. In its simplest format, support vectors are those data points that are scattered close to the hyperplane, hence providing difficulties during classification. The analysis of features presented section 7.5.4 resulted in the predetermination of Linear-SVM (LSVM) as the best possible classifier as illustrated in Figure 7.11. However, another 22 possible classifiers were also tested, as presented in the next section 7.5.7.

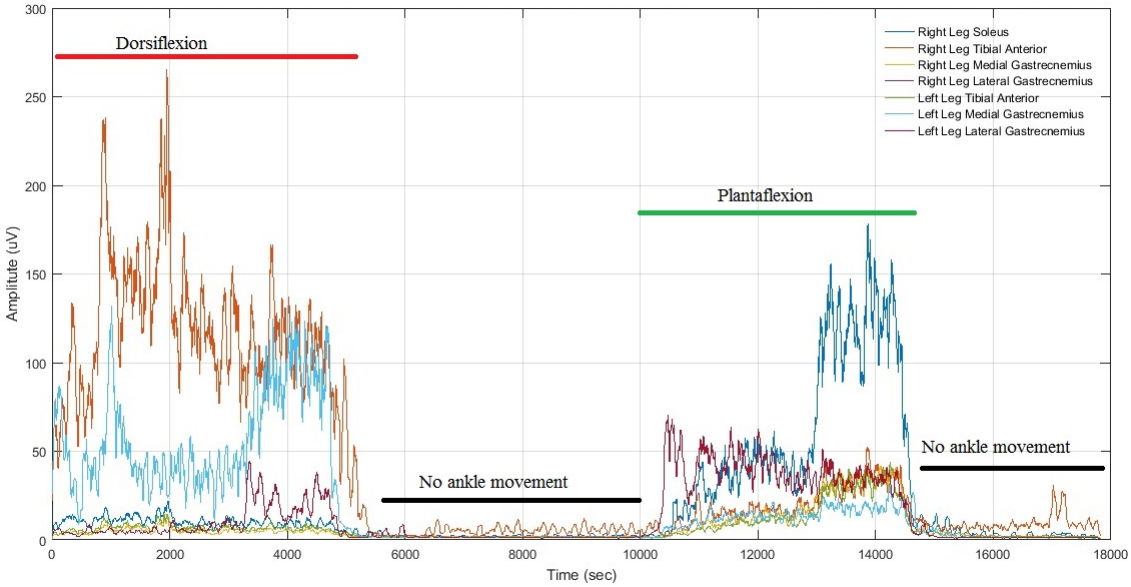

Figure 7.10: Labelled EMG signals during sagittal plane movements

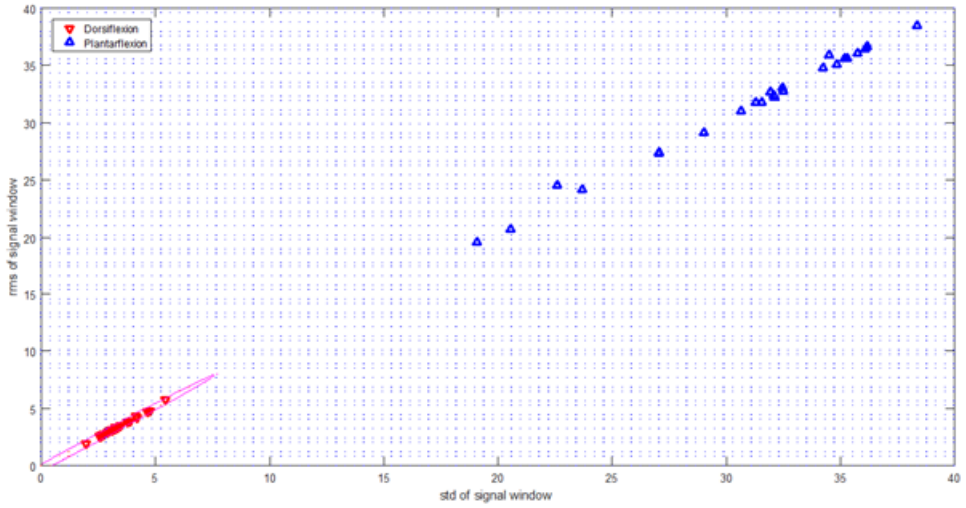

Figure 7.11: Using std and rms of the EMG signal as features

It is was deduced from the standard deviation (*std*) and root-mean-square (*rms*) values, extracted from labelled data for dorsiflexion and plantarflexion, that a hyperplane could be implemented. The linearity of the data was sufficient enough, to suggest LSVM as the initial possible classifier. Therefore, all that was needed was to develop the optimal hyperplane that could maximise classifier performance even in the event of poorly presented features, as illustrated in Figure 7.12. This will result in a more robust classifier. The underlying principle for LSVM was to maximise the margin around the separating hyperplane by increasing the separating distance, d.

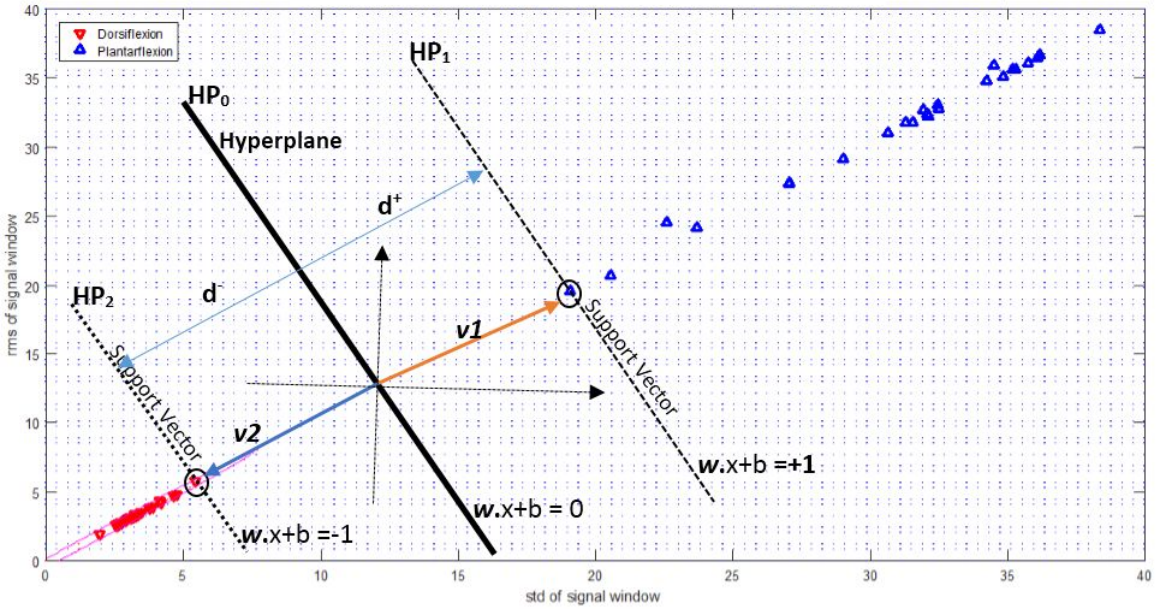

Figure 7.12: Illustration of LSVM technique on selected features

These support vectors (SV) had the capability of shifting the hyperplane, HP_0, when manipulated as compared to the other data points which were far from the hyperplane and not within the distance, d. The main role of the Support Vector Machine (SVM) algorithm was to optimally determine the position of the hyperplane and widening the distance, d. Therefore, the problem becomes an optimisation problem which was solved using an optimisation technique. The input to the SVM was a vector of features $(x_{mean}, x_{std}, , x_{ISS})$ extracted in the previous section 7.5.4 after application of PCA dimensionality reduction technique. The resultant output from the machine was a set of weights, w_i. Therefore the hyperplanes were represented as follows:

$$HP_1 \quad : \boldsymbol{w} \cdot \boldsymbol{x}_i + b = +1 \tag{7.38}$$

$$HP_2 \quad : \boldsymbol{w} \cdot \boldsymbol{x}_i + b = -1 \tag{7.39}$$

where $\boldsymbol{w}$ was the weight vector, $\boldsymbol{x}$, was the input vector (features) and b was the bias. The HP_0 was regarded as the median, where $w \cdot x_i + b = 0$. Therefore, d^+ was the shortest distance to the closest positive point, while the shortest distance to the negative point was regarded as d^- and, as a result, $|d^+| + |d^-| = d$, which was the margin of separation that needed to be increased so as to optimise classifier performance. Assuming the generalised approach that the distance, d, from a point (x_0, y_0) to any line $Ax + By + c = 0$ on a Cartesian plane is represented by:

$$d = \frac{Ax_0 + Bx_0 + C}{\sqrt{A^2 + B^2}} \tag{7.40}$$

and taking into consideration the hyperplanes representing the SV, then the distance, d^+, between HP_0 and HP_1 is derived as:

$$d^+ = \frac{|\boldsymbol{w} \cdot \boldsymbol{x}_i + b|}{\|w\|} = \frac{1}{\|w\|} \tag{7.41}$$

As a result, the total distance, d, between HP_1 and HP_2 was given by:

$$d = \frac{2}{\|w\|} \tag{7.42}$$

Therefore, when maximising the margin, one simply maximises $\|w\|$ given that there were no additional data points in between the two extreme hyperplanes, HP_1 and HP_2, such that:

$$HP_1 \quad : \boldsymbol{w} \cdot \boldsymbol{x}_i + b \geq +1 \qquad when \quad y_i = +1 \tag{7.43}$$

$$HP_2 \quad : \boldsymbol{w} \cdot \boldsymbol{x}_i + b \leq -1 \qquad when \quad y_i = -1 \tag{7.44}$$

Therefore, the Linear SVM classifier for the 2D discriminant was built on the basic form of:

$$f(x) = \boldsymbol{w}^T x_i + b \tag{7.45}$$

For LSVM, only the weight, w, was returned after training for the classification of new sEMG data which was presented as a vector of 23 features, $x_1, \cdots, x_n$. Therefore, for linearly separable features:

$$f(x) = \sum_{i=1}^{N} \alpha_i y_i (\boldsymbol{x}_i^T x) + b \tag{7.46}$$

where α_i is a slack variable $\boldsymbol{x}_i$, is the SV and the data point is represented as (x_i, y_i).

7.6 Results

The development of the robust myoelectric control architecture proved to be a broad field of study incorporating electronics, biomechanics, signal processing and artificial intelligence. Therefore, the results were presented in a modular manner as each field contributed differently to the final design. The quality and nature of an input signal to a control system influences overall performance of the system. This section is organised according to how the analysis of the EMG signal was done. Therefore, issues regarding signal distortion are presented and discussed as they affect the signal quality and ultimately the classifier performance. A novel technique for denoising the signal was then proposed. The denoised signal was then analysed with respect to the quantity and quality of features that were available for the development of the feature set. A dimensionality reduction technique was then applied to eliminate redundant features, thereby optimising the classifier performance. A LSVM classifier was modelled to fit the data and the classification *accuracy*, *sensitivity* and *specificity* was analysed.

7.6.1 Evaluation of noise inherent in the myoelectric control signal.

The recording of signals on an amputated residual limb is a challenge, and the skin movement and the changes on skin impedance contribute immensely to signal acquisition challenges. It should be noted that the skin at the residual stump is more loosely held as compared to the sound leg. According to [98], the current technologies are not immune to several noise interferences except for baseline noise and movement artefact noise. Therefore, there is a need to analyse the level of noise inherent in the myoelectric signal. Viljoen et al. [76] categorised the sources of noise in EMG signal as physiological and non-physiological, and these include movement artefact, changes in skin impedance and 50 Hz power line interference. The *Ag/AgCl* electrodes were used to record the sEMG signals from the three muscle sites, and an assessment was carried out on the behaviour of the signal during skin movement. To analyse the influence of the noise generated as a result of skin movement, the signal recorded during non-interference of the cable was compared to signals recorded during excessive cable movement, as illustrated in Figure 7.13.

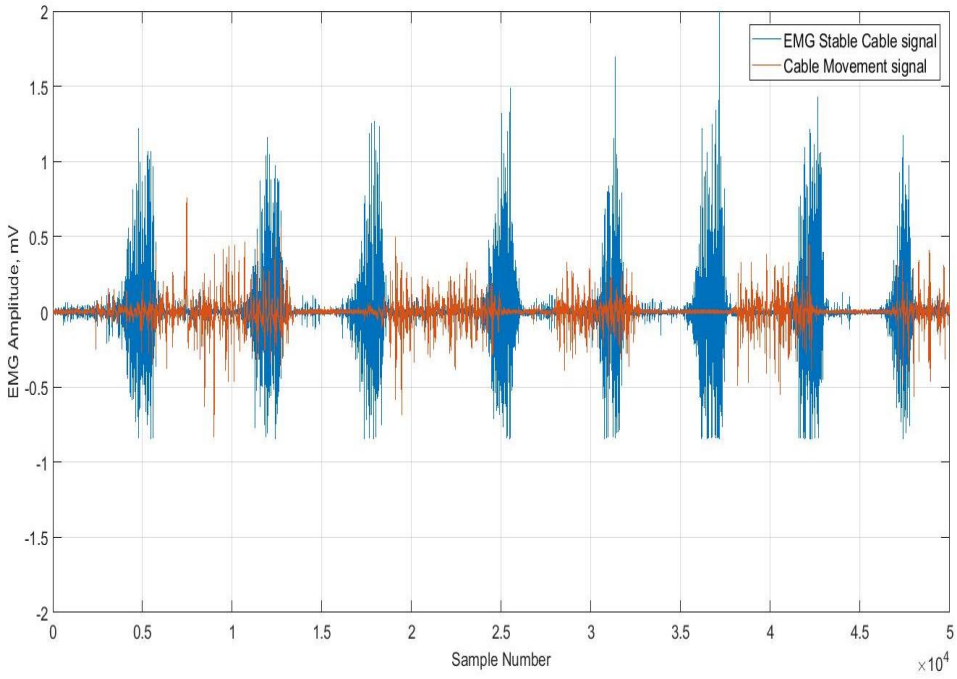

Figure 7.13: Noise signal due to cable movement and the noise free signal

The objective was to determine the extent to which the movement artefact was affecting the signal. The rapid increase in signal amplitudes in Figure 7.13 indicates the sudden application of shear forces resulting from peeling of the surface electrode. The slow increasing amplitudes were due to slow peeling. Similar findings were recorded by [327]. The signal was recorded from the Tibialis anterior muscle during sagittal movements from the output of the differential electrode amplifier before filtering was carried out. Luca [98] suggested that there is a need to have a trade-off between filtering out the noise and preserving the information within the signal. As a result, there is need to have a systematic way of selecting the amplifier gain and the filtering techniques. The differential amplifier gain, G, is given by:

$$G = 1 + \frac{49.4k}{R_G} \tag{7.47}$$

where R_G is the gain resistor and in this case $100\,\Omega$ was used. The idea was to provide the signal within the mV range while minimising the immediate amplification of the noise signal before the filtering section of the circuit. The power spectral analysis was then carried out on both signals so as to determine the dominant frequencies within the signal. During such a test, it is recommended that the sampling frequency and window size of the data segment remain constant over time [98]. The results generated are illustrated in Figure 7.14 for the noise signal. The spectrum showed how each frequency contributes to the overall signal structure and hence affects the signal features. The spectrum indicates that the most dominant frequencies resulting from cable movement artefact are within the ranges of 1-20 Hz. As a result, it is necessary to increase the cut-off frequency for the high pass filter to 20 Hz so that we could minimise the effects of noise due to cable or electrode movement.

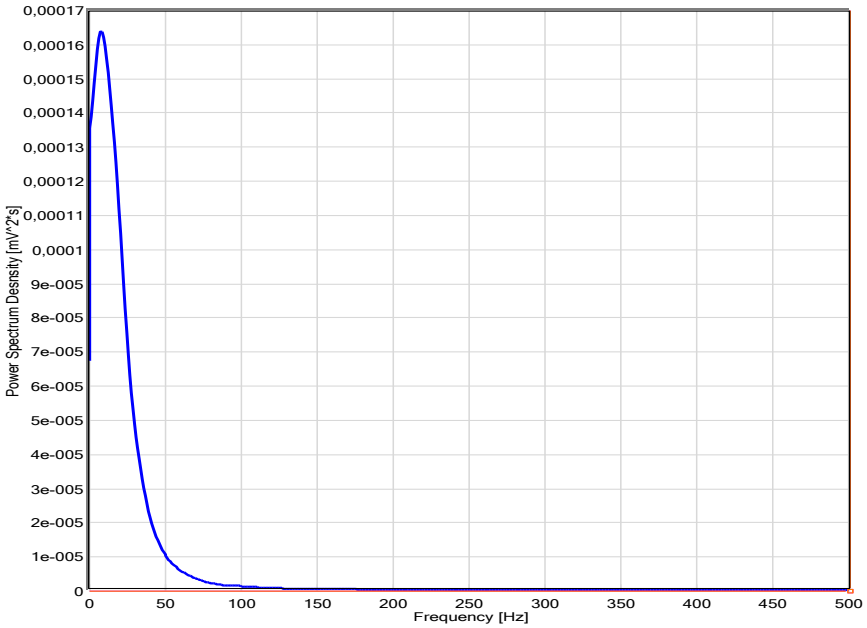

Figure 7.14: Frequency response of the noise signal

These results agree with the findings of [98] who suggested a 20 Hz cut-off frequency for high pass filter with a slope of 12 dB/Oct having the capability of removing movement artefact. The findings also support the work carried out by [327] who suggested that not all noise emanates from the electrode-skin, interface but also from general movement of the skin even when the cable is firmly secured. According to [98], skin movement due to electrode cable movement has a negative effect on the sEMG signal quality.

7.6.2 Electronic circuit performance analysis

The results presented in this section were achieved using Multisim (National Instruments, Texas, USA) and Matlab R2017a platforms. The developed embedded electronic control system was analysed so as to determine its reliability. Several analyses such as Bode plot, Monte Carlo analysis, noise analysis and AC analysis, were performed and the results were presented graphically. There was a need to analyse the circuit for the low pass filter performance so as to determine whether the selected circuit components achieve the desired cut-off frequency, f_{HC}, at the expected -3 dB. The results are illustrated in Figure 7.15. The roll off of the filter is important as it illustrates the filter response to the presence of noise. The attained frequency at -3 dB was 14.9940 Hz, but since the decrease in dB will result in an increase in frequency at -3 dB, the frequency will be approximately 15.40 Hz. The recommended cut-off frequency is 15 Hz [89],[180]. The exact value of the frequency at -3dB Hz was difficult to illustrate; therefore, the bode plot values were exported to an excel file and presented in Table 7.1.

Table 7.1: High pass filter performance

Frequency, Hz	**Voltage,** V
14.4544	0.661629
14.7911	0.678076
15.1356	0.694455
15.4882	0.710743
15.8489	0.726915
16.2181	0.742954

The desired $-3\,\text{dB}$ is equivalent to 0.707 of the voltage scale; hence, between 0.6945 and 0.7107 the frequency has a minimum of 15.1386 Hz and 15.4881 Hz respectively. Therefore, it can be concluded that the resistor values and capacitor values were within the desired range.

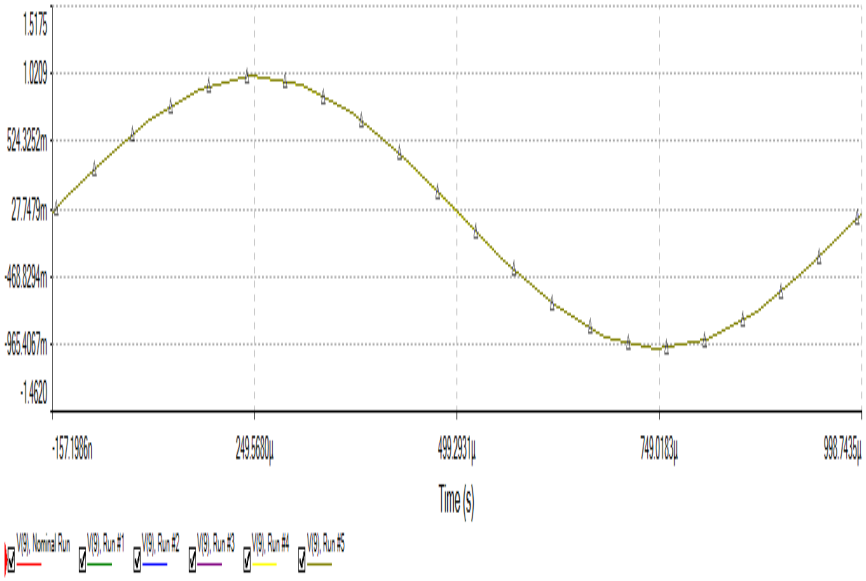

Figure 7.15: The Monte Carlo failure analysis

The failure to achieve the desired cut-off frequency has been attributed to the large tolerance of the circuit elements, such as the resistors and capacitors used to develop the filter. Tolerances were selected at 1% which was the minimum practical available value. However, to a less extent, this affected the circuit performance. The gain for the first stage components of the filter was kept at values less than 2 so as to avoid amplifying the noise. As a result, of the low gains, it was difficult to use high-value resistors and to achieve the desired frequency values of 15-500 Hz. Due to the variances in the high pass filter cut-off frequency, f_{HC}, and the low pass cut-off frequency, f_{LC}, the Monte Carlo analysis [328] was carried out so as to determine the effect of varying resistor tolerances and the results are illustrated in Figure 7.16.

The failure analysis results proved that after five runs varying the resistors within 0-5% of the nominal value the resistors were able to produce the same output as illustrated by the presence of a single line instead of five lines indicated on the legend below the graph. This proved that

the selected E12 series resistors were effective. Hence, the 3.4% error in the low pass filter is as a result of the low gain values. Embedded systems are always known to be unstable under varying input signal quality, as a result, a stability analysis was done for both filters within the band pass.

Figure 7.17 illustrates the Nyquist Analysis output of the filter transfer function, $H_{(s)}$, deduced earlier. The Nyquist analysis plot correlates the filter circuit stability to the region enclosed by the graph. If the point -1 lies within the smaller encircled region, the system is considered to be unstable. Since the encircled region stops at 0.1, this reveal that the filter results in a more stable system. Having selected the corner frequency as 15 Hz, the values of Capacitance, C, and resistance, R, were inversely proportional. The ratio between the output impedance of the amplifier and the value of the filter component resistance sets the transfer functions achieved at frequencies well above cut-off, therefore there was a need to correctly select the amplifier with the good Common Mode Rejection Ration. This was achieved through simulation in Multisim and the stability was then checked using Matlab R2017a.

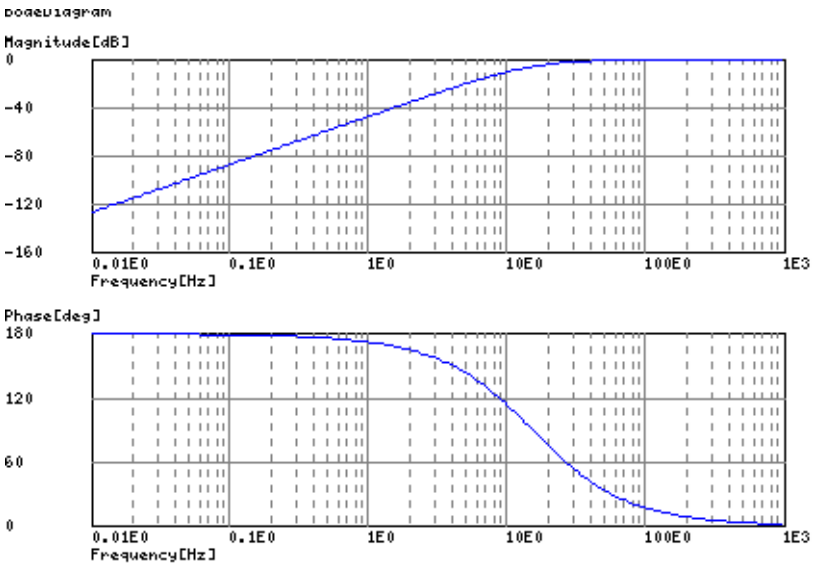

Figure 7.16: The bode plot and phase diagram for the high pass filter, $f_{HC} = 15\,\text{Hz}$

It was noted that the larger the value of resistance for the filters, the lower the transmission of signals at a frequency greater than 500 Hz. Hence, if impedance was too large it will mean that the capacitance will become so small that the parasitic capacitors (including the input capacitance of the amplifier) cause errors. For the high pass filter, the amplifier's output impedance does not play a parasitic role in the transfer function, so that the choice of smaller or larger resistor values is not so obvious. Stray capacitance in the circuit, including the input capacitance of the amplifier, makes the choice of small capacitors and large resistors undesirable. Also, being a high pass filter circuit, the bandwidth is potentially large and resistor noise associated with increased values became a concern. Then again, small resistors became a problem when the circuit impedance was too small for the amplifier to operate properly.

The proposed design is relevant to a signal acquisition circuit for pattern recognition based intelligent architectures for the control of robotic prosthetic limbs. Its high quality factor (Q),

noise tolerance and wide passband provided a good platform for learning algorithms in intelligent control architectures. The Sallen-Key architecture provided the much needed filtering circuit for both high pass and low pass filtering. However, it was noted during experiments that the gain resistors for both low pass and high pass filters strongly affected the performance of the filter at cut-off frequencies that is at -3 dB. Although literature suggested that there is a need for considering frequencies above $50Hz$ only, there are chances of having the system not reacting to low activation signals. The gains for the filters were kept at values less than 1.5 so as to avoid amplification of noise present in the signal. The use of the pre-amplification circuit with the aid of a precision and low power instrumentation amplifier enhances the capability of the protection circuit as it amplifies the signal to the shield and also amplifies the signal from the protection circuit if any voltage losses have been encountered by a gain of 10.

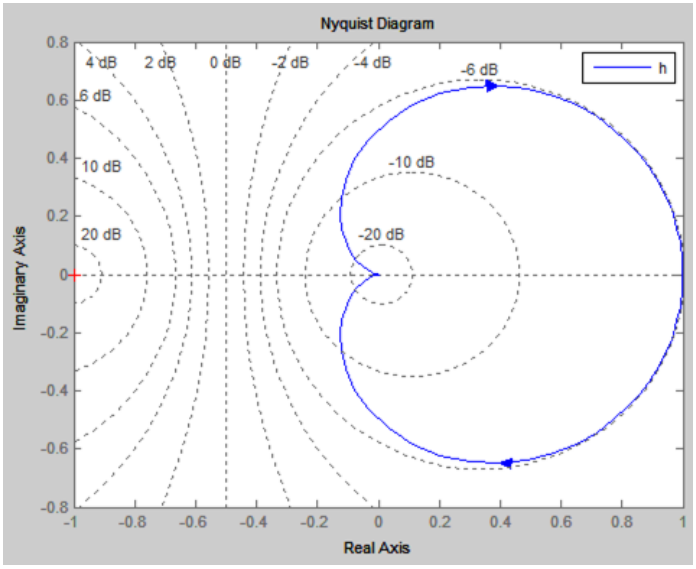

Figure 7.17: The AC analysis for the filtering and amplification circuit

7.6.3 EMG signal analysis

The sEMG signals were recorded from three different channels. Each channel represented a distinct muscle. The protocol presented in section 3.7.1 of the study illustrates the signal acquisition techniques. The signals were recorded with the intention of developing an input signal to a control architecture. Tibialis Anterior, Medialis Gastrocnemius and Lateralis Gastrocnemius muscles were identified as sources for the signal acquisition. The results reported in section 4.3.1 of the report illustrated the analysis of the signals during the determination of signal features necessary for developing the control architecture. The results presented in this section are from the developed architecture.

The sEMG signal passed through the user protection circuit consisting of a Zener barrier before the differential instrumentation amplifier. Such a set-up enabled AC coupling and DC component removal before filtering. Signal acquisition forms the initial stage for pattern recognition and influences the signal features which ultimately affects the classifier accuracy. The signals were recorded using the developed circuit (see Appendix D). In this section, Delysis EMGworks

Analysis software was also used for signal analysis. The signals were analysed for two principal sagittal motions (dorsiflexion and plantarflexion). The resultant analog signal is illustrated in Figure 7.18. A window length was selected with an overlap added on the subsequent windows and the offset was removed on all the signals. The signals were sampled at 1500 Hz.

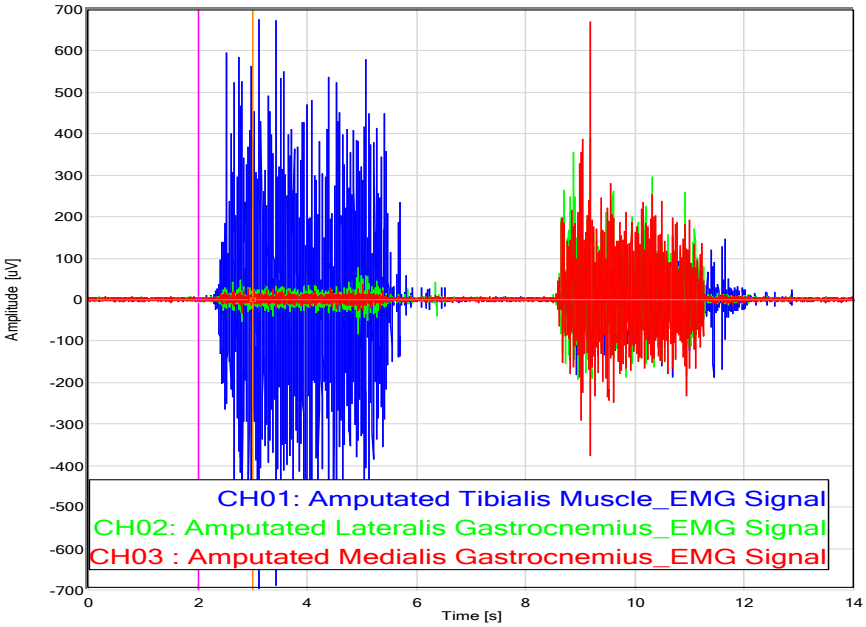

Figure 7.18: EMG signals from amputated leg

The vertical lines illustrate the beginning and the end of a dorsiflexion movement followed by a resting pause. However, the signal was later normalised and filtered so as to extract features more reliably. Both the time domain analysis and frequency domain analysis was carried out. The following sections present the detailed analysis.

- *Amplitude analysis*

  The stochastic nature of the sEMG signal presents challenges for controllers. There is a high probability that the signal will change its parameters with time, depending on the state of the muscle. The amplitude of a muscle which is experiencing fatigue is different to a muscle being flexed from rest. As a result, amplitude analysis was carried out on filtered, normalised and rectified signals and the resultant signal structure is presented in Figure 7.19. The root-mean-square (rms) envelope technique was applied with a window length, S, of 125 Hz and overlap of 62.5 Hz using normalised data of the Tibialis Anterior muscle. Thus, the rms was determined using the moving window. The data in each window, $f_{(s)}$, was calculated as:

$$rms = \sqrt{\frac{1}{S}\sum_{1}^{S} f^2(s)} \tag{7.48}$$

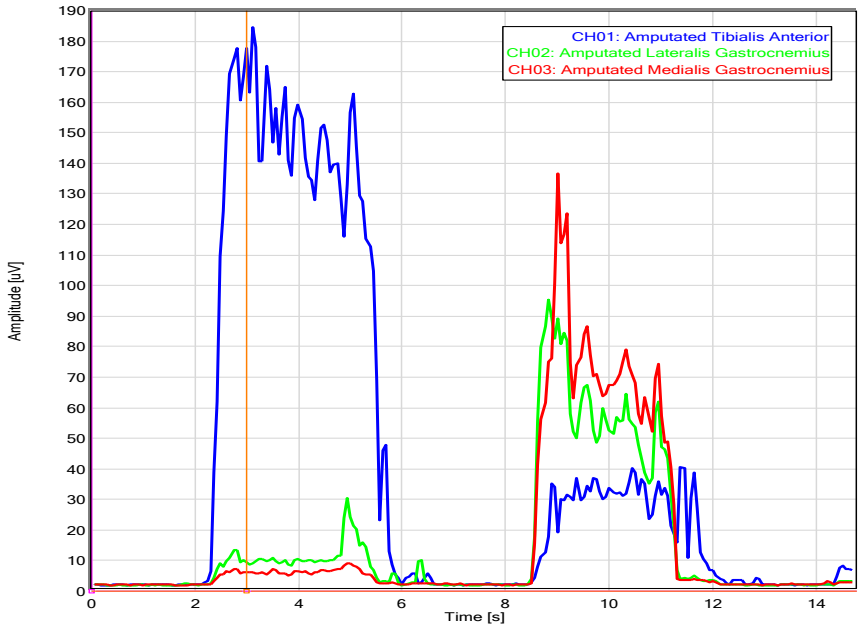

Figure 7.19: EMG signals amplitude representation from amputated leg

The amplitude analysis was mainly done to determine the distinction between the three muscles during intended movements. The Tibialis Anterior muscles show high amplitudes during dorsiflexion movement while the Gastrocnemius muscles (Medialis and Lateralis) shows dominance in terms of amplitude values during plantarflexion. Such distinction motivated the implementation of pattern recognition algorithms. The rms analysis strongly revealed that the amplitude is proportional to the force being exerted by the underlying muscle. The rms feature revealed the power of the signal in the time domain hence it is the most common tool used to determine the usability of a sEMG signal.

- *Power Spectral Density Analysis*

  The power spectral density (PSD) analysis was carried out in the frequency domain. With the aid of FT, the EMG signal was de-constructed into a collection of signals which slightly match the sine wave. The PSD analysis presents the extent to which each frequency power contributed to the structure of the signal. Therefore, the PSD analysis was carried out by squaring the FT of each data segment and then averaging them. The Fast FT (FFT) window length was chosen to be greater than the window length, S, and the FFT length was less than the number of samples within the recorded data.

  The p-Welch method [329] was used to compute the power spectral density analysis because this enabled the analysis of the data segments using Fourier Transform. This enabled fast computation of the non-stationary signals in the frequency domain. The WelchâĂŹs method is basically a modification of the BarllettâĂŹs method such that the subsequent data sets are allowed to overlap and hence the use of averaged modified periodograms during the analysis. Such a modification suggested by [329] enabled the section of the data to be twice the length previously proposed by Barllet [330]. Consider successive sequences are offset by D-points and each sequence is L-points long, then the i^{th} sequence is $x_i(n) = x(n+iD)$, where $n = 1, 2, \cdots, (L-1)$. If we require K sequence to immediately

cover the entire signal length, N, such that $N = L+D(K-1)$ and assuming that there is no overlap, then $(D = L)$ there will be $K = \frac{N}{L}$ subsequences of length, therefore $L = 125\,\text{Hz}$. However, for a 50% overlap, $D = \frac{L}{2}$ thus 62.50 Hz. Therefore, there was a need to have a trade-off between increasing L or increasing K, such that if L is increased then the variance of estimate is decreased and if K is doubled so is the spectral resolution. Therefore, the WelchâĂŹs estimate is described as:

$$E\{\widehat{p}_w(e^{j\omega})\} = \frac{1}{2\pi LU} P_x(e^{j\omega}) \times |W(e^{j\omega})|^2 \tag{7.49}$$

where $W(e^{j\omega})$ is the FT of the L-point data window, $w(n)$, and $\widehat{p}(e^{j\omega})$ is the periodogram of signal, $x_i(n)$. The PSD analysis results of the three channels is presented in Figure 7.20.

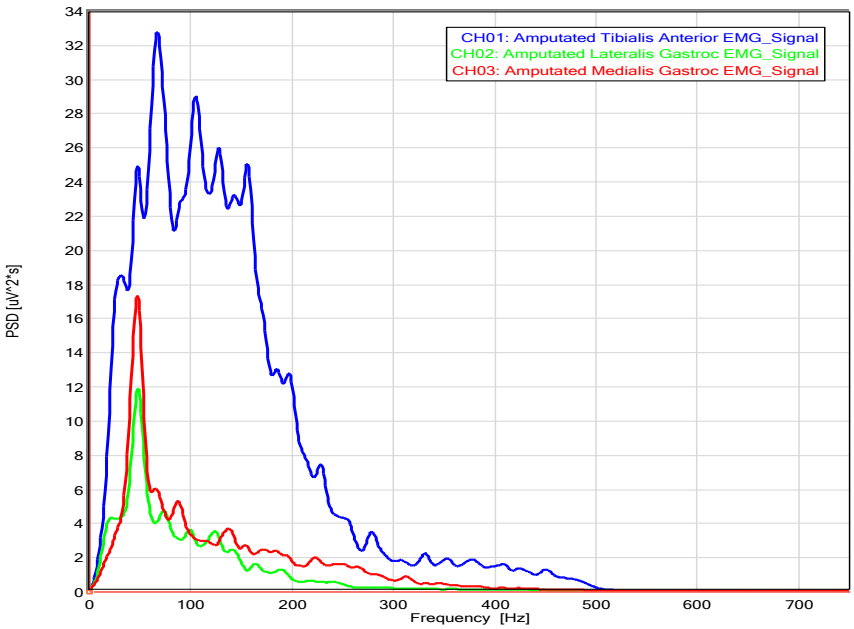

Figure 7.20: Power spectral density analysis of EMG signals from the amputated limb

Figure 7.20 shows that the Tibialis Anterior muscle has a wider bandwidth than the selected Gastrocnemius muscles. The 500 Hz low pass filter signal attenuation was very effective as there is no evidence of signals above the 500 Hz cut-off frequency. The 15 Hz high pass filter was also effective during recording of the signals as there was no signals with frequencies less than 15 Hz. However, the 50 Hz power line interference has a notable effect on the overall signal as it poses more power than any other frequency for the Gastrocnemius sEMG signals. It is apparent that the power line interference will remain inherent within the EMG signal as high signal peaks are recorded at 50 Hz for the Gastrocnemius muscles, largely due to their low-frequency values. Similar results were reported by [209] with regard to the continuous domination of 50 Hz on sEMG signals recorded on non-amputees. Any attempt to increase the high pass filter to a value greater than the 50 Hz resulted in the loss of valuable information from the Gastrocnemius signal, as illustrated in Figure 7.30.

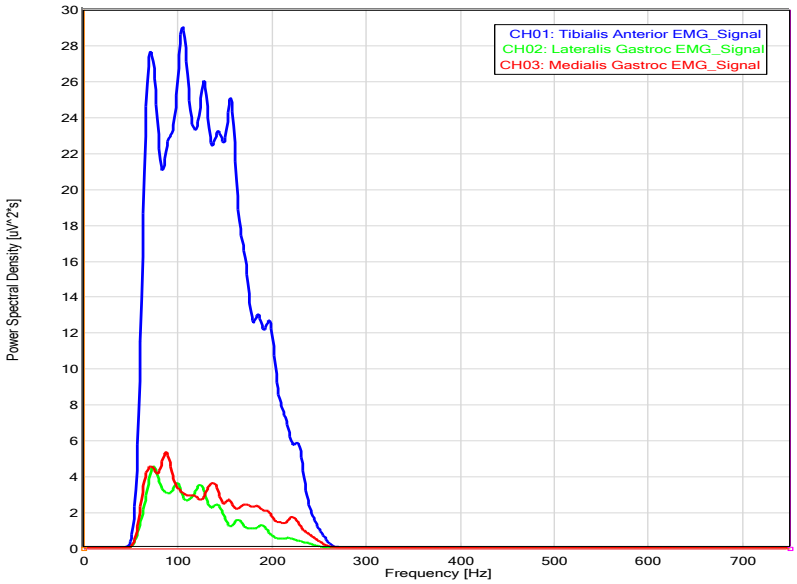

Figure 7.21: Power spectral density analysis of EMG signals after 50 Hz high pass filtering

The removal of the 50 Hz signal indicated the loss of significant signal power strength for the Gastrocnemius muscles. This caused a significant negative effect on the features of the signal in the frequency domain. The SENAIM and ISEK standards do not recommend the use of a notch filter so as to remove the 50 Hz interference because when applied it will distort the signal information due to roll off characteristics of the notch filter, thus affecting neighbouring frequencies. As a result, increasing the high pass filter to frequencies above 50 Hz, such as 60 Hz so that the roll of occurs before 50 Hz was achieved, thereby eliminating the 50 Hz noise signal, this was useful for control applications rather than diagnosis.

7.6.4 EMG Signal denoising analysis

The wavelet denoising technique was applied to signals from all three muscles from both the sound and the amputated leg. The comparison of the DWT, Savitzy Golay and Moving average was then carried out based on the Signal-to-Noise-Ratio (SNR) of the signal and the available noise inherent in the signal:

$$SNR = 10 \log \frac{EMG_{clean}}{EMG_{raw}} \tag{7.50}$$

where EMG_{clean} is the power of the denoised surface myoelectric signal and EMG_{raw} is the power of the original signal recorded from the Tibialis Anterior, Medialis Gastrocnemius and Lateralis Gastrocnemius during the dorsiflexion and plantarflexion respectively from the amputated leg. A t-test ($p < 0.05$) was performed to check for the significant differences of using the wavelet denoising technique as compared to the Savitzky Golay technique and the Moving Average technique for all three muscles for the sound leg and amputated leg. The average SNR parameter value for each technique was determined as illustrated in the Table 7.2. There were significant differences ($p = 9.7025 \times 10^{-11}$) between the signals denoised using DWT and Savitzky Golay technique and also between DWT and Moving average ($p = 3.7474 \times 10^{-7}$) with respect to Tibialis Anterior signals recorded from the amputated leg.

Table 7.2: Comparison of denoising techniques

Wavelet (SNR)	**Savitzky Golay** (SNR)	**Moving Average**(SNR)
32.9202	6.6902	0.9169
33.8065	5.1745	0.6810
36.0561	5.0772	0.58204
33.6701	4.7026	0.4870
34.1413	4.1144	0.4870
34.1189	5.1579	0.6422

When considering the signals from the Medialis Gastrocnemius muscle on the amputated leg, there were also significant differences ($p = 4.7780 \times 10^{-7}$) between the signals denoised using DWT and Savitzky Golay technique and also between DWT and Moving Average ($p = 2.1655 \times 10^{-6}$). The results were then compared between subjects and the average SNR for participant 1 was 28.5315 as compared to that of participant 2, which was 32.1637. However, there was no significant ($p = 1.8946$) difference in the denoising capability of the DWT between participants 1 and 2.

7.6.5 Analysis of signal features

The detected signals were recorded at a sampling frequency of 1500 Hz. According to [307], it is desirable to have a sampling frequency more than twice the highest frequency within the signal. Considering that the sEMG multichannel data acquisition circuit was operating at a bandwidth of 450 Hz, the post-processing values of 15-500 ms and 6^{th} order Butterworth band pass filter were implemented in Matlab R2017a. The 250 ms window size with a 30 ms overlapping window was implemented and the processing time was less than 300 ms per window, as recommended by ISEK and SENIAM standards [72]. The recorded signal length was restricted to over 17820 samples per exercise and this was done so as to achieve large data sets within small number of exercises so as to minimise the set-up times.

The segmented data was then structured into a table format representing a matrix of $m \times n$ rows and columns. The rows m represented the signal window or segmented data. Then the selected features were applied for every window (row of values). The total number of samples in a window, N_{sw}, were determined as:

$$N_{sw} = t_w \times F_s \tag{7.51}$$

where t_w is the window length processing time and, for this study $t_w = 250$ ms and F_s was the sampling frequency which was 1500 Hz. Using these values, the derived number of samples in a standard window was 375 samples, as shown in Figure 7.22.

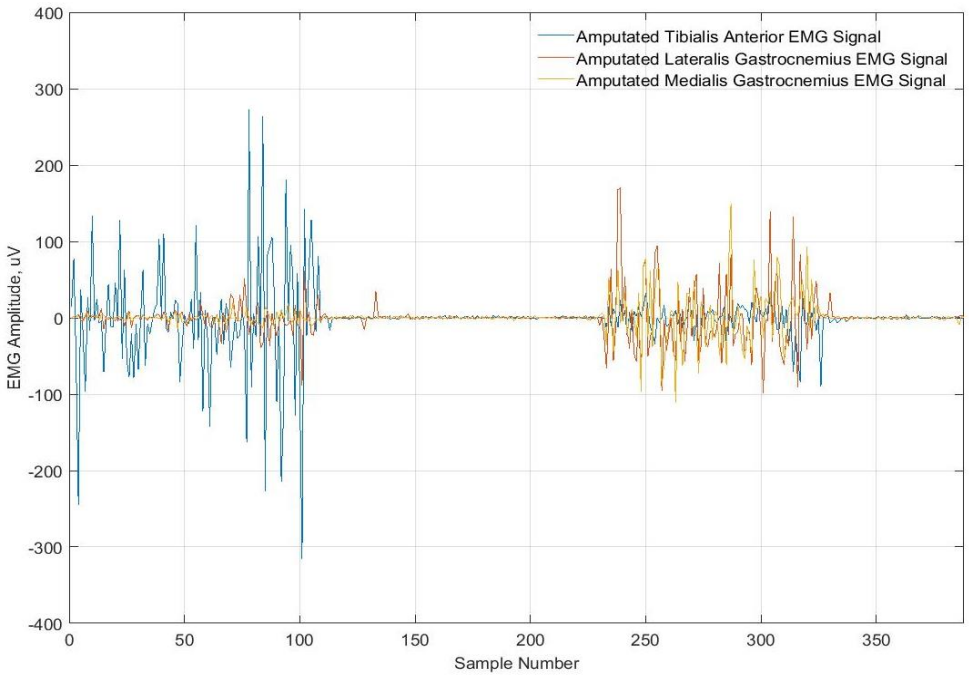

Figure 7.22: Window segment representation during ankle movement

The extracted feature values were combined into a single data set, x_{feat}, which was then used as an input data set to the classifiers. The vector elements are features described in section 7.5.4 as mean absolute deviation, mean absolute value, mean, zero crossing, wavelength, standard deviation, root-mean-square, integrated absolute value, auto regression coefficients, slope sign change, mean frequency, signal power and median frequency. A total of 11 extracted features were used to develop the feature vector. As a result, the total features for the whole control architecture were a product of a number of channels, N, and features per channel, x_{nf}, such that the feature vector had a total number of variables given by:

$$x_F = N \times x_{nf} \tag{7.52}$$

These features, x_F, were then used as an input vector to a classifier. An evaluation of the features based on the input vector is illustrated in Figure 7.23. The variables are termed predictors and their ability to separate classes provides an insight to the classifier performance. The visual inspection of the scatter plot presented in Figure 64 revealed that the mean and the root-mean-square features of the data provide a distinction between the three motion classes, which are dorsiflexion, plantarflexion and resting. Although the Tibialis Anterior muscle exhibited a distinction between resting and dorsiflexion, there was some similarity between plantarflexion and resting, as illustrated in Figure 7.23. This is a possible occurrence given that the Tibialis Anterior muscle is not actively involved in plantarflexion. Similar findings were reported by [180] during the development of the SENIAM standards. Since the Tibialis Anterior muscle was not highly involved in plantarflexion, a scatter plot of the Lateralis Gastrocnemius muscle signal is illustrated in Figure 7.24, indicating the ability of the mean and the root-mean-square features to separate the classes.

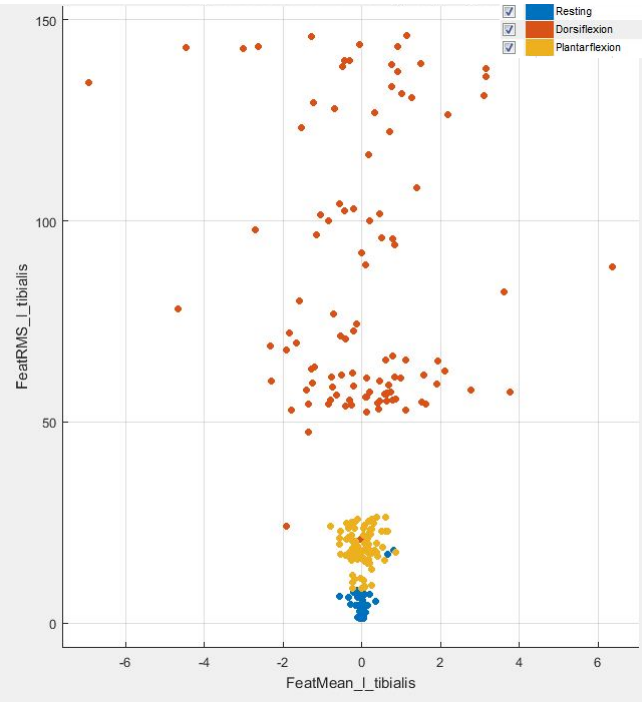

Figure 7.23: Feature analysis for rms and mean features of the Tibialis Anterior

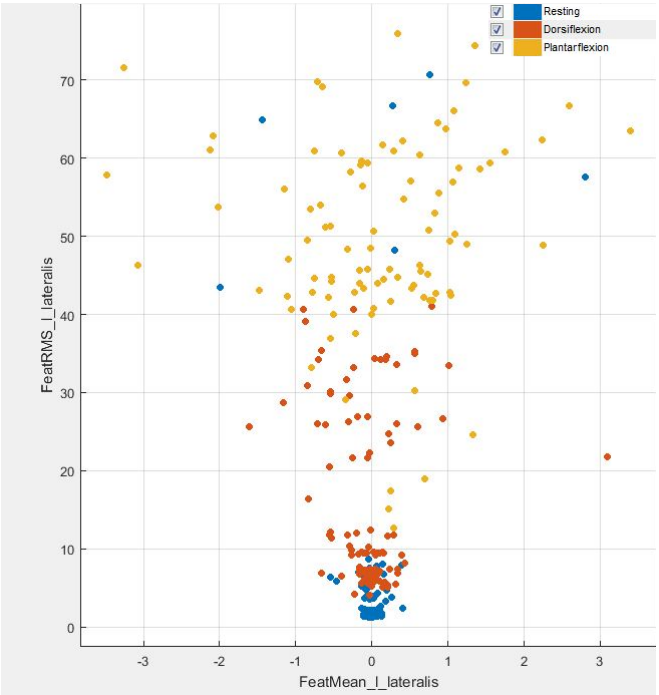

Figure 7.24: Feature analysis for rms and mean features of the Lateralis Gastrocnemius EMG signal

The visual inspection of the scatter plot presented in Figure 7.24 revealed that the Lateralis Gastrocnemius EMG signal was able to provide a separation between the plantarflexion and the dorsiflexion movements. However, there is a close relation between the dorsiflexion and the resting classes. This behaviour was expected because neither of the Gastrocnemius muscles (Lateralis and Medialis) are highly involved during dorsiflexion. It was, however, difficult to carry out feature selection using just scatter plots. As a result, dimensionality reduction was applied to automate the selection of the best possible features that could improve the classifier performance. The PCA dimensionality reduction technique was able to retain model free and unbiased features for optimising the classifier performance.

7.6.6 Evaluation of the classifier performance on training data

The classifier performed differently for several data sets presented to it in the format of feature vectors. There were 320 data sets of different lengths and variable exercises and movements as explained in the protocol in section 3.7 from two different amputees involving data from the amputated leg (left leg) and some from the sound leg (right leg). The information from the sound leg was used as a control so as to benchmark the performance of the classifier on the amputated leg. During classification, 20% of the data set was used as validation data and 80% as training data. Each data set had approximately 388 observations, thus an average of 124 160 windows were used in the study during the development of the control architecture. There were several classifiers mentioned in the literature with regard to myoelectric signals classification. As a way of determining an optimum classifier, several classifiers were tested. The results were presented in Figure 7.25, highlighting the tested classifiers and their classification accuracy on the available data.

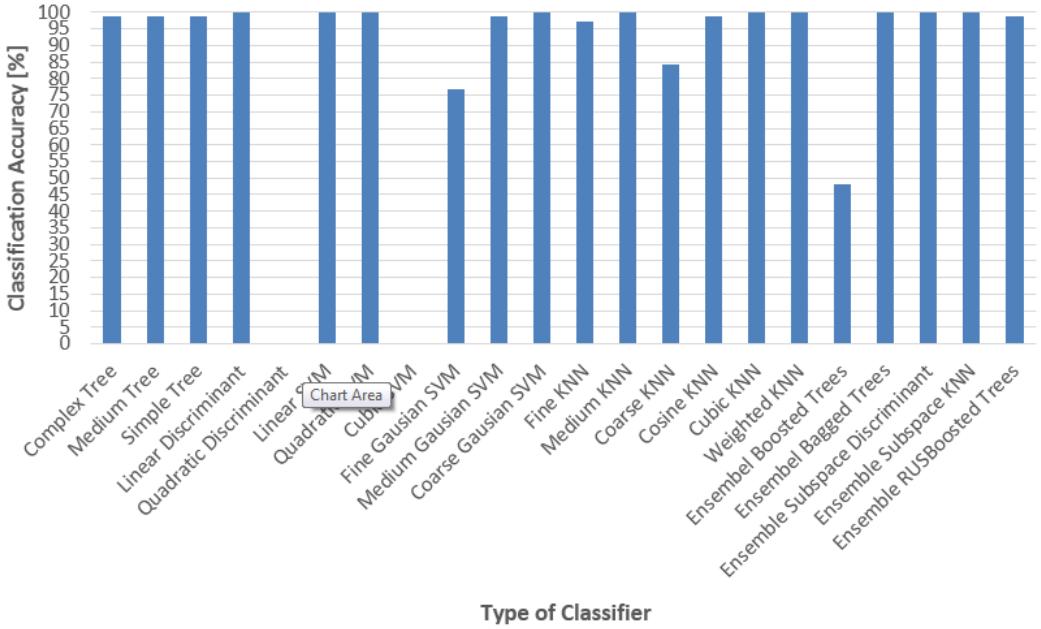

Figure 7.25: Averaged classifier performances based on all features

The quadratic discriminant classifier was unable to classify the data because some of the features were not compatible with the classifier. However, the linear discriminant classifier per-

formed with 99% accuracy on test data. Decision tree based classifiers performed very well with an accuracy of 98.7% and a processing time of 380 ms. The classification accuracy was not the only parameter that was under investigation: the processing time was also investigated for each classifier. The results for the average processing time for the three signal channels is illustrated in Figure 7.26.

As revealed in Figure 7.26, the high classification accuracy was achieved at the expense of a longer processing time. The Linear Discriminant classifier attained 100% accuracy on average but the processing time was much higher than that of the Simple Tree classifier with a difference of 244 ms. That is approximately a three-fold increase in processing time. Similar results were reported for Linear-SVM and Quadratic-SVM, which all produced classification of 100% accuracy at the expense of increased processing time. Ensemble classifiers also produced remarkable 100% classification accuracy but their processing time of 1032.70 ms was almost 300% more time consuming thanthe fine-KNN classifier which had 98.7% classification accuracy.

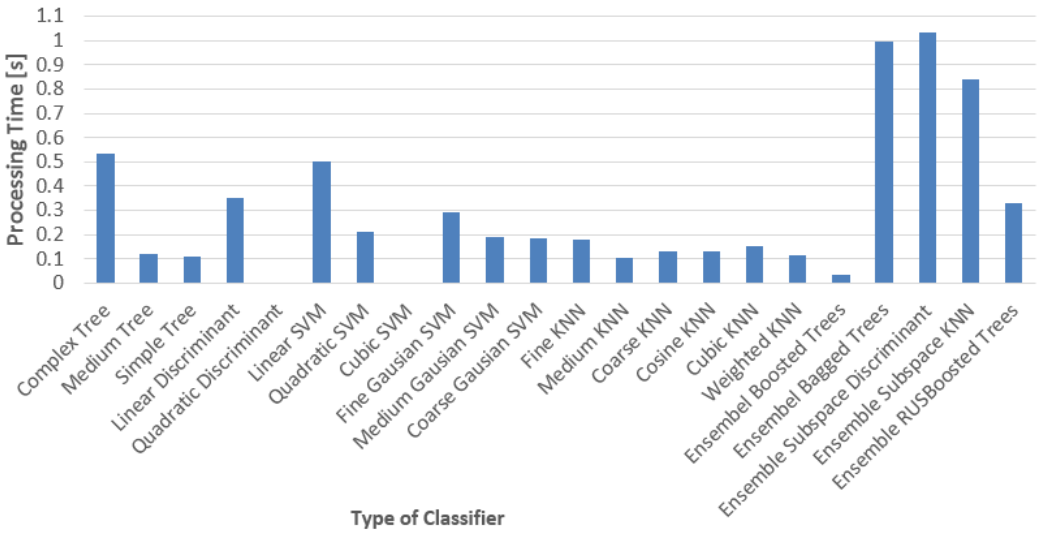

Figure 7.26: Classifier processing time based on all features

In an effort to reduce the processing time while maintaining higher classification accuracy of the classifiers, the Principle Component Analysis (PCA) was then implemented as a dimensionality reduction technique. This resulted in the removal of 10 variables, leaving 23 variables from the original 33 variables within the feature vector used in the initial analysis. The classification accuracy results of the remaining variables are illustrated in Figure 7.27 along with the initial results.

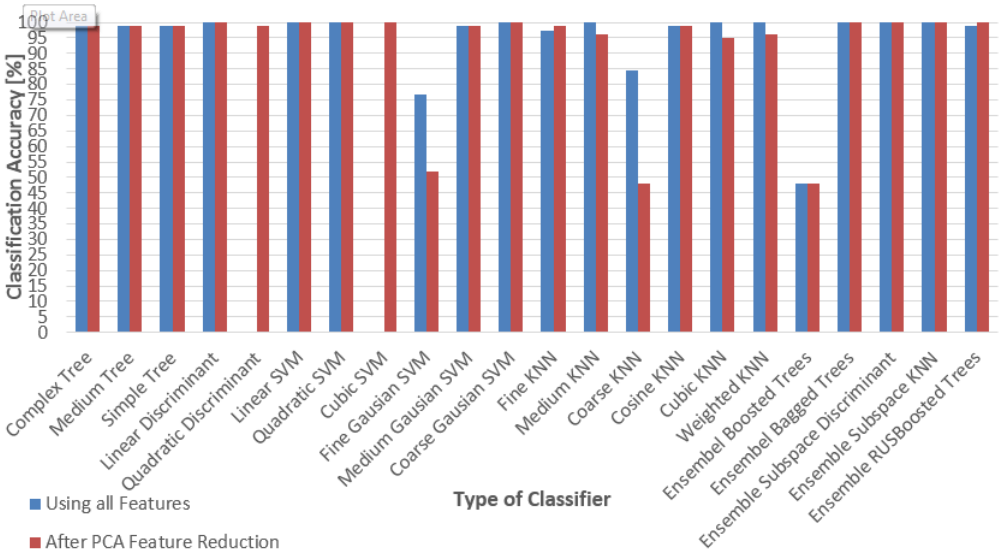

Figure 7.27: Classifier performance after the application of feature reduction technique

After the application of the PCA dimensionality reduction technique on the feature vector, the Quadratic Discriminant (QD) classifier, which failed to classify the initial data, was able to produce 98.7% classification accuracy. The Linear SVM exhibited a notable decrease in processing time from an average of 499 ms to 350 ms. Thus approximately a 30% decrease in processing time as shown in Figure 7.28.

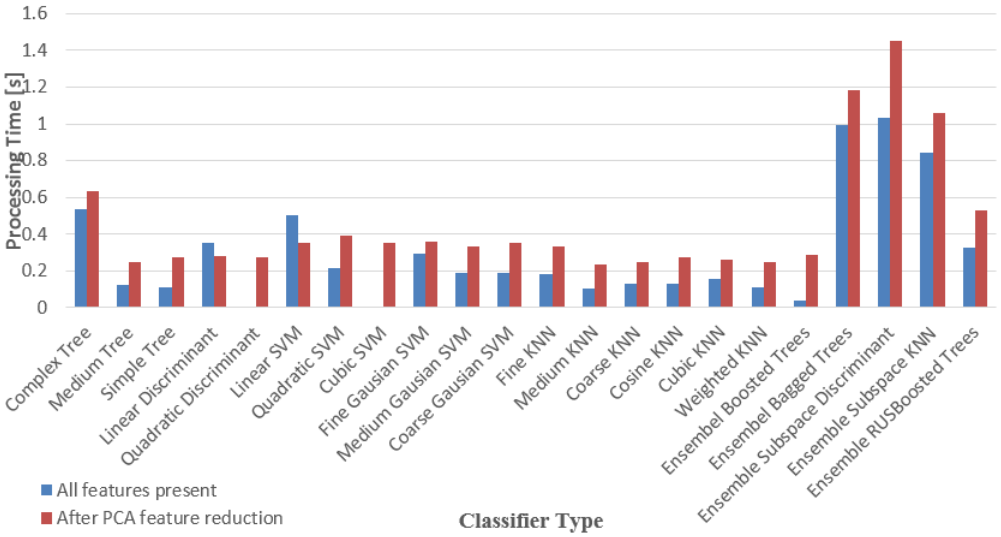

Figure 7.28: Comparison of processing times after feature reduction

A new classifier, cubic-SVM, was able to operate on the data after feature reduction and, as a result, a total of two extra classifiers were added which were not compatible with the initial set of the feature vector. Some classifiers were not compatible with auto-regression coefficients, mainly the 2^{nd}, 3^{rd} and 4^{th} coefficients. Therefore, there was a need to apply feature reduction

techniques as this will increase the number of potential classifiers in most instances. The Linear Discriminant and the Linear SVM showed both reduction in processing time and also consistency of 100% classification accuracy on all the feature vectors, both during training and on validation data. The structure of the Linear SVM was presented in section 7.5.7 as a Lagrangian dual problem of maximising the slack variables, α, with respect to the bias, b, and the weight, $\vec{w}$. The developed solution satisfied the relationships:

$$\vec{w} = \sum_{i=1}^{S} \alpha_i y_i \vec{x_i}, \qquad \sum_{i=1}^{S} \alpha_i y_i = 0 \tag{7.53}$$

Therefore:

$$maxL_D(\alpha_i) = \sum_{i=1}^{S} \alpha_i - \frac{1}{2} \sum_{i=1}^{S} \alpha_i \alpha_j y_i y_j (\vec{x_i} \cdot \vec{x_j}) \tag{7.54}$$

Such that:

$$\sum_{i=1}^{S} \alpha_i y_i = 0 \qquad and \qquad \alpha_i \geqslant 0 \tag{7.55}$$

The PCA technique enabled the optimal positioning of the hyperplane and also increased the margin that enabled better classification accuracy within the shortest possible time. The quality of the Linear-SVM was impressive as receiver operating characteristic (ROC) produced a value of 1. The area under the ROC curve is sufficient to cover all the available curve length. Since the classifier achieved 100% classification accuracy, the ROC curve exhibited a 90^0 angle and that alone shows that the classifier is good enough to classify the available signals. The performance of the classifier per given class was evaluated using the confusion matrix as in Figure 7.29.

The classifier presented 100% accuracy on labelled data (known data) and, as a result, there were no false negatives reported. Although there is close proximity in terms of features from Gastrocnemius (Medialis and Lateralis) sEMG signals to those recorded during resting and moving artefacts, the LSVM was able to correctly distinguish them. These results were based on training data. Initial results presented in this report indicated that there is no significant difference between sEMG signals from different amputees who had received similar a type of amputation. As a result, the training data was extracted from one participant during testing since the prototype was custom made for one participant. The EMG multichannel data acquisition unit, presented in Appendix C was the one used to acquire the signals. The data was segmented such that 80% of the data set was used for validation while the other 20% was used for validation. The same classifier used for training was the one used for testing. The number of instances were 77 during training and validation, however, the instances were varied during testing. See Appendix E for the averaged results. The test results with unknown or unlabelled data is presented in the next section.

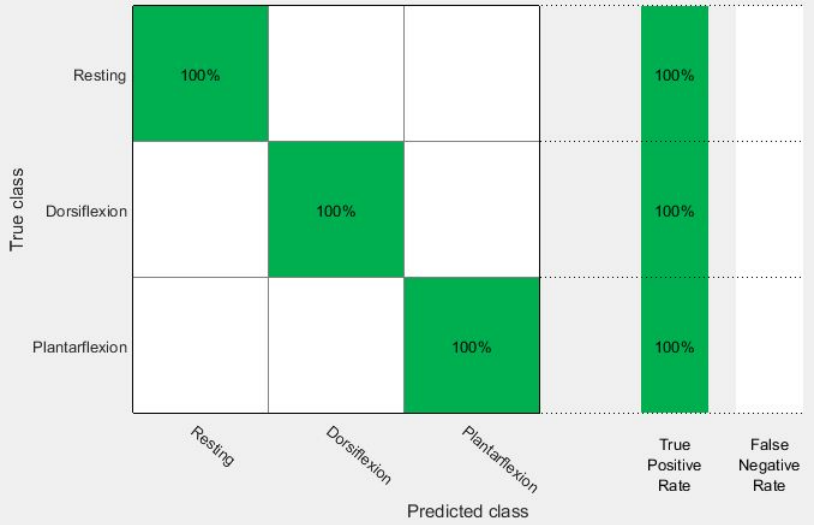

Figure 7.29: Confusion matrix on available motion classes

7.6.7 Control architecture validation by means of classifier performance evaluation on test data

This section presents the performance of the developed control architecture on *unknown data* recorded from the similar three muscle channels used during training. Therefore, the developed pattern recognition control architecture was then tested on unknown and unlabelled data which was recorded from the amputee during normal gait. The accumulated data sets were then post-processed, as explained in the section 7.5, and the same noise reduction and data segmentation techniques initially used on training data were applied. The only difference during testing was that the data was not pre-labelled as previously done. The performance of the control architecture will be reported in terms of classification accuracy. However, other characteristics such as *specificity* and *sensitivity* will also be reported.

A total of over 6 000 observations, of each equivalent to a processing window of a minimum of 350 ms were classified over a period of variable exercises performed both indoors and outdoors. One exercise had a minimum average of 428 observations. The outputs from the classifier were defined as follows:

- True Positive [TP] = Condition Present + Positive Result
- False Positive [FP] = Condition Absent + Positive Result [Type I error]
- False (invalid) Negative [FN] = Condition Present + Negative Result [Type II error]
- True (accurate) Negative [TN] = Condition Absent + Negative Result

Therefore:

$$Pression(class) = \frac{TP}{TP + FP} \tag{7.56}$$

$$Sensitivity(class) = Recal(class) = TruePositiveRates(class) = \frac{TP}{TP + FN} \tag{7.57}$$

$$Specificity(class) = TrueNegativeRates(class) = \frac{TN}{TN + FP} \tag{7.58}$$

The average values for the classifier performance are illustrated in Tables 7.3, 7.4 and 7.5, indicating how the three motion classes were correctly and falsely classified. For individual recordings of exercises refer to Appendix E.

Table 7.3: Classifier characteristics

Class	**1**	**2**	**3**
True Positive [TP]	262	101	119
False Positive [FP]	1	0	2
False Negative [FN]	1	1	1
True Negative [TN]	221	382	363

Table 7.4: Classifier performance

Class	**1**	**2**	**3**
Precision	0.997881	1	0.97987
Sensitivity	0.996148	0.989035	0.995495
Specificity	0.997409	1	0.993989

Table 7.5: Classifier performance evaluation based on confusion matrix

Rest	53.99843	0	0.11682243
Dorsiflexion	0	20.8438218	0
Plantraflexion	0.212415	0.2566773511	24.57183622
	Rest	**Dorsiflexion**	**Plantarflexion**
Motion Classes			

Based on the averaged confusion matrix, the overall classification accuracy of the pattern recognition control system was 99.25%, which is a 0.75% deviation from the training model. Efforts were made on trying to improve the classification accuracy during testing by increasing the high pass filtering to values above 20 Hz so as to eliminate movement artefact, but this actually reduced the classification accuracy of the model. Similarly, the median and moving average filters were also implemented in an effort to further clean the signal by removing periodically occurring signals, but there was no significant difference as the accuracy decreased.

7.7 Discussion

The use of pattern recognition control architectures presents an opportunity to implement machine intelligence. However, the study results revealed that there are several issues that govern the performance of machine intelligence in a control architecture. These factors include the quality of the signal, signal acquisition, processing techniques employed and the processing power of the main controller. It is, however, the performance of the pattern recognition technique used that determines the overall reliability of the control architecture. The LSVM classifier performed

very well even on low frequency signals from the Medialis and Lateralis muscles for plantarflexion movements. This was attributed to the ability of the sEMG signal acquisition system developed which was able to pick up signals on the surface, even of deep muscles which co-activate with the Gastrocnemius muscles [30]. The Soleus muscle, which was no longer accessible on the surface but was below the Gastrocnemius muscles on its insertion, had its activity picked up as co-activated signals on the surface of the Gastrocnemius muscle. This resulted in muscle crosstalk , hence increasing the noise levels.

The optimisation of the signal acquisition unit through the implementation of an adaptive filter enabled the acquisition of quality sEMG signals. However, the noise intereference had a significant effect on the system performance. Denoising techniques were compared using the SNR value such that, the higher the SNR value, the better the denoising technique. The high SNR values exhibited by the DWT technique is as a result of the ability to localise within the signal. The DWT recorded an SNR of 32.87 as compared to 7.77 and 0.94 for Savitzy Golay and Moving Average technique respectively. This has been attributed to the fact that the wavelets coefficients and the thresholding capabilities of DWT enable the use of the full-scale signal, hence localising in time and frequency to achieve a good SNR value. The ISEK standards [72] for reporting EMG signals simply stated that there is a need to have a good SNR value but it is not specific of any threshold value for the term *good*. However, in signal processing, it is well understood that $SNR > 25$ is regarded as a good value. On average the lowest SNR value recorded was 25.26 on the Medialis Gastrocnemius muscle of the amputated leg of participant 1. This was as a result of muscle crosstalk. The amount of noise expected in Gastrocnemius muscles (Medialis and Lateralis) were very high due to varying skin impedance, skin movement and close proximity of the muscles to the end of the stump of the residual limb. The skin was too lose and resulted in induced noise due to electrode movement.

In addition, the type of amputation has an influence on the nature of the skin attachment to the residual limb, thereby affecting the signal quality [7]. The bone bridging technique carried out on the amputees during the amputation procedure causes large muscle crosstalk and the presence of a large amount of noise causing the inefficiency of Savitzky Golay and Moving Average techniques. They recorded SNR values as low as 2.71 and 0.58 respectively on Gastrocnemius muscles. This will have a detrimental effect on the feature extractor and will subsequently reduce the classification accuracy of the pattern recognition based myoelectric system. As a result, the stability and plasticity properties of the system are altered to a large extent.

It was observed that the baseline noise depend highly on the nature of the recording equipment. However, even though validated commercial data acquisition tools were used to record EMG data, it is not the same equipment that was utilised for control systems. In a clinical set-up, the recording environment and the baseline noise from the recording equipment are pre-determined. However, in real-world prosthetic control, there are many uncertainties, such as changes in terrain, power line interference (50 Hz), electrode shifting and changes in skin impedances. These changes cause the accumulation of noise in the signal. Therefore, there was a need to have a reliable denoising technique within the control system such as the DWT. The superiority of DWT has been observed over the commonly used Savitzky Golay and Moving Average techniques. In most cases, researchers ignore the need for denoising and focus mostly on optimising the feature extractor and developing a complex classifier. As a result, this causes increased computational time and poor classification accuracy. Recording sEMG signals on non-amputated legs resulted in as much as 30% of the signal being recorded from inactive nearby

sites [85]. Therefore, using sEMG signals from amputated legs can cause a great deal of increased muscle crosstalk resulting in unstable myoelectric control systems. However, when correctly the denoising technique and filtering techniques were implemented, the proposed system presented useful sEMG signals.

These sEMG signals acquired when then used for feature extraction and provided a feature vector with variables which were separable. According to [30], increasing the number of channels increases the classification accuracy. A four channel system developed by [30] achieved a 97% classification accuracy, that is 1.8% less accurate than the system proposed in this study which attained 99.25% accuracy on unseen data using three channels. The application of dimensionality reduction has been proved to reduce computational time since some of the features could be occupying a high-dimensional space [50], [331]. This has been proved useful in this study as the removal of 10 variables within the feature vector decreased the computational time for LSVM classifier.

Quality input signals are a result of reliable data acquisition systems, and they offer an opportunity of using linear classifiers such as Linear Discriminant and Linear-SVM [331]. According to [50], a proper presentation of the signal will result in several classifiers being able to give recommendable results. This has been observed when Decision Trees and Ensemble Subspace KNN classifiers, presented in Figure 68, attained 100% classification accuracy although their processing times were undesirable.

The main objective for pursuing linear classifiers is because of their simplicity on implementation with embedded processors [30]. This led to the rejection of Decision Trees and Ensemble Subspace KNN classifiers. The selection of the large window length of 300 ms , as compared to the smaller window lengths such as 150 ms to 250 ms suggested by [332], was to improve feature stability. Small windows tend to introduce instability within the controller architecture, even though large window lengths increase actuation delay [30]. Feature instability may lead to poor repeatability thereby reducing the reliability of the overall myoelectric control system. The use of shorter window lengths could result in notable variability between features, leading to the degradation of the classifier [20].

The proposed design was able to meet the suggested important aspects of *controllability* for myoelectric systems [20], which are a *response time* of 350 ms on unseen or unknown data, an *accuracy* of 99.25% and *intuitive interface* achieved through the acquisition of a reliable input control signal using the developed multichannel sEMG signal acquisition unit.

7.7.1 Conclusion

The software and hardware requirements for a myoelectric control system were addressed. The pattern recognition system only utilised the sEMG signals from the three channels. The IMU sensors provided the feedback signals which was used within the knowledge base so as to provide system interlocks through conditional statements. The main goal of integrating the IMU and EMG sensors in a control architecture was achieved in a more synergistic way that also allowed the implementation of FSRs. The use of an ADS1298 integrated circuit provided a platform for the evaluation of the benefits of an adaptive filter. The filter had its filter coefficients changing to maintain the signal quality. The control system's signal acquisition circuitry exhibited robustness in the event of magnetic noise interference, skin impedance changes and electrode movement

artefacts but was susceptible to the 50 Hz power-line interference. The 15- 500 Hz bandwidth was used during the study through the implementation of a 15 Hz high pass filter and 500 Hz low pass filter using a 2^{nd} order Sallen-Key architecture. Furthermore, the adaptive on-board filtering resulted in more presentable sEMG signals from all the channels recorded.

Muscular crosstalk has been noted between the Gastrocnemius Muscles and the inaccessible Soleus muscle of the residual limb. The similarities in time domain features between Medial and Gastrocnemius muscles revealed the muscular crosstalk from the Soleus, which was considered to be beneath the Gastrocnemius muscles. The use of a 15 Hz as high pass filter cut-off frequency enabled the detection of Soleus and Gastrocnemius muscle crosstalk. The developed feature vector was then able to reliably provide separation properties for the classifier. The cable movement artefact is an unavoidable challenge for wearable devices. Efforts had been done to implement wireless technologies but hard wired systems proved to be less complex and reduces device processing time since wireless communication requires extensive processing of complex subroutines within the algorithm. Skin movement artefact was insignificant to the performance of the classifiers. As a result, the use of gelled electrodes was found to be reliable. However, the amputees preferred the use of dry electrodes as they do not require extensive skin preparation and they could easily be designed to be strap-on systems. Efforts made during experimentation using a bar electrode revealed that, it is difficult to position at the within the silicon socket lining and the presence of silicon cloth provided challenges on the proper electrode placement.

The MPU6050 is a 3^{rd} generation sensor which has the capability of on-board signal processing. Such a characteristic reduced the load on the main signal processor as most mathematical manipulations were done on-board of the MPU6050. Challenges were, however, experienced on the establishment of communication between the two IMU sensors and the microprocessor, and the only alternative was to use the I^2C protocol. The protocol was able to provide synchronisation between the IMU data and the sEMG data within the microprocessor. The dual IMU system of thigh and shank provided a more stable technique. Therefore, the position of the limb in space during normal gait was determined based on gait events such as heel-strike, double support, pre-swing and toe-off. The main objective of the IMU sensors was not to determine anatomical angles of the limb but to correctly predict the limb projection. The IMU sensors were actually used as feedback sensors along with FSRs placed on the foot.

A pattern recognition system based on myoelectric signal was developed and validated. The LSVM was modelled to accurately classify three motion classes (dorsiflexion, plantarflexion and resting) within the sagittal plane. The architecture is also composed of the principle component analysis (PCA) as a feature reduction module used during the training of the model. The use of PCA reduced the computational time and increases classification accuracy. The model classification accuracy on labelled data was 100%. However, on testing with unknown data, the architecture achieved 99.25% accuracy. The 0.75% error was attributed to variable properties of noise artefacts from cable movement, skin impedance and hardware components. Only the power-line interference remained constant across all data samples.

Therefore, the aforementioned results revealed that a robust pattern recognition control system is capable of classifying gait movements during walking, even in the event of noise interference. The validation of the control system was done in two stages. The initial stage involved validation based on classification accuracy which was presented in this section and the following section presents validation of the design based on functionality.

Chapter 8

Design validation through gait analysis

8.1 Introduction

The validation of the designed control architecture was carried out using gait analysis. The previous section 7.6.7 presented validation of the design based on classification accuracy, this section is mainly concerned on the validation based on how the proposed architecture has managed to restore gait of the amputee. The main advantage of the gait analysis method is that it presents the anatomical angles, orientation angles and distance variables of the lower limb [239]. As a result, it was possible to determine the extent to which the human gait has been restored through the powered prosthetic ankle. The ultimate goal of the powered limb was to provide locomotion and balance to the user. In the event of loss of input signal the powered ankle was suppose to prevent the unfortunate event of a fall.

8.2 The powered ankle prosthetic prototype

A prototype was developed to investigate the controllability characteristic of the powered ankle. The prototype consists of all the hardware developed during the course of the study. This includes the multichannel sEMG acquisition device, IMU sensors, FSRs, DC motor actuator and encoders. The sEMG signals were extracted from the identified Tibialis Anterior, Medialis Gastrocnemius and Lateralis Gastrocnemius muscles at the residual stump. The socket silicon lining was able to assist in holding the sEMG electrodes in place. Since the signals were not being extracted from the force bearing end of the residual stump the amputee did not show any signs of discomfort. The availability of the signals was tested using the Noraxon MR3 system prior to installing the designed active electrodes.

Two MPU6050 IMU sensors, based on the GY88 schematic architecture were used in the design. The IMU sensors were synchronised through the I2C communication protocol to eliminate a lagging factor in the control system. The sensors were installed such that the pitch could create a zero crossing between knee flexion and knee extension. The continuous streaming of the data was monitored through the use of LED signals. The recorded angles were then sent to the on-board SD card on the main control card (see Appendix D) for further analysis.

Initial experiments [55] revealed that the heel-strike, double support, single support and toe-off could be monitored using force sensitive resistors or load cells. However, the FSRs were preferred because the required system only needed an ON/OFF signal which could be used within

the knowledge base of the system to develop the IF-ELSE conditional statements. The inclusion of FSRs enabled the identification of the powered ankle transitions when on the ground such that when the FSR sensors were placed on the hindfoot and another on the midfoot, the conditional statements were structured as, for example, IF the Hindfoot-FSR is ON and the Midfoot-FSR is OFF then it is a heel-strike. These conditional statements, along with the IMU sensor values, were very useful in determining the gait events. They also aided in creating interlocks within the control architecture, thereby introducing robustness. The final design of the powered ankle is illustrated in Figure 8.1.

Figure 8.1: The crude prototype

The mechanical structure was made from aluminium in order to reduce the weight of the device. The overall weight of the system was approximately 3.8 Kg.

8.3 Methods and materials

The amputee was fitted with the designed powered prosthetic ankle. The system comprised of two IMU sensors, three EMG channels and two force resistive sensors. One IMU sensor was placed on the thigh (femur) and another IMU sensor was placed on the shank (tibia). The first FSR was place on the heel and the second one was placed at the toe. The FSR sensors were used to detect heel strike, double support and toe-off, that is transition phases between stance and swing in gait analysis. The IMU sensors were then used to predict the orientation of the limb in space. The data was then recorded as a *csv* file from all sensor channels. The control architecture was auto-calibration enabled for the double single phase of the gait. Noraxon IMU sensors were placed on the thigh, shank, foot and pelvis while sEMG sensors were placed on selected muscles of the lower limb. The Noraxon Myomotion system was then calibrated using the procedure explained in section 3 of the study. Furthermore, sEMG sensors were also placed

on the sound leg so as to compare the signal strength of the recorded data and also for developing labelled data for training the model. This was done to validate the model accuracy during offline post-processing of the data. The sensor placement is illustrated in Figure 8.2.

Figure 8.2: Sensor placement

The MyoMotion system was used to evaluate the anatomical and orientation angles of the subject as he walks on a treadmill and across the room. Two treadmill speeds were selected as 0.5 m/s and 0.8 m/s. The force plates within the specialised treadmill were then used to record force distribution on the amputee's foot. Several data sets were also generated for post-processing. The subject had initially been given an opportunity to walk around with the powered limb for approximately 15 minutes, both in the laboratory and outside the laboratory, allowing necessary adjustments to be done. The results generated were analysed and presented.

The statistical analysis was carried out to determine any significant difference between the acquired data and the data gained when the amputee was using a passive prosthetic limb, as previously reported in section 5.3 of the report. The reduction of raw motion data was carried out using Noraxon MR3 software. A second order Butterworth filter was used for the removal of specious markers and filtering of the data was achieved using a cut-off frequency of 15 Hz. Temporal-spatial data such as speed, stance percentage, and step length was determined. Signal parameters such as mean, peak and minimum values were also determined. Kinetic data, such as vertical ground reaction force and ankle, knee, and hip power, was compared with normative data within Noraxon and the data from the passive limb. Furthermore, Matlab functions were develop for post processing of the data and statistical analysis. The acquired data was analysed

for skewness using the Pearson's coefficient of skewness, a:

$$a = \frac{x_{mean} - x_{mode}}{x_{SD}} \tag{8.1}$$

where x_{SD} is the standard deviation and x_{mean} and x_{mode} are the mean values and mode of the variables. The data was considered normally distributed for $-0.5 < a < 0.5$. A paired t-test of unequal variance (level of significance, $p < 0.05$) was performed to determine whether there is significant differences between the powered ankle and the passive limb. The data was then evaluated to provide normative information for the amputee population when performing ambulatory-related activities using powered ankles.

8.4 Results

This section presents the results generated during the testing of the controlability of the powered ankle. The success of the design was evaluated based on its ability to restore normal gait. The ultimate goal of the study was to provide a reliable control architecture that could be used to improve the performance of already existing powered ankles by using sEMG signals to determine user intent and give feedback via encoder, FSRs and IMU sensors. Therefore, the results presented in this section are mainly for gait analysis.

8.4.1 Distance variables

The distance variables such as cadence, velocity, stride time, stride length and step time were analysed from the data recorded while the participant was walking on a treadmill. These parameters gives an indication on how the amputee performed as compared to non-amputees. The distance variables presented in this section were derived from the amputee performance when walking on a flat platform as illustrated in Figure 8.3. The results acquired include cadence, velocity, stride time, stride length, step time and stance time as illustrated in Table 8.1. These parameters were evaluated so as to determine anomalies using a benchmark of normal ambulators and knowledge of gait. The results of the t-test are also presented in Table 8.1.

Table 8.1: Comparison of powered ankle and passive ankle temporal distance factors

Item	Parameter	Unit	Powered Ankle	Passive	p-value
1	Cadence	$steps/min$	106.45 ± 2.10	107.23 ± 3.50	0.460
2	Velocity	m^{-s}	1.38 ± 0.04	1.410 ± 0.07	0.098
3	Stride time	s	5.9 ± 0.10	5.600 ± 0.18	1.720
4	Stride length	m	0.72 ± 0.02	0.794 ±0.03	1.642
5	Step time	s	1.15 ± 0.03	1.130 ± 0.05	1.524
6	Stance phase	gait % cycle	61± 0.551	59.00 ±2.58	0.486

Figure 8.3: Amputee walking with the prototype

8.4.2 Anatomical angles

The distance variables showed no significant difference between passive and powered ankle. As a result, there was a need to evaluate if the same performance could be concluded for anatomical angles. Therefore, a two-sample test was performed assuming unequal variances. The results prompted further investigations into the gait cycle of the amputee as there exists significant difference (since $p < 0.05$ as in Table 8.2) between the gait of results when using a powered ankle and when using a passive ankle. The results are shown in Table 8.2. The results presented in Table 8.2 revealed that there was significant difference but not to all anatomical angles. The results for the mean angle, minimum and peak angle are illustrated in Figure 8.4, 8.5 and 8.6 showed how the powered ankle performed as compared to the passive ankle and ankle from the sound leg.

Table 8.2: t-Test: Comparison of anatomical angles for significant difference between powered and passive ankles

Item	Movement	p - value
1	Hip flexion	0.0290
2	Hip abduction	0.043
3	Hip rotation	0.0257
4	Knee flexion	0.0406
5	Ankle dorsiflexion	0.035
6	Ankle inversion	0.0684
7	Ankle abduction	0.0588

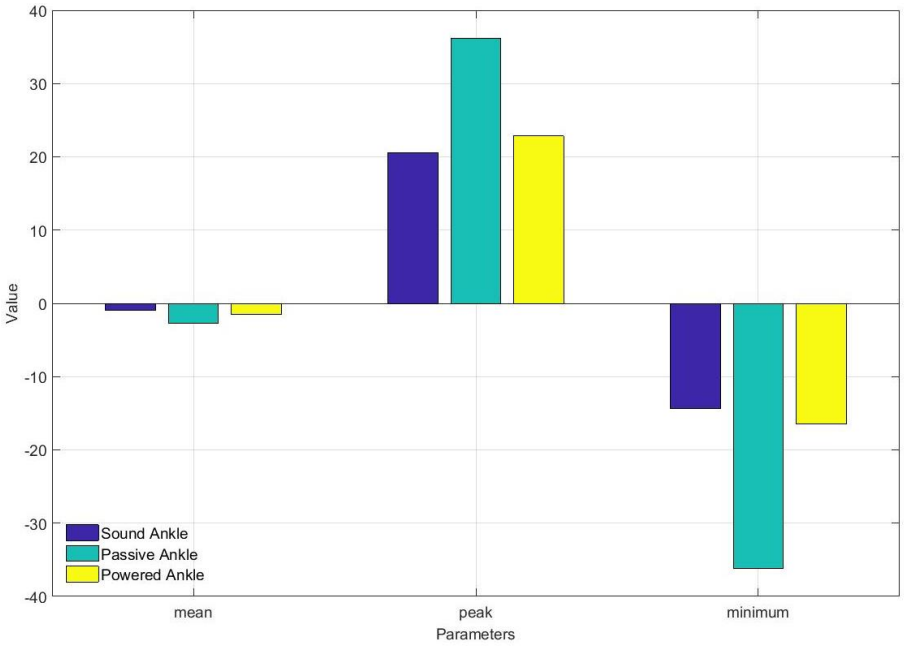

Figure 8.4: Comparison of the of the ankle angle passive prosthetic, powered prosthetic ankle to the ankle of the sound leg

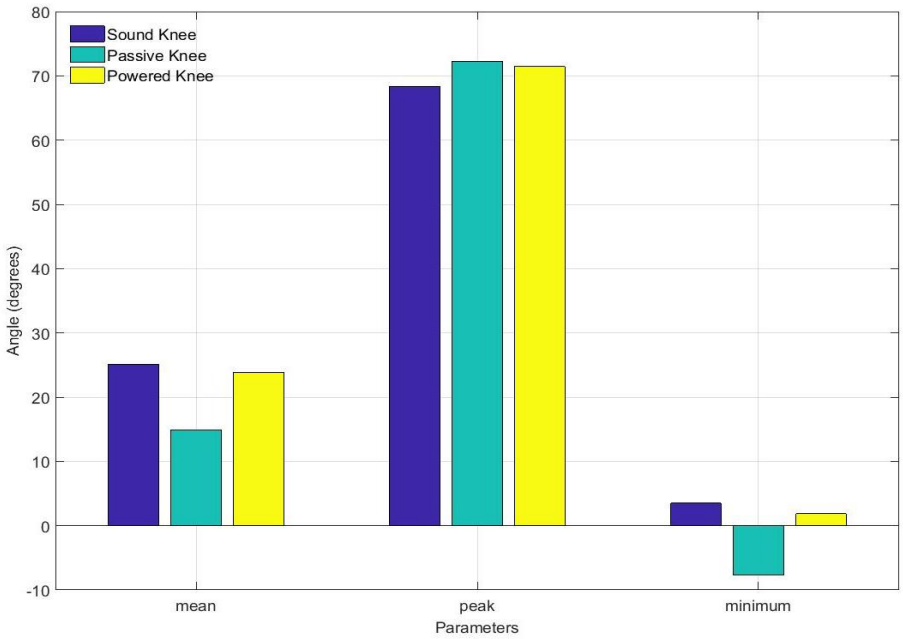

Figure 8.5: Comparison of the knee angle of the passive and powered ankles to the ankle of the sound leg

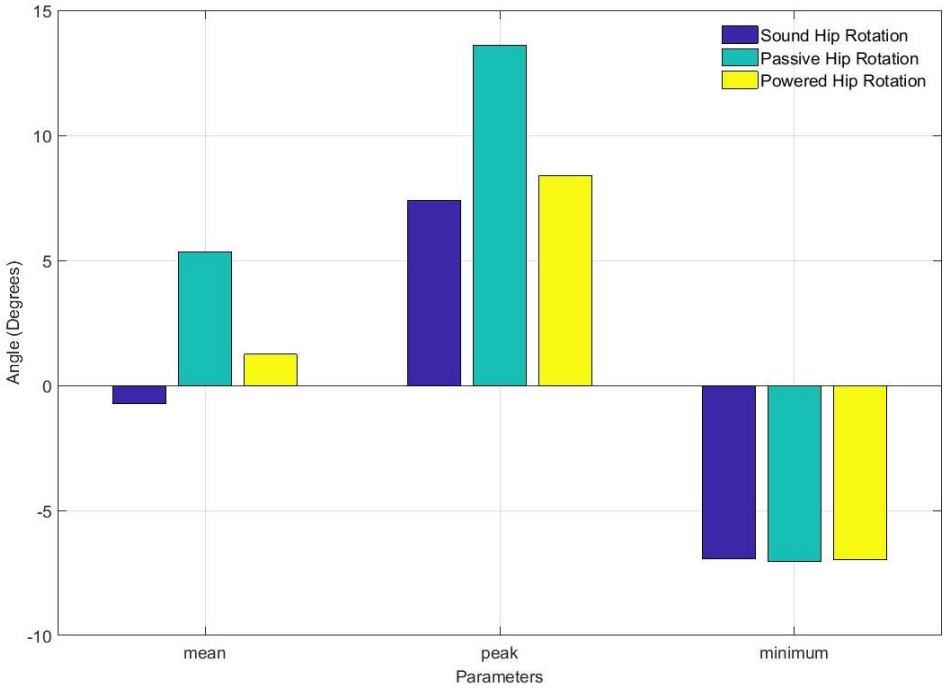

Figure 8.6: Comparison of the hip rotation of the passive and powered ankles to ankle of the sound leg

The hip rotation has reportedly been used as a compensatory mechanism to generate power for amputees to project the body forward. Figure 8.6 illustrates the hip rotation mean, peak and minimum angles. The gait plots are presented in Appendix F. These plots were an average of the total number of gait movements carried out on the treadmill and on the ground floor. The results are discussed in the following section.

8.5 Discussion

There was no significant difference with regard to the distance variables of the passive ankle performance as compared to the powered active ankle, as presented in Table 9. These findings also compliment the initial experimental results presented in section 5.3.1, comparing the passive ankle distance variables and variables from non-amputees which also revealed that there was no significant difference between non-amputees and amputees when normative data from non-amputees was used. Therefore, the powered ankle performed as expected. However, a closer analysis on each variable revealed some differences, though none significant. The cadence and the velocity for the powered ankle were less than that of the passive ankle. This could have been caused by the amputee's slow adaptation to the use of the device. The swing phase deviated by 1% from the non-amputee gait, thereby registering a 61%. The difference could not be categorised as late swing but this could be attributed to the delays within the DC motor actuation system.

Figure 8.4 revealed that the passive ankle maintained high angle values because of the stiffness of the ankle as compared to the powered ankle. The performance of the passive ankle largely depended on how effectively it returned to its original form as compared to the powered

ankle prosthetic, which could be positioned at any angle during walking in relation to the gait event. The dorsiflexion was activated during the heel-strike through to the loading response as expected but the torque delivered by the actuator caused positional errors due to delays. The mid-stance was determined as the period when the IMU sensors on the control systems were recording approximately 0^0, since this was designed as the zero crossing point. However, for the passive limb, the angle remains high irrespective of the foot projection. The powered ankle registered a peak angle of 22.85^0 which was approximately 2.20^0 higher than the angle from the sound leg. However, the passive ankle recorded a much higher average peak value of 36.20^0 which was a result of the lack of intuitive control of the device during the stance phase.

The results presented in Figure 8.5 revealed that there is a reduction in excessive knee flexion which was initially reported for the passive prosthetic limb. Although there was still evidence of a deviation of approximately 2.05^0 difference between the powered ankle and the sound leg, the difference could have been as a result of the amputee still being used to his previous body movements. The excessive knee extension experienced when using the passive limb during terminal stance and terminal swing was not observed on the powered ankle. This could have been attributed to the new actuation system as the powered ankle was able to be activated on all gait events, including terminal swing and terminal stance.

As the hip is responsible for generating power to project the body forward, the absence of plantar flexors caused the hip rotation to be reportedly high. The results presented in Figure 8.6 revealed that there is notable reduction in peak hip rotation by approximately 50% when using the powered ankle. This was due to the powered ankle's capability of providing the propulsive force in the absence of the plantar flexors.

The functionality of the powered active ankle was mainly governed by the actuator performance. However, the mechanics of the mechanical structure also had an impact on the overall performance of the device. The average peak dorsiflexion for adults is $12.64^0 \pm 3.95$SD [333] and the expected full range of motion is between 0^0 to 20^0. However, the intact non-amputated leg had an average peak dorsiflexion of $15^0 \pm 3$SD as compared to the average peak of $18.5^0 \pm 2$SD . The gait results (see Appendix F) also revealed that the prosthetic limb was able to achieve a stable stance phase. However, there were abnormalities during the swing phase, especially on the pre-swing phase where the ankle was supposed to exhibit the full range of motion on plantarflexion. The minimum plantarflexion angle achieved was as a result of the actuator experiencing an increase in torque demand. The plantarflexion maximum peak values were also inhibited by the excessive dorsiflexion and time delay that was being experienced by the actuator as it changed direction from forward to reverse. Therefore, the prosthetic limb produced a smooth limb projection during the stance phase as it utilised the full range of motion but experienced challenges during plantarflexion as the torque demand could not match the available torque.

The late swing phase on the prosthetic limb was observed as a result of prolonged loading response phase. The expected dorsiflexion and plantarflexion movement of the ankle, using normative data for subjects recorded on a treadmill as compared to the powered ankle, are shown in Appendix F. In comparison to the normative data, the prosthetic limb performed well for 61% of the gait cycle. The challenges with regard to smooth plantarflexion actuation are attributed to high torque demands as the motor will be trying to push the body up in contrast to the normal reaction force of the body.

8.6 Limitations of the study

The validation of the control architecture was based on single amputee.This was a small sample as compared to other previous studies. However, the number and length of activities were sufficient to provide conclusive results. The target control architecture is patient specific although approximately 85% of the system is universal. The carbon-flex foot which forms the basis of the foot and the socket were custom made. The control architecture's performance was highly influenced by the positioning of the IMU sensors on the amputee's shank even though the thigh position and orientation is expected to remain the same for every other individual. The positioning of the surface electrodes on the residual stump was very difficult due to the inner lining silicon cloth within the socket. Complex filtering algorithms are required to minimise cable movement artefacts. Such design requirements, if not implemented affects the performance of the device.

8.7 Conclusion

The testing and validation of the developed control architecture was presented in this section. The main emphasis was on evaluating the extent to which the developed control system could control a powered ankle. The goal was to evaluate the capability of the powered ankle for gait restoration by comparing the results to the passive prosthetic limb and the non-amputee gait results.

The results proved that the developed architecture was able to control the powered prosthetic ankle with the aid of sEMG signals, as the main control signal and the FSRs, encoder and IMU sensors were used to provide feedback. The system was able to correctly orientate the prosthetic foot with respect to the gait events. Challenges experienced during testing at the Neuromechanics laboratory included the magnetic interference experienced by the Noraxon IMU sensors each time the DC motor was being activated. As a result, in some instances, the values were not captured correctly during plantarflexion as the DC motor was being activated for longer periods as a way of providing the propulsive force (see Appendix F).

Although satisfactory results were achieved during the gait analysis, the crude prototype had limitations on the amount of torque the DC motor actuator could provide as compared to the required torque. The gait analysis results included the performance evaluation of the crude prototype. Therefore, the choice of machine mechanisms (links and cams) had an effect on the prototype performance. However, the concept proved to be useful and, if implemented, will go a long way on improving amputee gait. Thus, the study results were promising and revealed that continuous use of the device has the potential for gait restoration in lower limb amputees.

Chapter 9

Conclusion

9.1 Introduction

The desire to improve the daily lifestyle of the amputee community led to the development of an intelligent myoelectric control architecture in order to stabilise the use of prostheses. The main goal was to develop a control architecture which is capable of acquiring sEMG signals from identified muscle sites, intelligently deducing the intended move in the sagittal plane and deriving a reliable control signal that can be used to drive a powered ankle in a safe and reliable manner. This report presented the development of a robust myoelectric LSVM pattern recognition control architecture which is capable of intelligently driving a powered ankle with the aid of inertial sensors and force sensitive resistors. To achieve this goal of the study, the following objectives were realised:

- *Analysis of the effect of the passive mechanical prosthetic ankle on lower limb amputee gait.*

  The primary objective of *amputation rehabilitation* is to provide a means for the amputee to continue living a lifestyle similar to that of non-amputees with respect to mobility-related activities such as walking, running and standing. As a result, several types of amputation procedures are carried out with the aim of providing a rigid stump which could heal easily and could be interfaced with the available prosthetic limbs. In third world countries, the methods used to test the correctness of a prosthetic limb involves checking whether the amputee is comfortable with the prosthetic limb or not. However, our findings revealed that there are several other long-term and short-term effects associated with a *painless*, well fitted prosthetic limb.

  Gait analysis results revealed that there is no significant difference with regard to distance variables between amputees and non-amputees. However, upon examining the anatomical and orientation angles, it was observed that amputees exhibited excessive hip rotation. The excessive hip rotation was due to the compensatory behaviour of the hip to cover for the missing propulsive force during toe-off. The main purpose of the lower limb is to provide balance and locomotion. However, the forward projection of the body is as a result of the force generated by plantar flexors which assist during the pre-swing phase. For amputees, the missing plantar flexors cause excessive hip rotation and flexion which could result in unstable lumbar leading to a decrease in Gluteus Medius and internal oblique activity [230]. Amputees with passive mechanical limbs experienced early swing phase, and this has been attributed to the lack of stability of the amputated leg when it is positioned for single

support with the sound leg leading. This is due to a lack of balance and avoiding loading the body weight for a prolonged period during the single support phase.

The key issues of using a passive prosthetic limb are comfort and biomechanical restoration. The recommendations are based on the periodic adjustment of the mechanical passive prosthetic limbs to suite the amputee gait. The suggestion use of *comfort* as a variable for appropriateness of a prosthetic limb ignores the functionality component of the device. However, the results presented in this study revealed that passive prosthetic limbs neither have the capability of maintaining nor restoring normal gait. The lack of the propulsive force increases chances of poor range of motion (ROM) for the hip, knee and foot projection. The overall assessment of the anatomical and orientation angles reveal some characteristics of *spastic gait* due to lack of proper toe-off and poor foot projection on the amputated limb. The excessive hip flexion was caused by an attempt by the amputees to produce force to propel the body due to lack of plantar flexors. The poor ROM at the hip resulted in pelvis tilt which could lead to lower back pain. The excessive flexion and limited extension by the hip flexors could lead to lower back pain. These compensatory mechanisms may lead to long-term musculoskeletal system disorders due to stresses experienced by the lumbar spine. The results had been published in:

Garikayi, T., Van Den Heever, D. and Matope, S., 2017. Investigating the effects of passive mechanical ankle on unilateral osteomyoplastic transtibial amputees. *Journal of Musculoskeletal Research,* p.175-185.

- *The investigation of sEMG signal properties for ankle movements on transtibial amputees.*

The possibility of developing a reliable powered ankle to restore amputee gait relied on the availability of the control signal. In this study, sEMG was suggested as the control signal. However, the available literature was not sufficient to deduce the properties and characteristics of the available signal. As a result, experiments to investigate the properties of sEMG signals were carried out using two transtibial amputees. The available SENIAM and ISEK standards were insufficient to use during the recording the sEMG signals, although SENIAM standards were used for recording and ISEK standards were used for reporting. However, these available standards did not take into consideration the missing anatomical landmarks on the residual stump. They are well suited for clinical assessment of sEMG signals for diagnosis purposes on non-amputees.

There was significance difference between sEMG signals from the sound leg and those from the amputated leg. The signals from the amputated leg had approximately 35% signal power as compared to the sEMG from the sound leg. However, the signals from sound leg and the amputated leg had a similar bandwidth although, upon inspecting the power spectral density, it was observed that the signals from the amputated leg had 95% of its bandwidth within the 50% of the bandwidth of the signals from the sound leg. As a result, the muscular crosstalk between the Gastrocnemius muscles and the underlying inaccessible Soleus muscle contributed much to the frequencies below 40 Hz of the signal. Therefore, the high pass cut-off frequency was lowered to 15 Hz so that the lower frequencies could be captured and utilised, even in the form of muscular crosstalk, since it was unique only for plantarflexion.

The experimental results revealed that the Tibialis Anterior muscle responsible for dorsiflexion movement was active on the residual stump. However, the Soleus muscle, which is responsible for providing the plantarflexion, was inaccessible as it was covered by Gastrocnemius muscles. The Medialis Gastrocnemius and Lateralis Gastrocnemius muscles were also active and responsible for plantarflexion. The analysis results revealed that only three muscle sites could be used for myoelectric control and there was high demand for reliable filtering techniques so that quality signals could be acquired from the identified sites. The results concerning available muscles and their related sEMG signal characteristics had been published in:

Garikayi, T., Van den Heever, D. and Matope, S., 2018. Analysis of surface electromyography signal features on osteomyoplastic transtibial amputees for pattern recognition control architectures. *Biomedical Signal Processing and Control*, 40, pp.10-22.

- *Investigating the use of inertial sensors as feedback signals so as to improve adaptability, reliability and robustness of the architecture.*

Having identified the challenges involved with the use of passive prosthetic limbs and also revealing the signal properties of the sEMG, a reliable feedback system for the control architecture was determined. One of the major draw backs of the current passive and powered prosthetic limbs is the need for visual feedback on the performance of the device. This characteristic leaves the burden of completing the feedback loop to the amputee. A more novel approach was investigated in the use of IMU sensors to provide feedback concerning the performance of the limb. The technology had been well reported in the field of activity monitoring but is yet to be fully explored in the field of control systems. In gait analysis the signals are used to determine orientation and anatomical angles by calculating the angle between two IMU outputs. However, initial experimental results on gait analysis revealed that anatomical angles could be similar at different positions in gait or posture. For example, one can maintain the same knee angle while laying flat on the floor or standing. Therefore, to realise the intended objective, two IMU circuits were developed based on the MPU6050 IMU sensor. The initial experiments revealed that monitoring the shank alone will result in several similar features since the stride length of the amputees was around 1.09 s and the angle variations between gait events were small. Therefore, two sensor positions were identified as thigh and shank and the results generated from the IMU sensors were convincing as only the pitch output was used.

The system was optimised such that the orientation of the sensor (pitch angle) was considered to be the orientation of the limb segment (shank or thigh). The evidence of zero crossing between swing and stance for the shank improved the knowledge base performance. The IMU sensor outputs were used as feedback signals and not as input signals to the pattern recognition feature vector. The set-up provided control interlocks that improved the reliability of the architecture. The I2C communication protocol was used to synchronise the sensor outputs. The introduction of the IMU sensors also introduced robustness in the architecture since the IMU sensors were using the developed Kalman filter, which was able to predict the signal in the unfortunate event of loss of signal using previously acquired data. The results of the control system surpassed the previously reported performance of the Biomand the Triton Smart Ankle because the currently available technologies use the IMU sensors only to provide stiffness in the event of a fall, in other words, they provide

balance.

The proposed design has the capability for the establishment of closed loop feedback control. The other microprocessor based powered limbs, such as the Genium and C-Leg microprocessor versions, only use IMU sensors to provide actuation as the main control signal without any feedback on the limb performance. That is, they utilise feedforward control system. These systems assume that whatever control command initiated has been achieved. The encoders implemented in the proposed system provided the *true angle of the ankle* while the IMU sensors give feedback on the pitch angle of the shank and thigh with respect to the orientation of the IMU sensor. The results had been published in:

Garikayi, T., Van den Heever, D. and Matope, S., 2016, October. *Development of a health rehabilitation activity monitoring system for transtibial amputees* . South Africa Institute for Industrial Engineering Conference, 27-28 October, Stonehenge, Parys, South Africa, (p.177-190).

- *Development of the multichannel sEMG signal acquisition module*

The sEMG properties derived from the initial experiments on the characterisation of sEMG signals from the residual stump revealed that there is a need for a proper signal acquisition and processing module. The sEMG signals available were too weak and affected by muscle crosstalk. As a result, the necessary filtering and amplification techniques were developed, taking into consideration that only 35% signal power was available. The muscular crosstalk during plantarflexion between the inaccessible Soleus and the Gastrocnemius muscles was also considered as a noise artefact. The developed system consists of a second-order Sallen-Key bandpass filter which had a15 Hz high pass cut-off frequency and a 500 Hz low pass cut-off frequency. The system also consists of a BAS70XY diode barrier for of isolation the user from the circuit. The 24-bit ADS1298, with a data rate of 500 samples-per-second at a gain of 12 and having 16 channels was used for the acquisition of the signal. The adaptive filter coefficients used in the design enabled a clean output signal. Since the signal was acquired in differential mode, six channels were used for the three muscle sites.

The developed circuit can easily be used with any type of electrodes as the circuit was developed based on SENIAM and SEIK recommendations. As a contribution to the field of wearable rehabilitation devices, this design will provide a basis for future EMG based designs, as the signal acquisition stage is the most important stage in sEMG based rehabilitation devices. When packaged, the developed system had three terminals for the electrode interface, two terminals for power supply and a terminal for interfacing with the subsequent signal conversion circuit, making it a simple standalone device (See Appendix D). Recommendations are that the feedback resistors for the amplifiers use variable resistors which can be adjusted during circuit use. However, previous designs did not incorporate the protection circuit, hence for safety reasons this is now a prerequisite as detailed by the SENIAM regulations. The developed circuitry consisted of protection diodes which were responsible for isolating the circuit from the user in the unfortunate event of a current leakage through the electrodes.

The classification accuracy is highly affected by the nature of the input signal. Therefore, the 99.25% classification accuracy achieved by the classifier was a true reflection of the

signal acquisition performance. The Monte Carlo analysis and the Nyquist Analysis were both used to evaluate the signal acquisition circuit performance. The results revealed a stable and reliable circuit. Unfortunately, the circuit was affected by the 50 Hz power line interference. Similar challenges were reported in literature. However, to a great extent, the circuit achieved the targeted function.

- *The development of a robust myoelectric control architecture for a multifunctional artificial ankle.*

The initial results on the characterisation of the sEMG on the residual limb revealed that there are three available channels, namely Tibialis Anterior muscle (dorsiflexion), Medialis muscle (plantarflexion) and Lateralis Gastrocnemius muscle (plantarflexion). As a result, the application of myoelectric (sEMG controlled) control architecture was explored. The use of sEMG signals for clinical diagnostic purposes has been extensively been reported in literature but less literature is reported on their use in control systems. Some successful concepts had been developed by but the recommendations included the need for a more robust control architecture. Having defined robustness as failing gracefully, the use of sEMG signals alone in a control architecture could result in an unreliable system. The data acquired from the multichannel signal acquisition module was used to develop a feature vector which initially used 11 features per channel resulting, in 33 variables for the classifier. Initial results revealed unacceptable computational time lengths of over 700 ms. Therefore, PCA dimensionality reduction technique was applied and only 22 variables were left for the classifier to use. The reduction in feature vector resulted in decreased processing time and increased classification accuracy. Thus, the main thrust was to develop a pattern recognition system that is less complex and has recommendable classification accuracy (defined to be greater than 90%).

The literature survey indicated that linear classifiers are less complex, as a result, the options pursued included Linear Discriminant (LD) classifier or LSVM. However, the targeted classifiers were compared to 20 other classifiers. The Ensemble KNN and Decision Trees provided 100% classification accuracy on test data but had a three-fold processing time greater than LSVM and LD due to their complexity. LSVM and LD provided classification accuracy less than 100% on unknown data but had an acceptable processing time which was less than 300, ms. As a result, the LSVM classifier was chosen as it produced an average of 99.25% classification accuracy on unknown data.

In comparison with other previous studies, Hudgins et al. [107] used an Artificial Neural Network and achieved 91.2% for non-amputees and 85.5% on amputees and Nishikawa et al. [108] reported 91.5% with 1269.4, ms processing time which is almost four-fold the expected processing time. Other results were reported by Ajiboye and Wei [109] of 94-99% which could be an average of 96.4% using upper limbs sEMG values. However, the difference is that the lower limb has to deal with supporting the body during locomotion which increased the probability of skin movement artefact. Therefore, the 0.75% classification error could not be reduced through continuous training due to variability in skin impedance, movement artefact and power line interference. The achieved 99.25% classification accuracy is sufficient for the clinical viability of the device.

- *Testing the functionality of the developed control system architecture.*

  The testing of the developed concept was achieved through the use of fabricated crude powered ankle prototype. The powered ankle was simply a proof of concept, and the purpose of the test was to analyse the extend of the functionality of the developed system in real-life application. The prototype was made from aluminium material and consisted of a 12 V DC motor, a two-channel encoder, two FSRs, two IMU sensors, three channel sEMG acquisition unit and the microcontrollers. The system was installed on the participant. After calibration, the participant was tasked to walk on a treadmill. The treadmill speed was varied between 0.5 m/s and 0.8 m/s, resembling slow gait.

  The distance variables, anatomical angles and orientation angles were determined. A comparison was then made with the results from a passive mechanical limb. The results proved that the introduction of the propulsive force reduced the pelvis tilt. The device also exhibited recommendable foot projection, dorsiflexion and plantarflexion. However, the step size was reduced, and the stride duration increased. This was attributed to the reaction of the amputee to the new device. The use of prosthetic limbs takes time to practice and adapt to its functionality. This may take months or years, so even when the device functionality was working properly, it was regarded as a new extension of the human body by the user. The overall performance of the device could, however, be improved with regard to the mechanical mechanisms. To a greater extent, the device performance was achieved with respect to detecting human intention and controlling the powered ankle. These characteristics improved the amputee gait as compared to the use of the passive limb.

The design, development and testing of a myoelectric control system have been presented. The proposed design used sEMG, FSRs and IMU sensors within the control systems to improve the reliability of the control architecture. The use of sEMG signals for commercial powered ankles has not yet been reported to be clinically viable mainly because of the lack of a reliable sEMG signal, among other reasons. The BiOM, produced by MIT and now owned by Otto Bock ,only uses IMU sensors so is the Genium, C-Leg microprocessor based and the Triton Smart Ankle. The proposed design has the capability of utilising the sEMG signals, IMU sensors, FSRs and encoders to improve the reliability of the system. The current powered limbs require that the amputee move for a few steps before the system begins to operate. Otto Bock suggested that since because the user has no control over the performance of the powered limb, there is intuitive control (see Appendix G). However, one could argue that the intuitive control we introduced through the sEMG enabled the user to activate the powered ankle and has overall control *intuitively* of the orientation and performance of the leg.

The uniqueness of the developed design is that the user could tweak the powered ankle and correctly orientate the foot while standing to improve balance. The developed design, when walking, allow the limb to be adjusted based on the sEMG signals. The feedback sensors (IMU, encoders and FSRs) then checked the orientation and positioning of the whole lower limb and not just the foot. The major contribution of the proposed design in the field of the powered prosthetic limb is the provision of the propulsive force by the DC motor actuator through a lead-screw relative to the gait event(stance and swing phases). The system improved the toe-off and heel clearance thereby reducing excessive hip rotation and flexion reported for passive ankles.

9.2 Limitations of the study

Although the targeted goal was achieved, there are limitations associated with the developed control architecture. The major set-back of the design is that it could only operate on two motion classes, namely the dorsiflexion movement and the plantarflixion movement with the resting motion being considered as the transitional motion. Other movements such as abduction, adduction, inversion and eversion were not considered. However, during validation tests the participant revealed that only the dorsiflexion and plantarflexion could bring about positive changes on orientation angles such as hip rotation, knee flexion and pelvis tilt. As a result, the study was scoped to focus only on dorsiflexion and plantarflexion. The safety and control interlocks used within the design restricted the user to tweak or flex the ankle when seated or laying on the floor unless in upright position. Although these safety features were implemented to safeguard the amputee from actuating the device unless in motion or ready to walk, they limit the general requirements of the amputee to have full control of the device.

Power consumption of the device limited the length of time of the device could be used per day. Since the torque developed is related top the available power, the torque requirements of the ankle were limited by the available power from the 12 V battery. The 12 V DC motor used as the actuator has limited torque. Even though the lead screw technique was used for the drive it could not add much torque to the geared motor system, however, it actually increased the load to the motor.

Although the developed control architecture could work with any sEMG signals from the lower limb, it is limited to only three sEMG signal channels recorded in differential mode. Any attempt to reduce the available channels could reduce the classification accuracy of the system. An increase in signal channels causes an increase on the size of the feature vector which could lead to increased processing time thereby, reducing the effectiveness of the architecture. The developed control system architecture's signal acquisition system could only take up to eight signal channels when recorded in differential mode.

The developed dry electrode was efficient on recording the sEMG from all the three muscles sites. However, methods for securing the electrode to the residual stump were limited. The straps could not be used inside the silicon liner. Such limitations presence challenges for the clinical viability of the electrodes.

9.3 Recommendations

The goal of developing an intelligent and robust myoelectric control architecture was achieved. However, there are certain areas of the developed system that could be improved through further research. These improvements could further improve the functionality of the device and, as a result, improve the lifestyle of the amputees.

During testing the developed control system in real-time using a crude prototype, the participant complained about having a large control box with the battery hanging on his thigh. It is therefore, recommended that efforts be made to develop a system which is more compact and could be fitted within the prosthetic limb without attaching anything on the residual limb or body. Furthermore, the 12 V motor coupled to the lead screw generated a lot of noise during actuation. This noise was irritating the participant at times and suggestions are that a linear

actuator with high torque be developed specifically for powered ankles. This will reduce the noise generation, number of moving parts and also the overall volume and size of the device.

Although the use of two IMU sensors improved the system performance of the actuator, attaching the second IMU sensor on the thigh of the amputee was considered undesirable by the participant. It is therefore, suggested that efforts be made to achieve recommendable system performance by simply monitoring the shank (prosthetic limb) part without the need for the thigh.

Although the 99.25% classification accuracy is considered acceptable for myoelectric control, efforts can be made by future researchers to improve the classification accuracy to 100%. These suggestions if implemented could improve the performance of myoelectric control devices further than the reported results in this study.

The future for powered limb prosthetics is bright. The use of a myoelectric pattern recognition system is feasible and the intuitive control of the prosthetic limbs will revolutionise the rehabilitation device industry. If implemented, the developed control architecture will go a long way towards improving gait restoration, improving the ambulatory activities, reducing the impact of musculoskeletal disorders associated with use of passive limbs, reducing lower back pain as the pelvic tilt is improved and improving the amputee's lifestyle.

Appendices

Appendix A

Ethical clearance letter

UNIVERSITEIT·STELLENBOSCH·UNIVERSITY
jou kennisvennoot • your knowledge partner

Approved with Stipulations

Response to Modifications- (New Application)

04-Jul-2016
Garikayi, Talon T

Ethics Reference #: S16/05/093
Title: Development of myoelectric robust control architecture for lower limb prosthetic applications

Dear Mr Talon Garikayi,

The **Response to Modifications -** ***(New Application)*** received on **24-Jun-2016**, was reviewed by members of **Health Research Ethics Committee 2** via Expedited review procedures on **04-Jul-2016**.

Please note the following information about your approved research protocol:

Protocol Approval Period: **04-Jul-2016 -03-Jul-2017**

The Stipulations of your ethics approval are as follows:
The response to the review is generally satisfactory. The protocol is approved on condition that the remaining points regarding the Consent document (and related protocol) are addressed.
Consent form
1) Section 'If you do not agree to take part..':
Subject detail should be moved to the appropriate section e.g. What the study is about.
Correct grammar i.e. change "man" to "men" in the Consent document and Protocol.
2) Add the detail on procedures i.e. last paragraph of point 7 on MOD Letter, to section 'What will your responsibilities be', so that the subject will also immediately have an idea of the nature of activities to be performed, how long it will take, and the number of visits.
3) Mention under '..risks involved..' that potential discomfort may relate to skin irritation and adhesion of electrodes upon removal, subtle but safe voltage surges of surface electrodes, and falling during activities.

Please remember to use your **protocol number** (**S16/05/093**) on any documents or correspondence with the HREC concerning your research protocol.

Please note that the HREC has the prerogative and authority to ask further questions, seek additional information, require further modifications, or monitor the conduct of your research and the consent process.

After Ethical Review:
Please note a template of the progress report is obtainable on www.sun.ac.za/rds and should be submitted to the Committee before the year has expired. The Committee will then consider the continuation of the project for a further year (if necessary). Annually a number of projects may be selected randomly for an external audit.
Translation of the consent document to the language applicable to the study participants should be submitted.

Appendix B

Active electrode amplifier

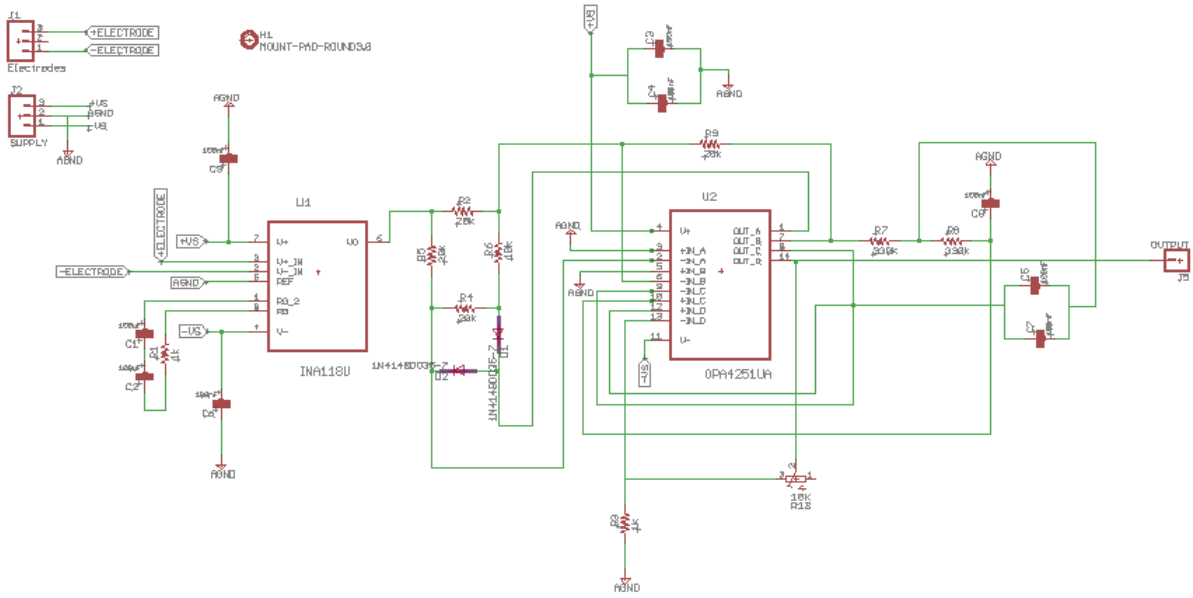

Appendix C

EMG multichannel data acquisition card

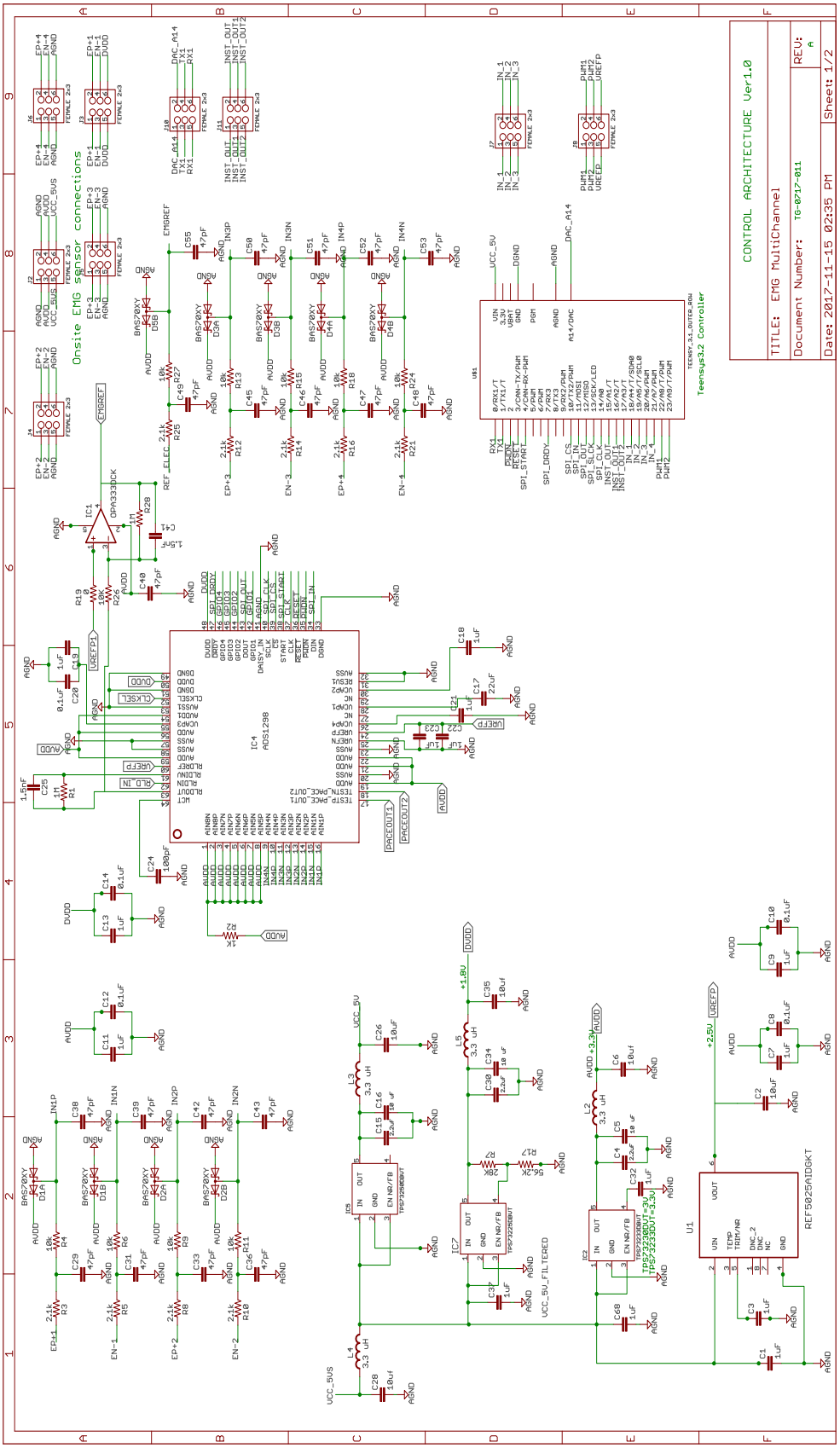

Appendix D

Main control card

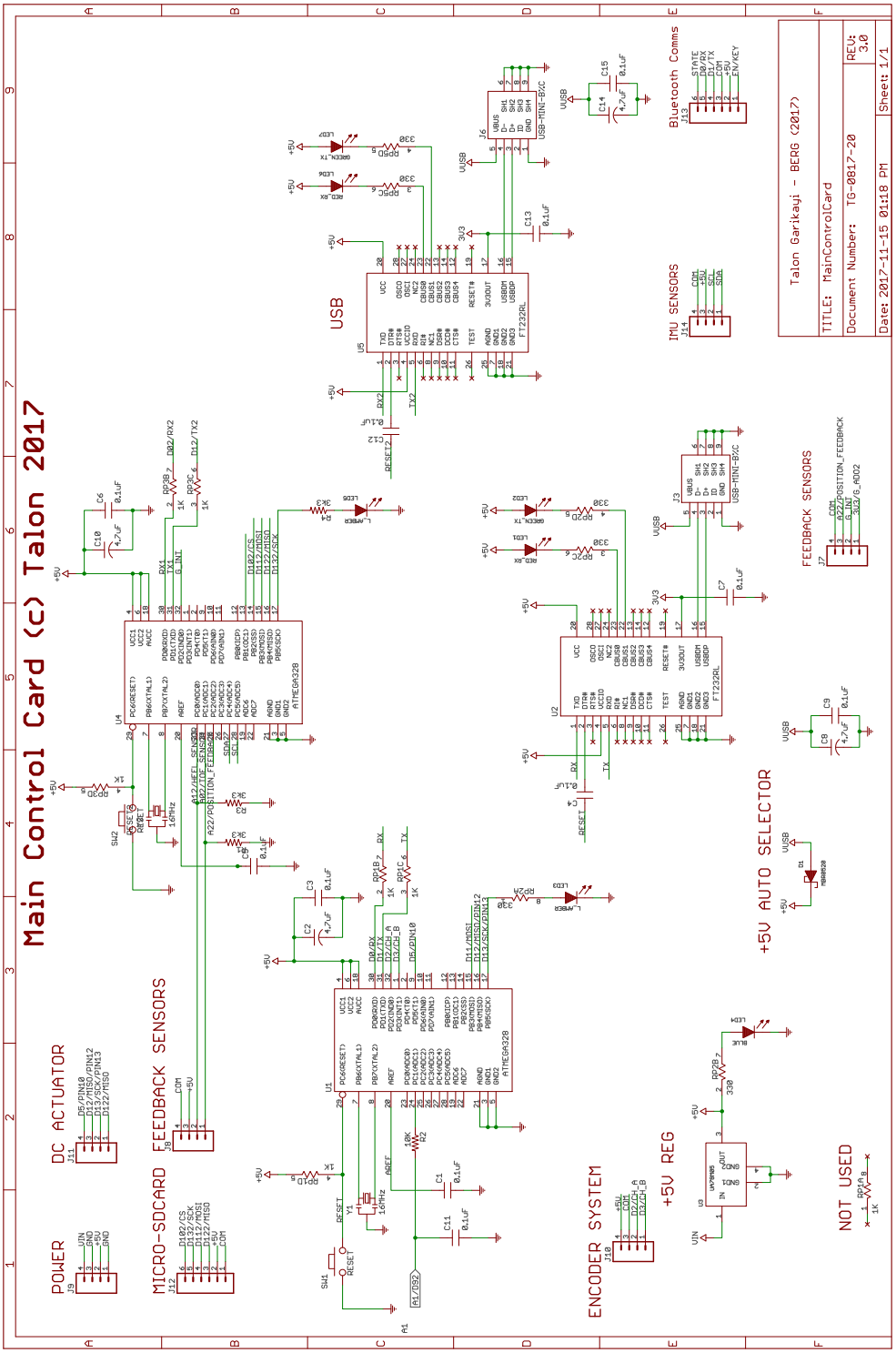

Appendix E

Classifier averaged results

Sub1Ex2

Total Observations 428

Confussion Matrix %

54.6729	0.0000	0.4673
0.0000	19.1589	0.0000
0.2336	0.0000	25.4673

Model Accuracy	0.9930	99%

Class	1	2	3
Precision	0.991525	1	0.990909
Sensitivity	0.995745	1	0.981982
Specificity	0.989637	1	0.996845

True Positive (TP)	234	82	109
False Positive (FP)	2	0	1
False Negative (FN)	1	0	2
True Negative (TN)	191	346	316

Sub1Ex3

Total Observations 487

Confussion Matrix %

54.6201232	0	0
0	22.38193	0
0.616016427	1.026694	21.35523614

Model Accuracy	0.98373	98%

Class	1	2	3
Precision	1	1	0.928571429
Sensitivity	0.988848	0.956140351	1
Specificity	1	1	0.979112272

True Positive (TP)	266	109	104
False Positive (FP)	0	0	8
False Negative (FN)	3	5	0
True Negative (TN)	218	373	375

Sub1Ex4

Total Observations 478

Confussion Matrix %

48.53556485	0	0
0	22.38494	0
0	0	29.0795

Model Accuracy	1	100%

Class	1	2	3
Precision	1	1	1
Sensitivity	1	1	1
Specificity	1	1	1

True Positive (TP)	232	107	139
False Positive (FP)	0	0	0
False Negative (FN)	0	0	0
True Negative (TN)	246	371	339

Sub1Ex5

Total Observations 545

Confussion Matrix %

58.16513761	0	0
0	19.44954	0
0	0	22.38532

Model Accuracy	1	100%

Class	1	2	3
Precision	1	1	1
Sensitivity	1	1	1
Specificity	1	1	1

True Positive (TP)	317	106	122
False Positive (FP)	0	0	0
False Negative (FN)	0	0	0
True Negative (TN)	228	439	423

AVERAGE VALUES

Class	1	2	3
Precision	0.997881	1	0.97987
Sensitivity	0.996148	0.989035	0.995495
Specificity	0.997409	1	0.993989

True Positive (TP)	262	101	119
False Positive (FP)	1	0	2
False Negative (FN)	1	1	1
True Negative (TN)	221	382	363

CONFUSSION MATRIX

Rest	53.99843	0	0.1682243
Dorsiflexion	0	20.8438218	0
Plantarflexion	0.212415	0.256673511	24.57183622
	Rest	Dorsiflexion	Plantarflexion

Appendix F

Gait plots

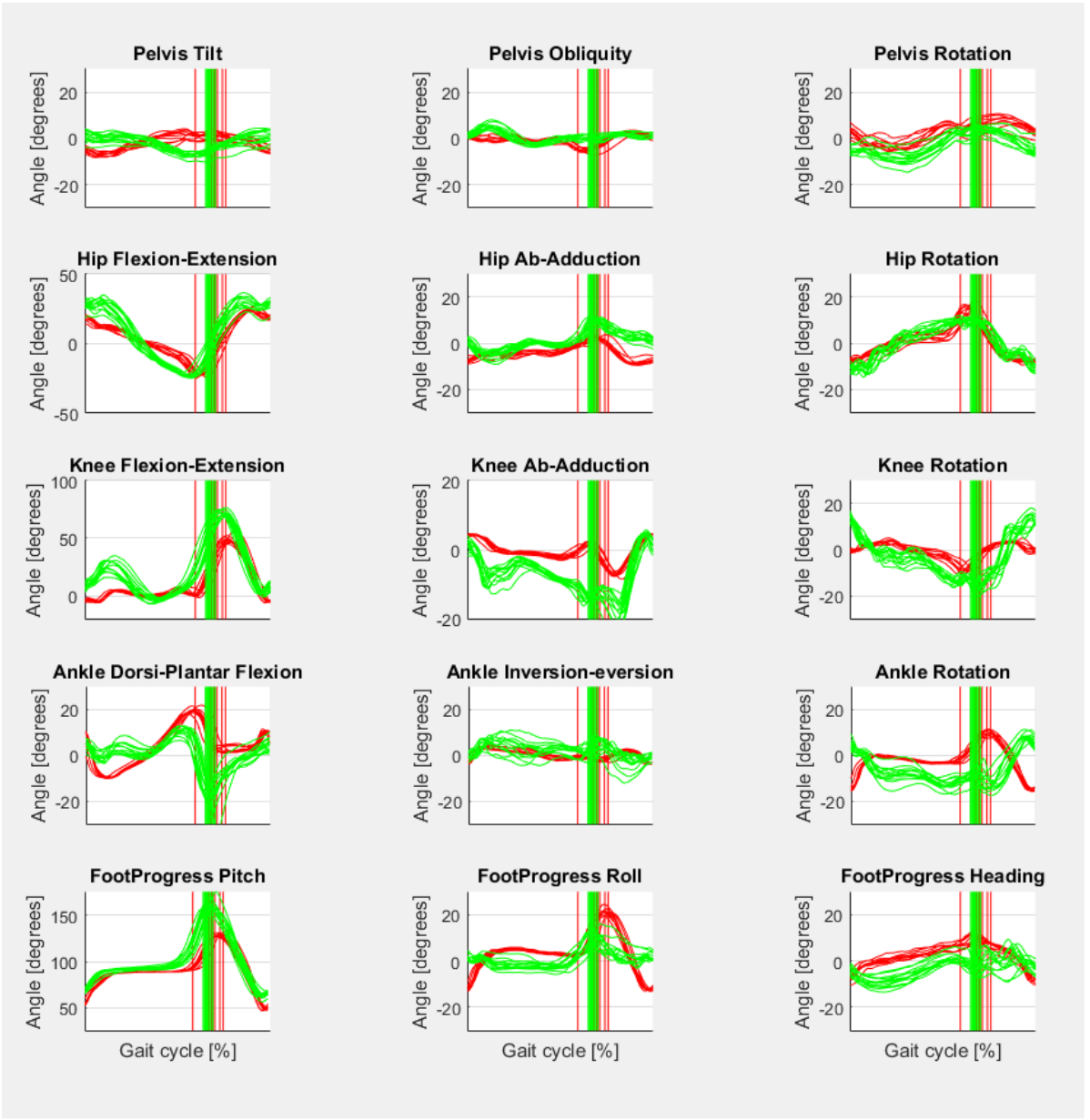

Appendix G

Commercial powered limbs

Mobility standards for more than 15 years

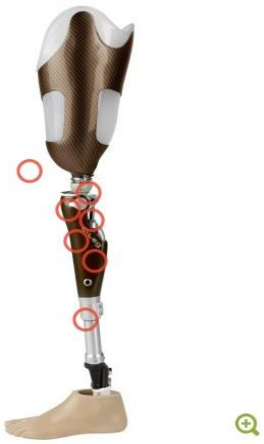

Confidence in the next step

The C-Leg has been setting fitting standards for transfemoral amputees since more than 15 years. More than 40,000 users worldwide rely on the C-Leg technology. The microprocessor-controlled leg prosthesis system is ideal for anyone with high stability and reliability requirements in everyday life. It also meets the demand for mobility and freedom. The knee joint is controlled by a complex sensor system, which permits adaptation to various walking speeds. Stability even in uncertain situations, walking slow or fast, negotiating slopes and walking down stairs step-over-step – the C-Leg supports these types of everyday mobility.

A Milestone in prosthetics

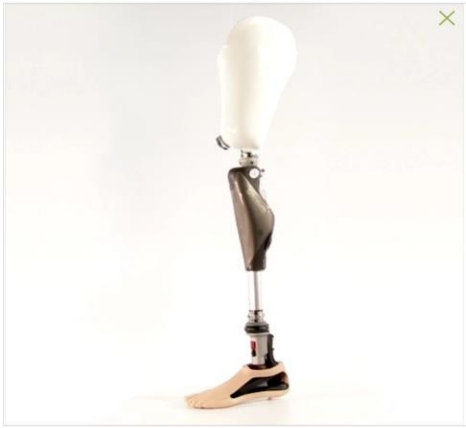

The Genium provides an intuitive, natural gait

The microprocessor-controlled Genium supports the natural movement pattern down to the details – without requiring the user to consciously control the joint. Everything happens in real time, regardless of the situation, and even forward-looking. This is made possible by the latest computer, sensor and control technology. The Genium responds intelligently to a wide variety of everyday situations. This is the closest a transfemoral leg prosthesis system has come to recreating a natural, physiological gait pattern.

Contact Us

Ask for our Patient Navigator

+27 (0) 87 806 2950

→ Send an email

Stay in touch

Sign up to receive occasional updates from Ottobock.

→ Sign up

Share with a friend

Facebook

List of References

[1] Parmar, N.: Mind controlled bionic limbs bring giant strides in prosthetics. *The National,www.thenational.ae*, 2012.

[2] Shi, L., Liu, X., Li, N., Liu, B. and Liu, Y.: Aging decreases the contribution of maxik channel in regulating vascular tone in mesenteric artery by unparallel downregulation of α-and β1-subunit expression. *Mechanisms of ageing and development*, vol. 134, no. 9, pp. 416–425, 2013.

[3] Bertram, M.Y., Jaswal, A.V., Van Wyk, V.P., Levitt, N.S. and Hofman, K.J.: The non-fatal disease burden caused by type 2 diabetes in south africa, 2009. *Glob Health Action*, vol. 6, no. Suppl 1, pp. 206–212, 2013.

[4] Hubbard, S., Smith, D.G. and Gambel, J.M.: Prosthetic cost projections for servicemembers with major limb loss from vietnam and oif/oef. *Journal of rehabilitation research and development*, vol. 47, no. 4, p. 387, 2010.

[5] Meek, S.G.: Prosthetic limbs. In: *NEUROPROSTHETICS: Theory and Practice*, pp. 793–810. World Scientific, 2017.

[6] Jimenez, M.C. and Fishel, J.A.: Evaluation of force, vibration and thermal tactile feedback in prosthetic limbs. In: *Haptics Symposium (HAPTICS), 2014 IEEE*, pp. 437–441. IEEE, 2014.

[7] Garikayi, T., van den Heever, D. and Matope, S.: Robotic prosthetic challenges for clinical applications. In: *Control and Robotics Engineering (ICCRE), 2016 IEEE International Conference on*, pp. 1–5. IEEE, 2016.

[8] Oskoei, M.A. and Hu, H.: Myoelectric control systemsâĂŤa survey. *Biomedical Signal Processing and Control*, vol. 2, no. 4, pp. 275–294, 2007.

[9] Markowitz, J., Krishnaswamy, P., Eilenberg, M.F., Endo, K., Barnhart, C. and Herr, H.: Speed adaptation in a powered transtibial prosthesis controlled with a neuromuscular model. *Philosophical Transactions of the Royal Society of London B: Biological Sciences*, vol. 366, no. 1570, pp. 1621–1631, 2011.

[10] Shenoy, P., Miller, K.J., Crawford, B. and Rao, R.P.: Online electromyographic control of a robotic prosthesis. *IEEE Transactions on Biomedical Engineering*, vol. 55, no. 3, pp. 1128–1135, 2008.

[11] Farina, D., Jiang, N., Rehbaum, H., Holobar, A., Graimann, B., Dietl, H. and Aszmann, O.C.: The extraction of neural information from the surface emg for the control of upper-limb prostheses: emerging avenues and challenges. *IEEE Transactions on Neural Systems and Rehabilitation Engineering*, vol. 22, no. 4, pp. 797–809, 2014.

[12] Menon, R., Di Caterina, G., Lakany, H., Petropoulakis, L., Conway, B. and Soraghan, J.: Study on interaction between temporal and spatial information in classification of emg signals in myoelectric prostheses. *IEEE Transactions on Neural Systems and Rehabilitation Engineering*, 2017.

[13] Muceli, S., Vujaklija, I., Jiang, N., Amsuess, S., Graimann, B., Aszmann, O. and Farina, D.: A biologically-inspired robust control system for myoelectric control. In: *Converging Clinical and Engineering Research on Neurorehabilitation II*, pp. 975–979. Springer, 2017.

[14] Li, G., Li, Y., Yu, L. and Geng, Y.: Conditioning and sampling issues of emg signals in motion recognition of multifunctional myoelectric prostheses. *Annals of biomedical engineering*, vol. 39, no. 6, pp. 1779–1787, 2011.

[15] Au, A.T. and Kirsch, R.F.: Emg-based prediction of shoulder and elbow kinematics in able-bodied and spinal cord injured individuals. *IEEE Transactions on Rehabilitation Engineering*, vol. 8, no. 4, pp. 471–480, 2000.

[16] Varol, H.A., Sup, F. and Goldfarb, M.: Multiclass real-time intent recognition of a powered lower limb prosthesis. *IEEE Transactions on Biomedical Engineering*, vol. 57, no. 3, pp. 542–551, 2010.

[17] Biddiss, E. and Chau, T.: Upper-limb prosthetics: critical factors in device abandonment. *American journal of physical medicine & rehabilitation*, vol. 86, no. 12, pp. 977–987, 2007.

[18] Benz, H.L., Yao, J., Rose, L., Olgac, O., Kreutz, K., Saha, A. and Civillico, E.F.: Upper extremity prosthesis user perspectives on unmet needs and innovative technology. In: *Engineering in Medicine and Biology Society (EMBC), 2016 IEEE 38th Annual International Conference of the*, pp. 287–290. IEEE, 2016.

[19] Patel, G.K., Dosen, S., Castellini, C. and Farina, D.: Multichannel electrotactile feedback for simultaneous and proportional myoelectric control. *Journal of Neural Engineering*, vol. 13, no. 5, p. 056015, 2016.

[20] Englehart, K. and Hudgins, B.: A robust, real-time control scheme for multifunction myoelectric control. *IEEE transactions on biomedical engineering*, vol. 50, no. 7, pp. 848–854, 2003.

[21] Whalen, A.J., Brennan, S.N., Sauer, T.D. and Schiff, S.J.: Observability and controllability of nonlinear networks: the role of symmetry. *Physical Review X*, vol. 5, no. 1, p. 011005, 2015.

[22] Hargrove, L.J., Li, G., Englehart, K.B. and Hudgins, B.S.: Principal components analysis preprocessing for improved classification accuracies in pattern-recognition-based myoelectric control. *IEEE Transactions on Biomedical Engineering*, vol. 56, no. 5, pp. 1407–1414, 2009.

[23] Castellini, C., Artemiadis, P., Wininger, M., Ajoudani, A., Alimusaj, M., Bicchi, A., Caputo, B., Craelius, W., Dosen, S., Englehart, K. *et al.*: Proceedings of the first workshop on peripheral machine interfaces: going beyond traditional surface electromyography. *Frontiers in neurorobotics*, vol. 8, p. 22, 2014.

[24] Wagner, J., Kim, J. and André, E.: From physiological signals to emotions: Implementing and comparing selected methods for feature extraction and classification. In: *2005 IEEE International Conference on Multimedia and Expo*, pp. 940–943. IEEE, 2005.

[25] Kaneko, K.: Characterization of stem cells and cancer cells on the basis of gene expression profile stability, plasticity, and robustness. *Bioessays*, vol. 33, no. 6, pp. 403–413, 2011.

[26] Veer, K. and Sharma, T.: A novel feature extraction for robust emg pattern recognition. *Journal of medical engineering & technology*, vol. 40, no. 4, pp. 149–154, 2016.

[27] Au, S.K., Dilworth, P. and Herr, H.: An ankle-foot emulation system for the study of human walking biomechanics. In: *Robotics and Automation, 2006. ICRA 2006. Proceedings 2006 IEEE International Conference on*, pp. 2939–2945. IEEE, 2006.

[28] Fekri, S., Athans, M. and Pascoal, A.: Issues, progress and new results in robust adaptive control. *International Journal of Adaptive Control and Signal Processing*, vol. 20, no. 10, pp. 519–579, 2006.

[29] Hargrove, L.J., Simon, A.M., Young, A.J., Lipschutz, R.D., Finucane, S.B., Smith, D.G. and Kuiken, T.A.: Robotic leg control with emg decoding in an amputee with nerve transfers. *New England Journal of Medicine*, vol. 369, no. 13, pp. 1237–1242, 2013.

[30] Scheme, E. and Englehart, K.: Electromyogram pattern recognition for control of powered upper-limb prostheses: State of the art and challenges for clinical use. *Journal of rehabilitation research and development*, vol. 48, no. 6, p. 643, 2011.

[31] Oskoei, M.A. and Hu, H.: Myoelectric based virtual joystick applied to electric powered wheelchair. In: *2008 IEEE/RSJ International Conference on Intelligent Robots and Systems*, pp. 2374–2379. IEEE, 2008.

[32] Guo, S., Pang, M., Gao, B., Hirata, H. and Ishihara, H.: Comparison of semg-based feature extraction and motion classification methods for upper-limb movement. *Sensors*, vol. 15, no. 4, pp. 9022–9038, 2015.

[33] Jiang, N., Dosen, S., Muller, K.-R. and Farina, D.: Myoelectric control of artificial limbsâĂŤis there a need to change focus?[in the spotlight]. *IEEE Signal Processing Magazine*, vol. 29, no. 5, pp. 152–150, 2012.

[34] Pieringer, D.S., Grimmer, M., Russold, M.F. and Riener, R.: Review of the actuators of active knee prostheses and their target design outputs for activities of daily living. In: *Rehabilitation Robotics (ICORR), 2017 International Conference on*, pp. 1246–1253. IEEE, 2017.

[35] Toledo, C., Leija, L., Munoz, R., Vera, A. and Ramirez, A.: Upper limb prostheses for amputations above elbow: A review. In: *Health Care Exchanges, 2009. PAHCE 2009. Pan American*, pp. 104–108. IEEE, 2009.

[36] Lura, D.J., Wernke, M.W., Carey, S.L., Kahle, J.T., Miro, R.M. and Highsmith, M.J.: Crossover study of amputee stair ascent and descent biomechanics using genium and c-leg prostheses with comparison to non-amputee control. *Gait & Posture*, vol. 58, pp. 103–107, 2017.

[37] Fite, K.B.: The socket interface. *Full Stride: Advancing the State of the Art in Lower Extremity Gait Systems*, p. 55, 2017.

[38] Tang, J., Jiang, L., Moser, D. and Zahedi, S.: The effect of integrated microprocessor controlled knee-foot for inclined walking-a preliminary study on linx. 2015.

[39] Shirota, C.: *Towards Effective Fall Prevention Mechanisms in Lower-Limb Prostheses: Trip Recovery in Transfemoral Amputees*. Ph.D. thesis, Northwestern University, 2015.

[40] AWAD, M., DEHGHANI, A., MOSER, D. and ZAHEDI, S.: Dynamic coupling characteristics of a semi-active knee prosthesis. In: *Nature-Inspired Mobile Robotics*, pp. 43–50. World Scientific, 2013.

[41] Connolly, C.: Prosthetic hands from touch bionics. *Industrial Robot: An International Journal*, vol. 35, no. 4, pp. 290–293, 2008.

[42] Van Der Niet, O. and van der Sluis, C.K.: Functionality of i-limb and i-limb pulse hands: Case report. *Journal of rehabilitation research and development*, vol. 50, no. 8, p. 1123, 2013.

[43] Bionics, T.: The i-limb hand. *Retrieved July 3rd*, 2009.

[44] Bogue, R.: Exoskeletons and robotic prosthetics: a review of recent developments. *Industrial Robot: An International Journal*, vol. 36, no. 5, pp. 421–427, 2009.

[45] Slade, P., Akhtar, A., Nguyen, M. and Bretl, T.: Tact: Design and performance of an open-source, affordable, myoelectric prosthetic hand. In: *Robotics and Automation (ICRA), 2015 IEEE International Conference on*, pp. 6451–6456. IEEE, 2015.

[46] Kannape, O.A. and Herr, H.M.: Split-belt adaptation and gait symmetry in transtibial amputees walking with a hybrid emg controlled ankle-foot prosthesis. In: *Engineering in Medicine and Biology Society (EMBC), 2016 IEEE 38th Annual International Conference of the*, pp. 5469–5472. IEEE, 2016.

[47] Schwartz, J.: Mind controlled bionic limbs bring giant strides in prosthetics. *The Boston Magazine,www.bostonmagazine.com*, 2013.

[48] Gardinier, E.S., Kelly, B.M., Wensman, J. and Gates, D.H.: A controlled clinical trial of a clinically-tuned powered ankle prosthesis in people with transtibial amputation. *Clinical Rehabilitation*, p. 0269215517723054, 2017.

[49] Reaz, M., Hussain, M. and Mohd-Yasin, F.: Techniques of emg signal analysis: detection, processing, classification and applications. *Biological procedures online*, vol. 8, no. 1, pp. 11–35, 2006.

[50] Hargrove, L.J., Englehart, K. and Hudgins, B.: A comparison of surface and intramuscular myoelectric signal classification. *IEEE Transactions on Biomedical Engineering*, vol. 54, no. 5, pp. 847–853, 2007.

[51] Sörnmo, L. and Laguna, P.: *Bioelectrical signal processing in cardiac and neurological applications*, vol. 8. Academic Press, 2005.

[52] Caggiati, A., Bergan, J.J., Gloviczki, P., Jantet, G., Wendell-Smith, C.P., Partsch, H., on Venous Anatomical Terminology, I.I.C.C. *et al.*: Nomenclature of the veins of the lower limbs: an international interdisciplinary consensus statement. *Journal of vascular surgery*, vol. 36, no. 2, pp. 416–422, 2002.

[53] Pitman, J. and John, L.: The non-invasive measurement of deep forearm muscle electromyography using surface electrodes. In: *She 25th Congress of the International Society of Biomechanics*, vol. 1, pp. 1–7. International Society of Biomechanic, 2014.

[54] McGill, S., Juker, D. and Kropf, P.: Appropriately placed surface emg electrodes reflect deep muscle activity (psoas, quadratus lumborum, abdominal wall) in the lumbar spine. *Journal of biomechanics*, vol. 29, no. 11, pp. 1503–1507, 1996.

[55] Garikayi, T., Van Den Heever, D. and Matope, S.: Investigating the effects of passive mechanical ankle on unilateral osteomyoplastic transtibial amputees. *Journal of Musculoskeletal Research*, p. 1750015, 2017.

[56] Binstead, J.T. and Bhimji, S.S.: Anatomy, lower limb, calf. 2017.

[57] Koshio, T., Sakurazawa, S., Toda, M., Akita, J., Kondo, K. and Nakamura, Y.: Identification of surface and deep layer muscles activity by surface emg. In: *SICE Annual Conference (SICE), 2012 Proceedings of*, pp. 1816–1821. IEEE, 2012.

[58] Kuiken, T.A., Dumanian, G., Lipschutz, R., Miller, L. and Stubblefield, K.: The use of targeted muscle reinnervation for improved myoelectric prosthesis control in a bilateral shoulder disarticulation amputee. *Prosthetics and orthotics international*, vol. 28, no. 3, pp. 245–253, 2004.

[59] Scheme, E. and Englehart, K.: Electromyogram pattern recognition for control of powered upper-limb prostheses: state of the art and challenges for clinical use. *Journal of Rehabilitation Research & Development*, vol. 48, no. 6, 2011.

[60] Rajaratnam, B., Goh, J. and Kumar, V.: A comparison of emg signals from surface and fine-wire electrodes during shoulder abduction. *International Journal of Physical Medicine & Rehabilitation*, 2014.

[61] Merletti, R., Parker, P.A. and Parker, P.J.: *Electromyography: physiology, engineering, and non-invasive applications*, vol. 11. John Wiley & Sons, 2004.

[62] Hakonen, M., Piitulainen, H. and Visala, A.: Current state of digital signal processing in myoelectric interfaces and related applications. *Biomedical Signal Processing and Control*, vol. 18, pp. 334–359, 2015.

[63] Hoozemans, M.J. and Van Dieen, J.H.: Prediction of handgrip forces using surface emg of forearm muscles. *Journal of electromyography and kinesiology*, vol. 15, no. 4, pp. 358–366, 2005.

[64] Bilodeau, M., Schindler-Ivens, S., Williams, D., Chandran, R. and Sharma, S.: Emg frequency content changes with increasing force and during fatigue in the quadriceps femoris muscle of men and women. *Journal of Electromyography and Kinesiology*, vol. 13, no. 1, pp. 83–92, 2003.

[65] Rechy-Ramirez, E.J. and Hu, H.: Stages for developing control systems using emg and eeg signals: A survey. *School of Computer Science and Electronic Engineering, University of Essex,*, 2011.

[66] Karimimehr, S., Marateb, H.R., Muceli, S., Mansourian, M., Mañanas, M.A. and Farina, D.: A real-time method for decoding the neural drive to muscles using single-channel intra-muscular emg recordings. *International Journal of Neural Systems*, p. 1750025, 2017.

[67] Parker, P., Englehart, K. and Hudgins, B.: Myoelectric signal processing for control of powered limb prostheses. *Journal of electromyography and kinesiology*, vol. 16, no. 6, pp. 541–548, 2006.

[68] Ives, C.T. and Doherty, T.J.: Influence of needle electrode depth on de-sta motor unit number estimation. *Muscle & nerve*, vol. 50, no. 4, pp. 587–592, 2014.

[69] Su, Y., Fisher, M.H., Wolczowski, A., Bell, G.D., Burn, D.J. and Gao, R.X.: Towards an emg-controlled prosthetic hand using a 3-d electromagnetic positioning system. *IEEE transactions on instrumentation and measurement*, vol. 56, no. 1, pp. 178–186, 2007.

[70] Chowdhury, R.H., Reaz, M.B., Ali, M.A.B.M., Bakar, A.A., Chellappan, K. and Chang, T.G.: Surface electromyography signal processing and classification techniques. *Sensors*, vol. 13, no. 9, pp. 12431–12466, 2013.

[71] Naik, G.R., Kumar, D.K., Weghorn, H. and Palaniswami, M.: Identification of number of independent sources in surface emg recordings using over complete ica. In: *The 1st International Conference on Signal Processing and Communication Systems, ICSPCS*. 2007.

[72] Merletti, R. and Di Torino, P.: Standards for reporting emg data. *J Electromyogr Kinesiol*, vol. 9, no. 1, pp. 3–4, 1999.

[73] Keshwani, N. and McLean, L.: State of the art review: intravaginal probes for recording electromyography from the pelvic floor muscles. *Neurourology and urodynamics*, vol. 34, no. 2, pp. 104–112, 2015.

[74] Tam, H. and Webster, J.G.: Minimizing electrode motion artifact by skin abrasion. *IEEE Transactions on Biomedical Engineering*, vol. 2, no. BME-24, pp. 134–139, 1977.

[75] Podrug, E. and Subasi, A.: Surface emg pattern recognition by using dwt feature extraction and svm classifier. In: *The 1st Conference of Medical and Biological Engineering in Bosnia and Herzegovina (CMBEBIH 2015), 13-15 March 2015*. 2015.

[76] Viljoen, S., Hanekom, T. and Farina, D.: Effect of characteristics of dynamic muscle contraction on crosstalk in surface electromyography recordings. *S. Afr. Inst. Electr. Eng*, vol. 98, pp. 18–28, 2007.

[77] Weir, R.F., Troyk, P., DeMichele, G. and Kerns, D.: Technical details of the implantable myoelectric sensor (imes) system for multifunction prosthesis control. In: *2005 IEEE Engineering in Medicine and Biology 27th Annual Conference*, pp. 7337–7340. IEEE, 2006.

[78] Leowinata, S., Hudgins, B. and Parker, P.: A pattern based continuous multifunction myoelectric control strategy. In: *[Engineering in Medicine and Biology, 1999. 21st Annual Conference and the 1999 Annual Fall Meetring of the Biomedical Engineering Society] BMES/EMBS Conference, 1999. Proceedings of the First Joint*, vol. 1, pp. 568–vol. IEEE, 1999.

[79] Benatti, S., Milosevic, B., Casamassima, F., Schonle, P., Bunjaku, P., Fateh, S., Huang, Q. and Benini, L.: Emg-based hand gesture recognition with flexible analog front end. In: *Biomedical Circuits and Systems Conference (BioCAS), 2014 IEEE*, pp. 57–60. IEEE, 2014.

[80] Merletti, R., Aventaggiato, M., Botter, A., Holobar, A., Marateb, H. and Vieira, T.M.: Advances in surface emg: recent progress in detection and processing techniques. *Critical ReviewsâĎć in Biomedical Engineering*, vol. 38, no. 4, 2010.

[81] Jamal, M.Z.: *Signal acquisition using surface EMG and circuit design considerations for robotic prosthesis*. INTECH Open Access Publisher, 2012.

[82] Day, S.: Important factors in surface emg measurement. *Bortec Biomedical Ltd publishers*, pp. 1–17, 2002.

[83] Hermens, H.J., Freriks, B., Disselhorst-Klug, C. and Rau, G.: Development of recommendations for semg sensors and sensor placement procedures. *Journal of electromyography and Kinesiology*, vol. 10, no. 5, pp. 361–374, 2000.

[84] Konrad, P.: The abc of emg. *A practical introduction to kinesiological electromyography*, vol. 1, pp. 30–35, 2005.

[85] De Luca, C.J.: Surface electromyography: Detection and recording. *DelSys Incorporated*, vol. 10, p. 2011, 2002.

[86] Han, J.-S., Bang, W.-C. and Bien, Z.Z.: Feature set extraction algorithm based on soft computing techniques and its application to emg pattern classification. *Fuzzy Optimization and Decision Making*, vol. 1, no. 3, pp. 269–286, 2002.

[87] Bien, Z., Chung, M.-J., Chang, P.-H., Kwon, D.-S., Kim, D.-J., Han, J.-S., Kim, J.-H., Kim, D.-H., Park, H.-S., Kang, S.-H. *et al.*: Integration of a rehabilitation robotic system (kares ii) with human-friendly man-machine interaction units. *Autonomous robots*, vol. 16, no. 2, pp. 165–191, 2004.

[88] Wojtczak, P., Amaral, T.G., Dias, O.P., Wolczowski, A. and Kurzynski, M.: Hand movement recognition based on biosignal analysis. *Engineering Applications of Artificial Intelligence*, vol. 22, no. 4, pp. 608–615, 2009.

[89] Hermens, H.J., Freriks, B., Merletti, R., Stegeman, D., Blok, J., Rau, G., Disselhorst-Klug, C. and Hägg, G.: European recommendations for surface electromyography. *Roessingh Research and Development*, vol. 8, no. 2, pp. 13–54, 1999.

[90] Jenkins, N.D., Housh, T.J., Bergstrom, H.C., Cochrane, K.C., Hill, E.C., Smith, C.M., Johnson, G.O., Schmidt, R.J. and Cramer, J.T.: Basic reporting and interpretation of surface emg amplitude and mean power frequency: a reply to vitgotsky, ogborn, and phillips. *European journal of applied physiology*, vol. 116, no. 3, pp. 659–661, 2016.

[91] Firoozabadi, S.M.P., Oskoei, M.A. and Hu, H.: A human-computer interface based on forehead multi-channel bio-signals to control a virtual wheelchair. In: *Proceedings of the 14th Iranian conference on biomedical engineering (ICBME)*, pp. 272–277. 2008.

[92] Kim, K.-H., Kim, H.K., Kim, J.-S., Son, W. and Lee, S.-Y.: A biosignal-based human interface controlling a power-wheelchair for people with motor disabilities. *ETRI journal*, vol. 28, no. 1, pp. 111–114, 2006.

[93] Song, J.-H., Jung, J.-W., Lee, S.-W. and Bien, Z.: Robust emg pattern recognition to muscular fatigue effect for powered wheelchair control. *Journal of Intelligent & Fuzzy Systems*, vol. 20, no. 1, 2, pp. 3–12, 2009.

[94] Merletti, R., Afsharipour, B. and Piervirgili, G.: High density surface emg technology. In: *Converging Clinical and Engineering Research on Neurorehabilitation*, pp. 1205–1209. Springer, 2013.

[95] Chan, F.H., Yang, Y.-S., Lam, F., Zhang, Y.-T. and Parker, P.A.: Fuzzy emg classification for prosthesis control. *IEEE transactions on rehabilitation engineering*, vol. 8, no. 3, pp. 305–311, 2000.

[96] Li, Y., Chen, X., Zhang, X. and Zhou, P.: Several practical issues toward implementing myoelectric pattern recognition for stroke rehabilitation. *Medical engineering & physics*, vol. 36, no. 6, pp. 754–760, 2014.

[97] Kale, S.N. and Dudul, S.V.: Intelligent noise removal from emg signal using focused time-lagged recurrent neural network. *Applied Computational Intelligence and Soft Computing*, vol. 2009, p. 1, 2009.

[98] De Luca, C.J., Gilmore, L.D., Kuznetsov, M. and Roy, S.H.: Filtering the surface emg signal: Movement artifact and baseline noise contamination. *Journal of biomechanics*, vol. 43, no. 8, pp. 1573–1579, 2010.

[99] Clancy, E., Morin, E.L. and Merletti, R.: Sampling, noise-reduction and amplitude estimation issues in surface electromyography. *Journal of Electromyography and Kinesiology*, vol. 12, no. 1, pp. 1–16, 2002.

[100] Mewett, D.T., Nazeran, H. and Reynolds, K.J.: Removing power line noise from recorded emg. In: *Engineering in Medicine and Biology Society, 2001. Proceedings of the 23rd Annual International Conference of the IEEE*, vol. 3, pp. 2190–2193. IEEE, 2001.

[101] De Luca, G.: Fundamental concepts in emg signal acquisition. *Copyright Delsys Inc*, 2003.

[102] Barreto, A.B., Scargle, S.D. and Adjouadi, M.: A practical emg-based human-computer interface for users with motor disabilities. *Journal of rehabilitation research and development*, vol. 37, no. 1, p. 53, 2000.

[103] Ijspeert, A.J. and Crespi, A.: Online trajectory generation in an amphibious snake robot using a lamprey-like central pattern generator model. In: *Proceedings 2007 IEEE International Conference on Robotics and Automation*, pp. 262–268. IEEE, 2007.

[104] Hu, T., Shen, L., Lin, L. and Xu, H.: Biological inspirations, kinematics modeling, mechanism design and experiments on an undulating robotic fin inspired by gymnarchus niloticus. *Mechanism and machine theory*, vol. 44, no. 3, pp. 633–645, 2009.

[105] Scott, R.N.: Myoelectric control of prostheses and orthoses. *Bulletin of prosthetics research*, vol. 7, p. 93, 1967.

[106] Parker, P.A. and Scott, R.N.: Myoelectric control of prostheses. *Critical reviews in biomedical engineering*, vol. 13, no. 4, pp. 283–310, 1986.

[107] Hudgins, B., Parker, P. and Scott, R.N.: A new strategy for multifunction myoelectric control. *IEEE Transactions on Biomedical Engineering*, vol. 40, no. 1, pp. 82–94, 1993.

[108] Nishikawa, D., Yu, W., Yokoi, H. and Kakazu, Y.: Emg prosthetic hand controller using real-time learning method. In: *Systems, Man, and Cybernetics, 1999. IEEE SMC'99 Conference Proceedings. 1999 IEEE International Conference on*, vol. 1, pp. 153–158. IEEE, 1999.

[109] Ajiboye, A.B. and Weir, R.F.: A heuristic fuzzy logic approach to emg pattern recognition for multifunctional prosthesis control. *IEEE Transactions on Neural Systems and Rehabilitation Engineering*, vol. 13, no. 3, pp. 280–291, 2005.

[110] Richard, P., Gander, R., Parker, P. and Scott, R.: Multistate myoelectric control: the feasibility of 5-state control. *Journal of rehabilitation R&D/Veterans Administration, Department of Medicine and Surgery, Rehabilitation R&D Service*, vol. 20, no. 1, pp. 84–86, 1983.

[111] Petrou, M.: Learning in pattern recognition. *Lecture notes in computer science*, pp. 1–12, 1999.

[112] Li, G.: *Electromyography pattern-recognition-based control of powered multifunctional upper-limb prostheses*. INTECH Open Access Publisher, 2011.

[113] Liu, Y.-H., Huang, H.-P. and Weng, C.-H.: Recognition of electromyographic signals using cascaded kernel learning machine. *IEEE/ASME Transactions on Mechatronics*, vol. 12, no. 3, pp. 253–264, 2007.

[114] Kuiken, T.A., Barlow, A.K., Hargrove, L.J. and Dumanian, G.A.: Targeted muscle reinnervation for the upper and lower extremity. *Techniques in Orthopaedics*, vol. 32, no. 2, pp. 109–116, 2017.

[115] Tkach, D.C., Young, A.J., Smith, L.H., Rouse, E.J. and Hargrove, L.J.: Real-time and offline performance of pattern recognition myoelectric control using a generic electrode grid with targeted muscle reinnervation patients. *IEEE Transactions on Neural Systems and Rehabilitation Engineering*, vol. 22, no. 4, pp. 727–734, 2014.

[116] Sup, F., Varol, H.A., Mitchell, J., Withrow, T.J. and Goldfarb, M.: Self-contained powered knee and ankle prosthesis: Initial evaluation on a transfemoral amputee. In: *2009 IEEE International Conference on Rehabilitation Robotics*, pp. 638–644. IEEE, 2009.

[117] Kapti, A.O. and Yucenur, M.S.: Design and control of an active artificial knee joint. *Mechanism and machine theory*, vol. 41, no. 12, pp. 1477–1485, 2006.

[118] Murphy, K.P.: *Machine learning: a probabilistic perspective*. MIT press, 2012.

[119] Williams III, T.W.: Progress on stabilizing and controlling powered upper-limb prostheses. *Journal of Rehabilitation Research & Development*, vol. 48, no. 6, pp. ix–ix, 2011.

[120] Hua, C.-C., Yang, Y. and Guan, X.: Neural network-based adaptive position tracking control for bilateral teleoperation under constant time delay. *Neurocomputing*, vol. 113, pp. 204–212, 2013.

[121] Chalhoub, N., Kfoury, G. and Bazzi, B.: Design of robust controllers and a nonlinear observer for the control of a single-link flexible robotic manipulator. *Journal of sound and vibration*, vol. 291, no. 1, pp. 437–461, 2006.

[122] Miao, Z., Wang, Y. and Yang, Y.: Robust tracking control of uncertain dynamic nonholonomic systems using recurrent neural networks. *Neurocomputing*, vol. 142, pp. 216–227, 2014.

[123] Pilarski, P.M., Dawson, M.R., Degris, T., Carey, J.P., Chan, K.M., Hebert, J.S. and Sutton, R.S.: Adaptive artificial limbs: A real-time approach to prediction and anticipation. *IEEE Robotics & Automation Magazine*, vol. 20, no. 1, pp. 53–64, 2013.

[124] Degris, T., Pilarski, P.M. and Sutton, R.S.: Model-free reinforcement learning with continuous action in practice. In: *2012 American Control Conference (ACC)*, pp. 2177–2182. IEEE, 2012.

[125] Lu, K., Wang, Q., Xue, J. and Pan, W.: 3d model retrieval and classification by semi-supervised learning with content-based similarity. *Information Sciences*, vol. 281, pp. 703–713, 2014.

[126] Elsafi, S.H.: Artificial neural networks (anns) for flood forecasting at dongola station in the river nile, sudan. *Alexandria Engineering Journal*, vol. 53, no. 3, pp. 655–662, 2014.

[127] Schleif, F.-M., Biehl, M. and Vellido, A.: Advances in machine learning and computational intelligence. *Neurocomputing*, vol. 72, no. 7, pp. 1377–1378, 2009.

[128] Ardestani, M.M., Chen, Z., Wang, L., Lian, Q., Liu, Y., He, J., Li, D. and Jin, Z.: Feed forward artificial neural network to predict contact force at medial knee joint: Application to gait modification. *Neurocomputing*, vol. 139, pp. 114–129, 2014.

[129] Prieto, A., Atencia, M. and Sandoval, F.: Advances in artificial neural networks and machine learning. *Neurocomputing*, vol. 121, pp. 1–4, 2013.

[130] Haykin, S.S., Haykin, S.S., Haykin, S.S. and Haykin, S.S.: *Neural networks and learning machines*, vol. 3. Pearson Upper Saddle River, NJ, USA:, 2009.

[131] Morita, S., Kondo, T. and Ito, K.: Estimation of forearm movement from emg signal and application to prosthetic hand control. In: *Robotics and Automation, 2001. Proceedings 2001 ICRA. IEEE International Conference on*, vol. 4, pp. 3692–3697. IEEE, 2001.

[132] Garikayi, T., Van den Heever, D. and Matope, S.: Analysis of surface electromyography signal features on osteomyoplastic transtibial amputees for pattern recognition control architectures. *Biomedical Signal Processing and Control*, vol. 40, pp. 10–22, 2018.

[133] Leung, W., Siebert, E.A. and Yun, J.: Measuring physical activity with accelerometers for individuals with intellectual disability: A systematic review. *Research in Developmental Disabilities*, vol. 67, pp. 60–70, 2017.

[134] Lipperts, M., van Laarhoven, S., Senden, R., Heyligers, I. and Grimm, B.: Clinical validation of a body-fixed 3d accelerometer and algorithm for activity monitoring in orthopaedic patients. *Journal of Orthopaedic Translation*, vol. 11, pp. 19–29, 2017.

[135] Godfrey, A., Del Din, S., Barry, G., Mathers, J. and Rochester, L.: Instrumenting gait with an accelerometer: A system and algorithm examination. *Medical engineering & physics*, vol. 37, no. 4, pp. 400–407, 2015.

[136] Nyan, M., Tay, F., Seah, K. and Sitoh, Y.: Classification of gait patterns in the time–frequency domain. *Journal of biomechanics*, vol. 39, no. 14, pp. 2647–2656, 2006.

[137] Sasaki, J.E., da Silva, K.S., da Costa, B.G.G. and John, D.: Measurement of physical activity using accelerometers. *Computer-assisted and web-based innovations in psychology, special education, and health. New York: Elsevier Inc*, pp. 33–60, 2016.

[138] Washabaugh, E.P., Kalyanaraman, T., Adamczyk, P.G., Claflin, E.S. and Krishnan, C.: Validity and repeatability of inertial measurement units for measuring gait parameters. *Gait & Posture*, vol. 55, pp. 87–93, 2017.

[139] Leardini, A., OâĂŹConnor, J.J. and Giannini, S.: Biomechanics of the natural, arthritic, and replaced human ankle joint. *Journal of foot and ankle research*, vol. 7, no. 1, p. 1, 2014.

[140] Wismans, J., Veldpaus, F., Janssen, J., Huson, A. and Struben, P.: A three-dimensional mathematical model of the knee-joint. *Journal of Biomechanics*, vol. 13, no. 8, pp. 677–685, 1980.

[141] Debski, R., Wong, E., Woo, S.L., Fu, F. and Warner, J.: An analytical approach to determine the in situ forces in the glenohumeral ligaments. *Journal of biomechanical engineering*, vol. 121, no. 3, pp. 311–315, 1999.

[142] Dettwyler, M., Stacoff, A., Kramers-de Quervain, I.A. and Stüssi, E.: Modelling of the ankle joint complex. reflections with regards to ankle prostheses. *Foot and ankle Surgery*, vol. 10, no. 3, pp. 109–119, 2004.

[143] Su, F.-C., Wu, W. and Wang, T.: Repeatability of kinematic data of the foot and ankle in gait. *BIOMEDICAL ENGINEERING APPLICATIONS BASIS COMMUNICATIONS*, vol. 12, no. 2, pp. 81–88, 2000.

[144] Allinger, T.L. and Engsberg, J.R.: A method to determine the range of motion of the ankle joint complex, in vivo. *Journal of biomechanics*, vol. 26, no. 1, pp. 69–76, 1993.

[145] Kepple, T., Stanhope, S., Lohmann, K. and Roman, N.: A video-based technique for measuring ankleâĂŤsubtalar motion during stance. *Journal of biomedical engineering*, vol. 12, no. 4, pp. 273–280, 1990.

[146] Kidder, S.M., Abuzzahab, F.S., Harris, G.F. and Johnson, J.E.: A system for the analysis of foot and ankle kinematics during gait. *IEEE Transactions on Rehabilitation Engineering*, vol. 4, no. 1, pp. 25–32, 1996.

[147] Hansen, A. and Starker, F.: Prosthetic foot principles and their influence on gait. *Handbook of Human Motion*, pp. 1–15, 2017.

[148] Giacomozzi, C. and Stebbins, J.A.: Anatomical masking of pressure footprints based on the oxford foot model: validation and clinical relevance. *Gait & Posture*, vol. 53, pp. 131–138, 2017.

[149] Tulchin, K., Orendurff, M., Adolfsen, S. and Karol, L.: The effects of walking speed on multisegment foot kinematics in adults. *Journal of applied biomechanics*, vol. 25, no. 4, p. 377, 2009.

[150] Kadaba, M.P., Ramakrishnan, H. and Wootten, M.: Measurement of lower extremity kinematics during level walking. *Journal of orthopaedic research*, vol. 8, no. 3, pp. 383–392, 1990.

[151] Davis, M., Ettinger, W., Neuhaus, J. and Mallon, K.: Knee osteoarthritis and physical functioning: evidence from the nhanes i epidemiologic followup study. *The Journal of rheumatology*, vol. 18, no. 4, pp. 591–598, 1991.

[152] Tuijthof, G.J.M., Zengerink, M., Beimers, L., Jonges, R., Maas, M., van Dijk, C.N. and Blankevoort, L.: Determination of consistent patterns of range of motion in the ankle joint with a computed tomography stress-test. *Clinical Biomechanics*, vol. 24, no. 6, pp. 517–523, 2009.

[153] Lundgren, P., Nester, C., Liu, A., Arndt, A., Jones, R., Stacoff, A., Wolf, P. and Lundberg, A.: Invasive in vivo measurement of rear-, mid-and forefoot motion during walking. *Gait & posture*, vol. 28, no. 1, pp. 93–100, 2008.

[154] Okita, N., Meyers, S.A., Challis, J.H. and Sharkey, N.A.: An objective evaluation of a segmented foot model. *Gait & posture*, vol. 30, no. 1, pp. 27–34, 2009.

[155] Procter, P. and Paul, J.: Ankle joint biomechanics. *Journal of biomechanics*, vol. 15, no. 9, pp. 627–634, 1982.

[156] Dul, J. and Johnson, G.: A kinematic model of the human ankle. *Journal of biomedical engineering*, vol. 7, no. 2, pp. 137–143, 1985.

[157] Scott, S.H. and Winter, D.A.: Talocrural and talocalcaneal joint kinematics and kinetics during the stance phase of walking. *Journal of biomechanics*, vol. 24, no. 8, pp. 743–752, 1991.

[158] Hicks, J.: The mechanics of the foot: I. the joints. *Journal of Anatomy*, vol. 87, no. Pt 4, p. 345, 1953.

[159] Wright, D.G., Desai, S.M. and Henderson, W.H.: Action of the subtalar and ankle-joint complex during the stance phase of walking. *J Bone Joint Surg Am*, vol. 46, no. 2, pp. 361–464, 1964.

[160] Isman, R.E., Inman, V.T. and Poor, P.: Anthropometric studies of the human foot and ankle. *Bull Prosthet Res*, vol. 11, pp. 97–108, 1969.

[161] Langelann, E.v.: Relative talotibial movements and relative tarsal movements. *A Kinematical Analysis of the Tarsal Joints*, pp. 135–265, 1983.

[162] Engsberg, J.R.: A biomechanical analysis of the talocalcaneal jointâĂŤin vitro. *Journal of biomechanics*, vol. 20, no. 4, pp. 429–442, 1987.

[163] Siegler, S., Chen, J. and Schneck, C.: The three-dimensional kinematics and flexibility characteristics of the human ankle and subtalar jointsâĂŤpart i: Kinematics. *Journal of biomechanical engineering*, vol. 110, no. 4, pp. 364–373, 1988.

[164] Leardini, A., Belvedere, C., Nardini, F., Sancisi, N., Conconi, M. and Parenti-Castelli, V.: Kinematic models of lower limb joints for musculo-skeletal modelling and optimization in gait analysis. *Journal of Biomechanics*, 2017.

[165] Wei, J., Meng, Q. and Badii, A.: Classification of human hand movements using surface emg for myoelectric control. In: *Advances in Computational Intelligence Systems*, pp. 331–339. Springer, 2017.

[166] Chandrasekharan, P.: *Robust control of linear dynamical systems*. Academic Press, 1996.

[167] Becker, K. and Voss, S.: Analyzing graceful degradation for mixed critical fault-tolerant real-time systems. In: *2015 IEEE 18th International Symposium on Real-Time Distributed Computing*, pp. 110–118. IEEE, 2015.

[168] Lee, P.A. and Anderson, T.: *Fault tolerance: principles and practice*, vol. 3. Springer Science & Business Media, 2012.

[169] Kyberd, P.J. and Chappell, P.H.: The southampton hand: an intelligent myoelectric prosthesis. *Journal of rehabilitation research and development*, vol. 31, no. 4, p. 326, 1994.

[170] Herr, H. and Wilkenfeld, A.: User-adaptive control of a magnetorheological prosthetic knee. *Industrial Robot: An International Journal*, vol. 30, no. 1, pp. 42–55, 2003.

[171] Ferris, D.P., Gordon, K.E., Sawicki, G.S. and Peethambaran, A.: An improved powered ankle–foot orthosis using proportional myoelectric control. *Gait & posture*, vol. 23, no. 4, pp. 425–428, 2006.

[172] Edwards, A.L., Dawson, M.R., Hebert, J.S., Sutton, R.S., Chan, K.M. and Pilarski, P.M.: Adaptive switching in practice: Improving myoelectric prosthesis performance through reinforcement learning. In: *Proc. of the Myoelectric Controls Symposium (MECâĂŹ14), Fredericton, New Brunswick*, pp. 69–73. Citeseer, 2014.

[173] Oskoei, M.A. and Hu, H.: Adaptive myoelectric control applied to video game. *Biomedical Signal Processing and Control*, vol. 18, pp. 153–160, 2015.

[174] Fariman, H.J., Ahmad, S.A., Marhaban, M.H., Ghasab, M.A. and Chappell, P.H.: Hand movements classification for myoelectric control system using adaptive resonance theory. *Australasian Physical & Engineering Sciences in Medicine*, vol. 39, no. 1, pp. 85–102, 2016.

[175] Rifaỳ, H., Abdessalem, M.B., Chemori, A., Mohammed, S. and Amirat, Y.: Augmented- 1 adaptive control of an actuated knee joint exoskeleton: From design to real-time experiments. In: *Robotics and Automation (ICRA), 2016 IEEE International Conference on*, pp. 5708–5714. IEEE, 2016.

[176] Prahm, C., Vujaklija, I., Kayali, F., Purgathofer, P. and Aszmann, O.C.: Game-based rehabilitation for myoelectric prosthesis control. *JMIR serious games*, vol. 5, no. 1, 2017.

[177] Koller, J.R., Jacobs, D.A., Ferris, D.P. and Remy, C.D.: Learning to walk with an adaptive gain proportional myoelectric controller for a robotic ankle exoskeleton. *Journal of neuroengineering and rehabilitation*, vol. 12, no. 1, p. 1, 2015.

[178] Sanz, R., Garcia, P., Albertos, P. and Zhong, Q.-C.: Robust controller design for input-delayed systems using predictive feedback and an uncertainty estimator. *International Journal of Robust and Nonlinear Control*, vol. 27, no. 10, pp. 1826–1840, 2017.

[179] Bryman, A. *et al.*: *Quantity and quality in social research*. Routledge, 2003.

[180] Stegeman, D. and Hermens, H.: Standards for surface electromyography: The european project surface emg for non-invasive assessment of muscles (seniam). *Enschede: Roessingh Research and Development*, pp. 108–12, 2007.

[181] Jänsch, J. and Birkhofer, H.: The development of the guideline vdi 2221-the change of direction. In: *DS 36: Proceedings DESIGN 2006, the 9th International Design Conference, Dubrovnik, Croatia*. 2006.

[182] Hiltmann, K., Thurnes, C., Adunka, R., Mayer, O., Koltze, K., Livotov, P. and Müller, W.: Vdi standard 4521: Status. 2015.

[183] Rivera, C.A., Poza, J., Ugalde, G. and Almandoz, G.: A knowledge based system architecture to manage and automate the electrical machine design process. In: *Electronics, Control, Measurement, Signals and their Application to Mechatronics (ECMSM), 2017 IEEE International Workshop of*, pp. 1–6. IEEE, 2017.

[184] Roozenburg, N.F. and Eekels, J.: *Product design: fundamentals and methods*, vol. 2. Wiley Chichester, 1995.

[185] Khushaba, R.N., Al-Ani, A. and Al-Jumaily, A.: Orthogonal fuzzy neighborhood discriminant analysis for multifunction myoelectric hand control. *IEEE Transactions on Biomedical Engineering*, vol. 57, no. 6, pp. 1410–1419, 2010.

[186] Isakov, E., Keren, O. and Benjuya, N.: TransîŞÿ tibial amputee gait: TimeîŞÿ distance parameters and emg activity. *Prosthetics and Orthotics International*, vol. 24, no. 3, pp. 216–220, 2000.

[187] Huang, H., Kuiken, T.A., Lipschutz, R.D. *et al.*: A strategy for identifying locomotion modes using surface electromyography. *IEEE Transactions on Biomedical Engineering*, vol. 56, no. 1, pp. 65–73, 2009.

[188] Preston, D.C. and Shapiro, B.E.: *Electromyography and Neuromuscular Disorders E-Book: Clinical-Electrophysiologic Correlations (Expert Consult-Online)*. Elsevier Health Sciences, 2012.

[189] Ashton, C., Junckerstorff, R., Bundell, C., Hollingsworth, P. and Needham, M.: Treatment and outcomes in necrotising autoimmune myopathy: an australian perspective. *Neuromuscular Disorders*, vol. 26, no. 11, pp. 734–740, 2016.

[190] Soderberg, G.L. and Knutson, L.M.: A guide for use and interpretation of kinesiologic electromyographic data. *Physical therapy*, vol. 80, no. 5, pp. 485–498, 2000.

[191] Christensen, A., Piper, A. and Jensen, D.: Emg and posture patterns in manual dc fulfillment. In: *IIE Annual Conference. Proceedings*, p. 2664. Institute of Industrial and Systems Engineers (IISE), 2015.

[192] Taylor, W., Kornaropoulos, E., Duda, G., Kratzenstein, S., Ehrig, R., Arampatzis, A. and Heller, M.: Repeatability and reproducibility of ossca, a functional approach for assessing the kinematics of the lower limb. *Gait & posture*, vol. 32, no. 2, pp. 231–236, 2010.

[193] Bateni, H. and Olney, S.J.: Kinematic and kinetic variations of below-knee amputee gait. *JPO: Journal of Prosthetics and Orthotics*, vol. 14, no. 1, pp. 2–10, 2002.

[194] Mokhlesabadifarahani, B. and Gunjan, V.K.: Methodology for working with emg dataset. In: *EMG Signals Characterization in Three States of Contraction by Fuzzy Network and Feature Extraction*, pp. 11–20. Springer, 2015.

[195] Bélaise, C., Dal Maso, F., Michaud, B., Mombaur, K. and Begon, M.: An emg-marker tracking optimisation method for estimating muscle forces. *Multibody System Dynamics*, pp. 1–25, 2017.

[196] Bornato, P., de Alessio, T. and Knaflitz, M.: A statistical method for the measurement of the muscle activation intervals from surface myoelectric signal gait. *IEEE Trans Biomed Eng*, vol. 45, pp. 287–299, 1998.

[197] Rainoldi, A., Melchiorri, G. and Caruso, I.: A method for positioning electrodes during surface emg recordings in lower limb muscles. *Journal of neuroscience methods*, vol. 134, no. 1, pp. 37–43, 2004.

[198] Mesin, L., Merletti, R. and Rainoldi, A.: Surface emg: the issue of electrode location. *Journal of Electromyography and Kinesiology*, vol. 19, no. 5, pp. 719–726, 2009.

[199] Camomilla, V., Cereatti, A., Cutti, A.G., Fantozzi, S., Stagni, R. and Vannozzi, G.: Methodological factors affecting joint moments estimation in clinical gait analysis: a systematic review. *Biomedical engineering online*, vol. 16, no. 1, p. 106, 2017.

[200] Ferrari, A., Benedetti, M.G., Pavan, E., Frigo, C., Bettinelli, D., Rabuffetti, M., Crenna, P. and Leardini, A.: Quantitative comparison of five current protocols in gait analysis. *Gait & posture*, vol. 28, no. 2, pp. 207–216, 2008.

[201] Miall, R.C. and Wolpert, D.M.: Forward models for physiological motor control. *Neural networks*, vol. 9, no. 8, pp. 1265–1279, 1996.

[202] Cleland, I., Kikhia, B., Nugent, C., Boytsov, A., Hallberg, J., Synnes, K., McClean, S. and Finlay, D.: Optimal placement of accelerometers for the detection of everyday activities. *Sensors*, vol. 13, no. 7, pp. 9183–9200, 2013.

[203] Blain, G.C.: Revisiting the critical values of the lilliefors test: towards the correct agrometeorological use of the kolmogorov-smirnov framework. *Bragantia*, vol. 73, no. 2, pp. 192–202, 2014.

[204] Dutta, A., Paulus, W. and Nitsche, M.A.: Facilitating myoelectric-control with transcranial direct current stimulation: a preliminary study in healthy humans. *Journal of neuroengineering and rehabilitation*, vol. 11, no. 1, p. 13, 2014.

[205] Liu, J., Ying, D. and Rymer, W.Z.: Emg burst presence probability: A joint time–frequency representation of muscle activity and its application to onset detection. *Journal of biomechanics*, vol. 48, no. 6, pp. 1193–1197, 2015.

[206] Soylu, A.R. and Arpinar-Avsar, P.: Detection of surface electromyography recording time interval without muscle fatigue effect for biceps brachii muscle during maximum voluntary contraction. *Journal of Electromyography and Kinesiology*, vol. 20, no. 4, pp. 773–776, 2010.

[207] Pohlert, T.: The pairwise multiple comparison of mean ranks package (pmcmr). *R package*, pp. 2004–2006, 2014.

[208] Armstrong, R.A.: When to use the bonferroni correction. *Ophthalmic and Physiological Optics*, vol. 34, no. 5, pp. 502–508, 2014.

[209] Phinyomark, A., Limsakul, C. and Phukpattaranont, P.: A novel feature extraction for robust emg pattern recognition. *arXiv preprint arXiv:0912.3973*, 2009.

[210] Goldberg, S.R., Anderson, F.C., Pandy, M.G. and Delp, S.L.: Muscles that influence knee flexion velocity in double support: implications for stiff-knee gait. *Journal of biomechanics*, vol. 37, no. 8, pp. 1189–1196, 2004.

[211] Mercer, J., Bezodis, N., DeLion, D., Zachry, T. and Rubley, M.: Emg sensor location: Does it influence the ability to detect differences in muscle contraction conditions? *Journal of Electromyography and Kinesiology*, vol. 16, no. 2, pp. 198–204, 2006.

[212] Farina, D., Merletti, R. and Enoka, R.M.: The extraction of neural strategies from the surface emg. *Journal of Applied Physiology*, vol. 96, no. 4, pp. 1486–1495, 2004.

[213] Merletti, R. and Farina, D.: Myoelectric manifestations of muscle fatigue. *Wiley Encyclopedia of Biomedical Engineering*, 2006.

[214] De Luca, C.J.: Physiology and mathematics of myoelectric signals. *IEEE Transactions on Biomedical Engineering*, , no. 6, pp. 313–325, 1979.

[215] Thongpanja, S., Phinyomark, A., Phukpattaranont, P. and Limsakul, C.: Mean and median frequency of emg signal to determine muscle force based on time-dependent power spectrum. *Elektronika ir Elektrotechnika*, vol. 19, no. 3, pp. 51–56, 2013.

[216] Shao, Y.H., Zhou, Y.S., Zhang, Y., Gu, Y.D., Fekete, G. and Fernandez, J.: Surface emg based muscle fatigue evaluation on neck-shoulder muscles while using single-monitor arm. In: *Journal of Biomimetics, Biomaterials and Biomedical Engineering*, vol. 29, pp. 61–67. Trans Tech Publ, 2016.

[217] He, J., Zhang, D., Jiang, N., Sheng, X., Farina, D. and Zhu, X.: User adaptation in long-term, open-loop myoelectric training: implications for emg pattern recognition in prosthesis control. *Journal of neural engineering*, vol. 12, no. 4, p. 046005, 2015.

[218] Zardoshti-Kermani, M., Wheeler, B.C., Badie, K. and Hashemi, R.M.: Emg feature evaluation for movement control of upper extremity prostheses. *IEEE Transactions on Rehabilitation Engineering*, vol. 3, no. 4, pp. 324–333, 1995.

[219] Boostani, R. and Moradi, M.H.: Evaluation of the forearm emg signal features for the control of a prosthetic hand. *Physiological measurement*, vol. 24, no. 2, p. 309, 2003.

[220] Phinyomark, A., Phukpattaranont, P. and Limsakul, C.: Feature reduction and selection for emg signal classification. *Expert Systems with Applications*, vol. 39, no. 8, pp. 7420–7431, 2012.

[221] Zaheer, F., Roy, S.H. and De Luca, C.J.: Preferred sensor sites for surface emg signal decomposition. *Physiological measurement*, vol. 33, no. 2, p. 195, 2012.

[222] Dudley-Javoroski, S. and Shields, R.K.: Muscle and bone plasticity after spinal cord injury: review of adaptations to disuse and to electrical muscle stimulation. *Journal of rehabilitation research and development*, vol. 45, no. 2, p. 283, 2008.

[223] Mai, A., Commuri, S., Dionne, C.P., Day, J., Ertl, W.J. and Regens, J.L.: Effect of prosthetic foot on residuum-socket interface pressure and gait characteristics in an otherwise healthy man with transtibial osteomyoplastic amputation. *JPO: Journal of Prosthetics and Orthotics*, vol. 24, no. 4, pp. 211–220, 2012.

[224] Ferris, A.E.: *Biomechanical assessment of Ertl and Burgess transtibial amputation techniques*. University of Northern Colorado, 2015.

[225] Taylor, B.C. and Poka, A.: Osteomyoplastic transtibial amputation: technique and tips. *Journal of orthopaedic surgery and research*, vol. 6, no. 1, p. 13, 2011.

[226] Dionne, C.P., Ertl, W.J. and Day, J.D.: Rehabilitation for those with transtibial osteomyoplastic amputation. *JPO: Journal of Prosthetics and Orthotics*, vol. 21, no. 1, pp. 64–70, 2009.

[227] Czerniecki, J.M., Turner, A.P., Williams, R.M., Thompson, M.L., Landry, G., Hakimi, K., Speckman, R. and Norvell, D.C.: The development and validation of the ampredict model for predicting mobility outcome after dysvascular lower extremity amputation. *Journal of vascular surgery*, vol. 65, no. 1, pp. 162–171, 2017.

[228] DeCoster, T.A. and Homedan, S.: Amputation osteoplasty. *The Iowa orthopaedic journal*, vol. 26, p. 54, 2006.

[229] Winter, D.A. and Sienko, S.E.: Biomechanics of below-knee amputee gait. *Journal of biomechanics*, vol. 21, no. 5, pp. 361–367, 1988.

[230] Cynn, H.-S., Oh, J.-S., Kwon, O.-Y. and Yi, C.-H.: Effects of lumbar stabilization using a pressure biofeedback unit on muscle activity and lateral pelvic tilt during hip abduction in sidelying. *Archives of physical medicine and rehabilitation*, vol. 87, no. 11, pp. 1454–1458, 2006.

[231] Zelik, K.E. and Adamczyk, P.G.: A unified perspective on ankle push-off in human walking. *Journal of Experimental Biology*, vol. 219, no. 23, pp. 3676–3683, 2016.

[232] Siebenrock, K., Kalbermatten, D. and Ganz, R.: Effect of pelvic tilt on acetabular retroversion: a study of pelves from cadavers. *Clinical orthopaedics and related research*, vol. 407, pp. 241–248, 2003.

[233] Karthikbabu, S., Chakrapani, M., Ganesan, S. and Ellajosyla, R.: Pelvic alignment in standing, and its relationship with trunk control and motor recovery of lower limb after stroke. *Neurology and Clinical Neuroscience*, vol. 5, no. 1, pp. 22–28, 2017.

[234] Eilenberg, M.F., Geyer, H. and Herr, H.: Control of a powered ankle–foot prosthesis based on a neuromuscular model. *IEEE transactions on neural systems and rehabilitation engineering*, vol. 18, no. 2, pp. 164–173, 2010.

[235] Segal, A.D., Orendurff, M.S., Klute, G.K., McDowell, M.L. *et al.*: Kinematic and kinetic comparisons of transfemoral amputee gait using c-leg® and mauch sns® prosthetic knees. *Journal of rehabilitation research and development*, vol. 43, no. 7, p. 857, 2006.

[236] Duval, K., Lam, T. and Sanderson, D.: The mechanical relationship between the rearfoot, pelvis and low-back. *Gait & posture*, vol. 32, no. 4, pp. 637–640, 2010.

[237] Al-Eisa, E., Egan, D., Deluzio, K. and Wassersug, R.: Effects of pelvic asymmetry and low back pain on trunk kinematics during sitting: a comparison with standing. *Spine*, vol. 31, no. 5, pp. E135–E143, 2006.

[238] Masouros, S., Bull, A. and Amis, A.: (i) biomechanics of the knee joint. *Orthopaedics and Trauma*, vol. 24, no. 2, pp. 84–91, 2010.

[239] Brown, B.J., Iorio, M.L., Hill, L., Klement, M., Mica, M.R.C., El-Amraoui, A. and Attinger, C.E.: Ertl below-knee amputation using a vascularized fibular strut in a nontrauma elderly population: a case series. *Annals of plastic surgery*, vol. 73, no. 2, pp. 196–201, 2014.

[240] Leardini, A., O'connor, J., Catani, F. and Giannini, S.: A geometric model of the human ankle joint. *Journal of biomechanics*, vol. 32, no. 6, pp. 585–591, 1999.

[241] Schmalz, T., Blumentritt, S. and Jarasch, R.: Energy expenditure and biomechanical characteristics of lower limb amputee gait:: The influence of prosthetic alignment and different prosthetic components. *Gait & posture*, vol. 16, no. 3, pp. 255–263, 2002.

[242] Klute, G.K., Berge, J.S., Orendurff, M.S., Williams, R.M. and Czerniecki, J.M.: Prosthetic intervention effects on activity of lower-extremity amputees. *Archives of physical medicine and rehabilitation*, vol. 87, no. 5, pp. 717–722, 2006.

[243] Fradet, L., Alimusaj, M., Braatz, F. and Wolf, S.I.: Biomechanical analysis of ramp ambulation of transtibial amputees with an adaptive ankle foot system. *Gait & posture*, vol. 32, no. 2, pp. 191–198, 2010.

[244] Light, C.M., Chappell, P.H. and Kyberd, P.J.: Establishing a standardized clinical assessment tool of pathologic and prosthetic hand function: normative data, reliability, and validity. *Archives of physical medicine and rehabilitation*, vol. 83, no. 6, pp. 776–783, 2002.

[245] Putz, R. and Pabst, R.: *Sobotta-Atlas of Human Anatomy: Head, Neck, Upper Limb, Thorax, Abdomen, Pelvis, Lower Limb; Two-volume set.* 2006.

[246] Young, A., Kuiken, T. and Hargrove, L.: Analysis of using emg and mechanical sensors to enhance intent recognition in powered lower limb prostheses. *Journal of neural engineering*, vol. 11, no. 5, p. 056021, 2014.

[247] Atkins, D.J., Heard, D.C. and Donovan, W.H.: Epidemiologic overview of individuals with upper-limb loss and their reported research priorities. *JPO: Journal of Prosthetics and Orthotics*, vol. 8, no. 1, pp. 2–11, 1996.

[248] James, D.A.: The application of inertial sensors in elite sports monitoring. In: *The Engineering of Sport 6*, pp. 289–294. Springer, 2006.

[249] Sprager, S. and Juric, M.B.: Inertial sensor-based gait recognition: a review. *Sensors*, vol. 15, no. 9, pp. 22089–22127, 2015.

[250] Mayagoitia, R.E., Nene, A.V. and Veltink, P.H.: Accelerometer and rate gyroscope measurement of kinematics: an inexpensive alternative to optical motion analysis systems. *Journal of biomechanics*, vol. 35, no. 4, pp. 537–542, 2002.

[251] Mechael, P., Batavia, H., Kaonga, N., Searle, S., Kwan, A., Goldberger, A., Fu, L., Ossman, J. *et al.*: *Barriers and gaps affecting mHealth in low and middle income countries: Policy white paper.* Columbia university. Earth institute. Center for global health and economic development (CGHED): with mHealth alliance, 2010.

[252] Brezmes, T., Gorricho, J.-L. and Cotrina, J.: Activity recognition from accelerometer data on a mobile phone. In: *International Work-Conference on Artificial Neural Networks*, pp. 796–799. Springer, 2009.

[253] Zheng, H., Black, N.D. and Harris, N.D.: Position-sensing technologies for movement analysis in stroke rehabilitation. *Medical and biological engineering and computing*, vol. 43, no. 4, pp. 413–420, 2005.

[254] Tao, Y. and Hu, H.: Building a visual tracking system for home-based rehabilitation. In: *Proc. of the 9th Chinese Automation and Computing Society Conf. In the UK*, pp. 343–448. 2003.

[255] Prathivadi, Y., Wu, J., Bennett, T.R. and Jafari, R.: Robust activity recognition using wearable imu sensors. In: *SENSORS, 2014 IEEE*, pp. 486–489. IEEE, 2014.

[256] Hou, H.: *Modeling inertial sensors errors using Allan variance.* Library and Archives Canada= Bibliothèque et Archives Canada, 2005.

[257] James, D., Busch, A. and Ohgi, Y.: Quantitative assessment of physical activity using inertial sensors. *Digit. Sport Perform. Enhanc. Compet. Evol*, vol. 122, pp. 122–135, 2009.

[258] Fei, Y., Song, Y., Xu, L. and Sun, G.: Micro-imu based wireless body sensor network. In: *Control Conference (CCC), 2014 33rd Chinese*, pp. 428–432. IEEE, 2014.

[259] Foerster, F. and Fahrenberg, J.: Motion pattern and posture: correctly assessed by calibrated accelerometers. *Behavior research methods, instruments, & computers*, vol. 32, no. 3, pp. 450–457, 2000.

[260] Lee, J. and Ha, I.: Real-time motion capture for a human body using accelerometers. *Robotica*, vol. 19, no. 06, pp. 601–610, 2001.

[261] Clark, W.A. and Geen, J.A.: Offset detection and compensation for micromachined inertial sensors. July 22 2014. US Patent 8,783,103.

[262] Foxlin, E.: Pedestrian tracking with shoe-mounted inertial sensors. *IEEE Computer graphics and applications*, vol. 25, no. 6, pp. 38–46, 2005.

[263] El-Sheimy, N., Hou, H. and Niu, X.: Analysis and modeling of inertial sensors using allan variance. *IEEE Transactions on instrumentation and measurement*, vol. 57, no. 1, pp. 140–149, 2008.

[264] Gay, V. and Leijdekkers, P.: A health monitoring system using smart phones and wearable sensors. *International journal of ARM*, vol. 8, no. 2, pp. 29–35, 2007.

[265] Anguita, D., Ghio, A., Oneto, L., Parra, X. and Reyes-Ortiz, J.L.: A public domain dataset for human activity recognition using smartphones. In: *ESANN*. 2013.

[266] Seel, T., Raisch, J. and Schauer, T.: Imu-based joint angle measurement for gait analysis. *Sensors*, vol. 14, no. 4, pp. 6891–6909, 2014.

[267] Chen, Y., Hu, W., Yang, Y., Hou, J. and Wang, Z.: A method to calibrate installation orientation errors of inertial sensors for gait analysis. In: *Information and Automation (ICIA), 2014 IEEE International Conference on*, pp. 598–603. IEEE, 2014.

[268] Sabatini, A.M.: Estimating three-dimensional orientation of human body parts by inertial/magnetic sensing. *Sensors*, vol. 11, no. 2, pp. 1489–1525, 2011.

[269] Madgwick, S.O., Harrison, A.J. and Vaidyanathan, R.: Estimation of imu and marg orientation using a gradient descent algorithm. In: *Rehabilitation Robotics (ICORR), 2011 IEEE International Conference on*, pp. 1–7. IEEE, 2011.

[270] Nguyen, H.-N., Zhou, J. and Kang, H.-J.: A calibration method for enhancing robot accuracy through integration of an extended kalman filter algorithm and an artificial neural network. *Neurocomputing*, vol. 151, pp. 996–1005, 2015.

[271] Stojanovic, V. and Nedic, N.: Robust kalman filtering for nonlinear multivariable stochastic systems in the presence of non-gaussian noise. *International Journal of Robust and Nonlinear Control*, vol. 26, no. 3, pp. 445–460, 2016.

[272] Li, W., Gong, D., Liu, M., Chen, J. and Duan, D.: Adaptive robust kalman filter for relative navigation using global position system. *IET Radar, Sonar & Navigation*, vol. 7, no. 5, pp. 471–479, 2013.

[273] Groves, P.D.: *Principles of GNSS, inertial, and multisensor integrated navigation systems*. Artech house, 2013.

[274] Roche, A.D., Rehbaum, H., Farina, D. and Aszmann, O.C.: Prosthetic myoelectric control strategies: a clinical perspective. *Current Surgery Reports*, vol. 2, no. 3, p. 44, 2014.

[275] Geng, Y., Samuel, O.W., Wei, Y. and Li, G.: Improving the robustness of real-time myoelectric pattern recognition against arm position changes in transradial amputees. *BioMed research international*, vol. 2017, 2017.

[276] Li, G., Schultz, A.E. and Kuiken, T.A.: Quantifying pattern recognitionâĂŤbased myoelectric control of multifunctional transradial prostheses. *IEEE transactions on neural systems and rehabilitation engineering: a publication of the IEEE Engineering in Medicine and Biology Society*, vol. 18, no. 2, p. 185, 2010.

[277] Thies, S.B., Kenney, L.P., Sobuh, M., Galpin, A., Kyberd, P., Stine, R. and Major, M.J.: Skill assessment in upper limb myoelectric prosthesis users: Validation of a clinically feasible method for characterising upper limb temporal and amplitude variability during the performance of functional tasks. *Medical Engineering & Physics*, vol. 47, pp. 137–143, 2017.

[278] Shehata, A.W., Scheme, E.J. and Sensinger, J.W.: The effect of myoelectric prosthesis control strategies and feedback level on adaptation rate for a target acquisition task. In: *Rehabilitation Robotics (ICORR), 2017 International Conference on*, pp. 200–204. IEEE, 2017.

[279] Yegnanarayana, B. and Sekhar, C.C.: Pattern recognition issues in speech processing. *Pattern Recognition*, vol. 10, p. 9789812386533_0019, 2001.

[280] Hargrove, L., Englehart, K. and Hudgins, B.: The effect of electrode displacements on pattern recognition based myoelectric control. In: *Engineering in Medicine and Biology Society, 2006. EMBS'06. 28th Annual International Conference of the IEEE*, pp. 2203–2206. IEEE, 2006.

[281] Rajesh, V., Reddy, D.K. *et al.*: Semg based human machine interface for controlling wheel chair by using ann. In: *Control, Automation, Communication and Energy Conservation, 2009. INCACEC 2009. 2009 International Conference on*, pp. 1–6. IEEE, 2009.

[282] Ahsan, M.R., Ibrahimy, M.I. and Khalifa, O.O.: Emg motion pattern classification through design and optimization of neural network. In: *Biomedical Engineering (ICoBE), 2012 International Conference on*, pp. 175–179. IEEE, 2012.

[283] Ortiz-Catalan, M., Brånemark, R. and Håkansson, B.: Biopatrec: A modular research platform for the control of artificial limbs based on pattern recognition algorithms. *Source code for biology and medicine*, vol. 8, no. 1, p. 11, 2013.

[284] Pasquina, P.F., Evangelista, M., Carvalho, A.J., Lockhart, J., Griffin, S., Nanos, G., McKay, P., Hansen, M., Ipsen, D., Vandersea, J. *et al.*: First-in-man demonstration of a fully implanted myoelectric sensors system to control an advanced electromechanical prosthetic hand. *Journal of neuroscience methods*, vol. 244, pp. 85–93, 2015.

[285] Piipponen, K.V.T., Sepponen, R. and Eskelinen, P.: A biosignal instrumentation system using capacitive coupling for power and signal isolation. *IEEE Transactions on Biomedical Engineering*, vol. 54, no. 10, pp. 1822–1828, 2007.

[286] Chan, A. and Englehart, K.: Continuous classification of myoelectric signals for powered prostheses using gaussian mixture models. In: *Engineering in Medicine and Biology Society, 2003. Proceedings of the 25th Annual International Conference of the IEEE*, vol. 3, pp. 2841–2844. IEEE, 2003.

[287] Kleene, S.J.: High-gain, low-noise amplification in olfactory transduction. *Biophysical journal*, vol. 73, no. 2, pp. 1110–1117, 1997.

[288] Horng, J.-W.: High-input impedance voltage-mode universal biquadratic filter using three plus-type cciis. *IEEE Transactions on Circuits and Systems II: Analog and Digital Signal Processing*, vol. 48, no. 10, pp. 996–997, 2001.

[289] Hogervorst, R. and Huijsing, J.: *Design of low-voltage, low-power operational amplifier cells*, vol. 374. Springer Science & Business Media, 2013.

[290] Strong, A.M.: Operational amplifier with jfet inputs having low input bias current and methods for using same. July 16 1996. US Patent 5,537,078.

[291] Bruschi, P., Del Cesta, F., Longhitano, A., Piotto, M. and Simmarano, R.: A very compact cmos instrumentation amplifier with nearly rail-to-rail input common mode range. In: *European Solid State Circuits Conference (ESSCIRC), ESSCIRC 2014-40th*, pp. 323–326. IEEE, 2014.

[292] Drung, D., Krause, C., Becker, U., Scherer, H. and Ahlers, F.: Ultrastable low-noise current amplifier: A novel device for measuring small electric currents with high accuracy. *Review of Scientific Instruments*, vol. 86, no. 2, p. 024703, 2015.

[293] Perreault, E., Hunter, I. and Kearney, R.: Quantitative analysis of four emg amplifiers. *Journal of biomedical engineering*, vol. 15, no. 5, pp. 413–419, 1993.

[294] Castellini, C. and van der Smagt, P.: Surface emg in advanced hand prosthetics. *Biological cybernetics*, vol. 100, no. 1, pp. 35–47, 2009.

[295] Tavakoli, M., Benussi, C. and Lourenco, J.L.: Single channel surface emg control of advanced prosthetic hands: A simple, low cost and efficient approach. *Expert Systems with Applications*, vol. 79, pp. 322–332, 2017.

[296] Capaday, C., Forget, R. and Milner, T.: A re-examination of the effects of instruction on the long-latency stretch reflex response of the flexor pollicis longus muscle. *Experimental brain research*, vol. 100, no. 3, pp. 515–521, 1994.

[297] Merrill, D.R., Lockhart, J., Troyk, P.R., Weir, R.F. and Hankin, D.L.: Development of an implantable myoelectric sensor for advanced prosthesis control. *Artificial organs*, vol. 35, no. 3, pp. 249–252, 2011.

[298] Hamza, N., Khriji, L. and Tourki, R.: Interference reduction and common mode rejection in electrocardiograph signal by removing the ground electrode. *Journal of Clinical Engineering*, vol. 42, no. 1, pp. 21–27, 2017.

[299] Malmivuo, J. and Plonsey, R.: *Bioelectromagnetism: principles and applications of bioelectric and biomagnetic fields*. Oxford University Press, USA, 1995.

[300] Baba, A. and Burke, M.: Measurement of the electrical properties of ungelled ecg electrodes. *International journal of biology and biomedical engineering*, vol. 2, no. 3, pp. 89–97, 2008.

[301] Jinhua, N. and Li, D.: Apparatus and methods for improving common mode rejection ratio. February 16 2016. US Patent 9,264,002.

[302] Velez, P., Naqui, J., Fernández-Prieto, A., Duran-Sindreu, M., Bonache, J., Martel, J., Medina, F. and Martin, F.: Differential bandpass filter with common-mode suppression based on open split ring resonators and open complementary split ring resonators. *IEEE Microwave and Wireless Components Letters*, vol. 23, no. 1, pp. 22–24, 2013.

[303] Huijsing, J.: *Operational amplifiers: theory and design*. Springer, 2016.

[304] Wang, J., Tang, L. and Bronlund, J.E.: Surface emg signal amplification and filtering. *International Journal of Computer Applications*, vol. 82, no. 1, 2013.

[305] Potvin, J. and Brown, S.: Less is more: high pass filtering, to remove up to 99% of the surface emg signal power, improves emg-based biceps brachii muscle force estimates. *Journal of Electromyography and Kinesiology*, vol. 14, no. 3, pp. 389–399, 2004.

[306] Devaprakash, D., Weir, G.J., Dunne, J.J., Alderson, J.A. and Donnelly, C.J.: The influence of digital filter type, amplitude normalisation method, and co-contraction algorithm on clinically relevant surface electromyography data during clinical movement assessments. *Journal of Electromyography and Kinesiology*, vol. 31, pp. 126–135, 2016.

[307] de Oliveira, I.H. and Balbinot, A.: Portable electrocardiograph based on the integrated circuit ads1294 using an android application as interface. *Health and Technology*, vol. 5, no. 2, pp. 147–154, 2015.

[308] Pashaei, A., Yazdchi, M.R. and Marateb, H.R.: Designing a low-noise, high-resolution, and portable four channel acquisition system for recording surface electromyographic signal. *Journal of medical signals and sensors*, vol. 5, no. 4, p. 245, 2015.

[309] Piccinini, D., Andino, N., Ponce, S., Roberti, M. *et al.*: Wearable system for acquisition and monitoring of biological signals. In: *Journal of Physics: Conference Series*, vol. 705, p. 012009. IOP Publishing, 2016.

[310] Son, D., Lee, J., Qiao, S., Ghaffari, R., Kim, J., Lee, J.E., Song, C., Kim, S.J., Lee, D.J., Jun, S.W. *et al.*: Multifunctional wearable devices for diagnosis and therapy of movement disorders. *Nature nanotechnology*, vol. 9, no. 5, pp. 397–404, 2014.

[311] Chi, Y.M., Deiss, S.R. and Cauwenberghs, G.: Non-contact low power eeg/ecg electrode for high density wearable biopotential sensor networks. In: *Wearable and Implantable Body Sensor Networks, 2009. BSN 2009. Sixth International Workshop on*, pp. 246–250. IEEE, 2009.

[312] Chi, Y.M., Jung, T.-P. and Cauwenberghs, G.: Dry-contact and noncontact biopotential electrodes: Methodological review. *IEEE reviews in biomedical engineering*, vol. 3, pp. 106–119, 2010.

[313] Klein, A. and Skrandies, W.: Total variation for the analysis of event-related potentials. *Journal of neuroscience methods*, vol. 275, pp. 33–44, 2017.

[314] Samar, V.J., Bopardikar, A., Rao, R. and Swartz, K.: Wavelet analysis of neuroelectric waveforms: a conceptual tutorial. *Brain and language*, vol. 66, no. 1, pp. 7–60, 1999.

[315] Liu, D., Li, C., Liu, J. and Long, K.: A novel signal separation algorithm for wideband spectrum sensing in cognitive networks. In: *Global Telecommunications Conference (GLOBECOM 2010), 2010 IEEE*, pp. 1–6. IEEE, 2010.

[316] Beck, T.W., Housh, T.J., Johnson, G.O., Weir, J.P., Cramer, J.T., Coburn, J.W. and Malek, M.H.: Comparison of fourier and wavelet transform procedures for examining the mechanomyographic and electromyographic frequency domain responses during fatiguing isokinetic muscle actions of the biceps brachii. *Journal of Electromyography and Kinesiology*, vol. 15, no. 2, pp. 190–199, 2005.

[317] Fukunaga, K.: *Introduction to statistical pattern recognition*. Academic press, 2013.

[318] Englehart, K., Hugdins, B. and Parker, P.: Multifunction control of prostheses using the myoelectric signal. 2000.

[319] Patil, S., Veeresh, P. and Mane, R.: Feature extraction and comparative classification of myoelectric signal for prosthetic arm control. *International Journal of Engineering and Innovative Technology*, vol. 3, no. 4, 2013.

[320] Rosli, M., Izni, N.A., Rahman, M.A.A., Balakrishnan, M., Mazlan, S.A. and Zamzuri, H.: The fusion of hrv and emg signals for automatic gender recognition during stepping exercise. *Telkomnika*, vol. 15, no. 2, 2017.

[321] Englehart, K., Hudgins, B., Parker, P.A. and Stevenson, M.: Classification of the myoelectric signal using time-frequency based representations. *Medical engineering & physics*, vol. 21, no. 6, pp. 431–438, 1999.

[322] Chu, J.-U., Moon, I., Lee, Y.-J., Kim, S.-K. and Mun, M.-S.: A supervised feature-projection-based real-time emg pattern recognition for multifunction myoelectric hand control. *IEEE/ASME Transactions on Mechatronics*, vol. 12, no. 3, pp. 282–290, 2007.

[323] Kotsiantis, S.B., Zaharakis, I. and Pintelas, P.: Supervised machine learning: A review of classification techniques. 2007.

[324] Hyvärinen, A., Karhunen, J. and Oja, E.: *Independent component analysis*, vol. 46. John Wiley & Sons, 2004.

[325] Rajalahti, T. and Kvalheim, O.M.: Multivariate data analysis in pharmaceutics: a tutorial review. *International journal of pharmaceutics*, vol. 417, no. 1, pp. 280–290, 2011.

[326] Candès, E.J., Li, X., Ma, Y. and Wright, J.: Robust principal component analysis? *Journal of the ACM (JACM)*, vol. 58, no. 3, p. 11, 2011.

[327] Roy, S.H., De Luca, G., Cheng, M., Johansson, A., Gilmore, L.D. and De Luca, C.J.: Electro-mechanical stability of surface emg sensors. *Medical & biological engineering & computing*, vol. 45, no. 5, pp. 447–457, 2007.

[328] Singhee, A. and Rutenbar, R.A.: From finance to flip flops: A study of fast quasi-monte carlo methods from computational finance applied to statistical circuit analysis. In: *Quality Electronic Design, 2007. ISQED'07. 8th International Symposium on*, pp. 685–692. IEEE, 2007.

[329] Welch, P.: The use of fast fourier transform for the estimation of power spectra: a method based on time averaging over short, modified periodograms. *IEEE Transactions on audio and electroacoustics*, vol. 15, no. 2, pp. 70–73, 1967.

[330] Wagoner, B. and Gillespie, A.: Sociocultural mediators of remembering: An extension of bartlett's method of repeated reproduction. *British Journal of Social Psychology*, vol. 53, no. 4, pp. 622–639, 2014.

[331] MScEE, Y.L., MScEE, K.E., MScEE, B.H. *et al.*: Evaluation of shoulder complex motion-based input strategies for endpoint prosthetic-limb control using dual-task paradigm. *Journal of rehabilitation research and development*, vol. 48, no. 6, p. 669, 2011.

[332] Smith, L., Lock, B. and Hargrove, L.: Effects of window length and classification accuracy on the real-time controllability of pattern recognition myoelectric control. In: *Proceedings of the 18th Congress of the International Society for Electrophysiology and Kinesiology*, pp. 16–19. 2010.

[333] Morais Filho, M.C., Reis, R.A.d. and Kawamura, C.M.: Evaluation of ankle and knee movement pattern during maturation of normal gait. *Acta Ortopédica Brasileira*, vol. 18, no. 1, pp. 23–25, 2010.